EVALUATION OF THE SEISMIC RESPONSE OF A REINFORCED CONCRETE FOOTING TO INCREASING PEAK GROUND ACCELERATION USING PSEUDO-DYNAMIC EXPERIMENTATION

SHANE HOSSELL

2019

UNIVERSITEIT VAN PRETORIA
UNIVERSITY OF PRETORIA
YUNIBESITHI YA PRETORIA

EVALUATION OF THE SEISMIC RESPONSE OF A REINFORCED CONCRETE FOOTING TO INCREASING PEAK GROUND ACCELERATION USING PSEUDO-DYNAMIC EXPERIMENTATION

SHANE HOSSELL

A project thesis submitted in partial fulfilment of the requirements for the degree of

MASTER OF ENGINEERING (STRUCTURAL ENGINEERING)

In the

FACULTY OF ENGINEERING

UNIVERSITY OF PRETORIA

March 2019

UNIVERSITEIT VAN PRETORIA
UNIVERSITY OF PRETORIA
YUNIBESITHI YA PRETORIA

THESIS SUMMARY

EVALUATION OF THE SEISMIC RESPONSE OF A REINFORCED CONCRETE FOOTING TO INCREASING PEAK GROUND ACCELERATION USING PSEUDO-DYNAMIC EXPERIMENTATION

SHANE HOSSELL

Supervisor:	Professor Chris Roth
Co-supervisor:	Professor Andrzej Kijko
Department:	Civil Engineering
University:	University of Pretoria
Degree :	Master of Engineering (Structural Engineering)

Southern Africa is characterised as a region of moderate seismicity with several instances of both natural seismicity and mining-related seismicity occurring within the last century. Evaluating the performance of a structure due to increasing seismic intensity is traditionally calculated post-earthquake using statistical means. However, the limited network of accelerometers in South Africa has prevented a detailed statistical analysis to be undertaken to determine the resultant structural damage to South African designed structures with increasing earthquake intensity. Therefore, this research investigates a method to relate damage to a structure with earthquake intensity by performing numerical analysis in combination with physical experimentation.

The pseudo-dynamic experimentation technique was utilised to evaluate the damage occurring in a reinforced concrete footing due to the overall response of a linear elastic two-storey, two-bay moment resisting steel frame structure that is subjected to earthquake excitation. The implicit Newmark's method with static condensation was utilized in the present study to solve the governing equation of motion of the multi-degree of freedom system. Five pseudo-dynamic

experiments were performed by scaling the El Centro ground motion record, which occurred in California on May 18, 1940, to produce peak ground accelerations that ranged between 0.34 g and 2 g. To supplement the pseudo-dynamic tests, two cyclic load tests were also undertaken. All the laboratory experiments were undertaken under a constant axial load for the duration of the applied earthquake excitation and utilised Rayleigh damping to model the energy loss with the overall linear elastic frame structure. Utilising the results produced during the experiments, an analytical hysteretic model and a damage index was formulated for the analysed reinforced concrete footing with the aim of interpolating damage at peak ground accelerations and overall structural fundamental period of vibration that were not evaluated during the laboratory test. The Park and Ang damage index was used in combination with the results to formulate damage curves and fragility curves for the reinforced concrete footing.

The pseudo-dynamic method provides a reliable method to relate damage suffered by the footing due to the overall structure's response to the applied earthquake excitation. The method enables the structural capacity and failure mechanisms of the reinforced concrete footing to be observed in relation to the seismic demand. The hysteretic response of the footings and energy dissipation characteristics were determined and was shown that the yield strength of the longitudinal reinforcement within the footing has a significant impact on the maximum shear capacity and damage incurred by the footing. The reinforced concrete footing could only sustain a maximum PGA before failure, which is related to the structure's natural frequency and overall energy loss within the structure. Five damage states can be determined for the reinforced concrete and are related to the design of the footing and material properties that comprise the footing. The damage is more pronounced with an increase in the number of cycles of vibration, particularly at displacements that exceed the yield strength of the reinforcement. An increase in the hysteretic energy dissipated by the reinforced concrete footing results in a concomitant increase in the observed damage to the footing in the form of concrete cracking, reinforcement yielding and spalling of the concrete. The investigation shows that the resultant damage to an individual structural component is complex and is dependent on several characteristics that define the structure.

DECLARATION

I, the undersigned hereby declare that:

- I understand what plagiarism is and I am aware of the University's policy in this regard
- The work contained in this thesis is my own original work;
- I did not refer to work of current or previous students, lecture notes, handbooks or any other study material without proper referencing;
- Where another person's work has been used this has been properly acknowledged and referenced;
- I have not allowed anyone to copy any part of my thesis;
- I have not previously in its entirety or in part submitted this thesis at any university for a degree

Signature of student: ________________

Name of student: Shane Hossell

Student number: 04413512

Date: April 2019

ACKNOWLEDGEMENTS

I wish to express my appreciation to the following organisations and persons who made this thesis possible:

- The University of Pretoria's Civil Engineering Department for the use of their facilities, materials and testing equipment;
- Prof. Roth, Prof. Kijko and Ms Ansie Smit for their guidance and support during the study;
- Mr. J. Scholtz, Mr. J. Botha, Mr. R Kock, Mr J Nkosi for their assistance in the Civil Engineering laboratory;
- Mr J. Clark, H. Booysen's for their assistance in the Sasol Laboratory for Mechanics
- MMI and the University of Pretoria's Natural Hazard Centre for the funding and support;
- Johannes Fourie and Tinette Brümmer for their assistance in reviewing the masters document;
- Marshalls Engineering and Cadcon for sponsoring the steel for the connections and the fabricating of the members
- NRF THRIP Funding TP 14072278140 for funding the materials for the laboratory tests;
- NRF funding grant No: 103724 and Grant: TP14072278140 for financial assistance; and
- To my father, Eugene Hossell, and my family for their continual love, support and encouragement during the study

TABLE OF CONTENTS

LIST OF FIGURES

LIST OF TABLES

LIST OF SYMBOLS

ω	Natural frequency of the structure in rads/s
μ	Ductility ratio
ζ	Structural damping ratio
γ	Newmark's parameter equalling ½ for the linear acceleration method
β	Either indicates Newmark's parameter equalling ¼ for the linear acceleration method or Park and Ang parameter indicating the extent of damage due to hysteresis
u	Displacement
du	Change in displacement
PGA	Peak ground acceleration
DI	Damage index
ρ_{st}	Steel density
ρ_m	Masonry density
ρ_c	Concrete density
Δt	Change in time
g	Gravity acceleration (9.81 m/s^2)
ρ_w	Confinement ratio
β_i	Logarithmic standard deviation
u_s	Non-linear spring displacement
p_t	Longitudinal steel ratio as a percentage
n_0	Normalised axial stress
k_s	Non-linear spring stiffness
a_0 & a_1	Rayleigh damping coefficients having units s^{-1} and s respectively

W_{SDL}	Distributed superimposed dead load
W_{LL}	Distributed live load
R_i	Measured restoring force from tests specimen
P_m	Point load due to masonry infill panels
P_{DL}	Point dead load
$[M]$	Mass matrix
$[K]$	Overall structural stiffness matrix
$\{I\}$:	Influence vector that accounts for the direction of the earthquake loading
F_s	Non-linear spring force
E_s	Strain energy
E_m	Kinetic energy
E_l	Total energy
E_c	Viscous damping energy
E_H	Hysteretic energy
$[C]$	Viscous damping matrix
h_t	Overall height of the structure used in building period formulas
$\{u_i\}$	Displacements at time step i
$\{\dot{u}_i\}$	Velocity vector at time step i
$\{\ddot{u}_i\}$	Acceleration vector at time step i
$\{\ddot{u}_{gi}\}$:	Ground acceleration at time step i

1 INTRODUCTION

1.1 BACKGROUND

The performance of structures during an earthquake of given intensity dictates the extent of damage and loss of life that becomes associated with the earthquake event. Quantifying the level of damage within a structure that has occurred during an earthquake is traditionally undertaken post-earthquake using statistical methods. However, this method is not suitable in areas with moderate seismicity as insufficient data are available to calibrate structural damage to an earthquake intensity parameter.

Southern Africa is characterised as a region of moderate seismicity, and due to the limited network of accelerometers within South Africa, a detailed statistical analysis of the level of damage that could occur within structures during future earthquakes has been prevented (Brandt, 2011). The previous century has been characterised by several earthquakes in South Africa, with the most widely documented being the Ceres-Tulbagh earthquake in 1969 of Richter magnitude 6.7. The Ceres-Tulbagh earthquake had an insured loss of US$ 7.4 million and a total uninsured loss amounting to approximately 3.5 times that of the insured loss. Extensive mining in South Africa, particularly in the gold mining districts of the Witwatersrand Basin, has resulted in at least four events in recent years that have caused significant structural damage (Kijko and Davies, 2003). Therefore, as noted in Kijko and Davies (2003), seismic risk faced by South African structures cannot be met with complacency and structures need to be evaluated against a range of earthquake intensities to quantify their seismic capacity and performance during an earthquake.

The typical engineering design process does not adequately quantify the level of performance that a structure can sustain during an earthquake. The procedure entails the analysis and design of structural components to satisfy the requirements of the South African structural design codes of practice, which tend to be prescriptive (Kijko and Davies, 2003). Therefore, the resultant performance of the structure and the components making up the structure are not thoroughly investigated at various earthquake intensities.

Quantifying the level of damage incurred by a structure due to increasing earthquake intensity is a complex task. Typically, structural components are evaluated using quasi-static methods to determine the response due to increasing load. However, the slow rate of the load applied onto the structure results in the inertia of the structure not being considered resulting in the response of the structure being independent of the applied earthquake loading. To relate earthquake intensity to damage, shake table testing or pseudo-dynamic testing provide a more accurate damage correlation with earthquake intensity. Shake table tests provide the most realistic means to evaluate damage at various intensities as it accounts for the inertial effects, and the time and frequency content of the ground motion. However, shake tables are very expensive, and it is difficult to evaluate large scale multi-story structures.

During pseudo-dynamic experimentation, part of the structure under investigation is physically tested in the laboratory in parallel with the dynamic time-stepping structural analysis of the overall structure that is mathematically modelled on the computer. The mathematical model of the overall structure incorporates both the mass and damping properties of the structure during the analysis with the physical model only accounting for the static force-displacement response of the test specimen. Pseudo-dynamic experimentation uses well established time integration numerical methods to determine the resultant displacement at the degree of freedom that couples the numerical model with the physical model. The displacement determined at the coupled degree of freedom is physically applied to the test specimen using a servo-controlled linear actuator. The resultant force on the structure is measured using a load cell and is subsequently fed back into the computational model and used in successive iterations and computations to calculate the new displacements.

The disadvantages associated with pseudo-dynamic tests is that they exclude time-dependent effects and can result in cumulative errors in the computational process. However, the advantages associated with the method include using the same equipment that is used to perform quasi-static tests and because of the time-independent nature of the experiment, the structural damage can be observed at each time step due to the slow application of the load. Advancements in computer software, the increase in the resolution of the control systems and data acquisition systems and the ability of pseudo-dynamic tests to incorporate the dynamic characteristics of a structure has made the method a feasible alternative to shake table tests to evaluate the performance of a structure at various earthquake intensities.

1.2 OBJECTIVE OF THE STUDY

The primary objective of the study was to use the pseudo-dynamic experimental method to relate structural damage incurred by a single axially loaded reinforced concrete footing, which forms part of a two-bay two-story moment resisting frame structure, to increasing earthquake intensity. Therefore, the purpose of the study was separated into the following objectives:

- To evaluate the feasibility and viability of using the pseudo-dynamic method with implicit time-stepping numerical methods to accurately relate the level of damage encountered by a reinforced concrete footing structural subcomponent, which forms part of an overall structural system subjected to an earthquake excitation, to increasing earthquake intensity;
- To utilise the pseudo-dynamic method to determine the structural capacity and failure mechanisms of the reinforced concrete footing structural component to be observed in relation to the seismic demand at various earthquake intensities. To determine the relationship between earthquake intensity and structural damage for the reinforced concrete footing by analysing the hysteretic cyclic response and energy dissipation characteristics at various earthquake intensities. To use the results obtained from experiments to formulate a damage index that can be used to quantify the expected level of damage at various earthquake intensities;
- To evaluate the response of the reinforced concrete structure at high peak ground accelerations (PGA) and to determine the maximum peak ground acceleration that the concrete section can endure for the analysed structural design and configuration; and
- To investigate the feasibility of using the pseudo-dynamic testing method to formulate damage curves and fragility curves for a structural subcomponent that forms part of an overall structural system. To determine the influence of the overall structure's fundamental period of vibration has on the level of damage experienced by the footing for the analysed structural design and configuration.

1.3 SCOPE OF THE STUDY

The susceptibility of damage to a reinforced concrete footing during an earthquake is dependent on several factors that relate to the type of structure placed on the footing and the type of earthquake ground motion that is imparted to the structure. The study focused on evaluating the pseudo-dynamic testing method using only the Newmark's implicit numerical time integration method to correlate damage incurred by the reinforced concrete footing to different earthquake intensities. Only a single ground motion record was used in the analysis with changes in the peak ground acceleration being the only variable. The El Centro earthquake record was selected as the input ground motion for the pseudo-dynamic analysis and the change in the peak ground acceleration was achieved by amplifying the record to obtain the required peak ground acceleration (PGA).

The reinforced concrete footing was subjected to a constant axial load for the duration of the earthquake record, and therefore the response of the footing due to a varying axial load was not investigated. Only a reinforced concrete footing of a single design that satisfied the minimum reinforcement requirements contained in SANS 10100-1:2000 was considered in this research. Therefore, the reinforced concrete footing dimensions, reinforcement and concrete mix design were all kept constant for each of the tests. All the footings were constructed using the same batch of concrete and reinforcement. Additional quasi-static cyclic load tests were conducted on the footings to determine the cyclic response to increasing deformation and to determine the maximum stiffness of the footing.

The frame structure, which was placed on the footing, remained linear elastic for the duration of the earthquake record. Only Rayleigh damping was incorporated into the analysis to account for damage and energy loss in the overall frame structure. The capacity of structural members and their connections within the overall frame structure is not considered during the analysis, and therefore, the formation of plastic hinges and the resulted loss of stiffness within the overall structure is not accounted for in the response of the reinforced concrete footing. Future studies can incorporate plastic hinges and determine the influence it has on the damage and fragility of the footings and the overall structure.

An analytical material model was developed by only using the results produced from the pseudo-dynamic experiments and the cyclic load tests to interpolate damage at peak ground accelerations and fundamental periods of vibration that were not undertaken during the laboratory experiments. The typical range of the fundamental periods of vibration were determined using building period formulas obtained from SANS 10160-4:2017. The fundamental period of vibration of the overall frame structure was varied by multiplying the stiffness of the each of the members by the same constant value, therefore ensuring that there is the same proportional variation in stiffness between each of the structural members. The fundamental period of vibration was not varied by altering the structural configuration or type of structure placed on the footing. A damage index was formulated using on the results produced in this research.

Damage curves and fragility curves were only produced for the designed reinforced concrete footing and moment resisting frame structure that was subjected to a single ground motion record. The fragility curves only consider a uniform distribution of fundamental periods of vibration of frame structures that could reasonably be placed on the reinforced concrete footing as the actual distribution of structures in an area is not known. The procedure following in this research could be used in future research to analyse the response of structures and structural components with varying configurations and designs to develop damage and fragility curves.

1.4 METHODOLOGY

The influence of earthquake intensity on the level of damage to the reinforced concrete footing was evaluated by using seven test specimens that were constructed from the same batch of reinforcing steel and 30 MPa concrete. Two cyclic load tests and five pseudo-dynamic tests were undertaken at PGAs of 0.34 g, 0.68 g, 0.78 g, 1 g and 2 g, which were obtained by amplifying the El Centro ground motion record. The reinforcement and concrete were obtained from commercial suppliers, which ensured that consistency was maintained between the materials used to construct the footings and the materials typically used in industry.

The pseudo-dynamic experimental method was used to establish a correlation between the level of damage encountered by the reinforced concrete footing, which forms part of a two-bay, two-story moment resisting steel frame structure, with earthquake intensity. Two stages were required to perform the pseudo-dynamic experiments with the first stage requiring the establishment of a physical test setup that would allow for a constant axial load to be applied to the test specimen for the duration of the earthquake record while allowing for a varying horizontal load, which was servo-controlled. Both the horizontal load and axial load needed to be applied simultaneously without any disruptions during the applied earthquake excitation.

The second stage required to undertake pseudo-dynamic experiments required the development and programming of an algorithm that would be used to control the actuators. The computer algorithm had to model the overall frame structure's mass, stiffness and applied static loading and was formulated using the equation of motion and Newmark's implicit time integration numerical method. The algorithm required two steps, with the first step requiring the formulation of the frame structure and the calculation of the initial state of the structure under static loading conditions. The second step entailed subjecting the structure to the earthquake excitation, and due to the implicit nature of the numerical method, the analysis required iteration until convergence at each time step. The horizontal displacement of the footing that was calculated from the numerical model was applied directly to the test specimen in the laboratory at each time increment, and the restoring force was measured using a load cell that was subsequently fed back into the algorithm to be used in further calculations.

Strain gauges were attached to the reinforcing bars to determine the strain at each time step, and four external displacement transducers were distributed along the height of the column to obtain additional displacement information at each time increment. Due to the implicit nature of the time-stepping algorithm used to perform the pseudo-dynamic tests, cyclic load tests were undertaken to determine the maximum stiffness of the footing, which was then used as an input into the pseudo-dynamic tests.

Due to the limited number of pseudo-dynamic tests undertaken, an analytical hysteretic model was developed from the results obtained from the cyclic load tests and pseudo-dynamic tests to complement and enable the interpolation of damage at peak ground accelerations and overall structural fundamental periods of vibration that were not undertaken during the pseudo-dynamic experiments. The result obtained from the cyclic load tests and pseudo-dynamic tests were subsequently used to formulate a damage index for the reinforced concrete footing. Ten-thousand numerical analysis were undertaken using the formulated analytical hysteretic model and damage index to determine the level of damage incurred by the footing over a range of peak ground accelerations and fundamental periods of vibration. The numerical analysis undertaken using the analytical hysteretic model utilised the same algorithm used to perform the pseudo-dynamic experiments, which entailed substituting the physical test setup with the analytical hysteretic model.

The results obtained by using the analytical hysteretic model were used to develop damage curves and contour damage plots, in terms of the overall structural fundamental period of vibration, for the reinforced concrete footing. The contour damage plots and curves were subsequently used to develop fragility curves assuming a uniform distribution and representative range of fundamental periods of vibration that could typically be obtained for structures placed on the footing. The results produced from the damage curves and fragility curves are related to predicted earthquake intensities and historical earthquake intensities in South Africa to infer predicted damage that a structure may sustain.

1.5 ORGANISATION OF THE REPORT

This report consists of the following chapters:

- Chapter 1 serves as an introduction to the report;
- Chapter 2 provides a literature study of the different concepts covered during the study;
- Chapter 3 provides the experimental test setup including the analysis and design of the overall frame structure and the reinforced concrete footing. The pseudo-dynamic experimental method is presented showing the physical test setup and the formulation of the algorithm used to perform the experiments;

- Chapter 4 discusses the analysis and detailed description of the results obtained from the cyclic load tests and pseudo-dynamic experiments;
- Chapter 5 provides the formulation of the analytical hysteretic model and damage results. The formulated damage index, the resultant damage and fragility curves are also presented and discussed;
- Chapter 6 contains the final conclusions and recommendations of the study; and
- Chapter 7 provides a list of references.

2 LITERATURE STUDY

This chapter explores the current understanding of pseudo-dynamic experimentation techniques used to analyse engineering structures and includes information on the non-linear time-stepping numerical models for solving the equation of motion. In the literature, numerous studies have been conducted on the pseudo-dynamic method; however, only the important contributions relevant to the current study are discussed. This literature review commences with a discussion on seismic risk in South Africa, followed by a discussion on the pseudo-dynamic experimentation concerning previous studies and the cyclic response of reinforced concrete. The final section of the literature study briefly discusses damage models and the formulation of damage and fragility curves from experimental data.

2.1 EARTHQUAKES

An earthquake is a naturally occurring phenomenon that typically does not pose a threat to humans; however, earthquakes become a hazard when considered in relation to structures and infrastructure due to the structure being subjected to the seismic excitation (Penelis & Kappos, 2010). Earthquakes have a severe impact on economic, social, psychological and political effects due to deaths and damage to infrastructure.

Earthquakes are ground vibrations that predominantly occur along plate boundary zones where one tectonic plate slides relative to another or subducts beneath the other or due to the fracturing of the crust (Penelis & Kappos, 2010). A schematic representation of the origin of earthquakes is shown in Figure 2-1.

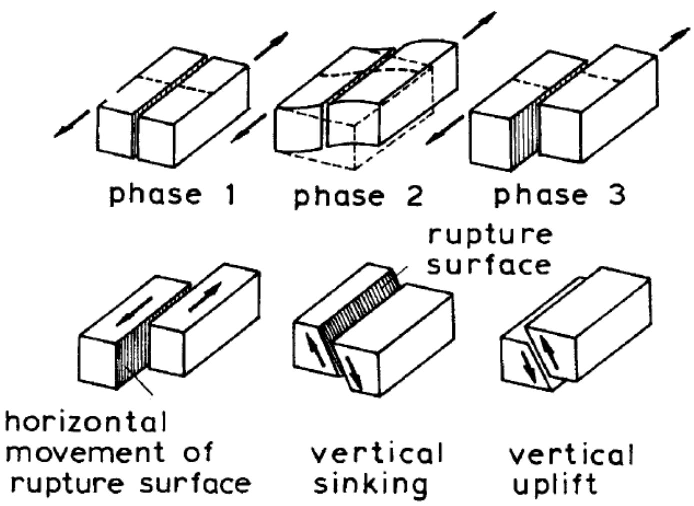

Figure 2-1 Origins of earthquakes (Penelis & Kappos, 2010)

In areas where plates move relative to one another, large amounts of energy build up over a relatively small area. As a result, these regions are responsible for more frequent and severe earthquakes. However, regions located within the boundaries of tectonic plates are generally rigid, which requires a much longer time to deform and build up energy (Kijko et al., 2015). South Africa is located within the boundaries of the African plate and is characterised as an area with moderate seismicity. Further information on the seismic hazard in South Africa and the tectonic makeup can be found in Brandt (2011).

Continents consist of vast geological histories that can comprise of up to 4 billion years. Earthquakes that occur in plate interiors are infrequent due to the slow speed of internal deformation, which can be associated with asperities in the mantle or faults in geological formations. However, Davies and Kijko (2003) indicate that the seismic risk faced by South Africa is non-negligible and therefore the risk of seismic activity needs to be considered when designing a structure. More alarming is that Kijko et al. (2015) conclude that structures designed to SANS Standard 10160 (SANS 10160-4, 2017) for a seismic load of 0.1 g are at significant seismic risk. Therefore, seismic hazard is an issue in South Africa that needs to be considered by the insurance industry and disaster management agencies as a probable threat to infrastructure and life (Kijko et al., 2015).

2.1.1 EARTHQUAKE MAGNITUDE AND INTENSITY

The magnitude of an earthquake is a measure of the amount of energy released at its point of origin in the form of seismic waves and is measured on the Richter scale. The largest earthquake to have been recorded had a magnitude of 8.9 on the Richter scale (Colombia-Ecuador, 1906; Japan, 1933) and is taken to be the largest earthquake to have ever occurred (Penelis & Kappos, 2010).

The damage caused by an earthquake is partly related to magnitude but is also related to several other factors such as the focal depth of the earthquake, the distance to the epicentre, and the geology and mechanical properties that make up the structures. The intensity provides a measure of quantifying the consequences that the earthquake will have on people and the structures in which they reside. Due to the complexity of the problem, empirical intensity scales have been formulated to quantify damage qualitatively. One of the most common intensity scales is the modified Mercalli (I_{MM}) scale, which has 12 intensity grades and can be related to peak ground acceleration and is shown in Table 2-1. Strong ground motions that are of interest to structural engineers are recorded using accelerograms and record the acceleration of the ground as a function of time. An example of a strong motion record shown in Figure 2-2.

Table 2-1 Modified Mercalli scale (Penelis & Kappos, 2010)

		Ground acceleration a ($\frac{cm}{sec}$)	$\frac{a}{g}$
I	Not felt except by a very few under especially favourable circumstances		
II	Felt only by a few persons at rest, especially on upper floors of buildings. Delicately suspended objects may swing	2, 3	
III	Felt quite noticeably indoors, expecially on upper floors of buildings, but many people do not recognize it as an earthquake. Standing motor cars may rock slightly. Vibration like passing truck. Duration estimated	4, 5, 6	0.005 g (at 5)
IV	During the day felt indoors by many, outdoors by few. At night some awakened. Dishes, windows, doors disturbed: walls make creaking sound. Sensation like heavy truck striking building. Standing motor cars rocked noticeably	7, 8, 9, 10	0.01 g (at 9)
V	Felt by nearly everyone: many awakened. Some dishes, windows, etc., broken; a few instances of cracked plaster; unstable objects overturned. Disturbances of trees, poles and other tall objects sometimes noticed. Pendulum clocks may stop	20, 30	
VI	Felt by all; many frightened and run outdoors. Some heavy furniture moved: a few instances of fallen plaster or damaged chimneys. Damage slight	40, 50, 60	0.05 g (at 50)
VII	Everybody runs outdoors. Damage negligible in buildings of good design and construction: slight to moderate in well-built ordinary structures: considerable in poorly built or badly designed structures; some chimneys broken. Noticed by persons driving motor cars	70, 80, 90, 100	0.1 g (at 100)
VIII	Damage slight in specially designed structures: considerable in ordinary substantial buildings, with partial collapse; great in poorly built structures. Panel walls thrown out of frame structures. Fall of chimneys, factory stacks, columns, monuments, walls. Heavy furniture overturned. Sand and mud ejected in small amounts. Changes in well water. Disturbs persons driving motor cars	200, 300	
IX	Damage considerable in specially designed structures: well-designed frame structures thrown out of plumb; great in substantial buildings, with partial collapse. Buildings shifted off foundations. Ground cracked conspicuously. Underground pipes broken	400, 500, 600	0.5 g (at 500)
X	Some well-built, wooden structures destroyed: most masonry and frame structures destroyed with foundations; ground badly cracked. Rails bent. Landslides considerable from river banks and steep slopes. Shifted sand and mud. Water splashed over banks	700, 800, 900, 1000	1 g (at 1000)
XI	Few, if any masonry structures remain standing, Bridges destroyed. Broad fissures in ground. Underground, pipelines completely out of service. Earth slumps and landslips in soft ground. Rails bent greatly	2000	
XII	Damage total. Waves seen on ground surfaces. Lines of sight and level distorted. Objects thrown upward into the air	3000, 4000, 5000, 6000	5 g (at 5000)

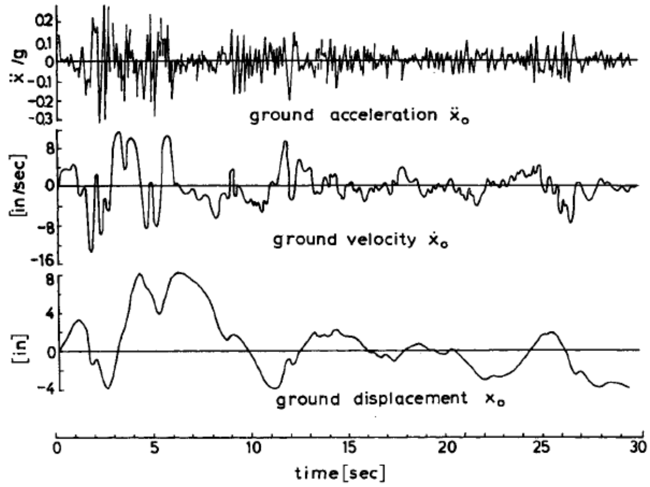

Figure 2-2 Example of a strong ground motion accelerogram of the El Centro earthquake on 18 May 1940 (N-S component) with the calculated velocity and displacement diagrams (Penelis & Kappos, 2010)

Intensity provides a single means of describing the effect that an earthquake has on human-made structures. The reason for using intensity (I_{MM}) to describe an earthquake as opposed to just using peak ground acceleration is that it considers the local condition inherent to a site, which is not possible when expressing an earthquake in terms of peak ground acceleration (Kijko et al., 2015). Many empirical relationships have been developed to correlate intensity with peak ground acceleration. Figure 2-4 shows various conversions that have been developed by various authors to relate intensity with maximum earthquake accelerations.

Discussions with Prof. A Kijko at the University of Pretoria's Natural Hazard Centre indicated that the correlation between peak ground acceleration and intensity developed by Ambraseys (1974) provided the best correlation for South African conditions. Figure 2-3 shows the maximum horizontal acceleration and maximum vertical acceleration against reported intensity between 1967 and 1974 during the study by Ambraseys (1974).

The solid dots shown in Figure 2-3 indicate the maximum horizontal acceleration and the open dots represents the maximum vertical acceleration. The stars indicate points obtained on hard ground, and the dots represent points on soft ground. Utilising the results from Figure 2-3 Ambraseys (1974) developed a first-order approximation for relating maximum horizontal acceleration and intensity, which is shown by Equation 2.1. The conclusions drawn by Ambraseys (1974) indicate that:

- There is a weak correlation between intensity and maximum ground accelerations due to the considerable variability in geologic conditions, foundation conditions, earthquake mechanisms and the type of accelerograms that are used;

- The maximum horizontal accelerations are in the order of 1.5 to 2.5 times greater than the vertical accelerations; and
- Accelerations on hard ground are more significant than those on soft ground.

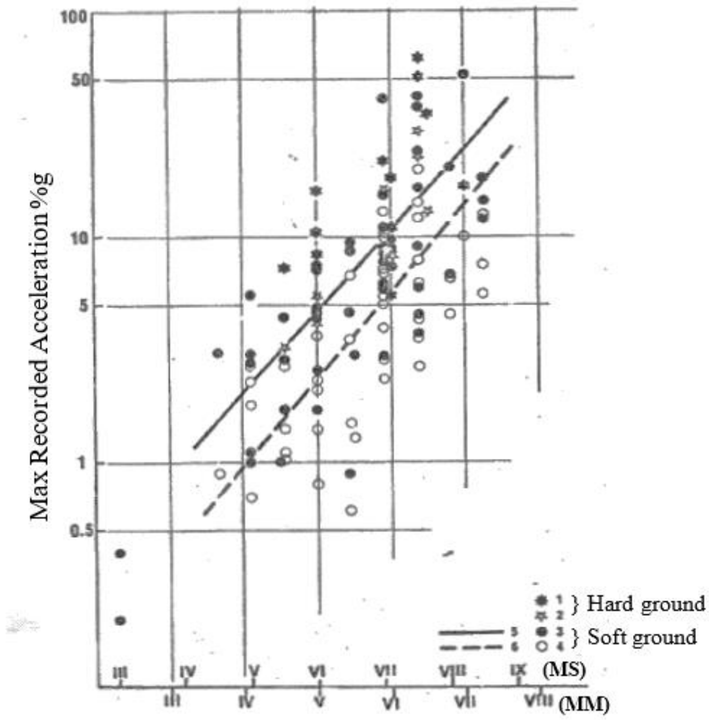

Figure 2-3 Plot of the maximum recorded acceleration versus reported intensity (Ambraseys, 1974)

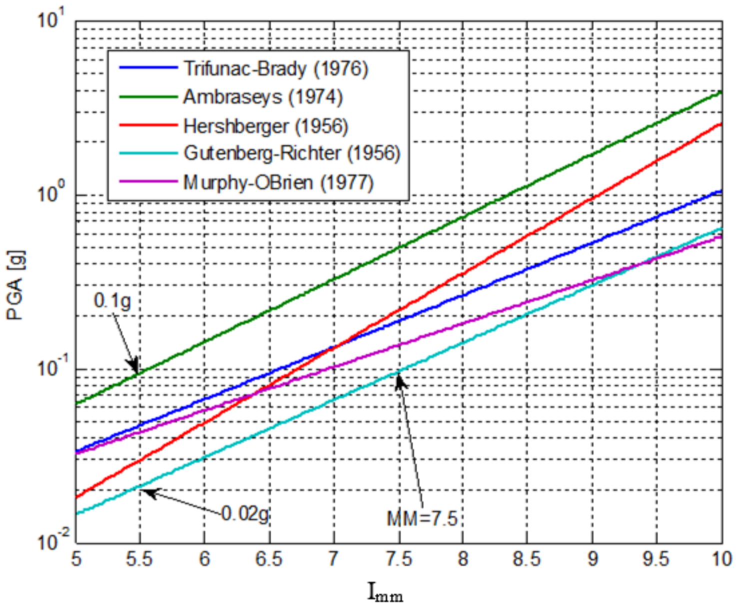

Figure 2-4 Peak ground accelerations conversions to intensity (IMM) relationships from different studies (Kijko, 2008)

$$\log(a_h) = -0.16 + 0.36(I_{MM}) \tag{2.1}$$

2.1.2 SEISMIC RISK IN SOUTH AFRICA

Two significant groups of seismicity occur in South Africa, namely natural seismicity and mining-related seismicity. The first recorded earthquake in South Africa occurred on Robben Island in 1620 and was recorded by the early Dutch settlers (Kijko et al., 2015). The 20th century predominately comprised of tectonic induced seismicity, with an example being the magnitude 6.0 to 6.5 seismic event that occurred on 31 December 1932 off the coast of Cape St Lucia (Kijko et al., 2015). Another example of a large magnitude earthquake occurring in South Africa is the Tulbagh-Ceres earthquake of magnitude 6.3 that occurred in 1969. The Tulbagh-Ceres earthquake resulted in extensive damage with examples of damage shown in Figure 2-5. The Tulbagh-Ceres earthquake was felt across the Western Cape and several buildings suffered severe damage, which ranged from large cracks to complete destruction. Twelve people lost their lives due to the earthquake, and the event produced an insured loss of US $ 7.4 million. However, the uninsured loss was estimated to be approximately 3.5 times higher than the insured damage (Kijko et al., 2015).

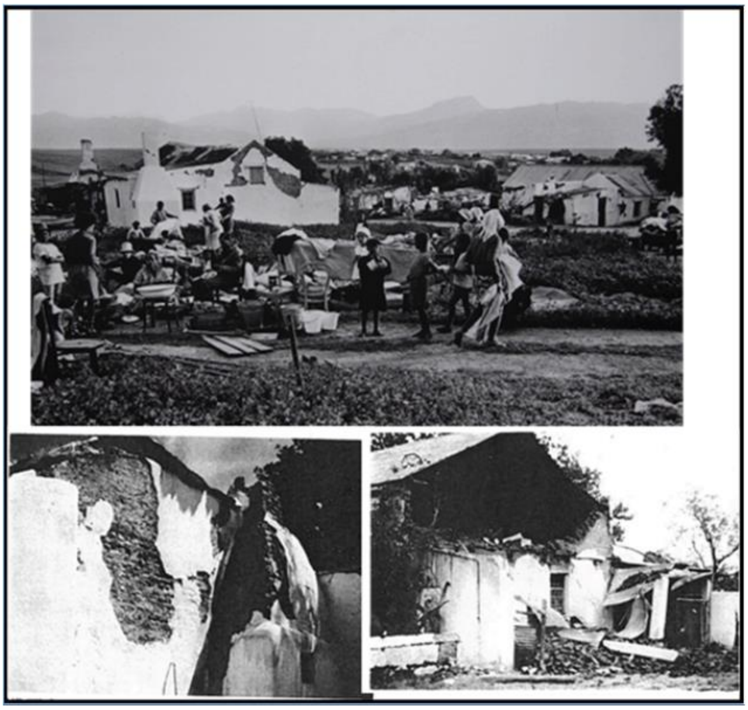

Figure 2-5 Resultant damage at Tulbagh after the Ceres earthquake of 29 September 1969 (Kijko et al., 2015)

Other examples of seismic events in South Africa include the Welkom earthquake in 1976 that resulted in the collapse of a six-story-high block of flats and incurred a total insured cost of R4.5 million. Figure 2-6 shows the collapse of the six-story building during the Welkom earthquake event. A seismic event that occurred in Anglovaal in 1998 resulted in an issued loss of R23 million (Kijko et al., 2015).

Figure 2-6 Collapse of a six-storey high block of flats due to the 1976 Welkom seismic event (Kijko et.al, 2015)

Figure 2-7 shows historical epicentral locations of seismicity in Southern Africa. Belt-like zones of seismicity characterise Southern Africa, which is surrounded by regions of low seismicity. The belt-like zones of seismicity extend from the African Rift Valley down into South Africa along the South African and Mozambique north-south border, which extends southwards into Kwa-Zulu Natal. Another belt of seismic activity occurs from east to west through southern KwaZulu Natal, Lesotho and the southern parts of the Free State (Brandt, 2011).

Due to limited information of historical earthquakes in South Africa, a probabilistic seismic hazard analysis is undertaken to produce a map showing the expected peak ground accelerations as a factor of gravitational acceleration ($g = 9.81\ m/s^2$) with a 10% probability of being exceeded within the next 50 years, which is shown in Figure 2-8. As noted in Kijko et al. (2015), due to the slow rate of deformation of the tectonic plates within South Africa, the repeat times of earthquakes range from thousands to tens of thousands of years. Due to this, instrumental and historical records cannot provide a comprehensive overview of the potential risk (Kijko et al., 2015).

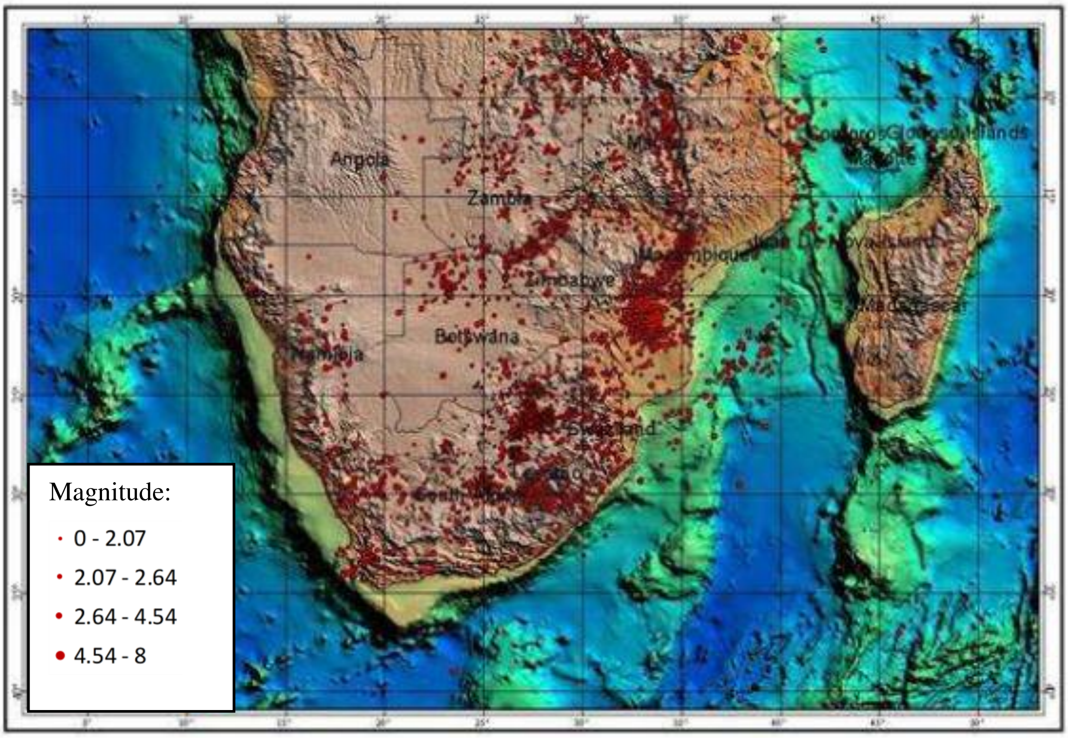

Figure 2-7 Seismic map of Southern Africa during the period of 1620 to 2010 (Brandt, 2011)

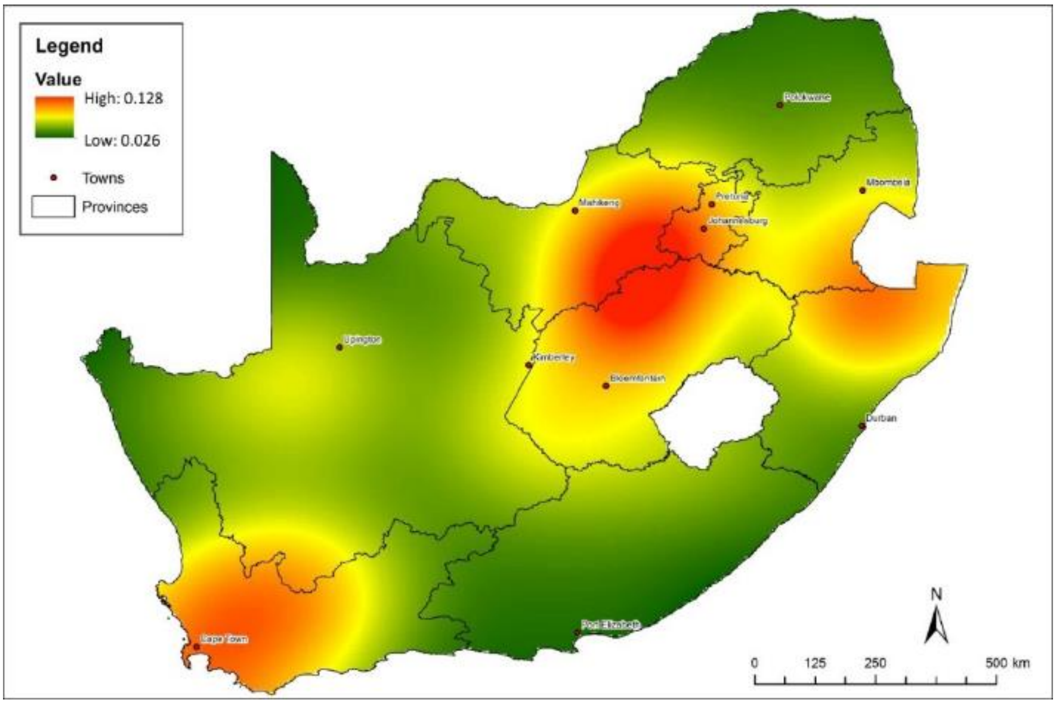

Figure 2-8 Expected peak ground acceleration (PGA) with a 10% probability of being exceeded at least once in a 50-year period (Kijko et. al. 2015)

2.1.3 SEISMICITY DUE TO MINING ACTIVITY

Many earthquakes that occur in Gauteng are due to mining activity within the region (Linzer et al., 2007). The largest seismic event that occurred in South Africa due to mining-related activity occurred in Stilfontein and happened on 9 March 2005. The seismic event recorded a 5.3 on the local Richter magnitude scale. Figure 2-9 shows some of the damage to buildings due to the seismic tremor in Stilfontein. Closure of the mine due to the earthquake resulted in large-scale socio-economic consequences for the people and the community that relied on the mine for their livelihood. Seismic events in mining regions will continue to happen if mining operations continue with the risk of seismic events continuing even after the mines have been decommissioned (Linzer et al. 2007). With increased development in regions of previous mining activity, the risk of damage to structures and infrastructure due to seismic activity is increasing. Also, due to the ever-increasing frequency of large-scale seismic activity within mining districts, the demand for more accurate identification and recording of epicentral locations in mining regions is required (Linzer et al., 2007). An earthquake of magnitude 5.5 occurred on 5 August 2014 in Orkney, South Africa, which is located at around 150 km southwest of Johannesburg. The Orkney earthquake is the largest recorded event to have occurred near a mining town and resulted in one death and damage to private houses (Manzunzu et al., 2017).

Figure 2-9 Structural damage due to the Stilfontein tremor of ML = 5.3 on 9 March 2005 (Linzer et al., 2007)

2.2 PSEUDO-DYNAMIC EXPERIMENTATION

In this section, a brief discussion is presented on the pseudo-dynamic testing technique and its background. Numerous studies have been conducted using the pseudo-dynamic testing method; however, this section only presents essential contributions and provides the relevant workflows and numerical time-stepping algorithms used during the research.

2.2.1 PSEUDO-DYNAMIC METHOD

The pseudo-dynamic testing technique is a computer controlled experimental method whereby the dynamic behaviour of the structure is mathematically calculated on a computer with the resultant displacement being statically imposed on a test specimen of the structure using servo-controlled actuators in an on-line procedure (Mosalam et al., 1997; Xing et al., 2007). Pseudo-dynamic testing emerged as an alternative to shake table testing in the 1960s and 1970s from the research done by Takanashi et al. (1975) as it produced a more controlled testing environment for large and heavy test specimens.

The pseudo-dynamic testing technique uses the same equipment as conventional quasi-static tests; however, the analysis is controlled by a closed loop system comprising of computer software that is integrated and runs in tandem with the quasi-static experiment (Kurt, 2010). Due to the inertia forces being modelled numerically, the test procedure does not need to be undertaken in real time (Takanashi et al., 1987; Pinto et al., 2004; Mosalam et al., 1997). The pseudo-dynamic method utilises well-established step-by-step time integration methods, whereby the calculated deformation is applied to the test specimen at any given time step at a common degree of freedom between the numerical model and the test specimen and the restoring force is measured using a load cell. The force obtained from the load cell is fed back into the computational model, which is used in successive iterations to determine the new deformation. The method utilises the same numerical approach generally undertaken in nonlinear structural dynamics; however, the structural restoring force is based on experimental feedback from load cells as opposed to an idealised hysteretic model (Shing & Mahin, 1984). Typical computational time domain analysis requires the idealisation of the non-linear response of the structure; however, pseudo-dynamic testing enables the true material response of the structure to be directly obtained from a physical model for the duration of the analysis (Mosalam et al., 1997).

The benefit of pseudo-dynamic testing is that it provides a better understanding of the seismic performance of a structure as it incorporates the overall response of the structure, the non-linear behaviour of the structural component, and the seismic excitation. Thereby, structural damage can be related to earthquake intensity, which is not possible during traditional quasi-static testing. The measured quantities from the actuators, calibrated displacement transducers and load cells are utilised in subsequent calculations, which enables both dynamic effects and progressive damage of the specimen to be observed for the duration of the experiment (Mosalam et al., 1997).

The pseudo-dynamic method comprises of two cycles as shown in Figure 2-10. The first cycle comprises of the calculation cycle, which requires the relevant software and hardware for solving the equation of motion using time-integration numerical methods. The second cycle of the pseudo-dynamic experiment comprises of the loading cycle, which requires the control system consisting of a servo-controlled hydraulic actuator for applying the calculated displacement to the test specimen and a load cell for reading the resultant restoring force (Takanashi et al., 1987).

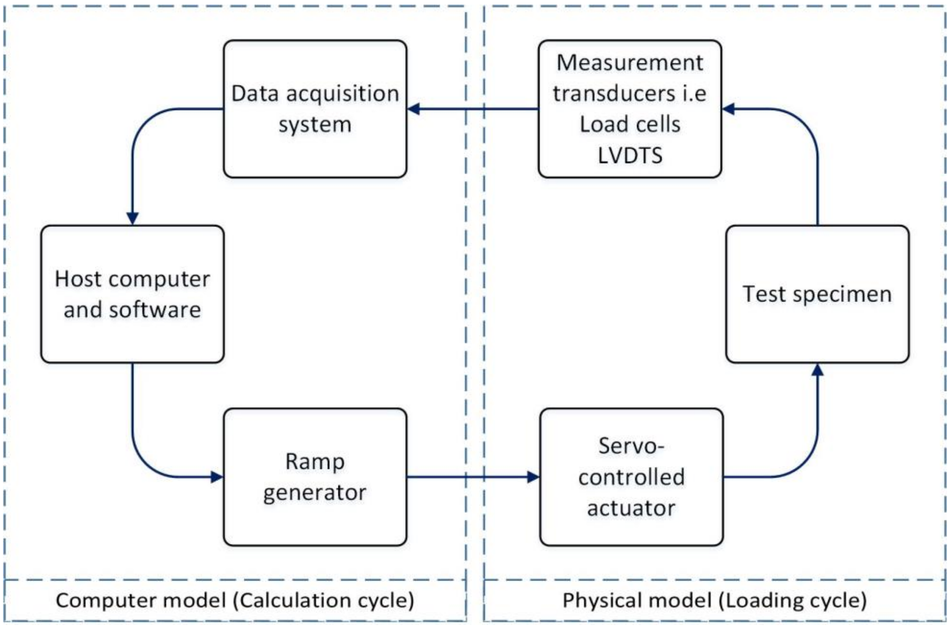

Figure 2-10 Pseudo-dynamic test loop adapted from Mosalam et al. (1997)

The advantages of pseudo-dynamic testing are indicated by Takanashi et al. (1975) as follows:

- The true non-linear restoring force characteristics of the structure with displacement can be considered without the need to assume a non-linear hysteretic model for the member;
- Testing can be performed on large structures including one to one scale structures or substructures with the use of electro-hydraulic actuators and load cells;

- The experiment can be analysed at each time-step, and the failure mechanism can be identified during the analysis. The test can be stopped at any point to inspect the structure and collect data; and
- Gravity loads can be incorporated into the analysis by utilising an actuator that applies the load before the commencement of the test to simulate the true stresses in the member such as axial stress in a column or bending stresses in a beam.

2.2.2 BACKGROUND TO THE PSEUDO-DYNAMIC METHOD

Pseudo-dynamic testing originated approximately forty years ago as an alternative to shake table testing with Takanashi et al. (1975) seen as one of the pioneers of the testing method (Kurt, 2010). Pseudo-dynamic testing is especially efficient when having to test structures that are too heavy or too large to be practically tested on available shake tables (Thewalt & Mahin, 1987). Pioneering work in pseudo-dynamic testing was done by Hakuno in 1969 (as cited by Takanashi et al., 1975) where he tested cantilever beams using an on-line system that comprised of an analogue computer and an electromagnetic actuator. However, the results produced by the test were rather poor due to the limitations of the available hardware. Following from the work that was done on cantilever beams, Takanashi et al. (1975) did substantial work in establishing the pseudo-dynamic technique by replacing the analogue computer with a more accurate digital computer. Modifications done by Takanashi et al. (1975) enabled the procedure to not have to operate in real time, thus producing a procedure that could be subjected to slow loading and pausing. The first pseudo-dynamic tests were restricted to planar test specimens that were subjected to a single horizontal component of base excitation (Takanashi et al., 1975; Shing & Mahin, 1984; Takanashi & Nakashima, 1987). However, the method can be easily adapted to be used to analyse three-dimensional response of structures with several components of base excitation (Thewalt & Mahin, 1987). Multi-degree of freedom testing was done by Chang (2009) whereby he subjected a one-storey frame to bidirectional loading.

The first pseudo-dynamic tests showed that the results were susceptible to measurement and control errors and subsequently resulted in research into error analysis (Takanashi et al., 1975). Numerous pseudo-dynamic experiments were done in Japan with 27 on-line tests being summarised in the journal paper by Takanashi & Nakashima (1987).

Pseudo-dynamic excitation enables the investigation of geometric nonlinearities, three dimensional and multi-support excitations and soils structure interaction all while subjecting the structure to an input earthquake excitation (Mahin et al., 1989). The practicability of pseudo-dynamic testing was shown in a report published by Mahin and Shing in 1985. Mahin and Shing (1985) demonstrated the pseudo-dynamic test by analysing a cantilever column as a single degree of freedom system with further tests being conducted on a strengthened steel structure. The tests undertaken by Mahin and Shing (1985) comprised of both shake table tests and pseudo-dynamic tests and confirmed that pseudo-dynamic is viable if conducted using well established analytical techniques combined with calibrated and precise loading and recording instruments (Kurt 2010).

Mahin et al. (1989) indicated that a series of investigations were undertaken through coordinated cooperation between the United States and Japan as part of the U.S.-Japan Cooperative Earthquake Research Program to investigate the limitations of the pseudo-dynamic testing method. Udagawa and Mimura (1991) investigated the seismic behaviour of frames with composite beams by using the pseudo-dynamic testing method and using the El Centro 1940 earthquake ground motion. The tests involved performing both cyclic load testing on the frames under constant displacement amplitudes to examine the safety of the frames. They indicated that it is not feasible to perform large-scale true time dynamic analysis using a large-scale servo-controlled hydraulic actuator, although Udagawa et al. (1984), and Takanashi and Udagawa (1989) said that displacement rate could not be neglected.

Mosalam et al. (1998) investigated the response of masonry infill frames using the pseudo-dynamic method and indicated that the pseudo-dynamic method provides an acceptable approximation of the dynamic response of a structure that is subjected to earthquake excitation.

Wang et al. (2006) investigated the response of a base isolated eight-storey building to a large earthquake using an on-line hybrid procedure. The analysis involved using ABAQUS (2003) finite element analysis software to analyse the overall response of an eight-storey superstructure and a physical model comprising of the base isolation layer and surrounding retaining walls. The resultant restoring force obtained from the physical test was input back into ABAQUS (2003) software at each cycle to solve for the resultant displacement.

The explicit Newmark's method was used by Wang et al. (2006) to solve for the unknown displacements at each time-step and was chosen due to its simplicity. The test used sub-structuring whereby part of the structure was modelled numerically with the remaining part of the structure tested in parallel within the laboratory. The test comprised of two models, the numerical model used to simulate the structural dynamics and the other model to obtain the restoring force from the physical model. The on-line hybrid system used by Wang et al. (2006) is shown in Figure 2-11 with their experimental test setup shown in Figure 2-12.

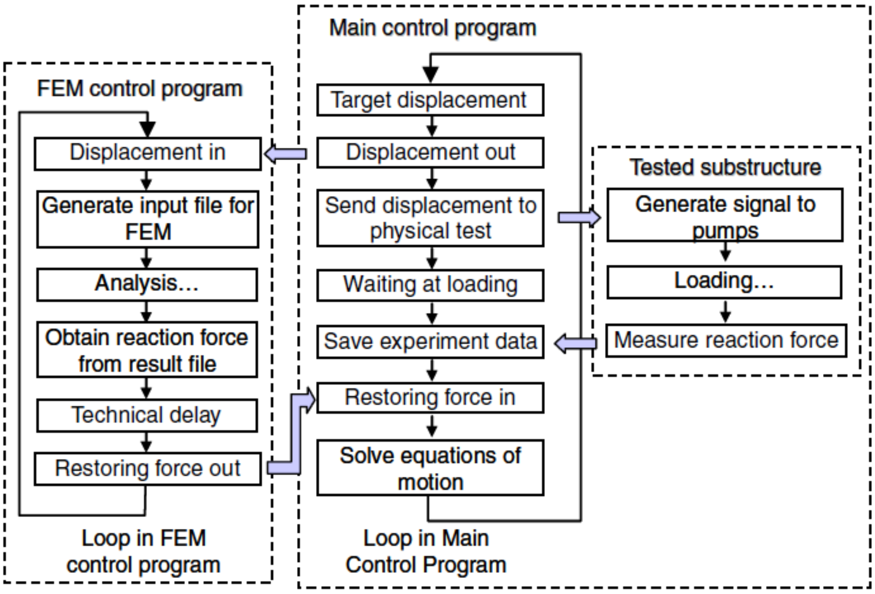

Figure 2-11 On-line hybrid system (Wang et al., 2006)

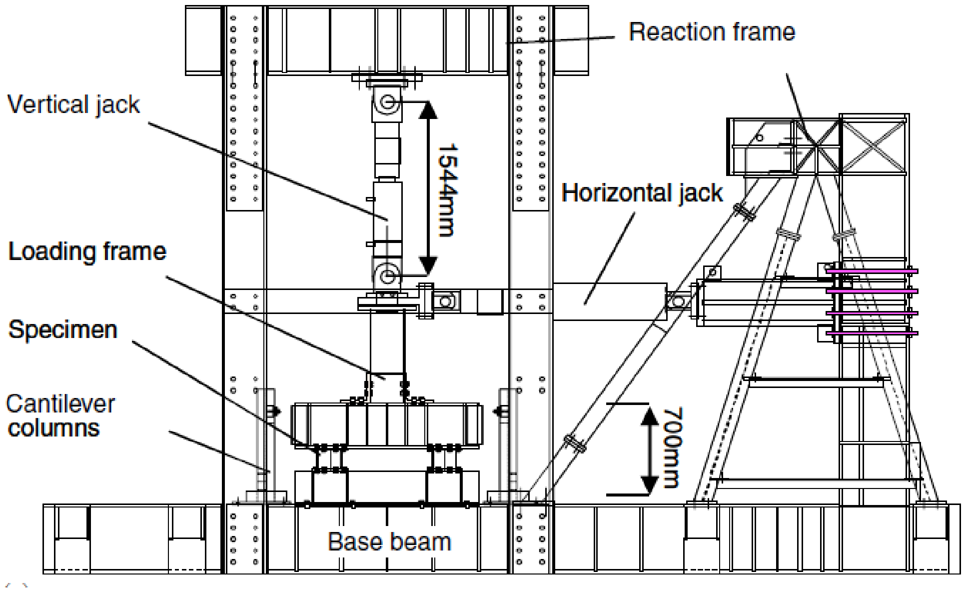

Figure 2-12 Loading system (Wang et al., 2006)

A multi-site hybrid simulation framework was developed at the University of Illinois at Urbana Champaign (Spencer et al., 2007) for piers of a bridge structure and is shown in Figure 2-13. The Ui-SimCor Hybrid Simulation Framework developed by Spencer et al. (2007) showed that the method provides a flexible and powerful method for using the pseudo-dynamic method to evaluate several components of an overall single structure utilising laboratories at three universities distributed across the Unites States of America. Spencer et. al (2007) indicated that hybrid-simulation can be gruelling task as it requires detailed knowledge of both numerical modelling and physical modelling tools, and the programming requirements to integrate the two methods. They indicate that it is necessary to use both numerical modelling and physical modelling to investigate the complex behaviour of reinforced concrete and the influence it has on the overall response of the structure.

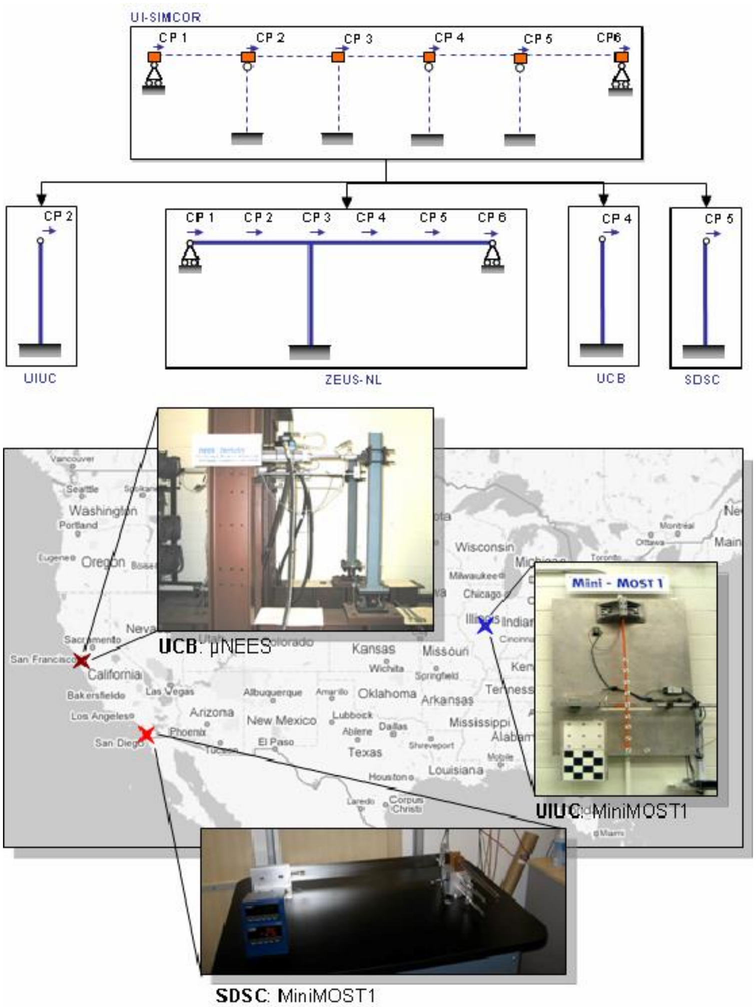

Figure 2-13 Three site hybrid simulation of piers of a bridge (Spencer et al., 2007)

Xing et al. (2017) performed pseudo-dynamic tests on concrete columns under earthquake loading. The column formed part of a four-bay, four storey prototype reinforced concrete planar frame structure and had a fundamental period of vibration of 0.8 s. Rayleigh damping was used to model the energy loss within the frame structure and a damping ratio of 5% was used with the first two modes of vibration. They concluded that the damage encountered by the reinforced concrete column is dependent on the displacement history of the structure, repeated load cycles, and the maximum displacement experienced by the structural member.

Li et al. (2019) used pseudo-dynamic tests on a two-story, two-bay reinforced concrete frame structures to investigate and compare the damage sustained by the moment resisting frame structure with and without the presence of an Energy-Dissipative Rocking Column (EDRC). The pseudo-dynamic tests were undertaken by solving the governing equation of motion using the central difference time integration method and used a damping ratio of 5%. There experiments showed that cracks occurred with minor concrete spalling at the column base due to the application of Shifang ground motion record produced during the 2008 Wenchuan Earthquake in China with a PGA of 0.55 g. The research undertaken by Li et al. (2019) shows that the pseudo-dynamic method provides an accurate method to relate the damage sustained by a structure with earthquake intensity.

2.2.3 FORMULATION OF PSEUDO-DYNAMIC METHOD

The pseudo-dynamic method was formulated from the time-discretised equation of motion for each time step, i, as shown by Equation 2.2. During pseudo-dynamic experimentation, Equation 2.2 is solved using numerical methods in a stepwise procedure with the restoring force, $\{R_i\}$, measured directly from the test specimen using a load cell (Kurt, 2010). The solution of the second order differential equation can either be solved using implicit or explicit numerical methods to solve for the displacements at each time step.

$$[M]\{\ddot{u}_i\} + [C]\{\dot{u}_i\} + [K]\{u_i\} + \{R_i\} = -[M]\{I\}\ddot{u}_{gi} \tag{2.2}$$

Where:

$[M]$:	Mass matrix
$[C]$:	Viscous damping matrix
$[K]$:	Overall structural stiffness matrix
$\{R_i\}$:	Measured restoring force vector from the test specimen
$\{\ddot{u}_i\}$, $\{\dot{u}_i\}$, $\{u_i\}$:	Nodal acceleration, velocities and displacements at time step i
$\ddot{u}_{gi}$:	Ground acceleration at time i
$\{I\}$:	Influence vector

The initial stiffness of the physical structure is generally chosen to be close to the maximum achievable stiffness of the test structure, which is generally the elastic stiffness of the structure. However, to ensure stability, the selection of the initial stiffness needs to be greater or equal to the maximum achievable tangent stiffness of the physical test structure (Pegan & Pinto, 2000).

Takanashi et al. (1975) indicated that the assessment of R_i is the most critical aspect in the analysis to achieve a satisfactory accuracy during the pseudo-dynamic testing. An appropriate numerical analysis time stepping method of enough accuracy is required to predict the incremental restoring force at the current time step utilising the data obtained from the preceding time step. Several numerical schemes are available to formulate a time-stepping approximation to the governing equation of motion as previously shown in Equation 2.2. The numerical schemes can be separated into purely explicit numerical methods such as the central difference method, which relies entirely on the results of the previous time-step, or purely implicit methods such as the Newmark's method, which relies on information of the previous time-step as well as information in the present time-step. Solving the equation of motion using explicit numerical integration methods can result in stability issues but was traditionally preferred over implicit methods as it eliminated the need for iteration (Mosalam et al., 1997). A mixture of implicit and explicit methods is also available, with an example being the operator splitting method (Mosalam et al., 1997). Thewalt and Mahin (1987) proposed a hybrid approach that uses the available experimental data, which includes both a digital computer and analogue voltage signals and summing amplifiers to solve the equation of motion.

In early applications of the pseudo-dynamic method, the difference equation was solved using the linear acceleration method. However, the method only produced reasonable results for flexible and straightforward structural systems (Takanashi & Nakashima, 1987). The linear acceleration method had issues in producing accurate results for stiff systems and systems with rapid changes in stiffness when estimating the instantaneous stiffness due to the accuracy limits of the measurement instruments. Takanashi et al. (1975) solved these issues by employing the central difference method, which mitigated the need for measuring the tangent stiffness at each increment and having to not solve the equation of motion in incremental form.

The central difference method enabled the direct input of the force reading produced by the load cell to be used in the equation of motion. Figure 2-14 shows the basic routine followed by Takanashi and Nakashima (1987) during the pseudo-dynamic method whereby the computed displacement is converted from a digital signal to an analogue signal using a digital to analogue converter (D/A). The analogue signal is then used to apply the displacement onto the structure and a force reading is taken using the load cell. The reading from the load cell is taken in the form of an analogue signal and is converted to a digital signal using an analogue to digital converter (A/D), which is subsequently fed back into the computer and used in subsequent calculations.

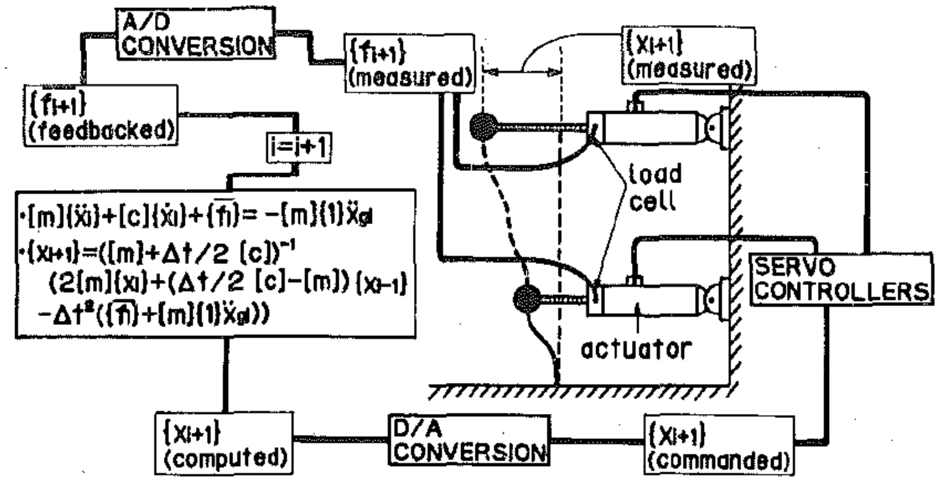

Figure 2-14 On-line algorithm adopted by Takanashi and Nakashima (1987)

Bursi and Shing (1996) discuss various implicit time stepping methods for non-linear problems, which includes the modified Newton iteration method. The modified Newton's method requires that the predictor stiffness $[K]$ used in the analysis to be greater than the actual stiffness of the structure. Mosalam et al. (1997) implemented the predictor-corrector algorithm, which produced an adequate control of experimental error propagation. The method enabled careful inspection and documentation of the complex cracking of infill masonry walls.

2.2.4 INHERENT LIMITATIONS AND ERRORS

Every test method involves a series of inherent limitations, and therefore several assumptions need to be made when performing pseudo-dynamic tests (Kurt, 2010). The first assumption that needs to be made is whether the structure can be accurately and precisely solved using the equation of motion and the resultant displacements can be applied to the structure with enough accuracy (Mahin et al., 1989). Mahin et al. (1989) described several limitations inherent to pseudo-dynamic testing that relates to the way the structure is idealised, damping effects within the structure and strain rate effects.

Assumptions need to be made on how the structure is discretised into a finite number of degrees of freedom and how the mass is subsequently lumped at the degrees of freedom. Damping effects are incorporated into the structure by assuming viscous damping, however, how energy is dissipated within the structure is complex (Mahin et al., 1989).

The rate of the load applied to the structure during a pseudo-dynamic test is much slower than real time dynamic tests and excludes time-dependent material effects, such as strain rate effects in the reinforcing steel. The time it takes for each time step can average at around 1 second resulting in tests being 100 times longer than the actual earthquake record, which can influence the response of structures subjected to impulse loading and short period structures (Mahin et al., 1989). Shing and Mahin (1988) investigated the rate of loading effects during pseudo-dynamic tests by comparing the response of an elastic/viscoplastic system with rate dependent characteristics with that of previous studies on the dynamic yield strength of mild steel. They showed that the dynamic response of mild steel had a 30% higher yield strength in comparison to that obtained during the pseudo-dynamic test.

Shing and Mahin (1990) investigated the experimental error effect in pseudo-dynamic testing by evaluating the error propagation characteristics of several algorithms. They found that the extent of error propagation depends on the numerical properties of the algorithm and the frequency characteristics of the test specimen. Response errors during the pseudo-dynamic testing are due to inherent errors in the displacement control system and the measurement system (Udagawa & Mimura, 1991).

The results obtained from the pseudo-dynamic experimentation are susceptible to the accuracy of the recording instruments and the numerical method used to solve the equation of motion (Mosalam et al., 1997). Several researchers investigated the reliability of the pseudo-dynamic method due to the potential of cumulative errors developing for the duration of the earthquake record. Calibration of the instruments needs to be ensured due to the sensitivity of the analysis to experimental error (Mosalam et al., 1997). The procedure employed during the pseudo-dynamic method can produce three significant sources of error, as shown by Shing & Mahin (1984):

- The reliability of the analytical techniques employed. The analogy of a discrete system does not necessarily account for the actual dynamic response of the continuous system. The prescribed damping may be an overly idealised energy dissipating mechanism;

- The numerical method employed can only produce an approximate solution to the equation of motion. The introduced numerical errors may result in the distortion of the actual dynamic response of the system; and
- Feedback errors from the experimental equipment. The errors introduced into the analysis through displacement control and restoring force feedback are inherently cumulative.

Despite the prospect of errors being introduced into the analysis, experiments done at the University of California Berkeley indicated that the pseudo-dynamic test method could be as reliable and realistic as shake table testing (Shing & Mahin, 1984). Mosalam et al. (1997) indicate that the recent trend in pseudo-dynamic testing is to use implicit numerical methods, such as Newmark's method, because of its superior stability properties.

2.3 IMPLICIT NEWMARK TIME INTEGRATION METHOD

The preference in the past has traditionally been towards explicit numerical methods because of the disinclination to numerical iteration at each time step. However, advancements in computational power and the increase in the resolution of computers have made using implicit numerical methods more favourable due to the superior stability properties it provides (Mosalam et al., 1997). Newmark's implicit method has been widely adopted in finite element analysis software to solve non-linear problems as it can be unconditionally stable for any time increment (Chopra, 2012). Therefore, the selection of the time increment only influences the accuracy of the solution and not the stability.

Newmark's method was developed in 1959 by N.M. Newmark and formulated from Equation 2.3 and Equation 2.4 (Chopra, 2012). The selection of the parameters γ and β determine the accuracy and stability of the solution. The average acceleration method has factors $\gamma = 1/2$ and $\beta = 1/4$ and results in an implicit and unconditionally stable solution (Chopra, 2012). A constant acceleration within the time interval $t \in [t_i \; t_{i+1}]$ is presumed and is graphically shown in Figure 2-15.

$$\dot{u}_{i+1} = \dot{u}_i + [(1-\gamma)\Delta t]\ddot{u}_i + (\gamma \Delta t)\ddot{u}_{i+1} \tag{2.3}$$

$$u_{i+1} = u_i + (\Delta t)\dot{u}_i + [(0.5-\beta)(\Delta t)^2]\ddot{u}_i + [\beta(\Delta t)^2]\ddot{u}_{i+1} \tag{2.4}$$

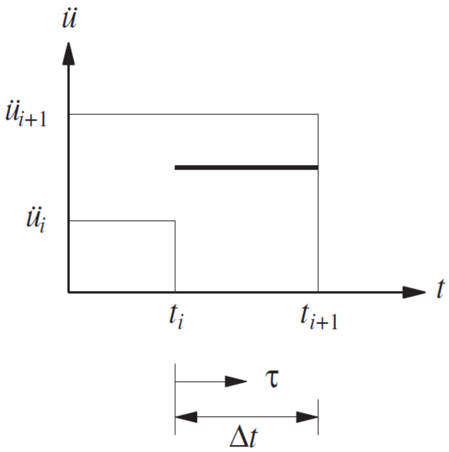

Figure 2-15 Newmark's constant average acceleration method (Chopra, 2012)

Newmark's method is an implicit numerical method, as it determines the solution at time $i + 1$ from the equilibrium condition at the same time $i + 1$ and therefore produces an equation whereby the resisting force $(f_s)_{i+1}$ is an unknown function of the unknown displacement u_{i+1}. As a result, Newton-Raphson iteration method is used to solve for the unknown force $(f_s)_{i+1}$ at time $i + 1$. The derivation of the Newton-Raphson method is obtained by expanding the resisting force $(f_s)^{j+1}$ in Taylor series about the known estimate $u^{(j)}$, with the full derivation shown in Chopra (2012).

The objective of the Newton-Raphson method is to solve for Equation 2.5 by reducing the force $R^{(j)}$ to zero, which is shown in Equation 2.6. The tangent stiffness at $u^{(j)}$ is given by ${k_T}^{(j)} = \left.\frac{\partial fs}{\partial u}\right|_{u^{(j)}}$ and by solving Equation 2.6 provides the $\Delta u^{(j)}$, which produces a better estimate of the resultant displacement in Equation 2.7. The process continues by incrementally increasing j within the time step i until the residual R is less than a specified tolerance at which point the next time step $i + 1$ is initialised (Chopra, 2012). Figure 2-16 shows graphically the Newton-Raphson iteration procedure that iterates within each time step i until convergence to a solution.

$$f_s(u) = P \tag{2.5}$$

$${k_T}^{(j)}\Delta u^{(j)} = P - {f_s}^{(j)} = R^{(j)} \tag{2.6}$$

$$u^{(j+1)} = u^{(j)} + \Delta u^{(j)} \tag{2.7}$$

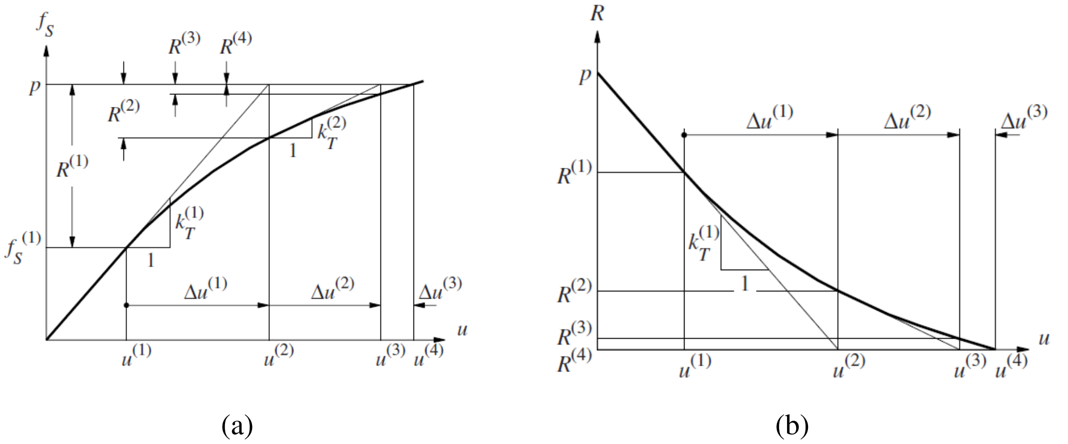

Figure 2-16 Newton-Raphson iteration procedure for time step *i* showing (a) convergence to the resultant force and (b) the residual force converging to zero (Chopra, 2012)

Newmark's method extends the Newton-Raphson method from a static problem to a dynamic problem by setting the resulting force, as previously shown in Equation 2.2, equal to the summation of the forces due to inertia, damping and stiffness within the structure and results in the formation of Equation 2.8 and Equation 2.9. The tangent stiffness ${k_T}^{(j)}$ for the nonlinear equilibrium of the dynamic problem is given by Equation 2.10 with the full derivation of the dynamic tangent stiffness provided in Chopra (2012). The resultant Newton-Raphson iteration method for a dynamic system is given by Equation 2.11 with the residual force vector being calculated using Equation 2.12.

$$\left(\hat{f}_s\right)_{i+1} = p_{i+1} \tag{2.8}$$

$$\left(\hat{f}_s\right)_{i+1} = m\ddot{u}_{i+1} + c\dot{u}_{i+1} + (f_s)_{i+1} \tag{2.9}$$

$$\left(\hat{k}_T\right)_{i+1}^{(j)} \equiv \frac{\partial \hat{f}_s}{\partial u_{i+1}} = (k_T)_{i+1}^{(j)} + \frac{\gamma}{\beta \Delta t} c + \frac{1}{\beta (\Delta t)^2} m \tag{2.10}$$

$$\left(\hat{k}_T\right)_{i+1}^{(j)} \Delta u^{(j)} = p_{i+1} - \left(\hat{f}_s\right)_{i+1}^{(j)} = \hat{R}^{(j)}{}_{i+1} \tag{2.11}$$

$$\hat{R}^{(j)}{}_{i+1} = p_{i+1} - (f_s)^{(j)}{}_{i+1} - \left[\frac{1}{\beta(\Delta t)^2} m + \frac{\gamma}{\beta(\Delta t)} c\right]\left((f_s)^{(j)}{}_{i+1} - u_i\right) + \left[\frac{1}{\beta(\Delta t)} m + \left[\frac{\gamma}{\beta} - 1\right] c\right] \dot{u}_i + \left[\left(\frac{1}{2\beta} - 1\right) m + \Delta t \left(\frac{\gamma}{2\beta} + 1\right) c\right] \ddot{u}_i \tag{2.12}$$

The adapted iteration technique using the Newton-Raphson method is similar in form to the static solution except the damping and inertia terms are included in both the residual force, $\hat{R}$, and the tangent stiffness k_T. Table 2-2, adopted from Chopra (2012), summarises the Newmark's method for the solution of the non-linear system. Step 3.6 in Table 2-2 requires the input of a hysteretic model that relates the calculated displacement $u_{i+1}^{(j+1)}$ to resultant force $(f_s)_{i+1}^{(j+1)}$, however, as previously discussed in Section 2.2, the calculated displacement $u_{i+1}^{(j+1)}$ in Step 3.5 is applied directly to the structure using a servo-controlled hydraulic actuator with the resultant force read from a calibrated load cell and fed back into the numerical model in Step 3.6. This circumvents the need to assume a hysteretic model and structural stiffness (Takanashi & Nakashima, 1987).

Table 2-2 Newmark's method for the solution of nonlinear systems (Chopra, 2012)

Special cases		
(1)	Average acceleration method $\left(\gamma = \frac{1}{2}, \beta = \frac{1}{4}\right)$	
1.0	Initial conditions	
	1.1	State determination $(f_s)_0$ and $(k_T)_0$
	1.2	$\ddot{u}_0 = \dfrac{p_0 - c\dot{u}_0 - (f_s)_0}{m}$
	1.3	Select Δt
	1.4	$a_1 = \frac{1}{\beta(\Delta t)^2}m + \frac{\gamma}{\beta \Delta t}c$; $a_2 = \frac{1}{\beta \Delta t}m + \left(\frac{\gamma}{\beta} - 1\right)$; $a_3 = \left(\frac{1}{2\beta} - 1\right)m + \Delta t\left(\frac{\gamma}{2\beta} - 1\right)c$
2.0	Calculations for each time instant $i = 0, 1, 2, \ldots$	
	2.1	Initialise $j = 1, u_{i+1}^{(j)} = u_i, (f_s)_{i+1}^{(j)} = (f_s)_i$, and $(k_T)_{i+1}^{(j)} = (k_T)_i$
	2.2	$\hat{p}_{i+1} = p_{i+1} + a_1 u_i + a_2 \dot{u}_i + a_2 \ddot{u}_i$
3.0	For each iteration, $j = 1, 2, 3 \ldots$	
	3.1	3.1 $\hat{R}_{i+1}^{(j)} = p_{i+1} - (f_s)_{i+1}^{(j)} - a_1 u_{i+1}^{(j)}$
	3.2	3.2 Check convergence: If the acceptance criteria are not met, implement steps 3.3 to 3.7, otherwise, skip these steps and go to step 4.0
	3.3	$(\hat{k}_T)_{i+1}^{(j)} = (k_T)_{i+1}^{(j)} + a_1$
	3.4	$\Delta u^{(j)} = \hat{R}_{i+1}^{(j)} \div (\hat{k}_T)_{i+1}^{(j)}$
	3.5	$u_{i+1}^{(j+1)} = u_{i+1}^{(j)} + \Delta u^{(j)}$
	3.6	State determination: $(f_s)_{i+1}^{(j+1)}$ and $(k_T)_{i+1}^{(j+1)}$ (Pseudo-dynamic loading cycle onto the test specimen)
	Replace j by $j + 1$ and repeat steps 3.1 to 3.6; denote final value as u_{i+1}	
4.0	Calculations for velocity and acceleration	
	4.1	$\dot{u}_{i+1} = \dfrac{\gamma}{\beta \Delta t}(u_{i+1} - u_i) + \left(1 - \dfrac{\gamma}{\beta}\right)\dot{u}_i + \Delta t\left(1 - \dfrac{\gamma}{2\beta}\right)\ddot{u}_i$
	4.2	$\ddot{u}_{i+1} = \dfrac{1}{\beta(\Delta t)^2}(u_{i+1} - u_i) - \dfrac{1}{\beta \Delta t}\dot{u}_i - \left(\dfrac{1}{2\beta} - 1\right)\ddot{u}_i$
5.0	Repetition for the next time step. Replace i by $i + 1$ and implement steps 2.0 to 4.0 for the next time step.	

2.4 FUNDAMENTAL PERIOD OF VIBRATION OF A STRUCTURE

The response of a structure to a given ground motion excitation is dependent on several characteristics inherent to the structure. The performance of the structure during an earthquake depends on the ability of the structure to absorb and dissipate energy including the frequency characteristics of the earthquake that correspond with the frequency characteristics of the structure (Chopra, 2012).

By solving Equation 2.13, with the stiffness matrix and mass matrix known, the scalar values ω_n^2 and vector Φ_n can be obtained. This produces n homogeneous algebraic equations for n modes of vibration. The natural period of vibration is determined by solving the eigenvalues for the non-trivial solution in Equation 2.13 by setting the determinate equal to zero as shown in Equation 2.14. The n roots, ω_n^2, are the natural frequencies of vibration of the structure and when ordered from smallest to largest, the smallest value is known as the fundamental frequency of vibration. The fundamental period of vibration is the typical vibration mode that is excited during a seismic event (Chopra, 2012).

$$\big[[\mathrm{K}] - \omega_n^2[\mathrm{M}]\big]\Phi_n = \{0\} \tag{2.13}$$

$$\det\big[[\mathrm{K}] - \omega_n^2[\mathrm{M}]\big] = 0 \tag{2.14}$$

2.4.1 BUILDING PERIOD FORMULAS

The fundamental period of vibration of structures appears in design codes for the calculation of the design base shear and lateral forces. Before completing the design of the structure, the fundamental period of vibration is unknown and therefore to circumvent this predicament, building codes provide empirical formulas that enable the estimation of the fundamental period of vibration for various building types and structural materials. Figure 2-17 provides historical fundamental periods of vibration from a database of 2622 Chilean buildings and shows that most fundamental periods for buildings show a linear relationship with increasing structural height (Lagos & Kupfer, 2012). Regression analysis of the database of the recorded fundamental period was used to develop empirical formulas for reinforced concrete moment resisting frame structures and steel moment resisting frame structures.

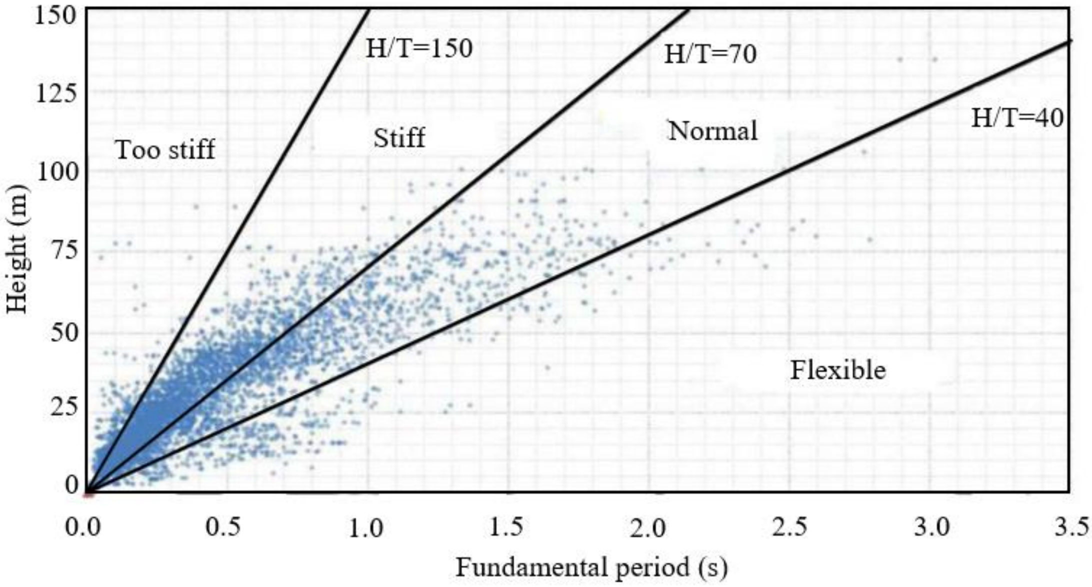

Figure 2-17 Comparison between fundamental periods and height of structures H for 2622 Chilean Buildings (Lagos & Kupfer, 2012)

SANS 10160-4:2017 provides building period formulas that can be used to estimate the fundamental period of vibration of a steel frame building, reinforced concrete moment resisting frame structures and other building types. Equation 2.15 enables the estimation of fundamental period of vibration of a steel frame moment resisting structures and Equation 2.16 provides the estimation of the fundamental period of vibration of reinforced concrete moment resisting frame structures as a function of the height of the structure. However, Goel and Chopra (1996) concluded that code formulas for concrete and moment resisting frame structures typically produce lower period values in comparison to measured periods.

$$T = 0.085 \times h_t^{3/4} \tag{2.15}$$

$$T = 0.075 \times h_t^{3/4} \tag{2.16}$$

2.5 RAYLEIGH DAMPING

Rayleigh damping provides a method of dissipating energy during a linear elastic structural analysis that is subjected to seismic loads (Hall, 2006) and can be used to account for energy loss in the linear computational portion of the pseudo-dynamic analysis. Numerical models used to solve vibrating structures consider three sources of energy dissipation, which includes energy dissipated through hysteretic non-linear material behaviour, energy radiation and damping in the structure (Hall, 2006). Incorporating damping into a linear elastic analysis is necessary as it accounts for complex non-linear behaviour of the structure that would otherwise be neglected. The mechanism by which the energy of a vibrating structure can be dissipated in a linear system is accounted for by equivalent viscous damping (Chopra, 2012). The viscous damping matrix is dependent on the distribution of stiffness within the structure, the mass of the structure and the natural modes of vibration of the structure (Park & Hashash, 2004).

Rayleigh damping is used to account for energy dissipation in a multi-degree of freedom system during a linear analysis and was proposed by Rayleigh and Lindsay (as cited in Park & Hashash, 2004). The damping matrix is assumed to be proportional to the mass matrix $[M]$ and the stiffness matrix $[K]$, using constants a_0 and a_1 as shown in Equation 2.17.

$$[C] = a_0[M] + a_1[K] \tag{2.17}$$

The constants a_0 and a_1 are calculated using Equation 2.18 and have units s^{-1} and s, respectively. Two significant modes are selected to solve for the constants and are assigned a damping coefficient. The damping coefficient assigned to each mode of vibration is equal as the damping coefficient is known to be frequency independent (Park and Hashash, 2004). The damping ratio is given by ζ at mode i with the damping ratio being the ratio of the mode's damping to critical damping (Hall, 2006). The natural frequency at a mode is given by ω_i. As can be seen from Figure 2-18, the damping ratio is only true at the two selected frequencies, with the damping typically being greater at frequencies less than ω_i and greater than ω_j. Frequencies between ω_i and ω_j tend to result in damping ratios less than the selected damping ratio ζ.

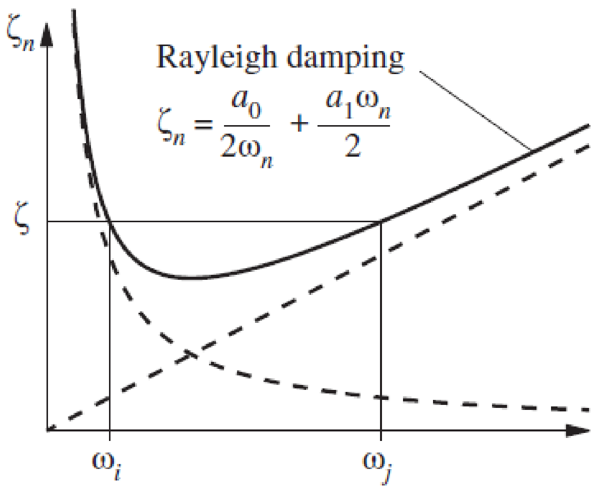

Figure 2-18 Rayleigh damping (Chopra, 2012)

$$\begin{bmatrix} \zeta \\ \zeta \end{bmatrix} = \frac{1}{2}\begin{bmatrix} \frac{1}{\omega_i} & \omega_i \\ \frac{1}{\omega_j} & \omega_j \end{bmatrix}\begin{Bmatrix} a_0 \\ a_1 \end{Bmatrix} \tag{2.18}$$

2.6 HYSTERETIC BEHAVIOUR OF REINFORCED CONCRETE COLUMNS

With the increase in world population and the subsequent increase urbanisation, more people and properties are at risk of impending natural hazards. As a result, the performance of reinforced concrete structures to natural hazard has gained research popularity amongst engineers to mitigate the devastating economic results and loss of life due to natural hazards such as earthquakes. Therefore, the prediction of the hysteresis behaviour of reinforced concrete is critical to understanding the performance of it during a seismic event (Sengupta & Li, 2017).

Over the last 50 years, hundreds of laboratory tests have been undertaken to determine the hysteretic behaviour of structural components for earthquake conditions (Chopra, 2012). Figure 2-19 shows the cyclic response of reinforced concrete and shows that the initial loading provides three stages of stiffness degradation for reinforced concrete. The figure also shows pinching effect upon unloading, which is evident by the reduction in stiffness as the load approaches zero. The monotonic loading response of reinforced concrete column forms the upper bound during a strong seismic excitation (Penelis & Kappos, 2010).

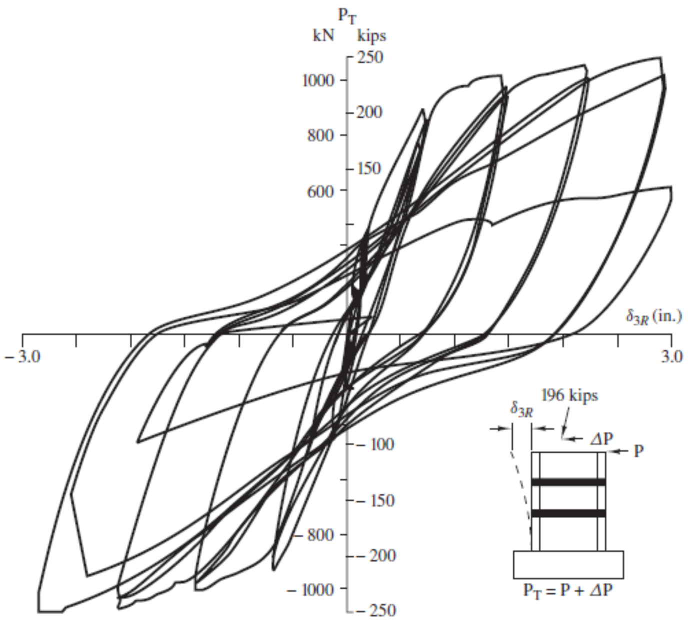

Figure 2-19 Force-deformation relationship for reinforced concrete (Chopra, 2012)

Low and Moehle (1987) did experimental studies on reinforced concrete columns subjected to multi-axial cyclic loading. Their study involved testing cantilever columns projecting from stiff foundation blocks and subjecting them to uniaxial cyclic lateral load histories with a constant axial load on the columns. The load-deflection curve for the constant axial load using imperial units is shown in Figure 2-20. From Figure 2-20, three regions of varying stiffness can be observed with the first corresponding to loading before flexural cracking, the second region being before reinforcement yielding but post the onset of cracking, and the final region is the yielding of the reinforcing bars. The hysteretic response as shown in Figure 2-20 is typical for reinforced concrete columns that are subjected to axial loads and do not encounter significant shear or anchorage weakening (Low & Moehle, 1987).

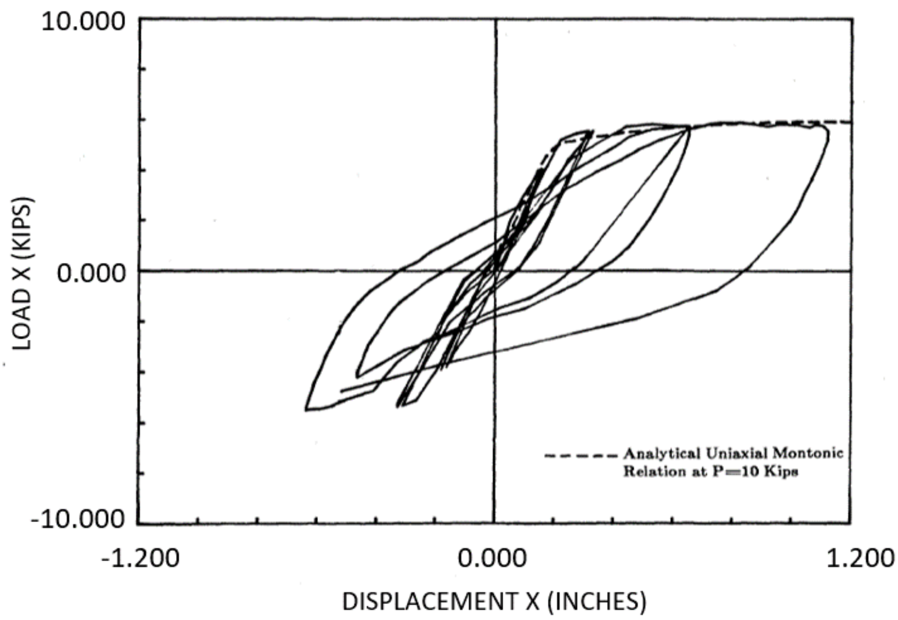

Figure 2-20 Lateral load versus lateral displacement for a column subjected to constant axial load (Low & Moehle, 1987)

The degradation response of reinforced concrete columns subjected to reversed cyclic loading is influenced by the applied axial loading on the column, which may or may not be favourable (Penelis & Kappos, 2010). Axial loading has the benefit of closing flexural and shear cracks in the concrete column. Penelis & Kappos (2010) indicated that the increase in axial load results in an increase in column stiffness and hysteresis loops with larger widths as shown in Figure 2-21. The flexural strength of a column varies substantially with the magnitude of the axial load and is related to the M-N interaction diagram for the section under consideration.

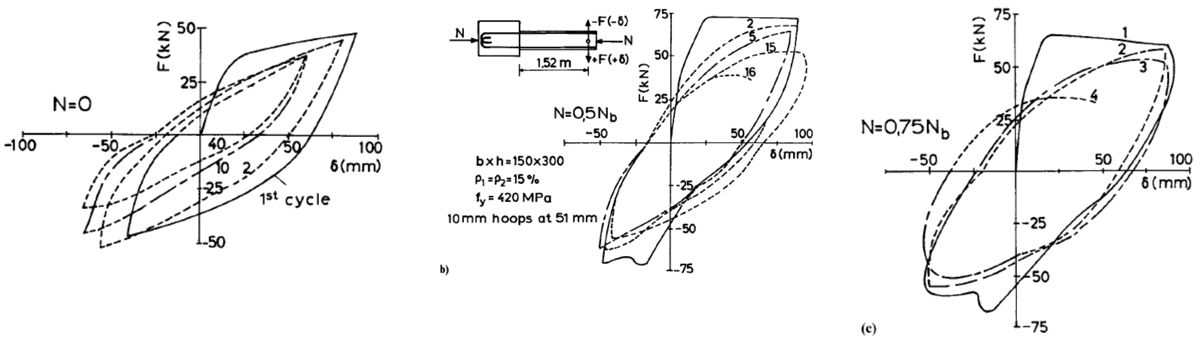

(a) (b) (c)

Figure 2-21 Hysteretic behaviour of elements with different levels of axial load (Penelis & Kappos, 2010)

2.6.1 CONFINEMENT AND DUCTILITY OF REINFORCED CONCRETE

The ability of reinforced concrete to undergo extensive plastic deformation enables the structural member to absorb more energy without a sudden and catastrophic collapse. Seismic design of reinforced concrete structures typically relies on the yielding of the steel reinforcement to provide for energy dissipation due to large deformations of the structure. Energy absorption and dissipation are fundamental for a structure to survive an earthquake and therefore ductility is critical in ensuring that a structure can sustain large plastic deformations before failure (Robberts & Marshall, 2010; Elmenshawi & Brown, 2009; Penelis & Kappos, 2010). However, uncertainty exists between the amount of ductility prescribed in design codes and actual ductility experienced during seismic events (Xing et al., 2017).

Figure 2-22 shows the stress-strain behaviour of reinforced concrete with different levels of confinement. Figure 2-23 shows the influence that rectangular hoops have on the concrete confinement response and the resultant stress concentrations that develop at the corners of the rectangular hoops (Penelis & Kappos, 2010). Parts of the concrete section produce zero confinement due to the outward deflection at the centre between bends of the rectangular hoop legs, as can be seen in Figure 2-23. Reinforced concrete columns with adequate longitudinal and lateral reinforcement can develop large amounts of ductility with a subsequent increase in strength (Cusson & Paultre, 1994; Penelis & Kappos, 2010). Confinement is initiated by the formation of internal bond cracks between the aggregates and the mortar, which increases the volume of the element (Kent and Park, 1971). Confinement has two critical advantages as it increases the strength of the concrete and increases the ductility of the concrete to strain values exceeding 0.35%, which is accepted as the maximum strain before failure in most codes (Penelis & Kappos, 2010).

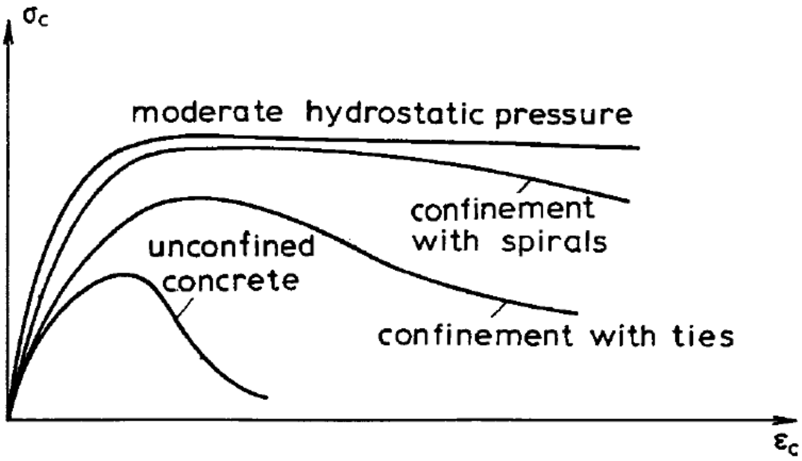

Figure 2-22 Stress-strain diagrams for concrete with different types of confinement (Penelis & Kappos, 2010)

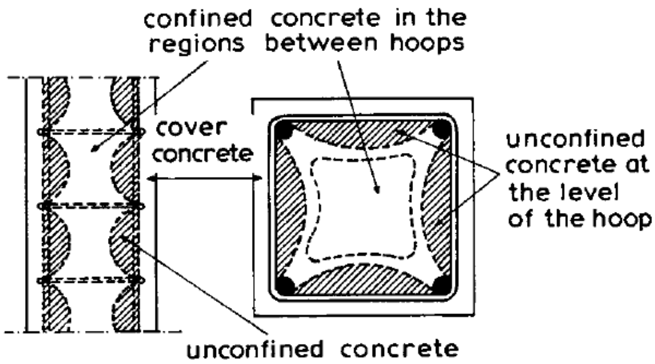

Figure 2-23 Influence of rectangular hoops on concrete confinement (Penelis & Kappos, 2010)

Kent and Park (1971) developed one of the first models for confined reinforced concrete models that only considered the increase in ductility due to rectangular confining steel without considering the increase in concrete strength. Figure 2-24 shows the results produced by Kent and Park (1971) for confined reinforced concrete with rectangular hoops. Passive confinement is provided to concrete in the form of closely spaced spirals or hoops and results in the concrete becoming confined once the stresses in the concrete approaches the uniaxial strength (Kent and Park, 1971). The Kent and Park (1971) model was modified by Scott et al. (1982) and Park et al. (1982) to account for concrete strength and ductility by considering confinement and the effect of strain rate. Mander et al. (1988) developed a model for confined concrete subjected to uniaxial compressive loading and confined by stirrups. The Mander et al. (1988) model considers various means of confining concrete and allows for cyclic loading and strain rate effect. The main parameters that influence the response of confinement in concrete are (Penelis & Kappos, 2010):

- The ratio of transverse reinforcement or volumetric ratio, ρ_w, defined as the ratio between the volume of hoops to the volume of the confined core;
- The yield strength of the transverse reinforcement, which results in an increase in confinement with an increase in strength;
- The compressive strength of concrete, with higher strength concrete being less ductile then lower strength concrete;
- The spacing of the hoops, with an increase in confinement resulting due to a reduction hoop spacing;
- The hoop pattern; and
- The longitudinal reinforcement.

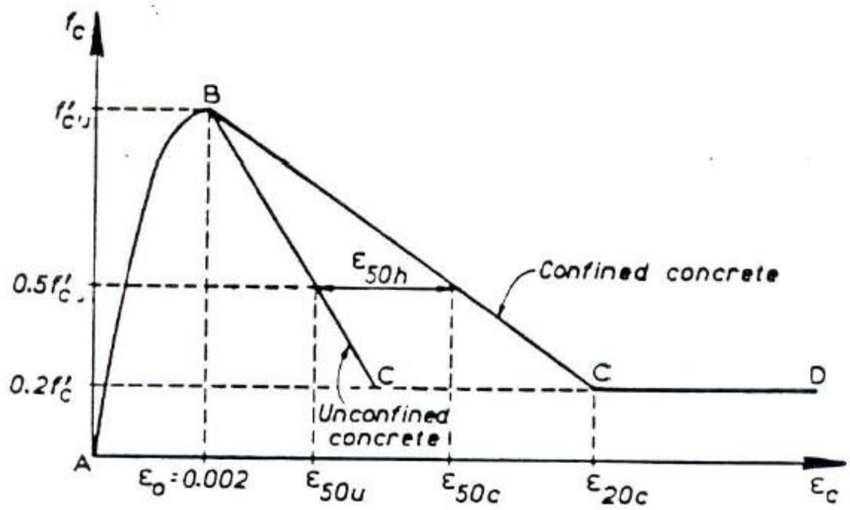

Figure 2-24 Proposed stress stain relationship for confined and unconfined concrete (Kent and Park, 1971)

Stress-strain models for confined concrete have been developed by Saatcioglu and Razvi (1992) and were based on a series of experimental tests on reinforced concrete columns. The proposed stress-strain relationship is given in Figure 2-25 with one of the experimental results shown in Figure 2-26. Concrete without any reinforcement that is subjected to uniaxial compressive load shows a brittle failure mechanism, however, confined concrete shows a substantial improvement in deformability (Cusson & Paultre, 1994). From Figure 2-26 the column can undergo a significant increase in deformation before failure with failure occurring at a strain of 4%, however, the decrease in strength with increase in strain is an indication that the concrete has spalled. The 4% failure strain, as shown in Figure 2-26, is significantly more than the 0.35% ultimate compressive strain as indicated in the South African standard for the design of structural concrete (SANS 10100-1, 2000), which indicates that a structure with adequate confining reinforcement can sustain much larger deformations before collapse. During inelastic load reversals, the ductility capacity of a structural element generally reduces due to an increase in shear deformation and bond deterioration (Park et al., 1984).

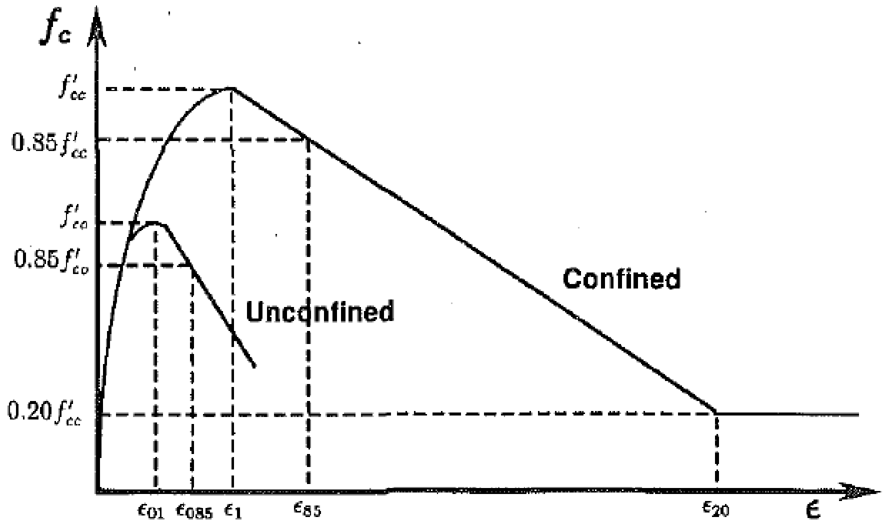

Figure 2-25 Proposed stress-strain relationship as given by Saatcioglu and Razvi (1992)

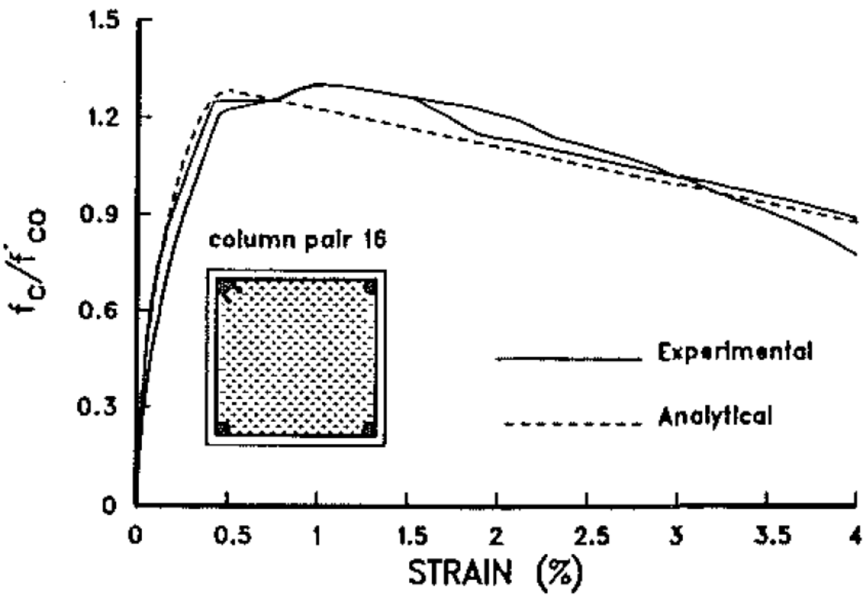

Figure 2-26 Normalised stress-strain diagram of a square column as tested by Razvi & Saatcioglu (1989)

2.6.2 PINCHING EFFECT IN REINFORCED CONCRETE

The pinching effect is commonly observed in the hysteretic response of reinforced concrete structures during the application of repeated cyclic loading, which is common during an earthquake (Yu et al., 2016). The pinching effect shown in the hysteretic loops is related to crack closure, shear crack sliding, shear lock, delayed closure of two cracked surfaces, slippage of reinforcement embedded in the concrete and concrete crushing to name a few. The pinching effect has been shown in experimental studies to result due to previous loadings and is revealed by a reduction in stiffness during reloading (Yu et al., 2016). Figure 2-27 shows the pinching effect in reinforced concrete and is characterised by the large reduction in stiffness with unloading and the subsequent increase in stiffness upon reloading once the cracks have closed in the direction of reloading.

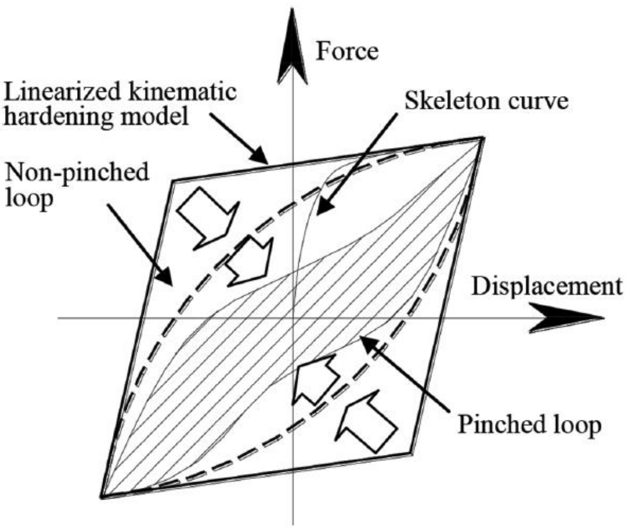

Figure 2-27 Pinching in reinforced concrete under cyclic loading (Yu et al., 2016)

Yu et al. (2016) undertook a combination of experimental tests and finite element modelling to investigate the mechanism of pinching in reinforced concrete columns. The contribution of the rebar and concrete to the pinching effect was analysed and found that the concrete results in a larger contribution to pinching than the reinforcement. Yu et al. (2016) attributes the delay in crack closure as one of the main contributions to pinching. The counteraction between material behaviour between concrete and reinforcement also plays a role in the formation of the pinching effect. During the unloading stage during cyclic loading, the forces in the steel may vary rapidly from tensile yielding to compressive yielding, which often occurs whilst the crack is still open. Reinforcing steel consists of a high elastic modulus and shows the Bauschinger effect after yielding, which is the property whereby the steel's yield strength reduces in the reverse direction to the initial loading (Yu et al., 2016).

2.6.3 BUCKLING OF LONGITUDINAL BARS

Figure 2-28 shows a flexural failure of a reinforced concrete member due to crushing and spalling of the concrete cover and subsequent buckling of the longitudinal bars. This failure mechanism typically occurs in members with high ductility that results in the member absorbing a significant amount of hysteretic energy. When the member reloads in the opposite direction to the initial loading and the reinforcing bar has been permanently deformed, the reloading occurs at a slope less than that of the unloading branch and decreases with increasing deformation, which contributes to the pinching effect.

Longitudinal bars that have undergone permanent elongation in the initial direction of loading prevents the cracks from closing during load reversal and reloading in the opposite direction. Provided the elongated bars do not yield in compression during load reversal, a force couple occurs between the longitudinal bars on either face. Buckling can occur in the longitudinal bars subjected to compression loading in areas where concrete spalling has occurred (Penelis & Kappos, 2010). In the book by Penelis & Kappos (2010) various analytical methods to determine the required stirrup spacing to prevent premature buckling have been formulated, but the methods are rather onerous.

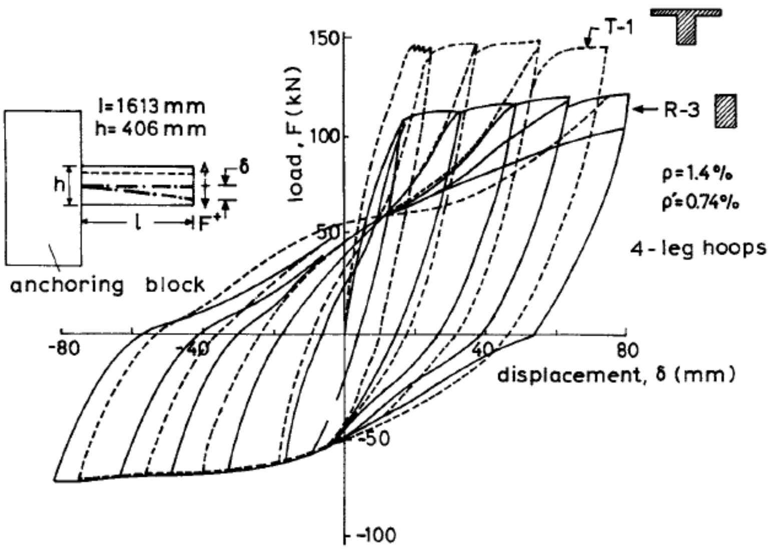

Figure 2-28 Reinforced concrete hysteresis loops subjected to cyclic loading (Penelis & Kappos, 2010)

Figure 2-29 shows various modes of longitudinal reinforcement buckling that can occur in reinforced concrete members subjected to cyclic loading. Determining the buckling length of a longitudinal bar is complicated as it depends on several factors such as the stirrup spacing, the stiffness of the stirrups and the extent of permanent elongation of the reinforcement when subjected to a compression load (Penelis & Kappos, 2010).

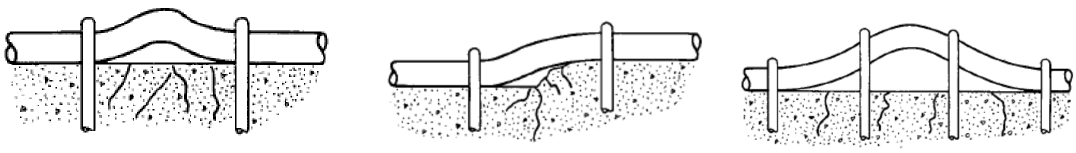

(a) **(b)** **(c)**

Figure 2-29 Different modes of longitudinal reinforcement buckling (Penelis & Kappos, 2010)

2.6.4 REINFORCED CONCRETE HYSTERETIC MODELS

Non-linear hysteretic models, such as bi-linear and tri-linear models, have typically been used to model the earthquake response of structures (Takanashi et al., 1975). However, the need to develop more realistic models that can account for stiffness and strength degradation of structural components is necessary to accurately determine the performance and resultant damage to structures at various earthquake intensities. The need for more accurate models stems from the inability of simplified analytical models to accurately account for non-linear behaviour of the structure due to uncertainty related to the material behaviour, local failure mechanisms, loss of stability and pinching effects in reinforced concrete members. Several analytical models have been proposed for reinforced concrete to mitigate the uncertainty of simplified models with some of the earliest models provided in Takanashi et al. (1975). Sengupta and Li (2017) undertook an extensive literature study on hysteresis models for reinforced concrete that were developed by various researchers. They performed comparative studies of the various hysteretic models by performing quasi static-cyclic load tests. Sengupta and Li (2017) concluded that elasto-plastic and degrading bilinear models do not capture the realistic hysteretic behaviour of reinforced concrete and does not incorporate the pinching effect experienced in reinforced concrete.

Ozcebe & Saatcioglu (1989) developed a hysteretic shear model for reinforced concrete members subjected to constant axial loads. Their purpose of the model is to predict the strength, stiffness and ductility response of reinforced concrete under cyclic loading. The model comprises of series of rules that describe the path of loading and unloading branches for the duration of the cyclic load or seismic loading. The model comprises of a primary curve (or backbone curve) that is considered as the force-displacement response under monotonic loading and is used as the envelope of the unloading and loading branches within the hysteretic model. The material model was derived from experimental data and statistical analysis with the comparison between the experimental and analytical model results presented in Ozcebe & Saatcioglu (1989). Comparing the hysteretic behaviour as shown in Figure 2-19 and the hysteretic model produced by Ozcebe & Saatcioglu (1989), the model closely approximates the hysteretic response of reinforced concrete. However, the unloading and reloading branches in the Ozcebe & Saatcioglu (1989) model follow a straight line to defined points of stiffness transition as shown in Figure 2-30. A full explanation of the hysteretic material model rules is provided in Ozcebe & Saatcioglu (1989). The material model is shown to predict the observed response of reinforced concrete under constant axial loads. From Figure 2-30 the model utilises the same cloverleaf hysteretic pattern as previously observed in Figure 2-19 and Figure 2-20.

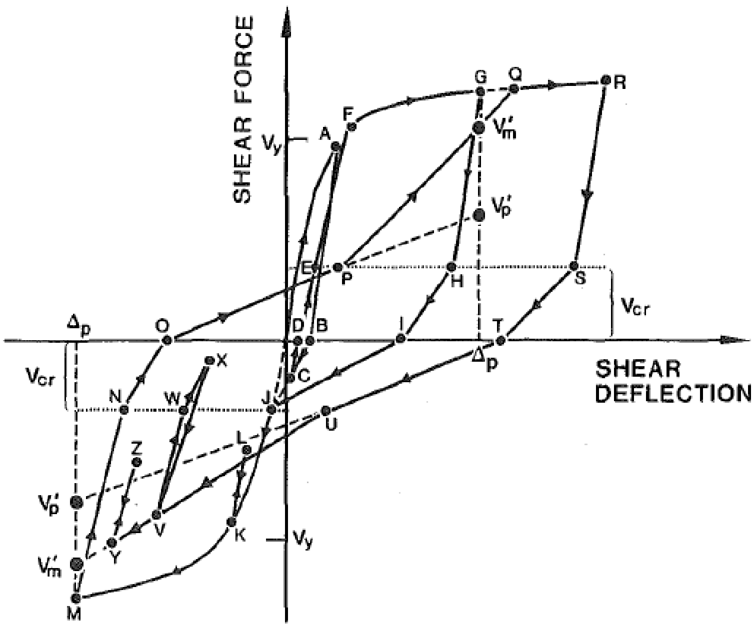

Figure 2-30 Hysteretic shear model developed by Ozecebe and Saatcioglu (1989)

Ibarra et al., (2005) used the data from Sezen (2000) to calibrate the hysteretic reinforced concrete model. Sezen (2000) undertook tests on columns with underprovided transverse reinforcement, and the column was connected to a rigid bottom beam and top beam to ensure double curvature bending. The tests were undertaken by subjecting the columns to a stepwise increasing cycle load with the experimental results from Sezen (2000) and analytical results from Ibarra et al. (2005) shown in Figure 2-31

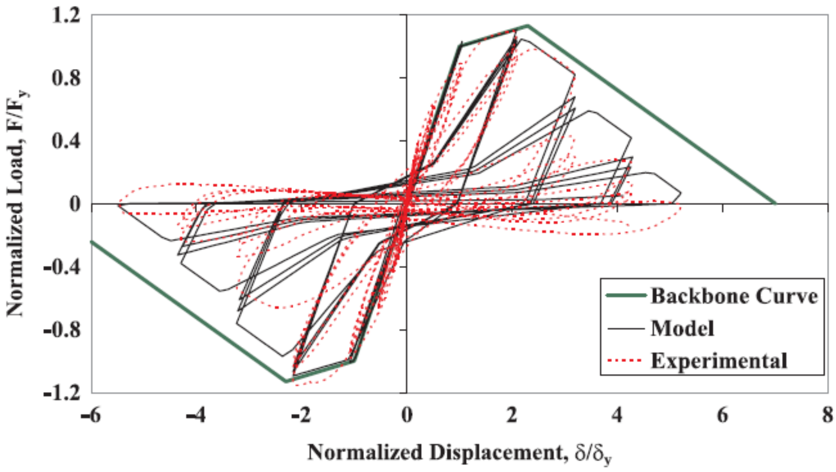

Figure 2-31 Hysteretic reinforced concrete model (Sezen, 2000; Ibarra et. al, 2005)

2.7 ENERGY AND HYSTERETIC ENERGY LOSS

Under serviceability limit states, structures are designed to absorb the energy within the structure without incurring damage upon loading and unloading. Upon unloading the structure should return to its initial position, which is achieved by ensuring that the structure remains in the elastic region. However, when a structure is subjected to large ground motions that result in substantial amounts of energy being imparted to the structure, a portion of the energy is temporarily stored as either kinetic or strain energy (Zahrah & Hall, 1984). The remainder of the energy is dissipated due to damping within the structure and the plastic deformation of structural components that make up the structure (Mosalam et al., 1997). Structures that are correctly designed should be able to sustain the imparted energy to the structure with minimal damage (Zahrah & Hall, 1984).

When the structure undergoes large deformations resulting in the structure being plastically deformed, energy is dissipated through hysteresis. Energy can be absorbed in the system by either recoverable energy or dissipated energy (Elmenshawi & Brown, 2009). The recoverable energy results in the structure returning to its original state under elastic deformation or recovering a portion of the plastic deformation upon unloading as shown in Figure 2-32. The ability to mitigate the earthquake effect due to the inelastic response of the structure is shown by the area enclosed by the hysteretic loop in Figure 2-32.

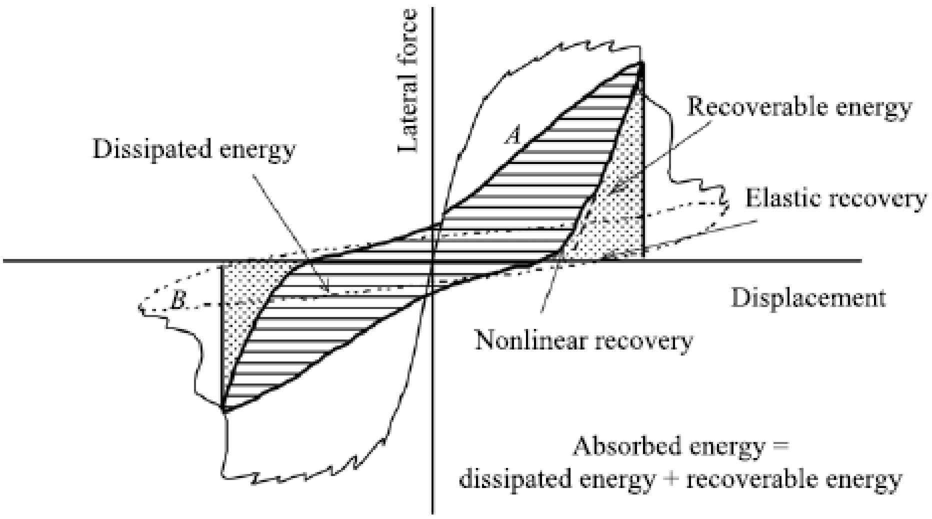

Figure 2-32 Recoverable and dissipated energy in a structural element (Elmenshawi & Brown, 2009)

The dissipated energy is due to the inelastic behaviour of the reinforcing steel, which results in excessive cracking of the concrete and permanent deformation of the structure. The energy dissipation capacity of a structural element is a critical factor during seismic design as the performance of the structure is significantly improved with an increase in the energy dissipation capacity of the structure before collapse (Elmenshawi & Brown, 2009).

The various energy terms can be deduced by integrating the equation of motion of an inelastic system as given in Equation 2.19 with respect to the change in displacement (Chopra, 2012). Energy being a scalar quantity allows the total energy input into the system to be quantified, thus enabling the overall response of the system to be assessed. The energy assessment in this section provides the response of the structure whereby the mass is acted on by a force calculated according to Equation 2.20. The kinetic energy in the system represents the energy imparted to the structure relative to the base of the structure and not due to the overall ground motion. It is the relative displacement and velocity that results in forces in the structure and subsequent damage. Therefore, it is more meaningful to quantify an energy expression in relative motion in respect of the base as opposed to the overall motion of the structure (Chopra, 2012).

$$\int_0^u [M]\{\ddot{u}(t)\}\{du\} + \int_0^u [C]\{\dot{u}(t)\}\{du\} + \int_0^u \{f_s(u)\}\{du\} = -\int_0^u [M]\{I\}\ddot{u}_g(t)\{du\} \tag{2.19}$$

$$\{P_{eff}\} = -[M]\{I\}\ddot{u}_g(t) \tag{2.20}$$

The total energy (E_T) input into the system is determined by integrating $\{P_{eff}\}$ with respect to the change in displacement. The total energy, as given by Equation 2.21, must equal the summation of kinetic, damping and stiffness energy. The distribution of the energy between the terms is a function of the structure's stiffness and mass characteristics (Chopra, 2012).

$$E_T(t) = -\int_0^u [M]\{I\}\ddot{u}_g(t)\,\{du\} \tag{2.21}$$

The kinetic energy (E_M), within the structures depends on the mass of the structure and its relative motion with respect to the ground. Equation 2.22 gives the kinetic energy as follows.

$$E_M(t) = \int_0^u [M]\{\ddot{u}(t)\}\,\{du\} = \int_0^{\dot{u}} [M]\{\dot{u}(t)\}\,\{d\dot{u}\} = \frac{m\dot{u}^2}{2} \tag{2.22}$$

The viscous damping energy (E_C) within the structure, which is determined as a function of the mass and stiffness matrices when considering Rayleigh damping, is given in Equation 2.23 (Chopra, 2012).

$$E_C(t) = \int_0^u [C]\{\dot{u}(t)\}\,\{du\} \tag{2.23}$$

The third term in Equation 2.19 is the strain energy in the structure due to the overall structural stiffness. The strain energy (E_S) can be separated into two terms, namely linear and non-linear/hysteretic strain energy as given by Equation 2.24. When analysing the structure, the structure can consist of regions of linear behaviour and regions of non-linear behaviour. Energy lost in the non-linear regions of the structure are determined by integrating the force-displacement relationship of the material at each time step.

$$E_S = E_K + E_H \tag{2.24}$$

The hysteretic energy absorbed within the structure is determined by integrating the force-displacement curve of the material between zero and the resultant displacement. Depending on the complexity of the material model, numerical methods need to be used, whereby the resultant change in energy is determined due to the change in displacement and force, which is then added to the overall energy. The energy absorbed due to the overall structural stiffness is given by the first term in Equation 2.25 and the hysteretic energy absorbed by a single non-linear element in the structure is given by the second term in the Equation 2.25.

$$E_S = \int_0^u [K]\{u(t)\}\{du\} + \int_0^u F_H(u)\, du \tag{2.25}$$

By studying the time history response of structural systems during seismic loading, valuable information can be obtained about the number of yield reversals, the displacement ductility of the structure and the duration of the earthquake record that is undergoing plastic deformation. Figure 2-33 shows the energy versus time response for a high-frequency, low-period structure subjected to the El Centro earthquake record. Figure 2-33 shows that energy stored incorporates a small proportion of the overall energy imparted to the structure with most of the imparted energy being dissipated almost immediately through damping and non-linear hysteretic behaviour.

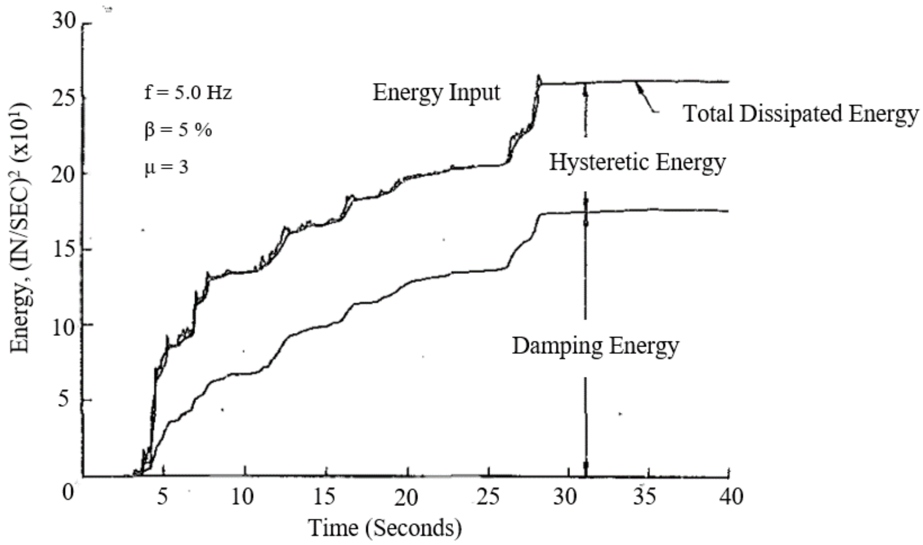

Figure 2-33 Energy versus Time for a structure subjected to the El Centro Earthquake Ground Motion (Zahrah & Hall, 1984)

Zahrah and Hall (1984) studied the earthquake energy absorption in a single degree of freedom structures. Their study focused on the amount of energy imparted to a structure and the amount of energy absorbed by each of the terms including inelastic deformations and damping. The research showed that peak ground acceleration is not a great measure of energy imparted to a structure and found that large amplitude and high-frequency components of acceleration do not correlate well with peak ground acceleration. Zahrah and Hall (1984) used the Newmark's method with linear acceleration in their experiments.

2.8 DAMAGE ASSESSMENT OF BUILDINGS

Seismic risk describes the probability of damage that an area can expect following a seismic event (Nielson, 2005). Most injuries and loss of life occur because of partial collapse or complete collapse of structures during a seismic event (FEMA P-58-1, 2012). Historically, moderate to severe seismic events have resulted in the collapse of reinforced concrete structures that were only designed for gravity loads with inadequate transverse reinforcement in columns (Jeon et al., 2014). It is necessary to determine the probability of collapse of a structure as a function of a ground motion intensity parameter and the type of failure that is being investigated to quantify the potential of structural collapse during an earthquake (FEMA P-58-1, 2012). Freeman (as cited by Davies & Kijko, 2003) undertook the first comprehensive study in 1932 to evaluate structural damage due to the applied forces caused by an earthquake. The study incorporated the impact that an earthquake would have on direct economic losses on essential facilities and infrastructure.

A study was undertaken after the 1971 San Fernando earthquake to investigate methods of correlating ground motion parameters to damage and losses with the result being the formation of damage probability matrices (Davies & Kijko, 2003). The extent of damage due to an earthquake, which ranges from none to collapse, was placed into various damage states. The damage states describe the extent of physical damage in words (Davies & Kijko, 2003).

2.8.1 PARK AND ANG DAMAGE INDEX

Performance based earthquake engineering evaluates the response of a structural component at various seismic hazard levels and therefore to undertake a comprehensive performance assessment the true response leading to the collapse of the structure needs to be considered (Ibarra et al., 2005). Performance based seismic design aims to accurately account for seismic structural damage and the associated risk (Ghosh et al., 2011). To approximate damage caused by a seismic event, a relationship between a ground motion parameter and damage to a structure is required (Rajabi et al., 2012). The amount of damage sustained by a structure can be represented by the maximum deformation of the structure, the number of yield cycles, and the amount of energy absorbed by the structure or structural component in the form hysteretic energy. A reinforced concrete member subjected to cyclic loading during a seismic event results in a reduction in the reinforced concrete columns ductility and ability to dissipate energy (Penelis & Kappos, 2010).

Seismic design philosophy and performance based seismic design involve the dissipation of energy by controlling the damage to the structure at moderate to strong earthquakes with the objective of preventing structural collapse (Ghosh et al., 2011). A damage index allows for the quantification of seismic damage to a structure and produces a dimensionless parameter that ranges between 0 for undamaged structures and 1 for structures that have collapsed. Intermediate values of damage indicate the extent of damage that the structure has incurred.

The most common approach to performance based seismic design entails designing a structure for a specified inelastic displacement and ductility demand. Assessment of the structure's performance often entails the use of the same parameters to determine the structure's various performance levels and limit states. Displacement of the structure in both the elastic and inelastic range can be used to quantify the extent of damage to the structure.

During an earthquake, reinforced concrete structures are generally damaged due to repeated stress reversals and large deformations. A damage index is a parameter that specifies the ratio between the demand placed on the member and the capacity of the member before failure (Rajabi et al., 2012). The relationship between damage and the structure's vulnerability is complex and depends on structural strength, ductility, seismic intensity and vibration characteristics of the earthquake. Damage indices are typically classified as either being cumulative or non-cumulative.

Non-cumulative damage indices only account for the maximum deformation of the structure, whereas cumulative damage accounts for both the maximum deformation and the cumulative hysteretic energy that is absorbed by the structure (Rajabi et al., 2012). The first damage indices were established in the early 1970s when non-linear analysis models were used to study the response of structures. Whitman (as referenced in Rajabi et al., 2012) produced one of the first models that related ground motion intensity with earthquake magnitude. The damage index formulated by Whitman was expressed using the modified Mercalli intensity criteria that concerned the cost to repair the structure in comparison to the reconstruction cost. The history of various damage indices is discussed in Rajabi et al. (2012).

The Park and Ang damage index is used to quantify the damage sustained by the structure and is considered as one of the most realistic measures of structural damage for reinforced concrete structures (Ghosh et al., 2011). The Park and Ang damage index is shown by Equation 2.26 (Park & Ang, 1985) and combines the cumulative energy demand with the ductility demand and has been supported by several researchers (Ghosh et al., 2011). The advantage of the Park and Ang damage index is its simplicity. Park and Ang (1985) proposed that a limiting damage index of 0.4 be used to separate the feasibility between repairing the structure and having to reconstruct the structure (the total loss of asset).

$$DI = \frac{d_m}{d_u} + \frac{\beta}{V_y d_u} \int dE_h \leq 1 \tag{2.26}$$

Where:

d_m: The absolute value of the maximum deformation applied to the member under dynamic loading

d_u: The ultimate deformation that the structure can sustain before failure under monotonic loading

dE_h: Cumulative value of hysteretic energy

V_y: The yield strength of the member

β: A non-dimensional, non-negative parameter

The selection of the non-dimensional non-negative constant β could have a considerable influence on the damage index. The Park and Ang damage index incorporates β into the definition to account for the response of the structure under cyclic load reversals. Empirical formulas have been proposed to calculate β by various authors, including Park and Ang (1985), which is given by Equation 2.27. Using a low value of β reduces the influence of low cycle fatigue and results in the damage being governed by the maximum displacement. A high value of β typically represents a structure that was poorly designed and detailed. Since the advent of the Park and Ang model in 1985, researchers have proposed various values for β for reinforced concrete columns that ranges from 0.05 to 0.24 (Ghosh et al., 2011).

Park et al., (1984) showed a negative correlation between β and the confining ratio ρ_w and a positive correlation between β and the shear span ratio $\frac{l}{d}$, longitudinal steel ratio p_t and axial stress n_0 through the numerous experiments that were conducted on reinforced concrete members. Park and Ang compared the experimentally determined β values with the results produced using Equation 2.27. Figure 2-34 shows the Park and Ang comparison between the analytical model and the experimental results and shows substantial dispersion of the results (Rajabi et al., 2012).

$$\beta = \left(-0.447 + 0.073\frac{l}{d} + 0.24n_0 + 0.314p_t\right) \times 0.7^{\rho_w} \tag{2.27}$$

With:

$\frac{l}{d}$: Shear span ratio (with $\frac{l}{d} = 1.7$ if $\frac{l}{d} \leq 1.7$)

n_0: Normalised axial stress (with $n_0 = 0.2$ if $n_0 < 0.2$)

p_t: Longitudinal steel ratio as a percentage (with $p_t = 0.75\%$ if $p_t < 0.75\%$)

ρ_w: Confinement ratio

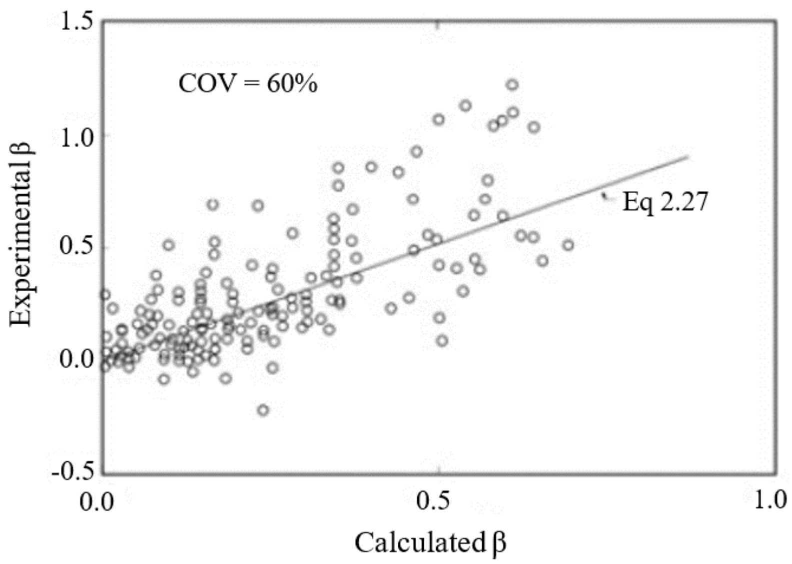

Figure 2-34 Park-Ang analytical and experimental comparison of β (Rajabi et al., 2012)

The ductility of the structure is given by μ, which is the ratio between the ultimate deformation (d_u) and the deformation at which the member yields (d_y), as shown in Equation 2.28.

$$\mu = \frac{d_u}{d_y} \tag{2.28}$$

Park et al. (1984) described three damage states for a structure in the following ranges: the structure is reparable when the damage index is less than 0.4, the structure is beyond repair when the damage index is greater than 0.4, but less than 1; and structure has collapsed when damage index is greater than 1. Ghosh et al. (2011) used the Park and Ang damage index in their work as it provides one of the most realistic measures of structural damage. Kunnath and Jenne (as cited by Ghosh et al., 2011) compared various damage indices with experimental observations and concluded that the Park and Ang damage index correlated the best with experimental observations and laboratory results. Therefore, due to its effectiveness at representing damage to reinforced concrete structures and its ability to incorporate hysteretic behaviour makes the Park and Ang (1985) damage model the most preferable when assessing the damage to a reinforced concrete structure.

2.8.2 FRAGILITY CURVES

Fragility functions are statistical distributions that quantify the probability of reaching prescribed damage states as a function of an earthquake intensity parameter (Jeon et al., 2014; FEMA P-58-1, 2012). Fragility functions provide a means for the quick assessment of the level of risk to a structure and can be generated using numerical models of structures by varying the loading intensity. There are several ways of determining fragility functions that include expert-based fragility functions, empirical fragility functions and analytical fragility functions with further details of each method given in Nielson (2005). Fragility functions are in the form of lognormal cumulative distribution functions with a median value of θ and a logarithmic standard deviation or dispersion β. Equation 2.29 provides a means to calculate fragility curves, and Figure 2-35 shows a typical lognormal fragility function.

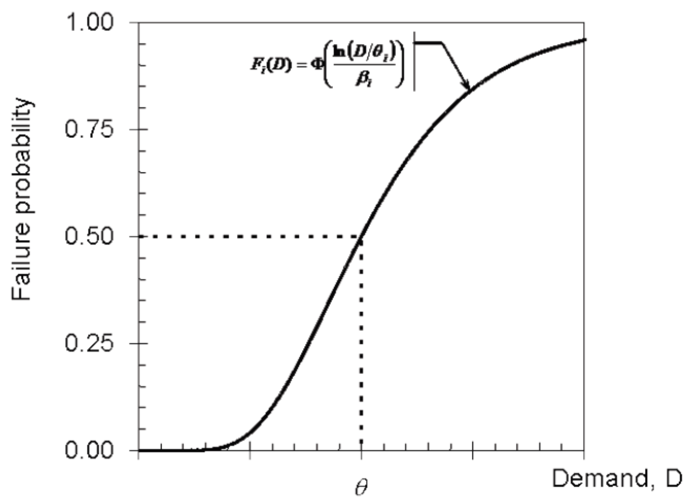

Figure 2-35 Typical lognormal fragility function (FEMA P-58-1, 2012)

$$F_i(D) = \Phi\left(\frac{ln(D/\theta_i)}{\beta_i}\right) \tag{2.29}$$

Where:

$F_i(D)$: Conditional probability that a structure will incur damage at damage state i

Φ: Standard normal (Gaussian) cumulative distribution function

D: Demand parameter

θ_i: Median value

β_i: Logarithmic standard deviation

FEMA P-58-1 (2012) prescribes a method for determining the fragility functions from actual demand data and provides Equation 2.30 to calculate the median θ and Equation 2.31 being used to calculate the random dispersion β_r. The total dispersion, β, is calculated using Equation 2.32.

$$\theta = e^{\left(\frac{1}{M}\sum_{i=1}^{M} ln(d_i)\right)} \tag{2.30}$$

$$\beta_r = \sqrt{\frac{1}{M-1}\sum_{i=1}^{M}\left(ln\left({}^{d_i}/_{\theta}\right)\right)^2} \tag{2.31}$$

Where:

M: Total number of tested specimens

d_i: Demand in test "i" at which the damage state first occurred

$$\beta = \sqrt{{\beta_r}^2 + {\beta_u}^2} \tag{2.32}$$

Where:

β_r: Random variability observed in the test data

β_u: Represents uncertainty in test data from real life conditions

Nielson (2005) used analytical methods during his doctoral studies to generate fragility curves for bridges from 3-D analytical models. The bridges were subjected to a range of ground motions, and probabilistic seismic demand models (PDSM) were generated for the analysis. Nielson (2005) indicates that one of the critical links during seismic hazard assessment is to determine the damage to critical structural components.

Jeon et al. (2014) developed fragility curves for non-ductile concrete frames using numerical models to investigate the failure of rigid beam-column joints by evaluating the nonlinear joint shear response, bond slip response, and column failure due to shear. Jeon et al. (2014) indicate that fragility functions should be developed using appropriate simulation techniques and a good understanding of how the material responds during an earthquake. The process for developing fragility function entails the following (Jeon et. al, 2014):

1. Choose response mechanisms to be considered;
2. Select a suite of N ground motions;
3. Perform nonlinear dynamic analysis for each of the N assigned ground motion pairs;
4. Record demand parameters in relation to the ground motion intensity at which the demand parameter was exceeded; and
5. Develop fragility curves from the results.

2.9 CONCLUSION OF THE LITERATURE STUDY

In this chapter, literature was presented on the prevalence of seismic activity within South Africa, the pseudo-dynamic experimentation technique and the determination of damage and fragility curves. Firstly, a brief overview of seismic activity in South Africa was presented with South Africa being considered a region of moderate seismicity, and it was shown that seismic risk in South Africa is non-negligible and should be considered when designing a structure.

The experimental technique known as pseudo-dynamic experimentation was discussed and it was shown how it enables the correlation between damage and peak ground acceleration to be determined all while accounting for the actual hysteretic response of the test specimen. When evaluating the damage to structures during an earthquake, several parameters need to be assessed to accurately quantify damage with increasing peak ground acceleration.

The pseudo-dynamic testing method is a two-stage procedure that contains a numerical model, which considers the response due to mass and damping of the overall structure, and the physical model under investigation. The calculated displacement at a shared degree of freedom between the numerical model and the physical test specimen is applied to the test specimen using a servo-controlled hydraulic actuator. The resultant force measured using a load cell is then fed back into the numerical model and used in subsequent calculations. The inherent limitations and errors associated with the method were investigated and shown that the method can be prone to cumulative errors, which can be mitigated by accurately calibrating the instruments and using high-resolution servo-controllers and data acquisition systems. Various numerical models can be used to perform the pseudo-dynamic experimentation, including both implicit and explicit numerical models. The implicit Newmark's method was discussed in further detail as it forms the basis of the pseudo-dynamic experimentation undertaken during this research.

The literature study goes on to discuss the hysteretic response of reinforced concrete, showing that the response of reinforced concrete is highly non-linear and subject to the pinching effect. The behaviour of reinforced concrete is dependent on whether the concrete has cracked, the reinforcement has yielded and concrete spalling. The response of reinforced concrete under monotonic loading results in a trilinear behaviour and forms the envelope to the unloading and reloading cycles.

A discussion on the Park and Ang damage model was presented and shows that the damage index incorporates both instantaneous damages due to the maximum deformation of the structure as well as cumulative damage due to hysteretic energy loss. The Park and Ang damage index is regarded as the most suitable model for analysing damage to a reinforced concrete structure. The literature study concludes by discussing the formulation of fragility curves using the results obtained from the experimental tests.

3 EXPERIMENTAL TEST SETUP AND ANALYSIS METHODS

3.1 GENERAL

This chapter describes the experimental program developed to study the resultant damage to an axially loaded reinforced concrete footing due to increased peak ground acceleration. The pseudo-dynamic experimentation, as discussed in Chapter 2, was used to correlate the resultant damage incurred by reinforced concrete footing, which forms part of a two-bay, two-storey unbraced frame structure with masonry infill walls, to increasing earthquake intensity. The focus of this research is the reinforced concrete footing as shown in Figure 3-1 that forms part of a hypothetical frame structure. A constant axial load from the structure occurs on the reinforced concrete footing for the duration of the earthquake record due to the symmetry of the structure. The procedure followed to design and analyse both the reinforced concrete footing and the conceptual frame structure is discussed in this chapter. The design of the frame structure and reinforced concrete footing only considered the gravity loads and the wind loads. Earthquake loading was not considered during the design of the frame structure and the reinforced concrete footing. The construction of the reinforced concrete footings and experimental procedure are also discussed in this chapter.

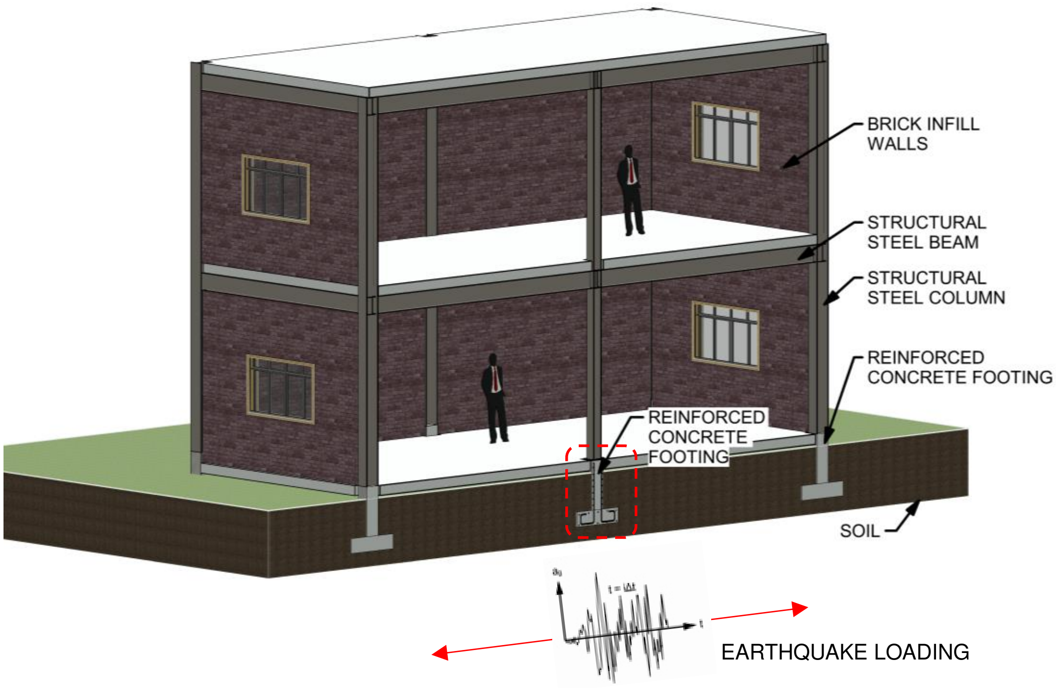

Figure 3-1 Conceptual model of the overall structure

The pseudo-dynamic analysis procedure will comprise of two parts, with the first part being the experimental test setup of the reinforced concrete footing in the laboratory, which contains the physical component of the pseudo-dynamic tests. The second part of the pseudo-dynamic test is the formulation of the numerical model using the Newmark's implicit time-stepping method with static condensation to eliminate the zero mass degrees of freedom and accounts for the overall structure that is placed on the reinforced concrete footing.

3.2 CHARACTERISTICS OF THE TESTED STRUCTURE

The structural element investigated during this research is a reinforced concrete footing under constant axial load that forms part of a hypothetical two-bay, two-storey linear elastic moment resisting frame structure founded on the footing. Figure 3-2 and Figure 3-3 illustrate the geometry of the frame structure used during the pseudo-dynamic tests. Due to limitations imposed on the project, the external columns were pin supported in the numerical model and therefore their contribution to the overall response of the structure was not considered. Only the non-linear lateral response of an internally located footing under constant axial load was considered in this research.

The axial load applied to the reinforced concrete footing had to be limited due to the capacity of the press frame that was available in the laboratory, which also limited the size of tests specimens that could be tested successfully in the laboratory. The mass distribution within the frame structure was selected to result in a 300 kN axial load being placed on the reinforced concrete footing. Most structures in South Africa are small to moderate size structures consisting of one to three stories and are generally the most critical structures. This is because they tend to be stiffer, thus producing lower periods of vibration and more substantial shear stresses at the base of the structure. The larger shear forces placed on the foundations result in more damage to the foundations.

The steel frame structure was divided into three segments, namely the internal columns, external columns and beams. The three segments enable a series of combinations of three steel sections that could be used to construct the steel frame structure. The width of each bay was selected to be 6 m with the storey heights selected to be 4 m as shown in Figure 3-3. The details of the structure used in the research are as follows:

- Consists of a steel moment resisting frame structure;
- The steel structure was founded on pad foundations that only allowed for the transfer of shear and axial load (i.e. pin connection);

- A 250 mm reinforced concrete slab spans in the transverse direction between the steel frames for each of the floors, which was selected to produce a 300 kN axial load on the central footing;
- The occupation of the structure is commercial/residential;
- Masonry infill panels with a thickness of 230 mm are used for the external walls; and
- The transverse span length between the frames was taken as 2.6 m, which is less than the typical span length used in buildings. A limitation had to be placed on the maximum axial load and the shear load placed on the foundations due to the available capacity of the actuators in the laboratory.

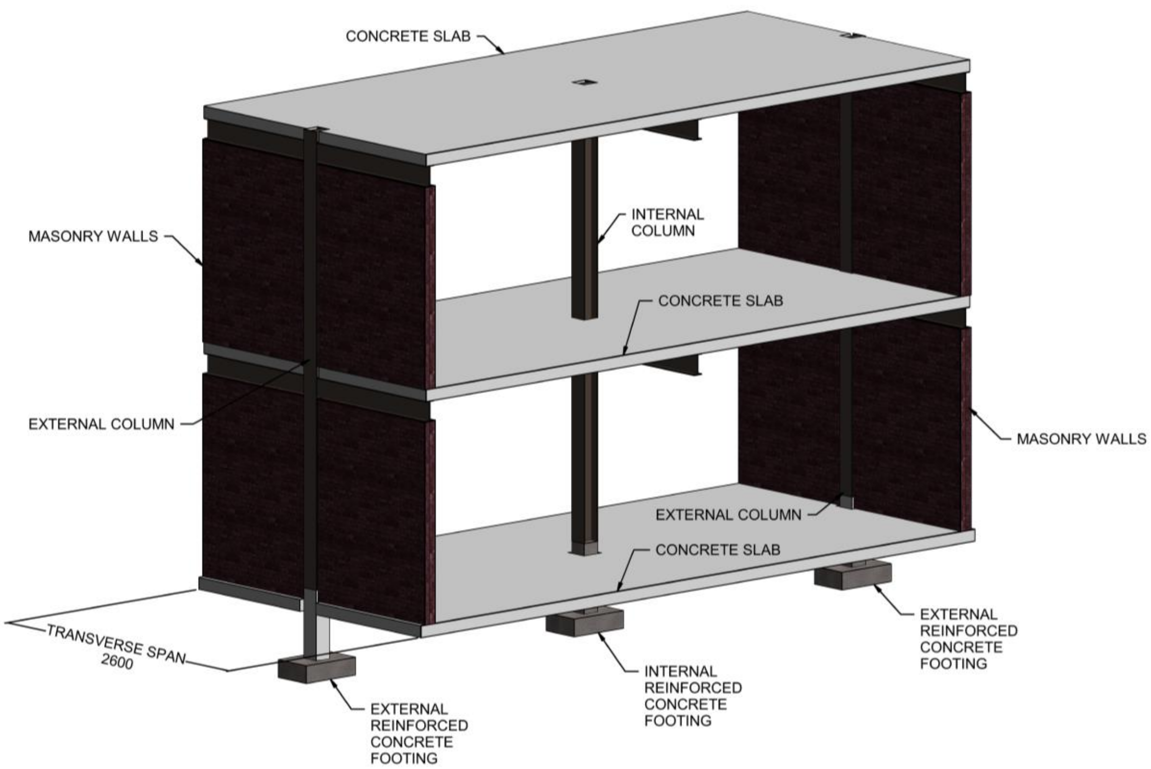

Figure 3-2 Characteristic 3D model of the frame structure

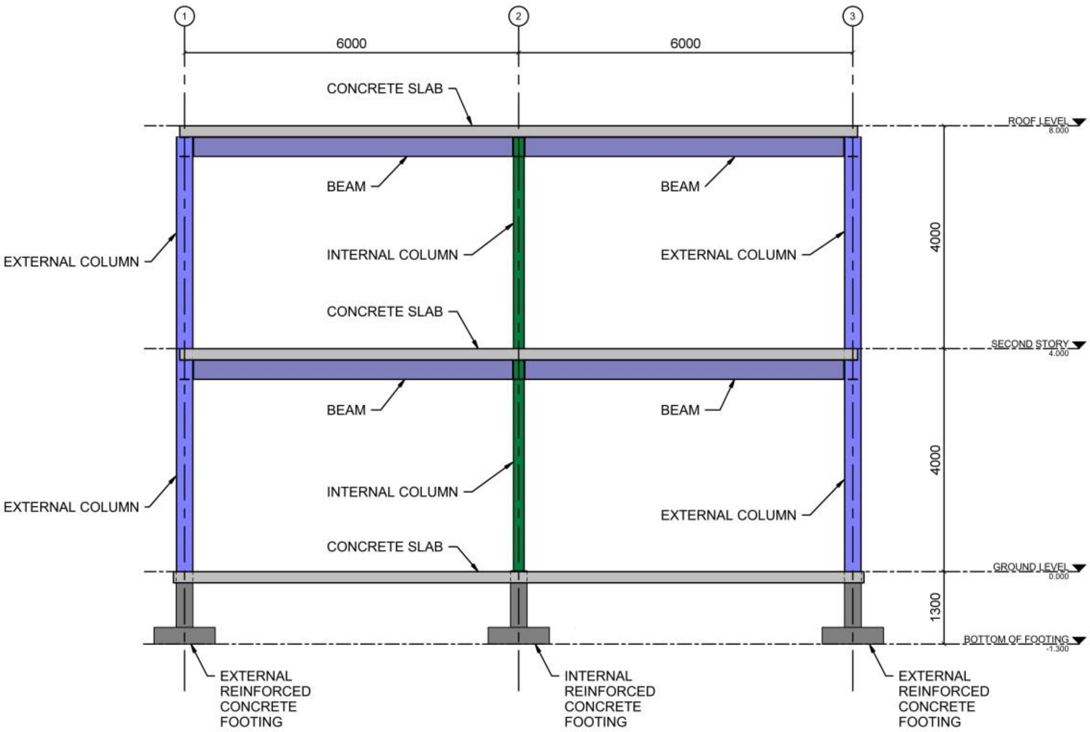

Figure 3-3 Characteristic section of the frame structure

3.3 LOADING ON THE TESTED STRUCTURE

This section describes the loading applied to the structure during the static analysis and pseudo-dynamic experiments. The design of the structure only considers gravity loading and wind loading with a description of the earthquake loading that is only applied to the structure during the pseudo-dynamic tests. The applied loads on the structure were determined using the following codes of practice:

- SANS 10160-1: 2011 Basis of structural design and actions for buildings and industrial structures – Part 1: Basis of structural design;
- SANS 10160-2: 2011 Basis of structural design and actions for buildings and industrial structures – Part 2: Self-weight and imposed loads; and
- SANS 10160-3:2011 Basis of structural design and actions for buildings and industrial structures – Part 3: Wind actions.

3.3.1 GRAVITY LOADS ON THE STRUCTURE

The static loads on the structure, which consists of the dead and live loads, were obtained from SANS 10160-2:2011 and remained constant for each of the pseudo-dynamic experiments. The dead loads (DL) on the structure comprised of the self-weight of the frame structure (W_{DL} and P_{DL}), the superimposed dead load consisted of the reinforced concrete slabs (W_{SDL}) and the masonry walls (P_m), and finally the live load that accounts for people that use the structure (W_{LL}). Distributed loads are indicated with a (W), and point loads are represented with a (P). Figure 3-4 shows static loading on the frame structure with the weight of the beams, concrete slab and live load being applied to the structure as a distributed load and the masonry walls and columns being applied to the structure as point loads. Table 3-1 shows the material properties used for the steel frame structure, concrete slab and masonry walls.

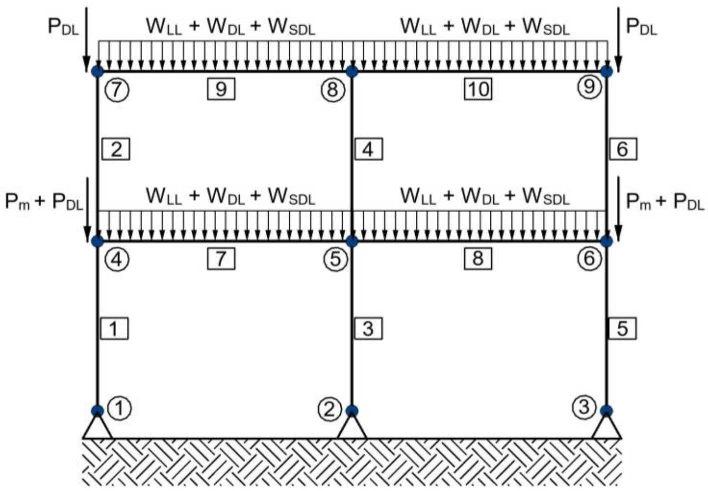

$$W_{LL} = 6.24\ kN/m$$
$$W_{SDL} = 15.3\ kN/m$$
$$P_m = 42.2\ kN$$

Figure 3-4 Static loading applied to the structure

Table 3-1 Material densities and applied loading used in design

Load Type	Value	Reference
Live loading	LL = 2.5 kN/m^2	Category B1 Table 1 SANS 10160-2:2011
Dead load - Self weight		
Concrete	ρ_c = 2400 kg/m^3	
Steel	ρ_{st} = 7850 kg/m^3	
Superimposed dead load		
Masonry	ρ_m = 1850 kg/m^3	

3.3.2 WIND LOADS ON THE STRUCTURE

The design wind loading on the structure was calculated using SANS 10160-3:2011 with the resultant unfactored design wind pressures on the structure shown in Figure 3-5. The wind loads were obtained by selecting Johannesburg, South Africa as the location of the structure with a regular cover of buildings surrounding the structure.

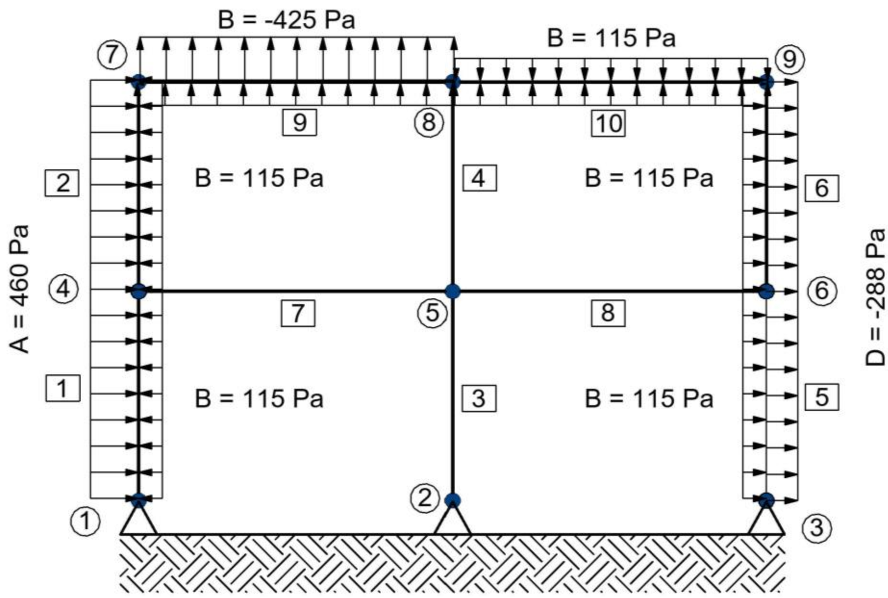

Figure 3-5 Wind pressure loading calculated from SANS 10160:3 2011

3.3.3 EARTHQUAKE LOADING ON THE STRUCTURE

The El Centro earthquake record was selected as the input ground motion for the pseudo-dynamic analysis. Figure 3-6 shows the El Centro, S00E of the event at Imperial Valley, California on May 18, 1940, and represents a strong ground shaking. Mosalam et al. (1997) indicate that the El Centro earthquake record is typical of the North American west coast earthquakes. The maximum acceleration during the ground motion record occurred at a time of 2.14 seconds. For each of the pseudo-dynamic tests, the peak ground acceleration was increased by scaling the amplitude of the El Centro earthquake.

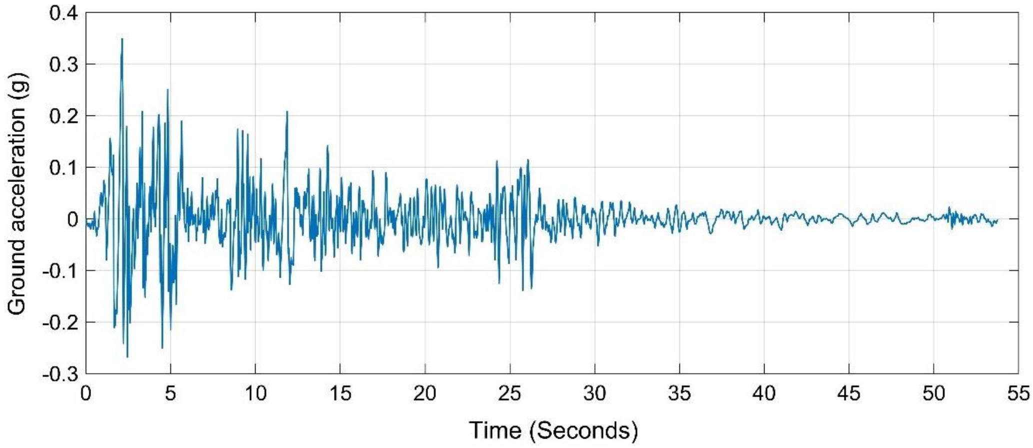

Figure 3-6 Acceleration record of the El Centro Earthquake

The elastic response spectrum of the El Centro earthquake is plotted in Figure 3-7 using a damping ratio of 5%. SANS 10160-4:2017 specifies four ground types for South Africa when determining the design elastic response spectrum. The ground type ranges from rock to sand and gravel, to clayey material. The objective during the analysis was to select a representative earthquake that closely follows the design response spectrum as provided in SANS 10160-4:2017. Figure 3-7 shows the elastic response spectrum of the El Centro ground motion record superimposed on the design elastic response spectra as specified in SANS 10160-4:2017. From Figure 3-7, it can be observed that the El Centro elastic response spectrum closely follows the design response spectra. Because of this, the El Centro earthquake was selected as the base earthquake for this research.

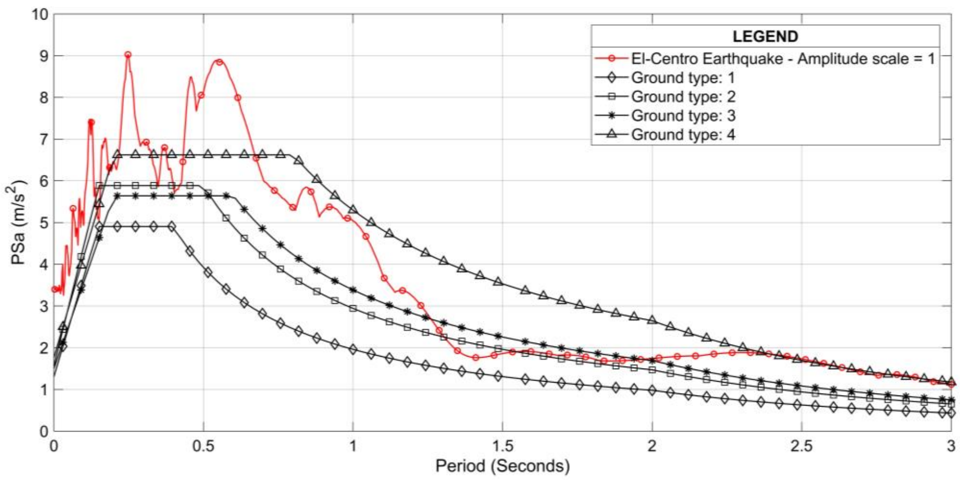

Figure 3-7 Elastic response spectrum of the El Centro earthquake with the design response spectra for the four ground types as specified in SANS 10160-4:2017

3.3.4 DESIGN LOAD COMBINATIONS

The critical load combinations acting on the structure are shown in Table 3-2 and were determined from SANS 10160-1:2011 for live load, dead load and wind load. For serviceability limit state, two load combinations, as shown in Table 3-2, are found to be critical. The first load combination governs the deflection of the beams and the second load combination determines the maximum horizontal deflection of the frame structure.

Table 3-2 Design load combinations

Serviceability Limit States
$\mathrm{STR1s} = 1.1\mathrm{DL} + 1.0\mathrm{LL}$
$\mathrm{STR2s_i} = 0.9\mathrm{DL} + 0\mathrm{LL} + 0.6\mathrm{WL_i}$
Ultimate limit state
$\mathrm{STR1} = 1.2\mathrm{DL} + 1.6\mathrm{LL}$
$\mathrm{STR2_i} = 1.2\mathrm{DL} + 1.6\mathrm{LL} + 1.3\mathrm{WL_i}$
$\mathrm{STR3_i} = 0.9\mathrm{DL} + 0\mathrm{LL} + 1.3\mathrm{WL_i}$
$\mathrm{STRP1} = 1.35\mathrm{DL} + 1\mathrm{LL}$
$\mathrm{STRP2_i} = 1.35\mathrm{DL} + 1\mathrm{LL} + 1\mathrm{WL_i}$

3.4 ANALYSIS AND DESIGN OF THE FRAME STRUCTURE

This section describes the results of the analysis and design of the planar steel frame structure with reinforced concrete floor slabs and masonry infill panels on the external columns. The structure was analysed using all prescribed sections available in the Southern African Steel and Construction Handbook (SAISC, 2010), with the most practical sections selected for the analysis. The frame structure was divided into three segments, as previously shown in Figure 3-3, with separate steel sections used for the beams, external structural columns and the internal structural columns.

During the analysis of the frame structure, only I-Sections are used for the beams, with H-Sections being used for the columns. The reinforced concrete floor slabs are assumed not to contribute to the stiffness and strength of the beams. The analysis and design of the sections are carried out using a script written in MATLAB (2017), which analyses the structure to determine the forces within each of the members with the actual stiffness properties of the design members. Once the analysis was completed, SANS 10162-1:2011 was used to design the members. The MATLAB (2017) program analysed the structure for each member combination of beam, internal column and external columns using the steel members obtained from Southern African Steel and Construction Handbook (SAISC, 2010). The analysis and design comprised of two steps: ultimate limit state (ULS) design, to ensure enough strength capacity and stability of the members, and serviceability limit state (SLS) design, to prevent excessive deflections during the day to day operations of the structure.

3.4.1 ULTIMATE LIMIT STATE DESIGN

The structure was analysed for each of the member combinations as previously shown in Figure 3-3 and the load combinations as specified in Table 3-2. The design of the structure considered the following during the design:

- All beams and columns are designed by incorporating both axial and uniaxial bending loads;
- The class of the section was selected to ensure local stability of the members;
- The columns are braced for out of plane buckling at storey heights;
- The beams are continuously braced for lateral torsional buckling due to the presence of the concrete slab along the top flange of the beam; and
- The beams and columns are analysed against the following interactions equations obtained from SANS 10162-1 (2011):
    - Cross-sectional strength;
    - Overall member strength; and
    - Lateral torsional buckling strength

From the analysis, regarding Table 3-2, it was found that load combination two governed the design of columns, whereas the load combination one dictated the design of the beams. Considering all the sections that satisfied the interaction equations as specified in SANS 10162-1 (2011), there were a total of 4095 steel member combinations for the external columns, interior columns and beam members that satisfy the ultimate limit state.

3.4.2 SERVICEABILITY LIMIT STATE

The second step in the design of the frame structure consisted of analysing the structure using the load combinations specified for the serviceability limit state loads, which are shown previously in Table 3-2. The analysis took all the members that satisfied the ultimate limit state design requirements and calculated the beam deflections and horizontal deflections for each of the storeys. The maximum allowed inter-storey deflection and overall structural deflection was obtained from SANS 10160-1:2011 and Figure 3-8 shows the points where the deflections were calculated and the design criteria that was used to limit the deflection. The maximum inter-storey deflections $(u_{1i}$ & $u_{2i})$, the overall structural deflection (u_g) and the deflection of the beams (u_{bi}) were determined for each of the load combinations.

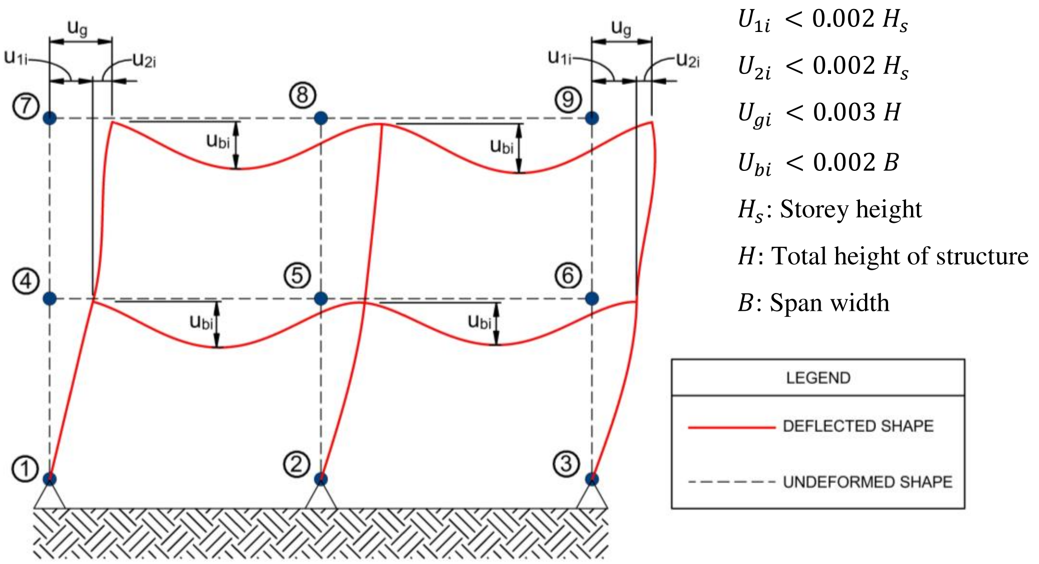

Figure 3-8 Deflection points on the frame structure for serviceability limit state design

The calculated deflections for each member combinations were compared to the maximum allowable deflection and disregarded if the member combination failed the design criteria. The total mass of the steel frame structure for each of the member combinations was calculated and sorted from the lowest mass to the largest mass, which is shown in Figure 3-9. Of the 4095 sections that satisfied the ultimate limit state criteria, 2272 combinations satisfied the serviceability limit state criteria.

As part of the serviceability limit state analysis, the fundamental period of vibration was calculated for each of the member combinations that satisfied the SLS and ULS designed requirements. The fundamental period of vibration for each frame member combination is plotted from lowest mass to the largest mass in Figure 3-10 and on average the natural period of vibration reduced with an increase in the mass of the steel frame. The variation in the natural period of vibration with an increase in mass was due to the variation in section properties, as the mass of the section does not increase as quickly as the stiffness of the section. Considering all possible steel section combinations that satisfy ultimate limit state and serviceability limit state conditions, the natural period of vibration of the frame structure under the given design conditions varied between 0.72 s and 1.28 s, with the average period of vibration equalling 1.05 s. However, considering the practical design and economic considerations, a frame structure producing the lowest mass that satisfies both the SLS and ULS design requirements would typically be used for the design of the steel frame structure.

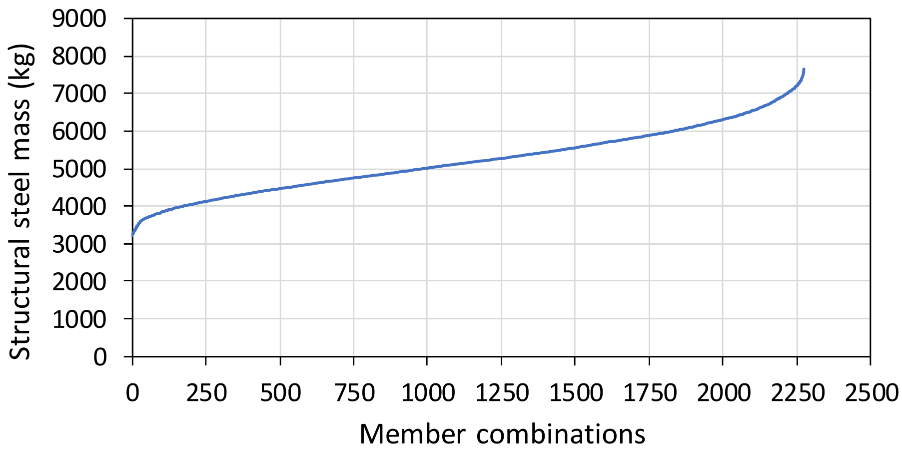

Figure 3-9 Mass distribution for all the member combinations satisfying SLS and ULS design ordered from lowest mass to largest mass

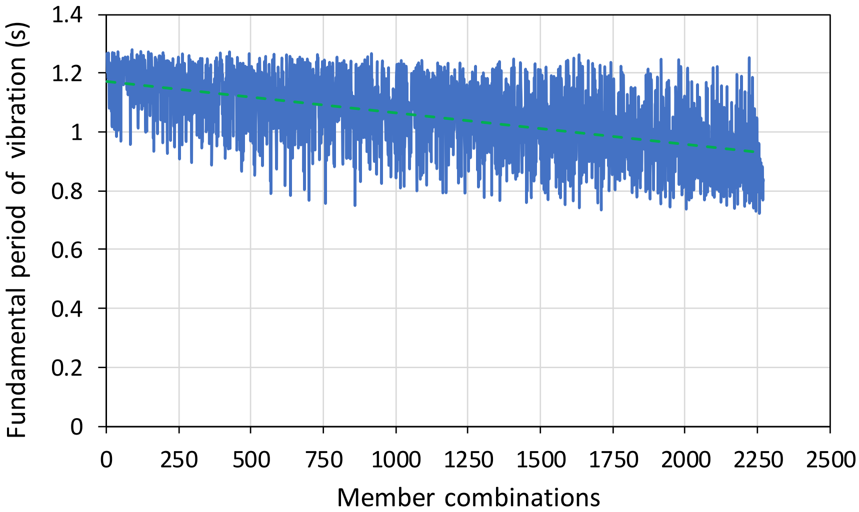

Figure 3-10 Fundamental period of vibration for each of the member combinations satisfying ULS and SLS design

The final design selected for the steel moment resisting frame structure to be used during the pseudo-dynamic experiments is shown in Figure 3-11 and corresponds to an overall natural period of vibration of 0.86 s. To optimise the design a separate steel section member was used for the internal column and external columns with the ratio of the moment of inertia between the internal column to the external column equalling 0.2.

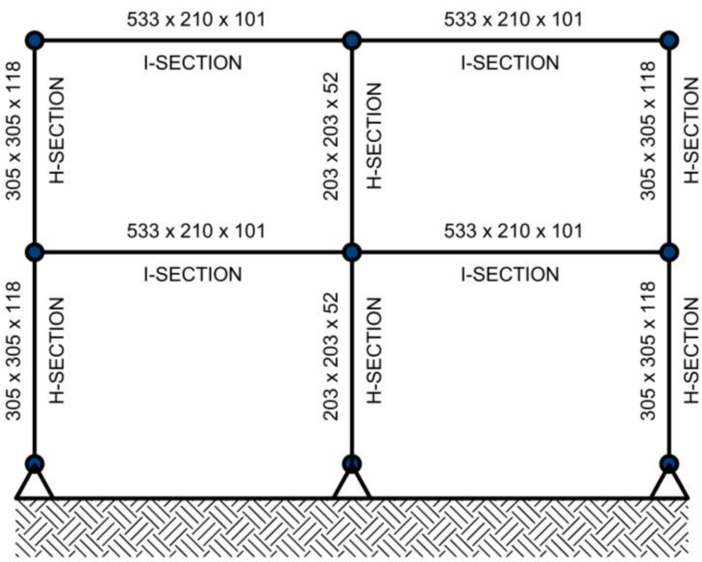

Figure 3-11 Member design for the steel moment resisting frame structure

3.5 TEST SPECIMENS – REINFORCED CONCRETE FOOTINGS

The reinforced concrete footings used in this research were designed using SANS 10100-1:2000 to satisfy the ultimate limit state, serviceability limit state and practical design considerations. The footings are considered representative of those that would typically be used in low to moderately tall structures of one to three stories that only carry axial load.

3.5.1 DESIGN OF THE FOOTINGS

Eight reinforced concrete footings were constructed at the University of Pretoria's experimental farm with a base size of 1100 x 700 x 300 mm and column size of 300 x 300 x 1000 mm. Four M16 L-Shape Class 8.8 holding down bolts were fixed within the reinforcement cage before the concrete was cast to allow for a shear connection between the base plate of the steel column and the top of the reinforced concrete footing.

The characteristic design yield stress of 450 MPa and a Young's Modulus of 200 GPa was used for the design of the reinforcement. The characteristic compressive strength of concrete specified and used during the design was 30 MPa. Using the concrete and reinforcing steel design parameters resulted in the reinforced concrete column only required minimum reinforcement to resist gravity and wind loads and comprised of 4 x Y12 reinforcing bars, with one bar placed at each of the column corners. The reinforced concrete footings all had the same design and configuration as shown in Figure 3-12.

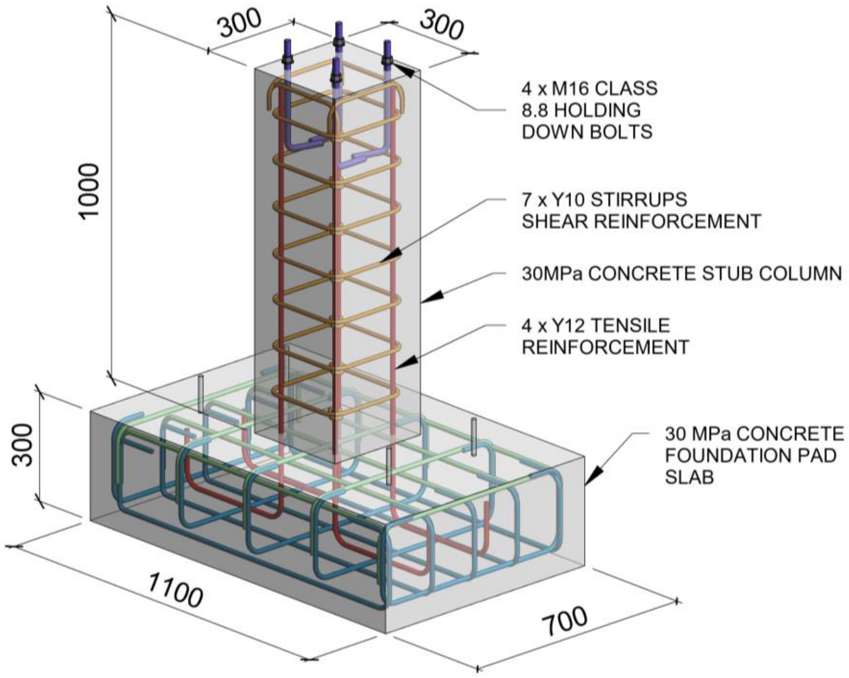

Figure 3-12 Three-dimensional visualisation of the reinforced concrete footing (Units in mm)

Shear reinforcement consisted of seven Y10 reinforcing stirrups placed at 150 mm centres within the column. The reinforced concrete base slab comprised of five Y12 bars spaced at 150 mm centre to centre in both the long and short spans. Both top and bottom reinforcement are provided, and a concrete cover of 30 mm was used for all the reinforcement.

The footings were designed to sustain the reactions for each of the ultimate limit state load cases determined at node number 2, as shown previously in Figure 3-8, during the analysis and design of the frame. The internal reinforced concrete footing is only considered during this study and will not be subjected to a varying axial load for the duration of the applied earthquake excitation due to the symmetry of the frame structure. The structural supports during the frame analysis were modelled as pin supports and therefore only axial and shear loads are applied to the footing, with the moment being equal to zero. The internal footing will have zero shear load applied to it under only gravity loading due to the symmetry of the frame structure.

The design of the reinforced concrete footing also needed to consider the practical design considerations by ensuring that there was sufficient space for the connection of the base plate of the steel column to the reinforced concrete stub column. The resultant axial load and bending moment at the critical section for design is shown in Figure 3-13 and occurs at the interface between the column and the concrete base slab. The maximum moment was calculated by multiplying the shear force applied to the HD-bolts by the height of the column. The concrete stub column was considered stocky according to SANS 10100-1:2000, and therefore the required tensile reinforcement for the column could be obtained by only using the MN-interaction diagram shown in Figure 3-14.

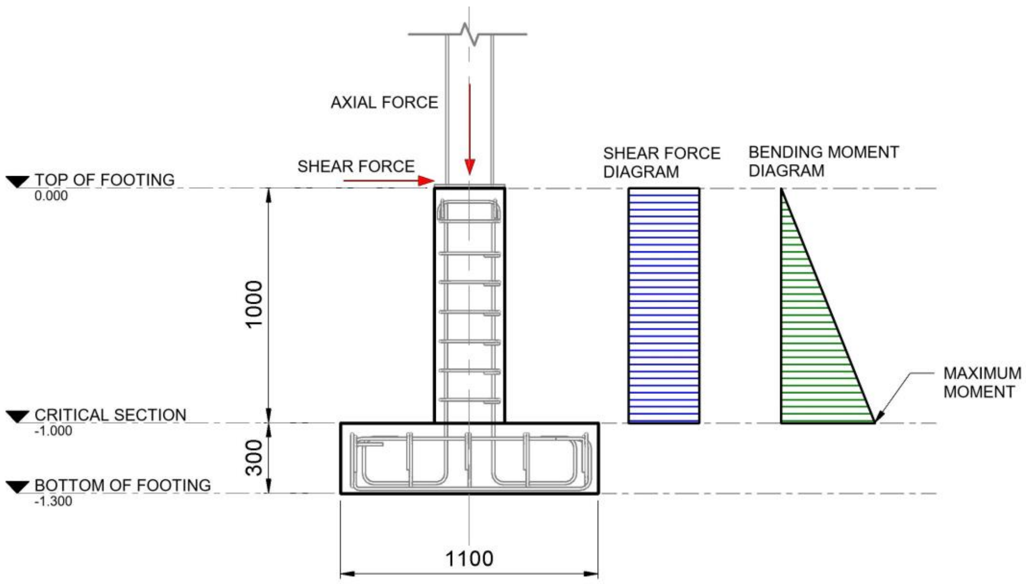

Figure 3-13 Analysis of the reinforced concrete footing

Only minimum reinforcement, with a reinforcement ratio of 0.4% according to SANS 10100-1:2000, was required for the given loading and column dimensions. The MN-interaction diagram and reinforcement layout for the reinforced concrete section with a 300 x 300 mm column and 4Y12 reinforcing bars is shown in Figure 3-15. As can be seen from Figure 3-15, the applied static loads on the footing due to gravity loads and wind loads are much lower than the available capacity of the footing. Therefore, the footing has additional capacity to carry larger shear loads.

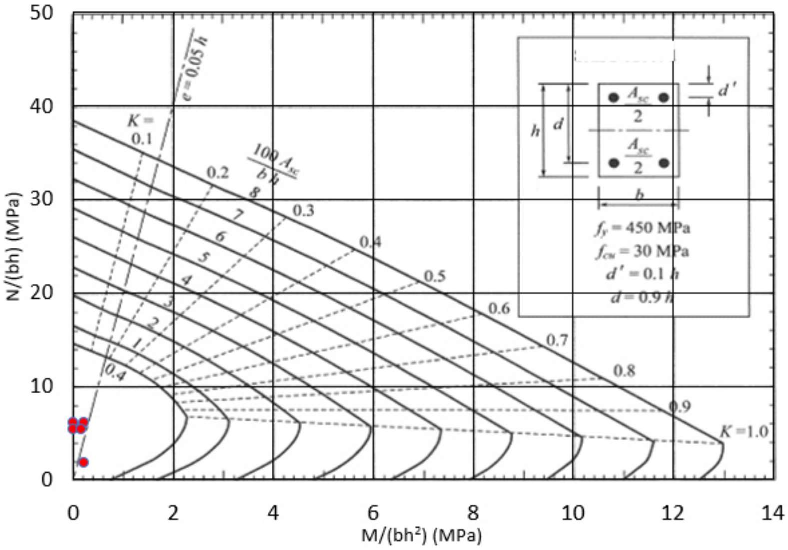

Figure 3-14 Design of reinforced concrete column for the ULS load cases (SANS 10100.1:2000)

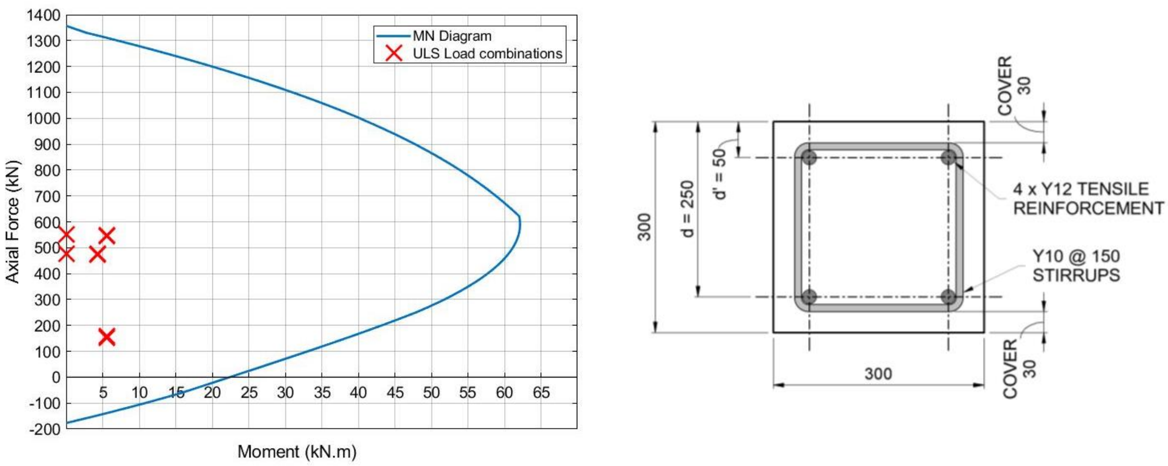

(a) **(b)**

Figure 3-15 Design of the reinforced concrete column showing (a) the MN-Interaction diagram for the column of the footing at ULS and (b) a section through the reinforced concrete column of the footing

3.5.2 MATERIALS AND CONSTRUCTION OF THE FOOTINGS

The reinforced concrete footings were constructed at the University of Pretoria's experimental farm and were cast monolithically in an upright position. The footings were cast monolithically to prevent a cold joint from forming between the base slab and the stub column. A lid on the base slab shuttering was provided to allow for a single concrete pour of the base slab and column. Figure 3-16 shows the shuttering for the reinforced concrete footings and the base slab lid. Figure 3-17 shows the reinforcing cages for the footings with four Y12 tensile reinforcement bars and seven Y10 stirrups. Threaded rods were placed at each of base slab corners to enable the lid to be bolted down to prevent uplift during the casting of the concrete. The threaded rods were also used to lift and transport the footings from the experimental farm to the laboratory to ensure that the integrity of the concrete stub column was not compromised before testing. Figure 3-18 shows the holding down bolts and the templates that were used to position the bolts within the concrete column. The holding down bolts consisted of four M16 Class 8.8 L-Shape bolts placed on a 180 mm x 180 mm grid.

Figure 3-16 Reinforced concrete footing shuttering with base slab lid

Figure 3-17 Reinforcement cages for the concrete footings

(a) (b)

Figure 3-18 Holding down bolts and template

Concrete was obtained from a commercial company to ensure that the concrete used in each of the footings remained consisted and was representative of concrete that would typically be used in industry. A concrete cube strength at 28 days of 30 MPa was specified and used to cast the footings, and Figure 3-19 shows the casting of the reinforced concrete footings. The footings were left to cure for 28 days before removing the shuttering. Concrete cube tests were done to determine the strength of the concrete after 28 days with the results shown in Table 3-3. The concrete cube tests show that an average cube strength of 32 MPa was obtained and therefore the specified cube strength of 30 MPa was reached at 28 days.

Table 3-3 Concrete cube tests at 28 days

Cube	**Weight in air (grams)**	**Weight in water (grams)**	**Applied load (kN)**	**Concrete cube strength (F_{cu}) (MPa)**
1	1486	2476	332	33.2
2	1502	2496	298	29.8
3	1486	2478	328	32.8
			Average:	32.0

Tension coupon tests were undertaken on the reinforcing bars to determine the strength of the bars used to construct the reinforcement cages. Figure 3-20 shows the stress-strain curve for a Y12 reinforcement bar taken from the same batch of steel used to construct the reinforcement cages for the footings. The reinforcement yielded at a stress of 545 MPa, which corresponds to a strain of 0.3%.

Figure 3-19 Concrete casting of the reinforced concrete footings

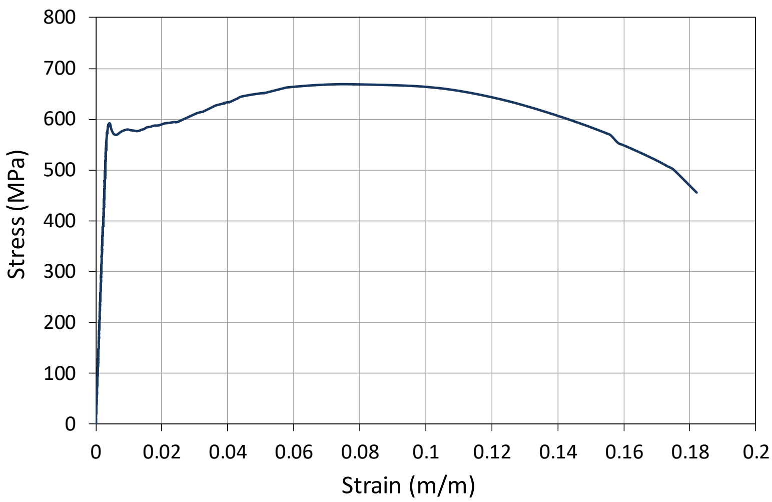

Figure 3-20 Stress-Strain curves for reinforcement

3.6 PSEUDO-DYNAMIC EXPERIMENTAL METHOD

The formulation of the numerical model used to perform the pseudo-dynamic experiment is presented in this section using the implicit Newmark's method with static condensation to remove the zero rotational mass degrees of freedom. The procedure followed in this study comprised of replacing the internal pin support of the frame structure at the location of the reinforced concrete footing with a mass-spring system as shown in Figure 3-21. The dynamic response of a linear multi-degree of freedom system with a single non-linear translational degree of freedom was solved using Equation 3.1.

$$\underbrace{[M]\{\ddot{u}(t)\} + [C]\{\dot{u}(t)\} + [K]\{u(t)\}}_{\substack{Linear\\component}} + \underbrace{[K_s(t)]\{u(t)\}}_{\substack{Non-linear\\component}} = \underbrace{\{P\}}_{\substack{Static\\load}} - \underbrace{[M]\{I\}\ddot{u}_g(t)}_{\substack{Earthquake\\loading}} \tag{3.1}$$

Where:

$[M]$:	The lumped mass matrix of the frame structure including the mass of the reinforced concrete footing
$[C]$:	Rayleigh damping matrix for the elastic part of the frame structure
$[K]$:	Linear elastic stiffness matrix of the frame structure
$\{\ddot{u}(t)\}$, $\{\dot{u}(t)\}$, $\{u(t)\}$:	Acceleration, velocity and displacement vector respectively
$[K_s(t)]$:	Lateral non-linear spring stiffness matrix of the reinforced concrete footing
$\{I\}$:	Influence vector that accounts for the horizontal direction of the earthquake loading
$\ddot{u}_g(t)$:	Ground acceleration

Figure 3-21(a) shows the discretised numerical model used in the pseudo-dynamic analysis with the equivalent mass-spring system. The boundary conditions comprised of two pin supports at the external columns with the internal reinforced concrete footing idealised as a single degree of freedom consisting of a constant lumped mass that was supported laterally by a massless non-linear spring of stiffness $k_s(t)$. The horizontal displacement was taken at the top of the column where the steel column of the frame structure connects to the footing using a base plate and holding down bolts. The degree of freedom $\{u_s = u_1\}$ shown in Figure 3-21 couples the calculation cycle with the physical test specimen. The total mass of the reinforced concrete footing was lumped together into a single mass with dynamic effect considered in the numerical model.

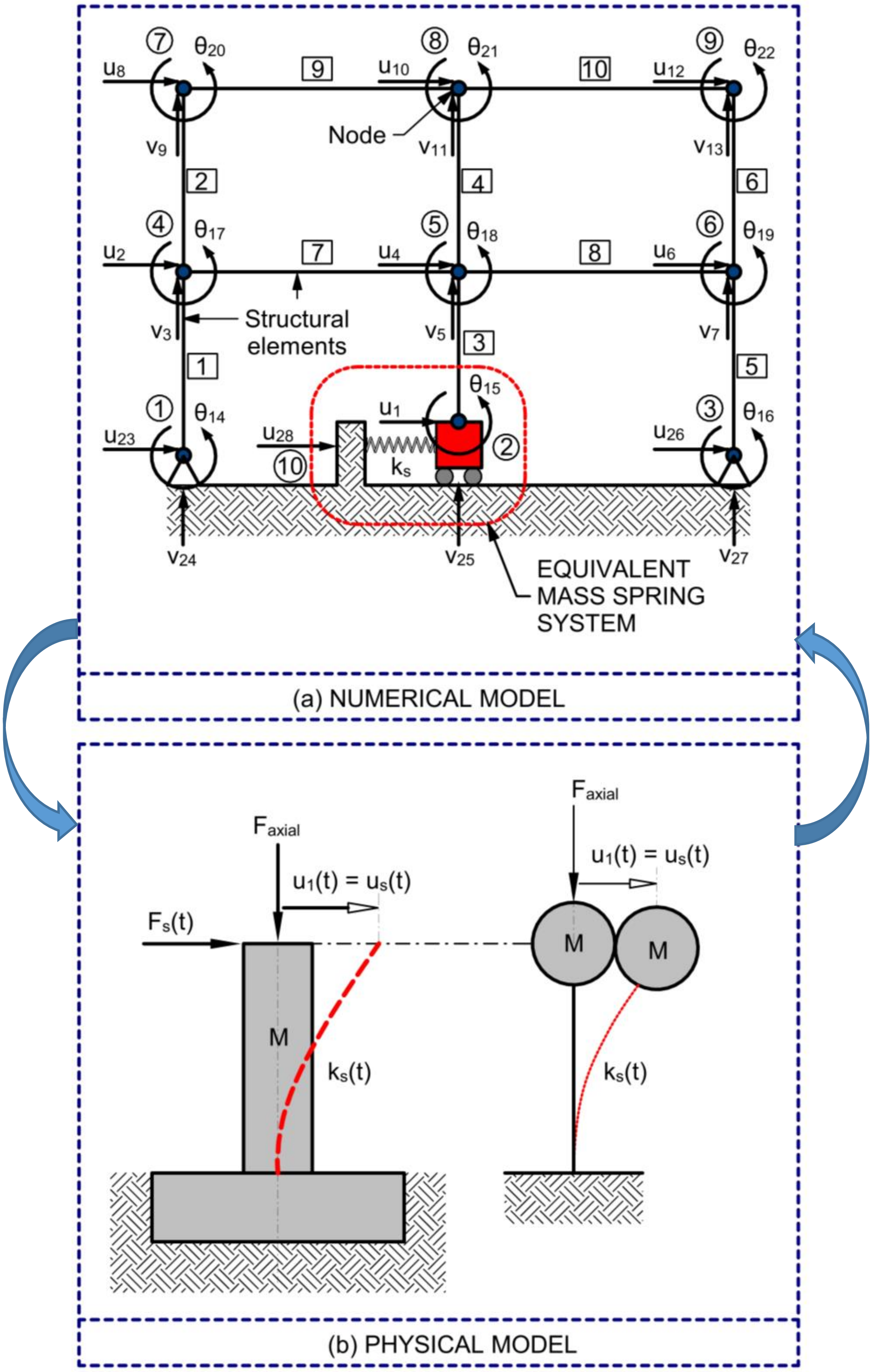

Figure 3-21 Pseudo-dynamic numerical model and physical model

3.6.1 PSEUDO-DYNAMIC ANALYSIS ASSUMPTIONS

To limit the scope of the project several assumptions had to be made regarding the distribution of stiffness and mass within the structure. The assumptions made during the derivation and formulation of the numerical model are as follows:

- The pseudo-dynamic analysis was run considering only a single design for the steel frame structure and the reinforced concrete footing. Therefore, the analysis only considers a single natural period of vibration, which would otherwise vary depending on the selection of the members used to construct the frame;
- The steel frame was modelled using beam elements with 6 degrees of freedom, with two translational and one rotational degree of freedom per node. Because the frame structure will remain linear elastic for the duration of the earthquake record, energy loss due to the non-linear behaviour that would otherwise occur during an earthquake was simulated using Rayleigh damping. Only the first two natural modes of vibration are used to determine the Rayleigh damping coefficients. Failure to incorporate energy loss within the rest of the structure by assuming zero damping will give an unrealistic view of the damage sustained by the footing, and therefore damping needs to be incorporated into the overall structural model that may otherwise experience non-linear behaviour. The downside to not incorporating nonlinearity into the rest of the structure means that the influence that the degradation of stiffness and subsequent increase in the natural period of vibration is not considered when studying the response of the reinforced concrete footing;
- The single lumped mass was used for the reinforced concrete footing, and therefore discrete material responses within the foundation are not considered;
- The only nonlinearity incorporated into the analysis was the lateral deformation of the footing, and therefore any reduction in stiffness of the overall structure will only be due to the stiffness degradation of the footing; and
- During the pseudo-dynamic tests, a constant axial load was applied to the footing with only the horizontal load varying. The constant loads comprised of the static loads on the structure under serviceability limit state loading, which only includes the gravity loads due to the dead weight of the structure and a nominal live load.

3.6.2 LOADING CYCLE PHYSICAL TEST SETUP

A conceptual model of the experimental test setup is shown in Figure 3-22 and the setup within the laboratory is shown in Figure 3-23. The schematic layout showing the front and back view of the experimental test setup with the test setup dimensions and each of the components is shown in Figure 3-24 and Figure 3-25. The test setup comprised of two actuators and two load cells with the vertical actuator being used to simulate the 300 kN constant axial load applied by the overall structure on the footing, which corresponds to the degree of freedom v_{25} in Figure 3-21. The horizontal actuator was used to simulate the horizontal shear load on the footing during the earthquake loading due to the overall dynamic response of the frame structure. The displacement u_s calculated in the computer model was applied directly to the footing using the horizontal actuator with the corresponding force F_s measured using the horizontal load cell [LC1]. The horizontal force was subsequently fed back into the numerical model at which time the numerical model computation continued.

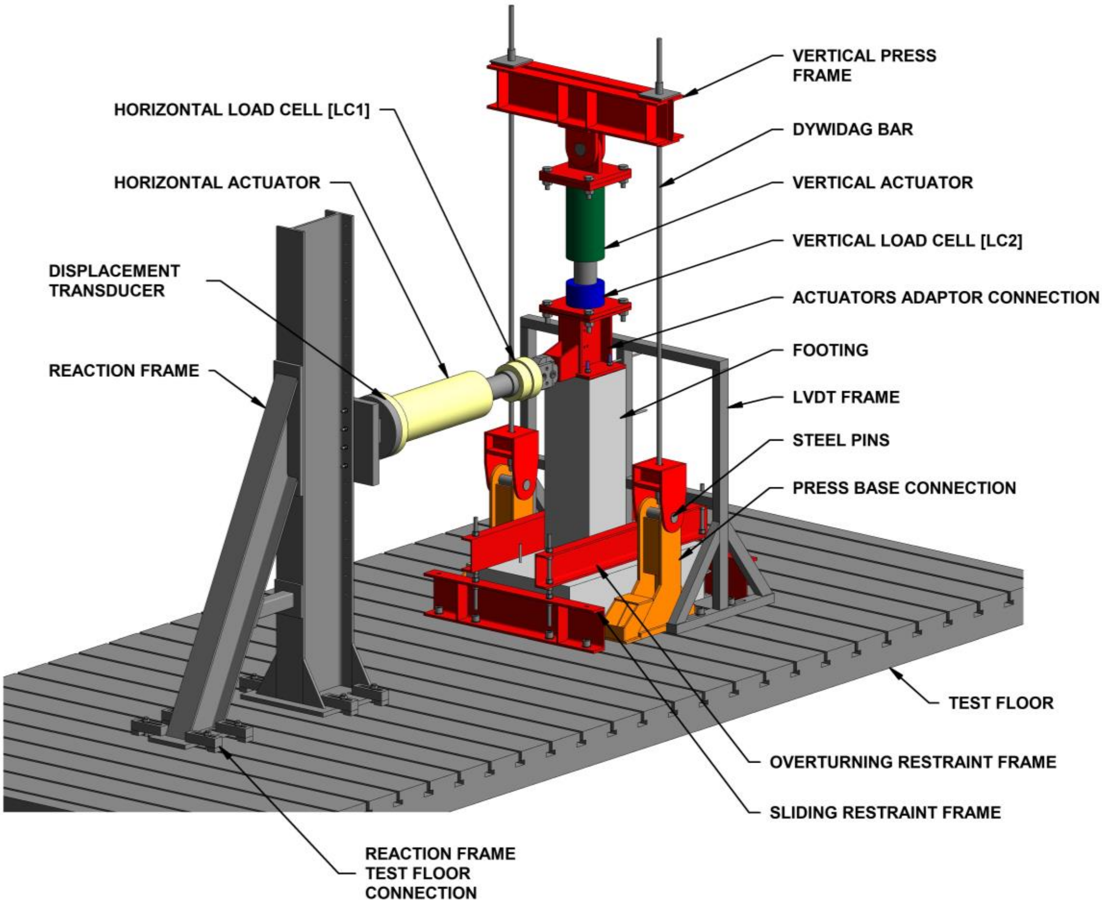

Figure 3-22 Conceptual experimental test setup

Figure 3-23 Experimental test setup in the University of Pretoria's Sasol Laboratory

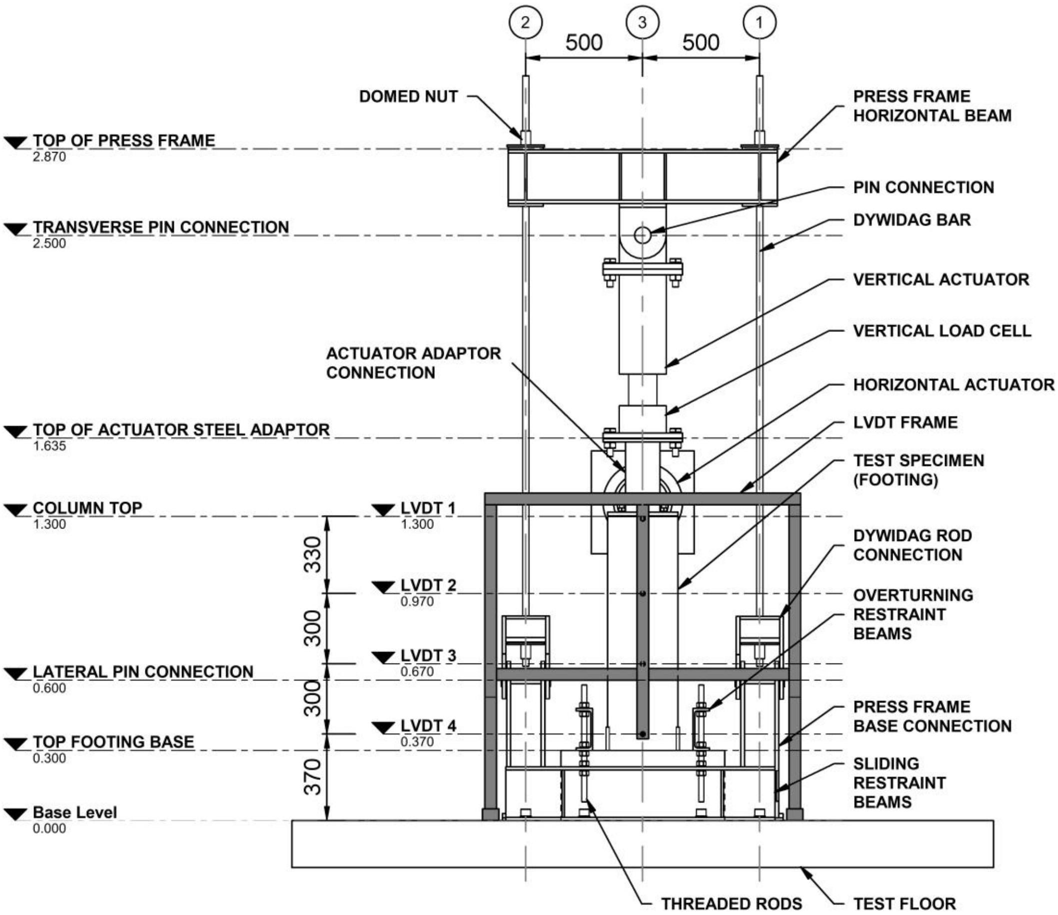

Figure 3-24 Back elevation of the pseudo-dynamic experimental test setup

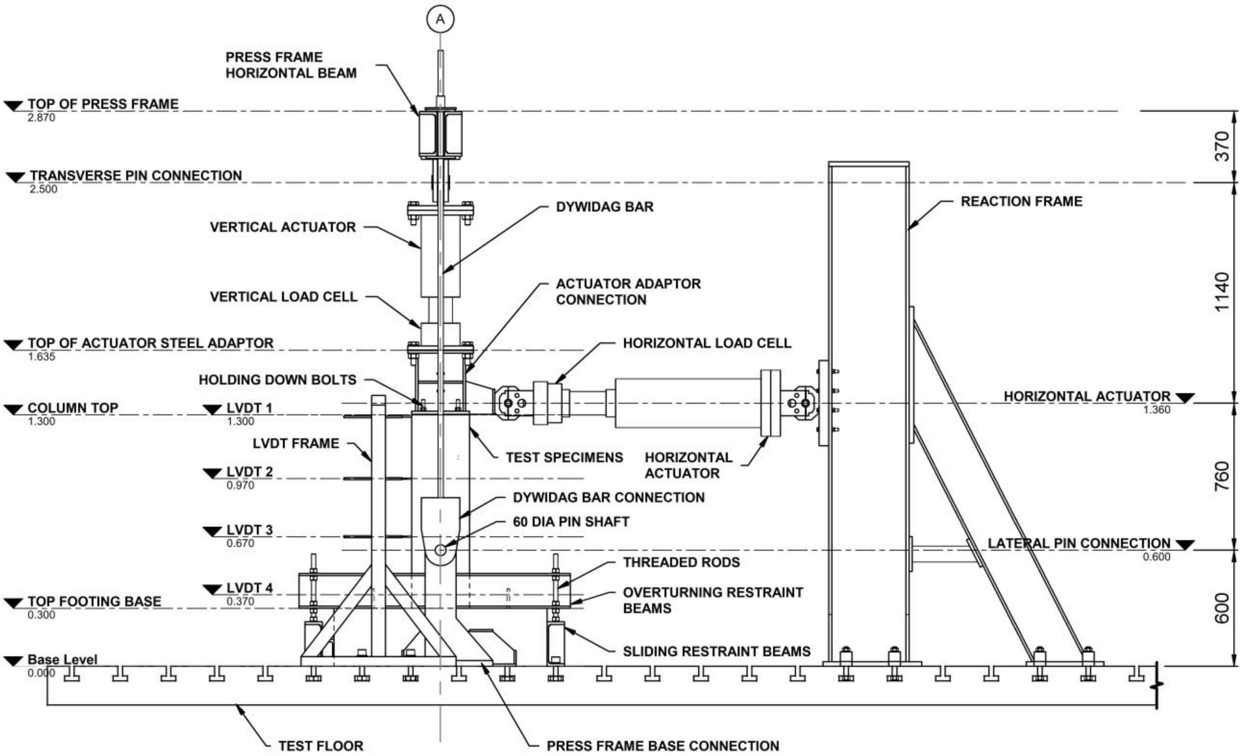

Figure 3-25 Side elevation of the pseudo-dynamic experimental test setup

Figure 3-26 shows the hardware and software that was used to integrate the calculation cycle with the loading cycle. Two control loops were used in the experimental tests with the first control loop being used under force control to maintain the vertical axial load on the reinforced concrete footing. The second control loop was used under displacement control to apply the horizontal displacement calculated in the numerical model onto the reinforced concrete footing at each iteration within each time step. A linear ramp function was used to apply the load incrementally and delay the rate of lateral load applied onto the footing. The objective of the ramp function was to mitigate dynamic effects during the analysis due to large changes in calculated displacements between iterations.

Figure 3-26 also shows a third path that comprised of additional instruments attached to the experimental test setup. Strain gauges were attached to two of the four longitudinal reinforcing bars, with a reinforcing bar with strain gauge being placed on each column face in the direction of loading. The strain gauges were applied at the base of the column where the maximum moment was expected. Four additional linear displacement transducers were placed at equal increments over the length of the column with the aim to compare the results with the internal displacement transducer in the horizontal actuator.

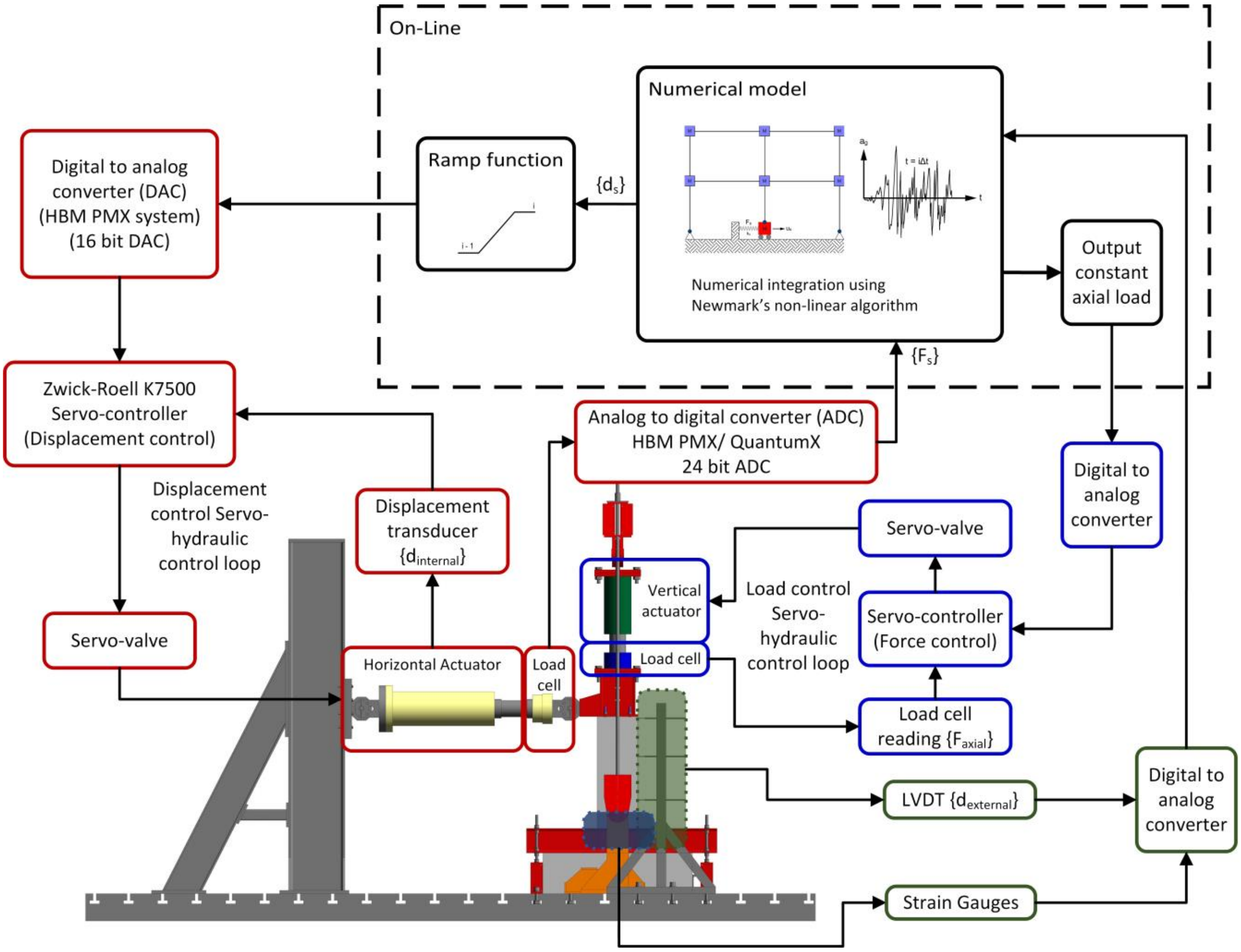

Figure 3-26 Schematic illustration of external components of the pseudo-dynamic experiment

3.6.3 CALCULATION CYCLE NUMERICAL MODEL

The non-linear Newmark's implicit method using the average acceleration method was used to perform the pseudo-dynamic experiments, and Figure 3-27 shows the pseudo-dynamic algorithm used to run the analysis. The script that was developed to run the pseudo-dynamic analysis is given in Appendix A. The algorithm was adapted to incorporate static condensation to eliminate the rotational free degrees of freedom with zero mass within the overall frame structure. The unknown displacements and forces within the structure using the initial state of the structure are solved at each time-step:

$$i = 1,2,3 \dots n \qquad with \;\; t = i\Delta t$$

With n being the total number of time steps in the earthquake record and t being the time in seconds at any point within the analysis. The average acceleration method produces an unconditionally stable solution and therefore the selection of the time step only influenced the accuracy of the solution and not the stability of the solution. For each time step "i" within the earthquake record, iteration, "j", was required due to the implicit relationship between the restoring force matrix $(f_s^*)_i$ and the unknown displacement of the structure at $(u)_i$ as shown in Step 15 in Figure 3-27. Therefore, the stiffness of the footing must be assumed before the calculation at each time step can be initialised. The initial stiffness of the footing had to be determined before the pseudo-dynamic analysis could commence. The selection of the initial lateral stiffness of the footing had to be considered carefully because assuming a stiffness that was lower than the maximum true elastic stiffness of the footing would produce premature damage to the footing at the start of each time step. Selecting a stiffness lower than the elastic stiffness of the footing can also produce instability problems in the convergence of the solution.

Reinforced concrete is a highly non-linear material, and with the application of the applied loading at the beginning of each time step, an initial out of balance residual force vector was produced. As a result, the structure was no longer in force or energy equilibrium. In general, the displacement applied to the structure results in a restoring force that differs from that of the restoring force that was calculated using the initially maximum stiffness of the structure. Because of this, the stiffness of the footing (k_s) between the previous time step and the current time step was updated at each iteration until there was convergence to a solution. Once the solution converged, and equilibrium within the structure was achieved, the next time step "i" can commence. Force and energy equilibrium had to be ensured within a certain level of accuracy by specifying a convergence criterion at the start of the pseudo-dynamic analysis, which was less than the resolution of the data acquisition system.

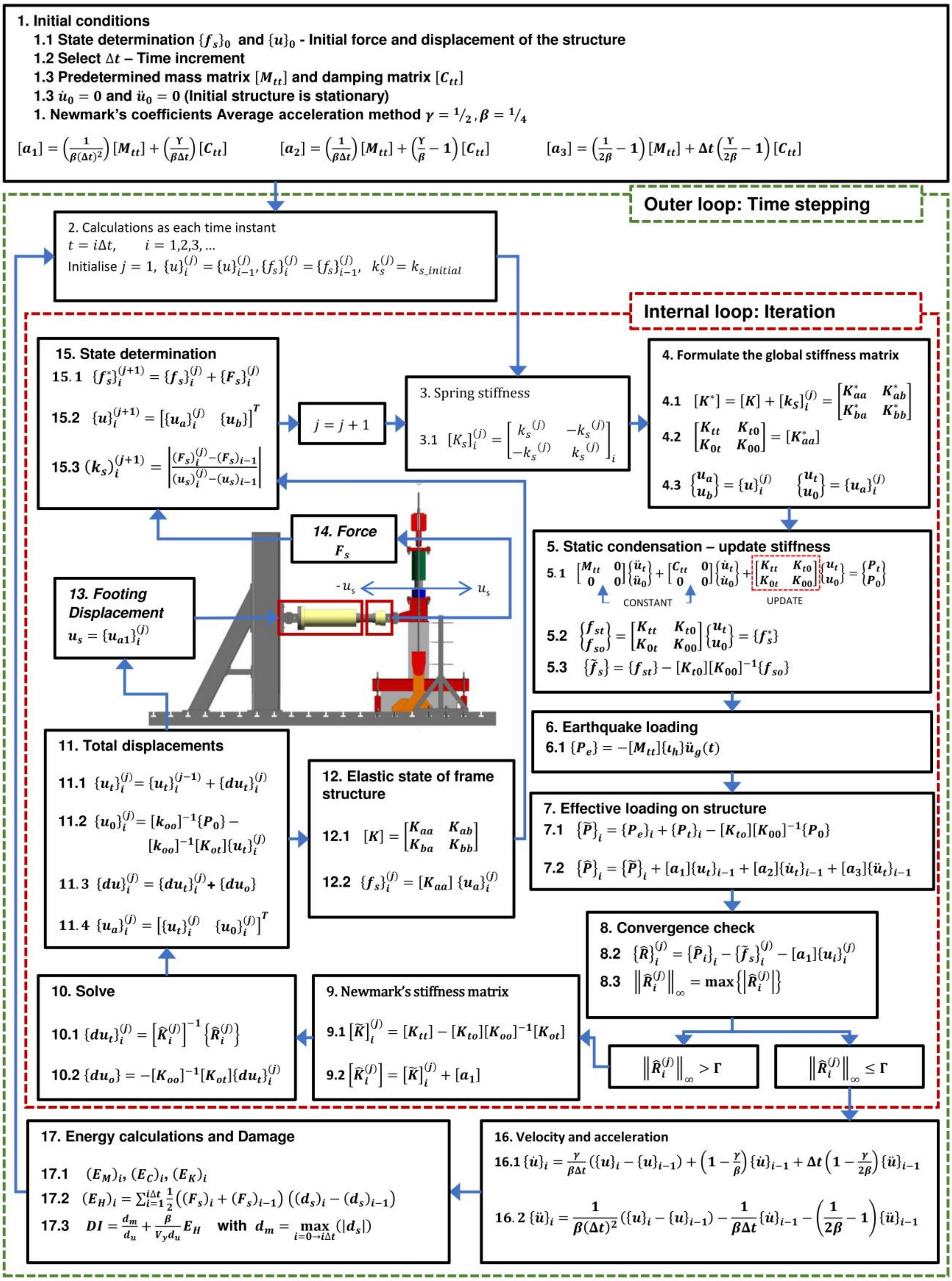

Figure 3-27 Pseudo-dynamic numerical model algorithm

The initial calculations consisted of analysing the structure under static loading to determine the initial state of the structure before the application of the earthquake excitation. Equation 3.2 needs to be solved for the unknown displacements, using the applied gravity loads, to determine the static distribution of load in the structure. Equation 3.3 is the initial stiffness matrix of a spring element that was used for the lateral displacement of the footing and includes the position within the overall global stiffness matrix.

$$[K]\{u\}_0 + [K_s]_0\{u\}_0 = [K^*]_0\{u\}_0 = \{P\} \tag{3.2}$$

$$[K_s]_0 = \begin{array}{cc} \begin{array}{ccc} u_1 & \cdots & u_{28} \end{array} & \\ \begin{bmatrix} k_{s0} & \cdots & -k_{s0} \\ \vdots & \ddots & \vdots \\ -k_{s0} & \cdots & k_{s0} \end{bmatrix} & \begin{array}{c} u_1 \\ \vdots \\ u_{28} \end{array} \end{array} \qquad \text{with} \quad u_s = u_1 \tag{3.3}$$

Where $\{P\}$ is the statically applied point loads on the structure and $[K]$ represents the overall global elastic stiffness matrix of the frame structure that was formulated using beam elements. The matrix $[K_s]_0$ is the initial stiffness matrix of the reinforced concrete footing with k_{s0} the initial stiffness of the spring element at time equal to zero. The vector given by $\{u\}_0$ was the initial displacements of the structure before the earthquake loading was applied to the structure.

Beam elements were used to model the frame structure with three degrees of freedom associated with each node to reduce computation demand. Regarding Figure 3-21(a), the structure was discretised into ten beam elements with ten nodes. Nodes one through nine of the frame structure comprised of three degrees of freedom (two translational and one rotational degree of freedom) whereas node ten only consisted of a single translational degree of freedom. Node ten only provides a horizontal translational boundary condition for the non-linear idealised spring element used to model the lateral displacement of the footing. This results in 28 degrees of freedom.

The degrees of freedom of the frame structure was numbered such that the translational free degrees of freedom were numbered first followed by the rotational free degrees of freedom and finally the support degrees of freedom, which have zero displacement. Figure 3-28 shows the degrees of freedom for the frame structure and the order in which they were numbered. During the static analysis, the numbering of the free degrees of freedom is not critical. However, during the dynamic analysis, only the translational free degrees of freedom are considered to contain mass with the inertia effects due to rotational degrees of freedom being neglected. Therefore, the static condensation method was used to eliminate the rotational free degrees of freedom from the dynamic analysis. The order that the degrees of freedom were numbered was done to ameliorate the formulation of the statically condensed mass and stiffness matrices.

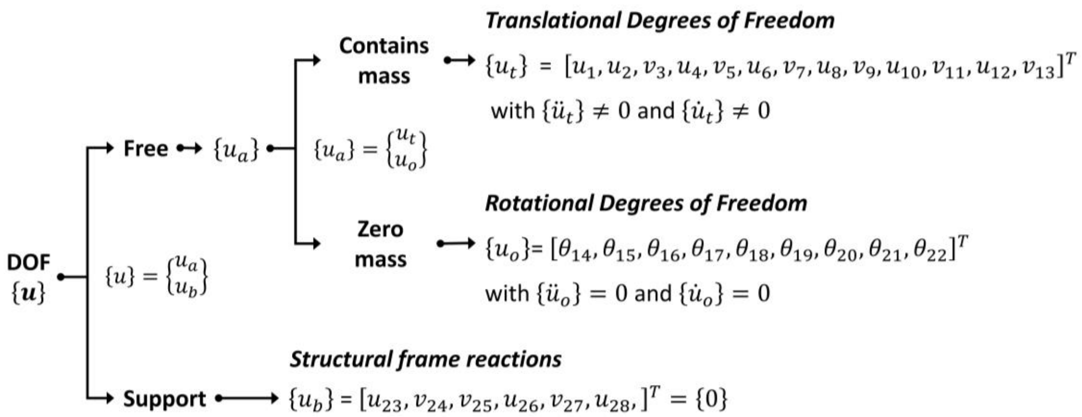

Figure 3-28 Degrees of freedom numbering

Before the structure was subjected to the earthquake loading, the structure would have initial displacements and forces in the members due to gravity loading from the dead load of the structure and live load under serviceability limit states. The same loadings as presented in Section 3.3.1 were used with the applied loading on the numerical model shown in Figure 3-29 to ensure an axial load of 300 kN was produced on the central footing. As the calculations are only done at the nodes, the point loads and moments at the nodes due to the distributed loading was determined using the fixed end reactions as shown in Figure 3-30.

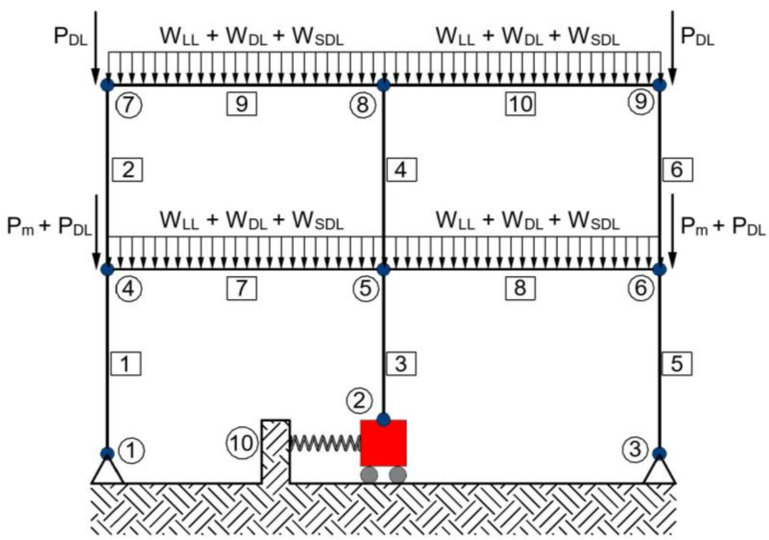

Figure 3-29 Static loading applied to the numerical model

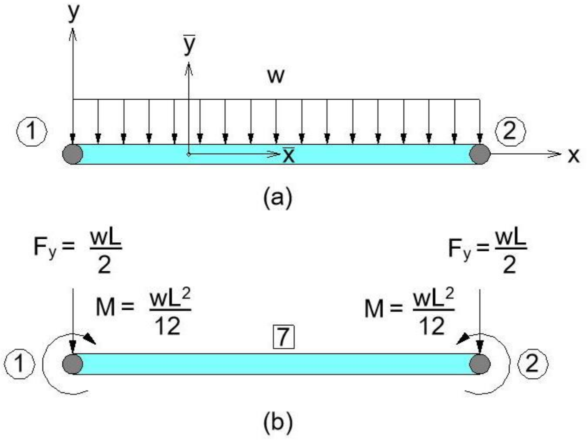

Figure 3-30 Fixed-end reactions due to a uniformly distributed load

The primary objective of the static analysis was to obtain the initial condition or state of the structure before applying the earthquake loading. The overall stiffness matrix $[K^*]$ consists of both the stiffness components from the frame structure and spring element as shown in Equation 3.4. In Equation 3.4 the subscript "b" indicates components of the stiffness matrix relating to the supports and subscript "a" relating to components associated with the free degrees of freedom as previously alluded to in Figure 3-28. The first subscript in the stiffness matrix in Equation 3.5 relates to the force component of a degree of freedom and the second subscript relates to the displacement component.

$$[K^*] = \underbrace{[K]}_{\substack{Frame\\Stiffness\\Matrix\\(Linear)}} + \underbrace{[K_s]}_{\substack{Spring\\Stiffness\\Matrix\\(Non-Linear)}} = \begin{bmatrix} K_{aa}^* & K_{ab}^* \\ K_{ba}^* & K_{bb}^* \end{bmatrix} \tag{3.4}$$

$$\begin{Bmatrix} P_a \\ P_b \end{Bmatrix} = \begin{bmatrix} K_{aa}^* & K_{ab}^* \\ K_{ba}^* & K_{bb}^* \end{bmatrix} \begin{Bmatrix} u_a \\ u_b \end{Bmatrix} \qquad \text{Where } \{u_b\} = \{0\} \tag{3.5}$$

Using Equation 3.5, the unknown displacements $\{u_a\}$ was obtained by solving Equation 3.6 with the reactions determined using Equation 3.8. The initial forces at each of the degrees of freedom $\{f_s^*\}$ under static conditions were obtained from the applied loads on the structure in global coordinates as shown in Equation 3.9.

$$\{u_a\} = [K_{aa}^*]^{-1}\{P_a\} \tag{3.6}$$

$$\{u_{s0}\} = \{u_a\} \tag{3.7}$$

$$\{P_b\} = [K_{ba}^*]\{u_a\} \tag{3.8}$$

$$\{f_s^*\} = [K_{aa}^*]\{u_a\} = \{P_a\} \tag{3.9}$$

The mass matrix $[M]$ was formulated by lumping the mass of the beams, columns and floor slab equally amongst the corresponding nodes as shown in Figure 3-31. All the mass associated with the masonry walls was lumped at the base node as it was assumed that the mass would not be attached to the top beam. Inertial effects due to the mass rotation have not been considered in this analysis. Therefore, the masses associated with rotational free degrees of freedom are equal to zero. The mass matrix is formulated from the following masses within the structure:

- Self-weight of the columns and beams;
- Dead load from the concrete floor slabs;
- Nominal live load from occupants and other non-structural items; and
- Mass of the masonry infill panels.

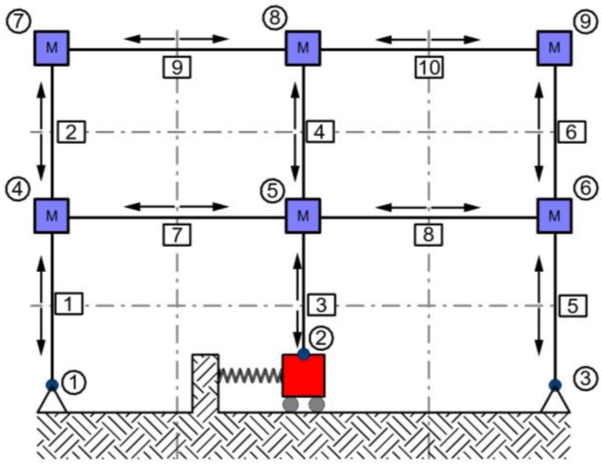

Figure 3-31 Distribution of mass within the structure to the nodes

The rotational degrees of freedom that contain zero mass were eliminated from the dynamic analysis using static condensation. It is therefore assumed that energy dissipation only occurs in the mass degrees of freedom. Therefore, the diagonal elements in the mass matrix $[M]$ that contain zero entry values need to be eliminated from the dynamic analysis during the time stepping analysis. The process entails ordering the mass matrix in such a manner that the first diagonal entries within the mass matrix correspond to the degrees of freedom that contain mass and the subsequent diagonal entries containing zero mass. The ordering of the degrees of freedom was shown previously in Figure 3-21(a) when the degrees of freedom were numbered.

Numbering the translational free degrees of freedom followed by the rotational degrees of freedom results in the formulation of Equation 3.10 without having to reorder the matrix $[K_{aa}^*]$. The degrees of freedom $\{u_t\}$ corresponds to free degrees of freedom that contain mass (free translational degrees of freedom) and $\{u_0\}$ corresponds to free degrees of freedom that contain zero mass (rotational degrees of freedom). The statically condensed equation of motion, which includes damping, containing all the degrees of freedom is written in partitioned form is shown in Equation 3.10. Equation 3.11 shows the statically condensed form that excludes the support degrees of freedom.

$$\begin{bmatrix} \boldsymbol{M_{tt}} & \boldsymbol{0} & 0 \\ \boldsymbol{0} & \boldsymbol{0} & 0 \\ 0 & 0 & 0 \end{bmatrix} \begin{Bmatrix} \ddot{u}_t \\ \ddot{u}_0 \\ 0 \end{Bmatrix} + \begin{bmatrix} \boldsymbol{C_{tt}} & \boldsymbol{0} & 0 \\ \boldsymbol{0} & \boldsymbol{0} & 0 \\ 0 & 0 & 0 \end{bmatrix} \begin{Bmatrix} \dot{u}_t \\ \dot{u}_0 \\ 0 \end{Bmatrix} + \begin{bmatrix} \boldsymbol{K_{tt}} & \boldsymbol{K_{t0}} & \\ \boldsymbol{K_{0t}} & \boldsymbol{K_{00}} & K_{ab} \\ & K_{ba} & K_{bb} \end{bmatrix} \begin{Bmatrix} \boldsymbol{u_t} \\ \boldsymbol{u_0} \\ u_b \end{Bmatrix} = \begin{Bmatrix} \boldsymbol{P_t} \\ \boldsymbol{P_0} \\ P_b \end{Bmatrix} \tag{3.10}$$

$$\begin{bmatrix} M_{tt} & 0 \\ 0 & 0 \end{bmatrix} \begin{Bmatrix} \ddot{u}_t \\ \ddot{u}_0 \end{Bmatrix} + \begin{bmatrix} C_{tt} & 0 \\ 0 & 0 \end{bmatrix} \begin{Bmatrix} \dot{u}_t \\ \dot{u}_0 \end{Bmatrix} + \begin{bmatrix} K_{tt} & K_{t0} \\ K_{0t} & K_{00} \end{bmatrix} \begin{Bmatrix} u_t \\ u_0 \end{Bmatrix} = \begin{Bmatrix} P_t \\ P_0 \end{Bmatrix} \tag{3.11}$$

Where:

$$\begin{bmatrix} K_{tt} & K_{t0} \\ K_{0t} & K_{00} \end{bmatrix} = [K_{aa}^*], \quad [u_a] = \begin{Bmatrix} u_t \\ u_0 \end{Bmatrix}, \qquad P_a = \begin{Bmatrix} P_t \\ P_0 \end{Bmatrix}$$

And:

$[M_{tt}]$: Mass matrix that corresponds to the free translational degrees of freedom

$[C_{tt}]$: Rayleigh damping matrix that is determined from $[M_{tt}]$ and $[K_{tt}]$

$[K_{tt}]$: Stiffness matrix consisting of free translational degrees of freedom with assigned mass

$\{\ddot{u}_t\}$: Accelerations of the translational degrees of freedom with mass

$\{\ddot{u}_0\}$: Accelerations of the free rotational degrees of freedom

$\{\dot{u}_t\}$: Velocities of the free translational degrees of freedom

$\{\dot{u}_0\}$: Velocities of the free rotational degrees of freedom

$\{u_t\}$: Displacements of the free translational degrees of freedom

$\{u_0\}$: Displacements of the free rotational degrees of freedom

Multiplying through with Equation 3.11 produces Equation 3.12 and Equation 3.13. Equation 3.13 allows for the static relationship between $\{u_0\}$ and $\{u_t\}$ to exist due to the lack of presence of inertia and damping terms and is reordered in Equation 3.14. Any static loads applied to degrees of freedom with zero mass is also incorporated into Equation 3.13.

$$[M_{tt}]\{\ddot{u}_t\} + [C_{tt}]\{\dot{u}_t\} + [K_{tt}]\{u_t\} + [K_{t0}]\{u_0\} = \{P_t\} \tag{3.12}$$

$$[K_{0t}]\{u_t\} + [K_{00}]\{u_0\} = \{P_0\} \tag{3.13}$$

$$\{u_0\} = [K_{00}]^{-1}\{P_0\} - [K_{00}]^{-1}[K_{0t}]\{u_t\} \tag{3.14}$$

Equation 3.14 is substituted into Equation 3.12 with the resultant expression shown in Equation 3.15.

$$\begin{aligned}&[M_{tt}]\{\ddot{u}_t\} + [C_{tt}]\{\dot{u}_t\} + \big[[K_{tt}] - [K_{t0}][K_{00}]^{-1}[K_{0t}]\big]\{u_t\} \\ &= \{P_t\} - [K_{t0}][K_{00}]^{-1}[K_{0t}]\{P_0\}\end{aligned} \tag{3.15}$$

Simplifying Equation 3.15 results in the following expressions:

$$[M_{tt}]\{\ddot{u}_t\} + [C_{tt}]\{\dot{u}_t\} + \big[\tilde{K}\big]\{u_t\} = \{\tilde{P}\} \tag{3.16}$$

$$\big[\tilde{K}\big] = [K_{tt}] - [K_{t0}][K_{00}]^{-1}[k_{0t}] \tag{3.17}$$

$$\{\tilde{P}\} = \{P_t\} - [K_{t0}][K_{00}]^{-1}[K_{0t}]\{P_0\} \tag{3.18}$$

$$\{P_t\} = \{P_g\} + \{P_f\} = -[M_{tt}]\{I\}\ddot{u}_g + \{P_f\} \tag{3.19}$$

The static loads in the structure or state of the structure $\{f_s^*\}$ at each time increment was separated into two components as shown in Equation 3.20 with $\{f_{st}\}$ representing the translational degrees of freedom and $\{f_{s0}\}$ representing the rotational degrees of freedom. The state of the structure due to static condensation $\{\tilde{f}_s\}$ is defined in Equation 3.21 and derived by multiplying out Equation 3.20 and reordering the terms such that Equation 3.22 is produced.

$$\{f_s^*\} = \begin{Bmatrix} f_{st} \\ f_{s0} \end{Bmatrix} = \begin{bmatrix} K_{tt} & K_{t0} \\ K_{0t} & K_{00} \end{bmatrix} \begin{Bmatrix} u_t \\ u_0 \end{Bmatrix} \tag{3.20}$$

The derivation of $\{\tilde{f_s}\}$ using Equation 3.20 is as follows:

$$\{f_{st}\} = [K_{tt}]\{u_t\} + [K_{t0}]\{u_0\}$$

$$\{u_0\} = [K_{00}]^{-1}\{f_{s0}\} - [K_{00}]^{-1}[K_{0t}]\{u_t\}$$

$$([K_{tt}] - [K_{t0}][K_{00}]^{-1}[K_{0t}])\{u_t\} = \{f_{st}\} - [K_{t0}][K_{00}]^{-1}\{f_{s0}\}$$

$$[\widetilde{K}]\{u_t\} = \{f_{st}\} - [K_{t0}][K_{00}]^{-1}\{f_{s0}\}$$

$$\{\tilde{f_s}\} = [\widetilde{K}]\{u_t\} \tag{3.21}$$

$$\{\tilde{f_s}\} = \{f_{st}\} - [K_{t0}][K_{00}]^{-1}\{f_{s0}\} \tag{3.22}$$

To produce the damping matrix $[C_{tt}]$ required the calculation of the first two natural periods of vibration of the structure by solving the determinant for Equation 3.23 for the non-trivial solution. Equation 3.24 was used to solve for the Rayleigh damping coefficients a_0 and a_1 using a 5% ($\xi = 0.05$) damping ratio and the natural periods of vibration of the structure calculated using Equation 3.23. The first two modes of vibration contribute significantly to the overall response of the structure, with both modes of vibration being assigned the same damping value. SANS 10160-4:2017 traditionally uses a damping value of 5%, as the design elastic response spectra within the code are derived using a 5% damping value. Upon solving for the statically condensed mass and stiffness matrices, the damping matrix $[C_{tt}]$ can be calculated using Equation 3.25.

$$\left[[\widetilde{K}] - \omega_n^2[M_{tt}]\right]\varphi_n = \{0\} \tag{3.23}$$

$$\frac{1}{2}\begin{bmatrix} 1/\omega_1 & \omega_1 \\ 1/\omega_2 & \omega_2 \end{bmatrix} \begin{Bmatrix} a_0 \\ a_1 \end{Bmatrix} = \begin{Bmatrix} \xi \\ \xi \end{Bmatrix} \tag{3.24}$$

$$[C_{tt}] = a_0[M_{tt}] + a_1[K_{tt}] \tag{3.25}$$

The only non-linear component in the structure was due to the lateral stiffness $(k_s(t))$ of the reinforced concrete footing. Therefore, the stiffness matrix of the frame structure remains constant for the duration of the experiment. Within each iteration within a timestep, the spring stiffness $k_s(t)$ was updated in Equation 3.26, which was then incorporated back into the overall global stiffness matrix.

$$[K_s]_i^{(j)} = \begin{array}{c} \begin{array}{ccc} u_1 & \cdots & u_{28} \end{array} \\ \begin{bmatrix} {k_s}^{(j)} & \cdots & -{k_s}^{(j)} \\ \vdots & \ddots & \vdots \\ -{k_s}^{(j)} & \cdots & {k_s}^{(j)} \end{bmatrix} \end{array} \begin{array}{c} u_1 \\ \vdots \\ u_{28} \end{array} \quad \text{with} \quad u_s = u_1 \tag{3.26}$$

The earthquake loading on the frame structure was determined by using Equation 3.27 with the influence vector $\{I\}$ only including the horizontal translational free degrees of freedom. The effective loading $\{\tilde{P}\}_i$ was calculated in Equation 3.28 and accounts for the static load components due to static condensation of the frame structure and the earthquake loading. Equation 3.28 is then substituted into the familiar Newmark equation, which is shown in Equation 3.29.

$$\{P_e\}_i = -[M_{tt}]\{I\}\left(\ddot{u}_g\right)_i \tag{3.27}$$

$$\{\tilde{P}\}_i = \{P_e\}_i + \{P_t\}_i - [K_{to}][K_{00}]^{-1}\{P_0\} \tag{3.28}$$

$$\left\{\hat{P}\right\}_i = \{\tilde{P}\}_i + [a_1]\{u\}_{i-1} + [a_2]\{\dot{u}\}_{i-1} + [a_3]\{\ddot{u}\}_{i-1} \tag{3.29}$$

The unbalanced load on the structure for each degree of freedom was determined using Equation 3.30. The infinity norm of a vector was used to determine whether the residual vector had converged to a solution within the specified convergence criteria. Once the convergence criterion has been achieved, the next time step was initialised. The infinity norm determines the maximum absolute value within the residual vector produced in Equation 3.30. The stop criteria in the research was selected to be 5 x 10^{-5} and was selected to be less than the resolution of the data acquisition system, which had a resolution of 0.003.

$$\{\hat{R}\}_i^{(j)} = \{\hat{P}\}_i - \{\tilde{f}_s\}_i^{(j)} - [a_1]\{u\}_i^{(j)} \tag{3.30}$$

$$\left\|\hat{R}_i^{(j)}\right\|_\infty = \max\left\{\left|\hat{R}_i^{(j)}\right|\right\} \tag{3.31}$$

If the stop criterion was not met, the following calculations were performed to update the displacements and internal forces within the structure. The statically condensed stiffness matrix was determined using Equation 3.32 and was added to the Newmark's coefficient matrix $[a_1]$ to produce the Newmark's stiffness matrix $\left[\hat{K}_i^{(j)}\right]$ as shown in Equation 3.33.

$$[\tilde{K}]^{(j)} = [K_{tt}] - [K_{to}][K_{oo}]^{-1}[K_{ot}] \tag{3.32}$$

$$\left[\hat{K}_i^{(j)}\right] = [\tilde{K}]^{(j)} + [a_1] \tag{3.33}$$

The change in displacement due to the unbalanced residual vector is calculated indicatively using Equation 3.34. The change in displacement was added to the current displacement of the structure at the degrees of freedom with mass from the previous iteration, which is indicated in Equation 3.35.

$$\{du_t\}_i^{(j)} = \left[\hat{K}_i^{(j)}\right]^{-1}\{\hat{R}\}_i^{(j)} \tag{3.34}$$

$$\{u_t\}_i^{(j)} = \{u_t\}_i^{(j-1)} + \{du_t\}_i^{(j)} \tag{3.35}$$

Equation 3.36 is solved to determine the change in deflection of the zero-mass degrees of freedom. Equation 3.37 is used to determine the overall displacement of the zero-mass degrees of freedom, which requires the displacements for static rotational degrees of freedom. The overall displacement of the structure was subsequently combined into a single vector $\{du\}_i^{(j)}$ that was ordered according to the degrees of freedom as defined in Figure 3-21(a).

$$\{du_o\} = -[K_{oo}]^{-1}[K_{ot}]\{du_t\}_i^{(j)} \tag{3.36}$$

$$\{u_0\}_i^{(j)} = [k_{oo}]^{-1}\{P_0\} - [K_{oo}]^{-1}[K_{ot}]\{u_t\}_i^{(j)} \tag{3.37}$$

Equation 3.38 produces the total displacement of the structure that includes both the zero-mass and mass degrees of freedom while the change in displacement is given by Equation 3.39. For Equation 3.38 and Equation 3.39, the values within the vectors are ordered consecutively according to the numbering of the degrees of freedom shown previously in Figure 3-21(a).

$$\{u_a\}_i^{(j)} = \left[\{u_t\}_i^{(j)}, \{u_0\}_i^{(j)}\right]^T \tag{3.38}$$

$$\{du_a\}_i^{(j)} = \left[\{du_t\}_i^{(j)}, \{du_o\}^{(j)}\right]^T \tag{3.39}$$

The state of the structure $\{f_s^*\}$ and $\{u_s\}$ was subsequently updated within a given iteration "j" in each timestep "i". Because the only non-linearity in the system was the lateral displacement of the reinforced concrete footing, the force and displacements components due to the frame structure can be calculated using Equation 3.40 and Equation 3.41.

$$\{f_s\}_i^{(j)} = [K_{aa}]\{u_a\}_i^{(j)} \tag{3.40}$$

$$\{u_s\}_i^{(j)} = \{u_a\}_i^{(j)} \tag{3.41}$$

The force component F_s from the lateral displacement of the reinforced concrete footing was read from the horizontal load cell from the physical test setup and added to the respective degree of freedom in $\{f_s^*\}$. The updated $\{f_s^*\}$ is shown in Equation 3.42. The stiffness of the footing can be updated once the restoring force of the reinforced concrete footing was fed back into the numerical model from the horizontal load cell. The stiffness of the footing was determined by using the previous time steps displacement and force components and the calculated total displacement and measured restoring force in the current time step and iteration. The stiffness of the reinforced concrete footing was calculated using Equation 3.43.

$$\{f_s^*\}_i^{(j)} = \{f_s\}_i^{(j)} + \{F_s\}_i^{(j)} \tag{3.42}$$

$$(k_s)_i^{(j+1)} = \left|\frac{(F_s)_i^{(j)} - (F_s)_{i-1}}{(u_s)_i^{(j)} - (u_s)_{i-1}}\right| \tag{3.43}$$

Figure 3-32 and Figure 3-33 shows a hypothetical example of a change in slope from positive to negative that was run for two cases whereby the absolute value of the calculated stiffness is used and when it is not used. Using the absolute value of the slope, as shown in Equation 3.43, results in the rate of convergence to the solution being slower than that produced by not taking the absolute value. In both cases, the solution converged to the same point on the negative slope and the only benefit with using the absolute value is that the load increments that are applied by the horizontal load actuator to the structure are much smaller. The smaller load increments in combination with the ramp function, as described in Figure 3-26, ensures a slow rate of loading onto the test specimen thus preventing dynamic effects being imparted on the footing.

Figure 3-32 and Figure 3-33 show that the point $(u_s)_{i-1}$ does not necessarily coincide with the inflection/yield point of the analytical model used to describe the reinforced concrete section. During the pseudo-dynamic experiment on the physical test specimen, the reinforced concrete cyclic behavior is not known, and the actual F_s values are obtained from the horizontal load cell [LC1] as shown previously in Figure 3-22. The error at the inflection points in the material response is remedied by reducing the time increments.

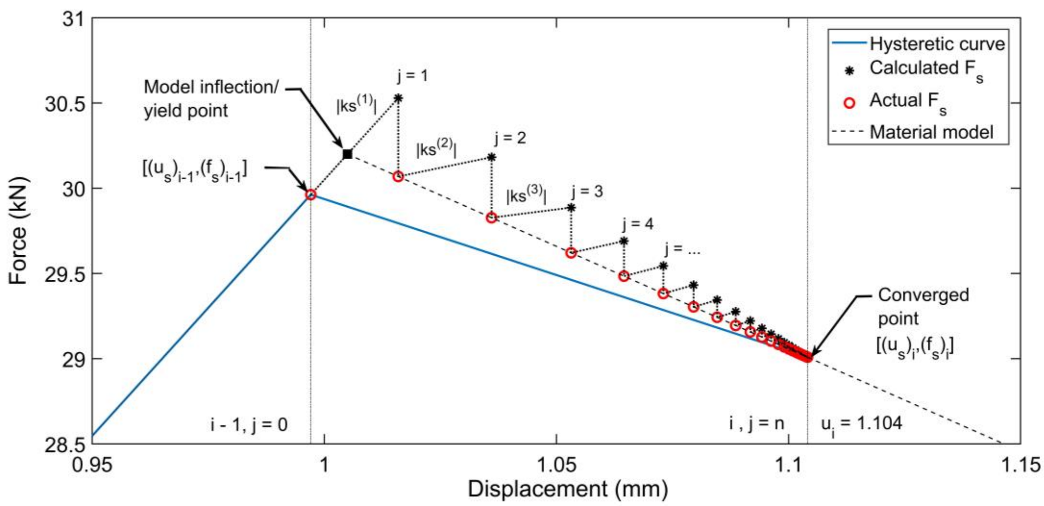

Figure 3-32 Newton-Raphson iteration at an inflection point where the slope changes from positive to negative with the absolute value used for the computational slope k_s

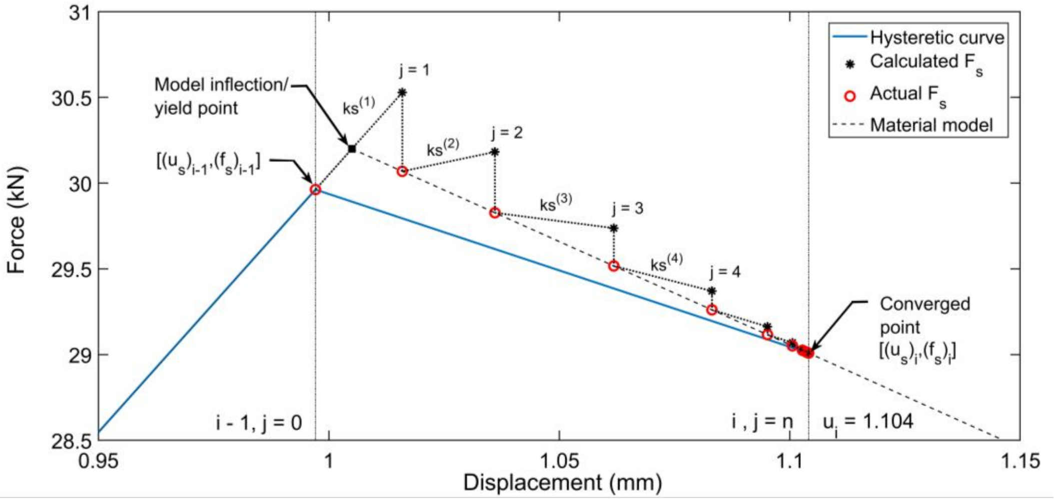

Figure 3-33 Newton-Raphson iteration at an inflection point where the model slope changes from positive to negative and the computation slope ks being either positive or negative

Figure 3-34 and Figure 3-35 shows the Newton-Raphson iteration on a negative slope. Figure 3-34 shows the iteration in a time step whereby the absolute value of the stiffness is used for each iteration and therefore produces more iterations with smaller displacement increments. Figure 3-35 shows the iteration that produces fewer iteration steps as the stiffness can either be positive or negative. However, the displacement steps produced at each iteration are much larger. The stiffness $k_s{}^{(1)}$ is equal to the initial stiffness of the structure and corresponds to the maximum stiffness that the test specimen can achieve.

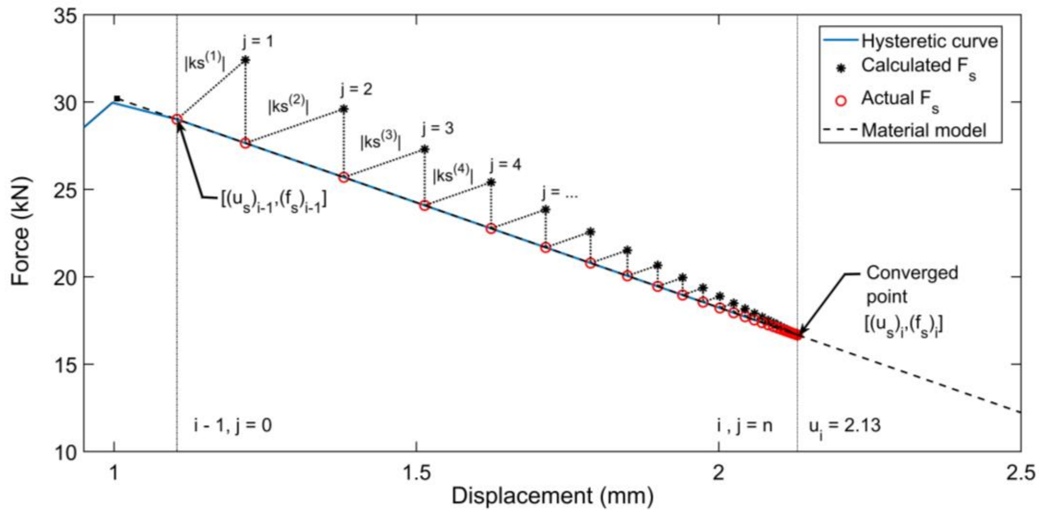

Figure 3-34 Newton-Raphson iteration on a negative slope with the computational slope ks taken as only positive

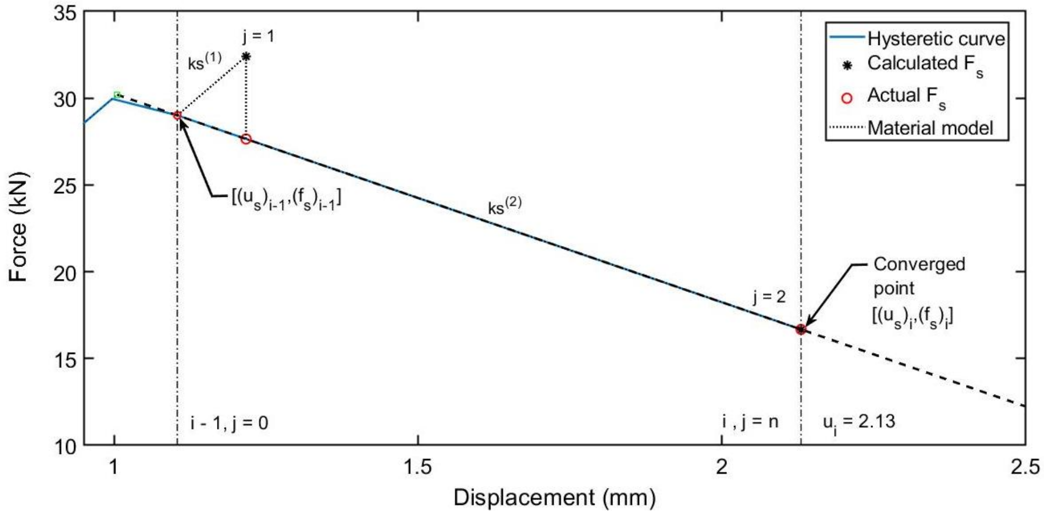

Figure 3-35 Newton-Raphson iteration on a negative slope with the computation slope ks being either positive or negative

3.6.4 ENERGY AND DAMAGE CALCULATIONS

The expressions for the various energy terms in this study were determined numerically at each time increment and were determined by cumulatively summing the change in energy at each time increment for the duration of the experiment. The initial energy expressions at the start of the analysis are equal to the work done by the statically applied loads, which is equal to the energy absorbed by the structure as shown in Equation 3.44. At the start of the analysis the structure was stationary, and therefore the kinetic energy and damping energy were equal to zero. Because the structure is symmetrical, the lateral displacement of the internal footing was equal to zero under gravity loads, which results in the hysteretic energy being equal to zero before the analysis starts.

$$(E_k)_0 = \frac{1}{2}\{P\}^T\{u\}_0 = \frac{1}{2}[[K^*]_0\{u\}_0]^T\{u\}_0 \tag{3.44}$$

Energy (E_T) was imparted to the structure once the structure was subjected to the earthquake excitation. During the analysis, a portion of the energy was temporally stored as kinetic energy (E_M) and strain energy (E_K), with the rest being dissipated in the form of damping energy (E_C), and hysteretic energy (E_H). The total energy was calculated using Equation 3.45 and Equation 3.46. The expressions for each of the energy terms is given by Equation 3.47 to Equation 3.50.

$$\{P^*\}_i = \{P\} - \{P_e\}_i \tag{3.45}$$

$$(E_T)_i = (E_k)_0 + \sum_{i=1}^{i} \frac{1}{2}[\{P^*\}_i + \{P^*\}_{i-1}]^T[\{u\}_i + \{u\}_{i-1}] \tag{3.46}$$

$$(E_M)_i = \sum_{i=1}^{i} \frac{1}{2}\left[[M_{tt}]\{\ddot{u}_t\}_i + [M_{tt}]\{\ddot{u}_t\}_{i-1}\right]^T[\{u_t\}_i - \{u_t\}_{i-1}] \tag{3.47}$$

$$(E_C)_i = \sum_{i=1}^{i} \frac{1}{2}\left[[C_{tt}]\{\dot{u}_t\}_i + [C_{tt}]\{\dot{u}_t\}_{i-1}\right]^T[\{u_t\}_i - \{u_t\}_{i-1}] \tag{3.48}$$

$$(E_K)_i = \frac{1}{2}[[K^*]_0\{u\}_0]^T\{u\}_0 + \sum_{i=1}^{i} \frac{1}{2}\left[[K]\{u\}_i + [K]\{u\}_{i-1}\right]^T[\{u\}_i - \{u\}_{i-1}] \tag{3.49}$$

$$(E_H)_i = \sum_{i=1}^{i} \frac{1}{2}((F_s)_i + (F_s)_{i-1})((d_s)_i - (d_s)_{i-1}) \tag{3.50}$$

Summing the energy terms results in Equation 3.51

$$(E_M)_i + (E_C)_i + (E_K)_i + (E_H)_i = (E_T)_i \tag{3.51}$$

The damage to the structure was determined by using the Park and Ang (1985) damage index that is shown in Equation 3.52 with the terms defined previously. During the pseudo-dynamic tests, the maximum displacement $\{d_u\}$ and shear force $\{V_y\}$ is not known, therefore needs to be assumed and compared to the result once the experiment is done. At which point the maximum displacement and shear force can be updated.

$$DI = \frac{d_m}{d_u} + \frac{\beta}{V_y d_u}(E_H)_i \leq 1 \qquad with \qquad d_m = \max_{i=0 \to n}(|d_s|) \tag{3.52}$$

3.6.5 TESTING INSTRUMENTATION

The pseudo-dynamic analysis algorithm was written in CatmanAP (2016) software, which uses Visual Basic Programming Language. HBM CatmanAP (2016) software enabled the integration between the hardware and software, which allowed the script to calculate the displacement of the footing and transfer the calculated displacement value as a calibrated output voltage (±10V) to the servo-controller. Once the actuator had reached its final position and stabilised, the resultant restoring force was read from the load cell back into the script, and the script continued running.

Figure 3-36 shows the interface that was created with CatmanAP (2016) to monitor the progress of the pseudo-dynamic experiment. The interface enabled the real-time visualisation and interpretation of the hysteretic response and energy characteristics of the structure to be compared with the resultant damage encountered by the footing as the earthquake progressed. The interface also enabled the monitoring of the convergence of the iterations and the number of iterations required before satisfying the stop criterion.

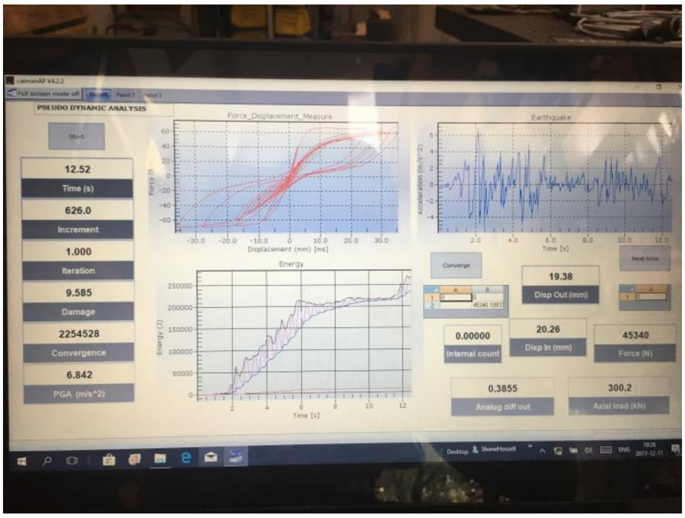

Figure 3-36 Pseudo-dynamic analysis computer interface

The calculated displacement determined from the numerical model was converted from a digital signal to an analogue output signal (DAC) that ranged between ±10 V. The HBM PMX data acquisition system shown in Figure 3-37 was used to integrate the computer software with the servo-controller by converting the digital signal produced by the computer to an analogue output voltage that is used to control the position of the horizontal actuator. The data acquisition system has a 16-bit digital to analogue converter (DAC) and produced an output resolution of 0.003 mm for the horizontal actuator with a stroke length of 200 mm.

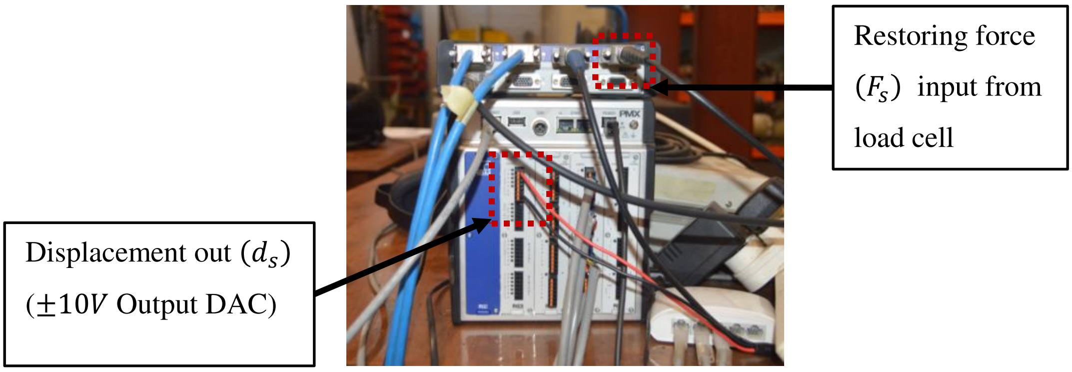

Figure 3-37 HBM Quantum X and PMX Data acquisition system with analogue output

Two Zwick-Roell K7500 servo-controllers are shown in Figure 3-38 and were used during the pseudo-dynamic analysis to control the servo-valves and actuators. The first Zwick-Roell servo-controller was used under displacement control with an input voltage from the HBM PMX system. The constant axial load of 300 kN applied to the footing was controlled by using the second Zwick-Roell Servo-controller under force control.

Figure 3-38 Zwick-Roell K7500 Servo-controllers

A 100 kN hydraulic servo-controlled actuator is shown in Figure 3-40 and was used to place the horizontal load on the reinforced concrete footing. Once the actuator had reached its final position at each iteration within each time step, and the load reading had stabilised, a reading was taken from the horizontal load cell and input back into the computer using a Quantum X

MX840B amplifier as was shown previously in Figure 3-37. The load reading was calibrated such that 1 V = 10 kN as is shown in Figure 3-39(b).

The axial load that was placed on the footing from the frame structure was simulated using a vertical actuator and load cell as shown in Figure 3-41. The axial compression load that was placed on the footing was equilibrated using a custom press frame that only allowed for the transfer of tension forces and not bending moments due to the application of the lateral load. Free rotation of the vertical actuator was achieved by using a pin connection as shown in Figure 3-41 and Figure 3-42.

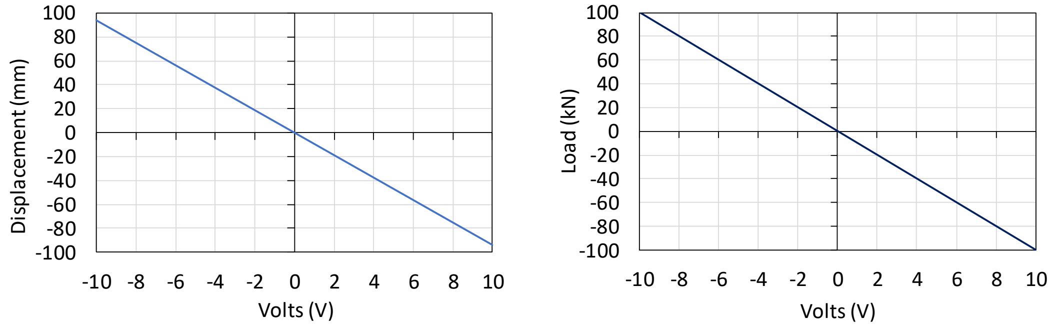

(a) Displacement transducer **(b) Load cell**

Figure 3-39 Relationship between voltage and (a) Displacement of the actuator and (b) Input force from the horizontal load cell

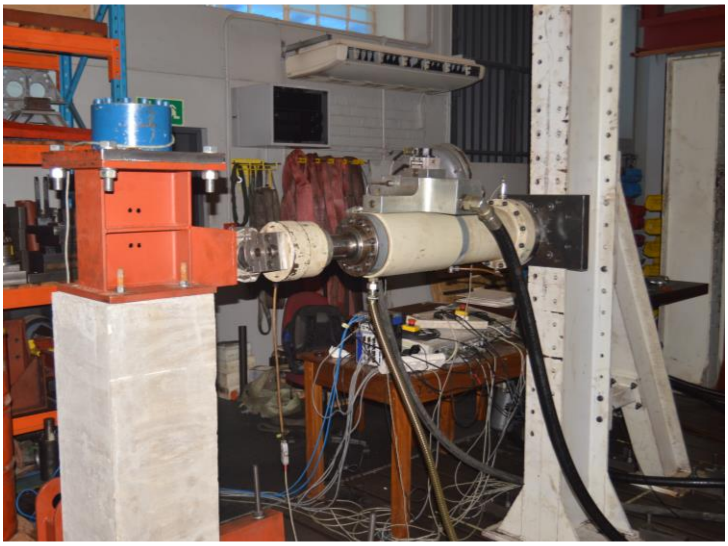

Figure 3-40 Horizontal servo-controlled hydraulic actuator

The reinforced concrete footings were connected to the test floor using steel channel sections and threaded rods as shown in Figure 3-42. Sliding was prevented by placing a channel section on either side of the footing in the direction of the applied lateral load and bolted to the test floor. However, if the static friction coefficient of 0.57 as indicated Rabbat & Russell (1985) was used between concrete and steel with an applied axial load of 300 kN, the shear resistance at the base of the footing due to friction was approximately 170 kN, which is larger than the capacity of the horizontal actuator. Therefore, the channel sections provided additional safety against sliding.

Overturning of the footing was prevented by placing two channel sections across the top of the footing base slab and securing them to the test floor using threaded rods, which is also shown in Figure 3-42. The overturning restraint beams were designed to sustain a maximum overturning moment of 150 kN.m. Figure 3-42 also shows the base connection of the press frame to the test floor with the pin connection from the Dywidag threaded rods. For each of the press frame base connections, 4 x M24 Class 10.9 bolts were used to fix the press frame base steel component to the test floor. Figure 3-43 shows the steel actuator connection to the reinforced concrete footing with the base plate connected to the top of the reinforced concrete footing using four M16 Class 8.8 holding down bolts.

Figure 3-41 Vertical servo-controlled hydraulic actuator with press frame

Figure 3-42 Sliding and overturning restraint beams, and the vertical press frame connection to the test floor

Figure 3-43 Steel actuator adaptor connection to the footing with the base plate and holding down bolts

The strain gauges, which were attached to the reinforcing bars, were placed in a half bridge configuration with both strain gauges active and at 90 degrees to each other. The half bridge configuration ensured that temperature effects were negated. The characteristics of the strain gauges are shown in Table 3-4. Figure 3-44 shows the position of the strain gauges on the reinforcing bars, which were cast into the reinforced concrete footings.

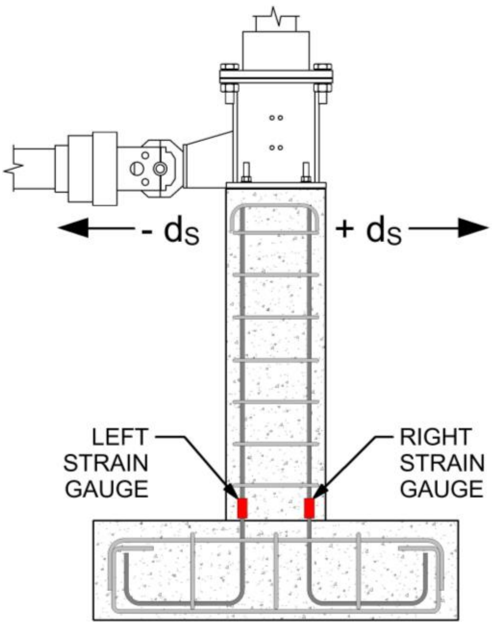

Figure 3-44 Strain gauges placement position on tensile reinforcement

The Y12 tensile bars had to be modified slightly to provide a clean surface for the strain gauges to be attached, with Figure 3-45 showing the strain gauges attached to the reinforcing bars. To ensure that a smooth surface was provided on the bars, the ribs on the Y12 bars had to be removed at the localised position where the strain gauges were going to be placed. The strain gauges on the reinforcement were waterproofed by first painting a sealant over them and their connecting wires and then using shrink tubing to ensure the strain gauges were watertight during the casting of the concrete. Figure 3-36 shows the sealed strain gauges on the reinforcement within the reinforcement cages. The strain gauges cables were loosely fastened to the bars to allow for movement during the casting of the concrete.

Table 3-4 Characteristics of the strain gauges used in the footings

Parameter	Value
Gauge type	TML-YEFLA-5-3LJC
Gauge length	5 mm
Gauge factor	2.14 ± 1%
Gauge resistance	119.5 ± 0.5 Ω


Figure 3-45 Strain gauge attachment to the reinforcing bars

Figure 3-46 Strain gauges fixed to reinforcing bars

3.6.6 TESTING PROCEDURE AND SEQUENCE

Five pseudo-dynamic tests were conducted on the reinforced concrete footings to determine the extent of damage with increasing peak ground acceleration, with the final experimental setup shown in Figure 3-47. The initial horizontal stiffness of the reinforced concrete footing was required before the pseudo-dynamic analysis could commence and to enable the elastic natural period of vibration of the structure to be determined. The first two footings were subjected to cyclic loading to get an indication of the initial stiffness of the footings and to test the displacement transducer within the horizontal actuator.

Once the initial stiffness had been determined, the pseudo-dynamic tests could commence. For each test, the frame structure and static loading were kept constant with the only variable being the peak ground acceleration, which was determined by scaling the El Centro ground motion record. Each pseudo-dynamic experiment commenced by initialising the actuators and ensuring the load on the footing was equal to zero. The 300 kN axial load was then applied to the footing, and once the axial load had reached 300 kN, the horizontal actuator was initialised on the servo-controller, and the pseudo-dynamic test could commence. The initial calculation within the software ensured that all the instruments were zeroed, and the static analysis was performed before commencing the pseudo-dynamic analysis. Time stepping, and iteration commenced upon completion of the initial calculations. The peak ground accelerations used for the pseudo-dynamic experiments, which were obtained by scaling the amplitude of the El Centro earthquake record, are as follows:

- Specimen 1: A maximum peak ground acceleration of 0.34 g;
- Specimen 2: A maximum peak ground acceleration of 0.68 g;
- Specimen 3: A maximum peak ground acceleration of 0.78 g;
- Specimen 4: A maximum peak ground acceleration of 1 g; and
- Specimen 5: A maximum peak ground acceleration of 2 g.

Figure 3-47 Pseudo-dynamic analysis control system

4 EXPERIMENTAL RESULTS

In this chapter, the results obtained from the cyclic load tests and pseudo-dynamic tests are presented, analysed and discussed. The evolution of damage to the reinforced concrete footing with increasing earthquake intensity and cycles of vibration are discussed, compared, and conclusions are drawn. The hysteretic response of the footings and the energy characteristics of the structure are presented due to the applied scaled El Centro ground motion record for each of the pseudo-dynamic experiments.

4.1 CYCLIC LOAD TESTING

Cyclic load tests were undertaken to determine the maximum horizontal elastic stiffness of the reinforced concrete footing under an applied axial load of 300 kN. The maximum horizontal stiffness produced from the cyclic load tests was required as an input into the pseudo-dynamic experiments. Figure 4-1 shows the two cyclic load tests that were undertaken under displacement control whereby the lateral displacement was incrementally increased by 1 mm with each cycle of vibration. Appendix B shows the algorithm used to perform the cyclic load test.

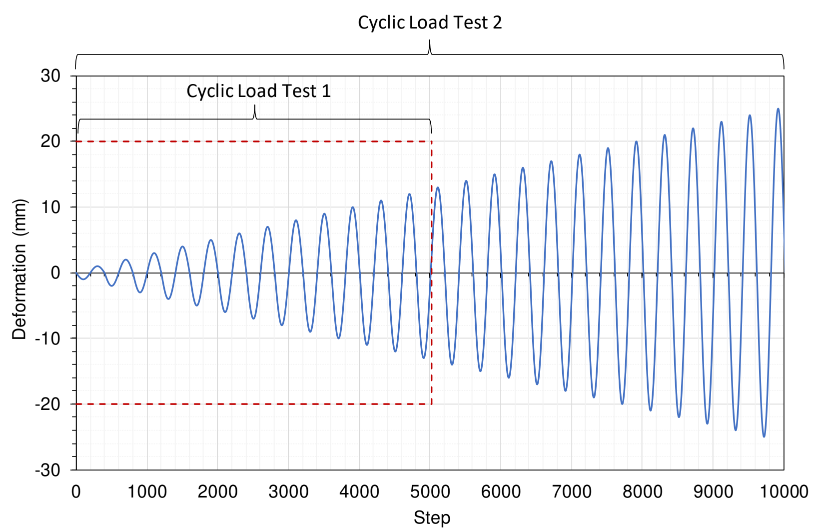

Figure 4-1 Incrementally applied cyclic load independent of time

The first cyclic load test was undertaken to evaluate the test setup and hardware and to provide an initial understanding of the lateral behaviour of the reinforced concrete footing. Figure 4-2 shows the lateral hysteretic response of the reinforced concrete footing with an applied axial load of 300 kN. Cracking of the concrete was evident by the reduction in lateral stiffness at a deformation of 1 mm and at a corresponding restoring force of 21 kN, which can be observed by the reduction in lateral stiffness that is shown in Figure 4-2. Therefore, a maximum elastic stiffness of 21000 N/mm is produced for the section. A single horizontal crack opened at the base of the column at the interface between the concrete slab and the column. With each cycle of vibration, the horizontal crack increased in size and became more apparent without the formation of additional cracks.

However, during the cyclic load test, the experimental test rig experienced unexpected vibrations when the footing was displacement in the positive direction (extension of the hydraulic actuator piston) from its initial position, which can be seen in Figure 4-2. The test was stopped at a maximum lateral deflection of 13 mm due to the vibrations of the press frame. The vibrations were due to the single top pin connection between the vertical actuator and the top press beam not having a flush connection, which resulted in the top beam rotating relative to the vertical actuator causing an unbalanced load and the subsequent vibrations. To mitigate the vibrations in the test frame, 5 mm steel packing plates were placed in the gap between at the pin connection, which is shown in Figure 4-3.

As the cyclic load test was stopped at a maximum displacement of 13 mm, a static load test was done on the same specimen by applying an incrementally increasing negative lateral deformation (retraction of the actuator) to the footing with an applied axial load of 300 kN, which is also shown in Figure 4-2. The static load test was terminated at a maximum deformation of 20 mm with the formation of a large horizontal crack at the base of the column and the spalling of the concrete at the top of the column at the holding down bolts. Figure 4-4 shows the damage to the reinforced concrete column at the end of the cyclic load test and the static load test.

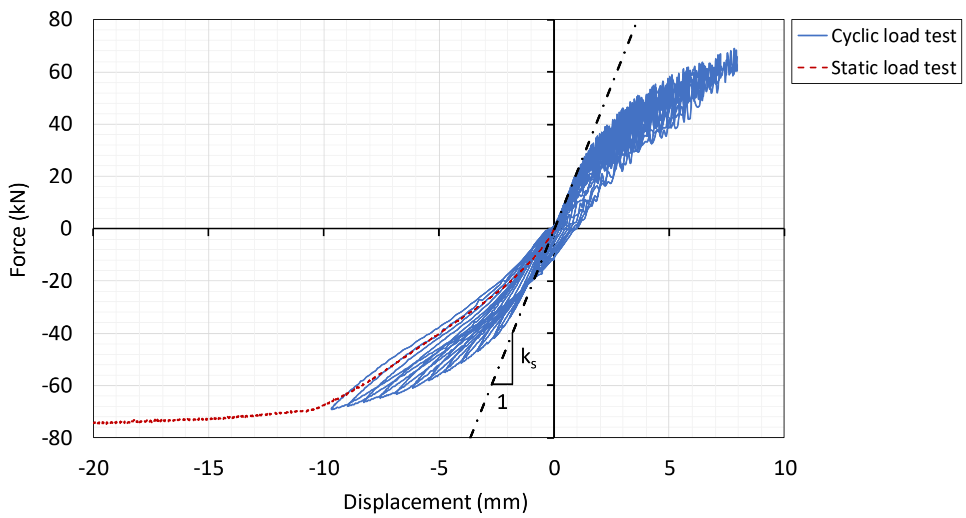

Figure 4-2 Hysteretic response for cyclic load test one

Figure 4-3 Top beam connection stiffening of the press frame

(a) **(b)**

Figure 4-4 Cracking during the first cyclic load test

Figure 4-5 shows the hysteretic response for the second cyclic load test. The cyclic load test was undertaken by incrementally increasing the lateral cyclic displacement by 1 mm after each vibration cycle up to a maximum lateral displacement of ±25 mm. The backbone curve is also shown in Figure 4-5 and forms the envelope to the unloading and reloading branches. The maximum stiffness of the footing (k_s) was obtained from the backbone curve before the concrete started to crack and produced a lateral stiffness of 14536 N/mm. The resultant stiffness from the cyclic load tests is less than the calculated flexural stiffness from first principles for a cantilever member. The stiffness of the footing is not only governed by the flexural stiffness of the reinforced concrete but also influenced by the connection between the base plate and the concrete column and the connection of the footing with the test floor.

The hysteretic response shows a distinct change in stiffness in the backbone curve at 2 mm with a corresponding shear force of 29 kN, which indicates the onset of concrete cracking. A further increase in the lateral displacement of the footing resulted in the stiffness tending to zero, which occurs at an applied deformation of 8 mm and at a corresponding shear force of 66 kN. The flattening of the backbone curves indicates that the lateral capacity of the footing had been reached under the applied axial load and therefore the maximum horizontal force that can be transmitted from the ground into the structure had been reached. Visible pinching can be observed with each cycle of applied load and is likely due to the incompatibility between the material behaviour of reinforcing steel and concrete and the delayed closure of the crack upon load reversal. Upon load reversal the plastically elongated reinforcing steel is first mobilised in compression prior to the closure of the crack in the direction of unloading and reloading. The vertical axial load applied to the footing most likely also contributed to the pinching effect because as the horizontal load is removed, the vertical load overcomes the overturning moment produced by the horizontal force and attempts to stabilise the section by returning the footing back to its original vertical position as can be observed in Figure 4-5.

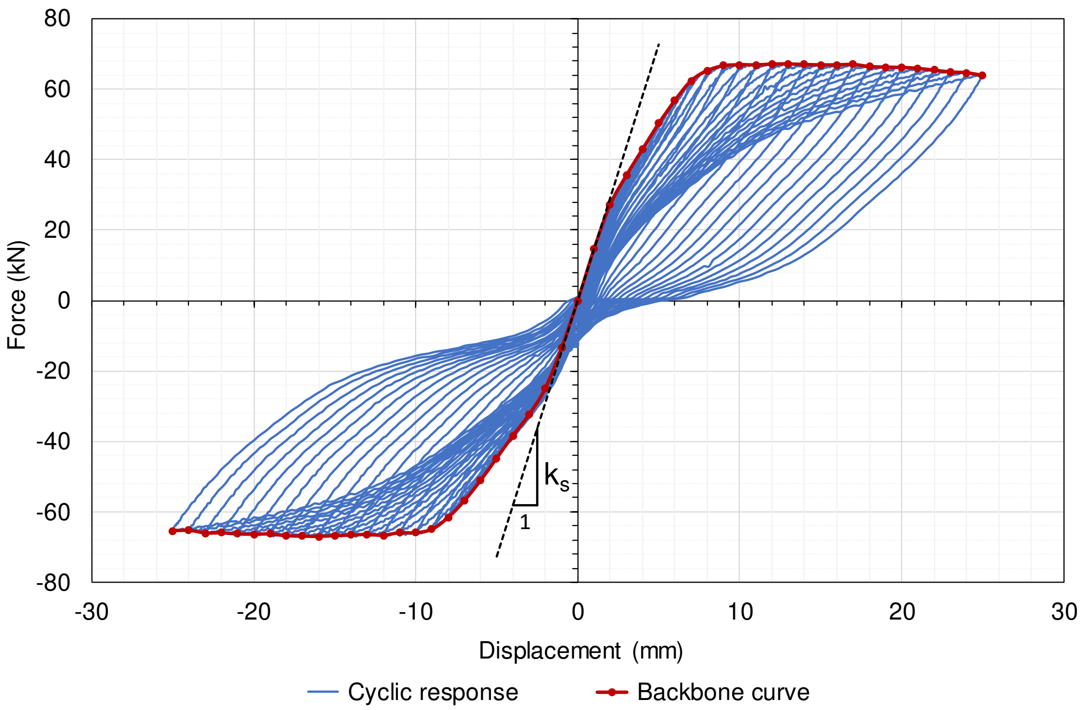

Figure 4-5 Hysteresis curves for cyclic load test two

Figure 4-6 shows that cracking occurred at approximately 40 mm from the base of the column with a single horizontal flexural crack occurring on each face of the column in the direction of the applied shear load. The cracks on either side of the footing were less than 1 mm in width before the reinforcement yielded. However, upon yielding the size of the cracks increased substantially and with a further increase in the displacement amplitude and with each cycle of vibration, the extent of spalling of the concrete increased. The spalling of concrete was found to be exacerbated with repeated cyclic loading of the footing and became more severe post yielding of the reinforcement. Therefore, because of the spalling of the concrete, a slight decrease in the maximum shear capacity of the footing can be observed with an increase in lateral deformation. At the maximum applied displacement of ±25 mm the test was stopped at which point a 5 mm crack had opened at the base of the concrete column, which can be seen in Figure 4-6.

(a) **(b)**

Figure 4-6 Cracking at the base of the reinforced concrete column during the cyclic load testing

Figure 4-7 shows the strain gauge readings for the cyclic load test up until yielding of the reinforcement. Once the tensile strain in the reinforcement exceeded the proportional limit, there is a reduction in the change in strain between corresponding cycles of vibration. This is contrary to what is expected as the strain should increase with a reduction in lateral stiffness of the reinforced concrete footing.

The observed compression strains in Figure 4-7 differed between the two bars, indicating that the position of the actuator connection to the test specimen and the loading direction could have influenced the response of the footing. As the left reinforcing bar approaches the maximum tensile strain, the compressive strain tends to reduce in the right reinforcing bar, indicating that the neutral axis was closer to the compression reinforcement at the maximum strain in the left reinforcing bar. This can also justify why the hysteretic curve is unsymmetrical in Figure 4-5. Figure 4-8 shows the lateral shear force applied at the top of the column with each load step. The shear capacity of the column is reached once the strain in the reinforcement exceeds the proportional limit and the yield stress of the longitudinal reinforcement. The results obtained from the cyclic load tests were considered when determining the initial lateral stiffness, k_{s0}, for the reinforced concrete footings during the pseudo-dynamic tests.

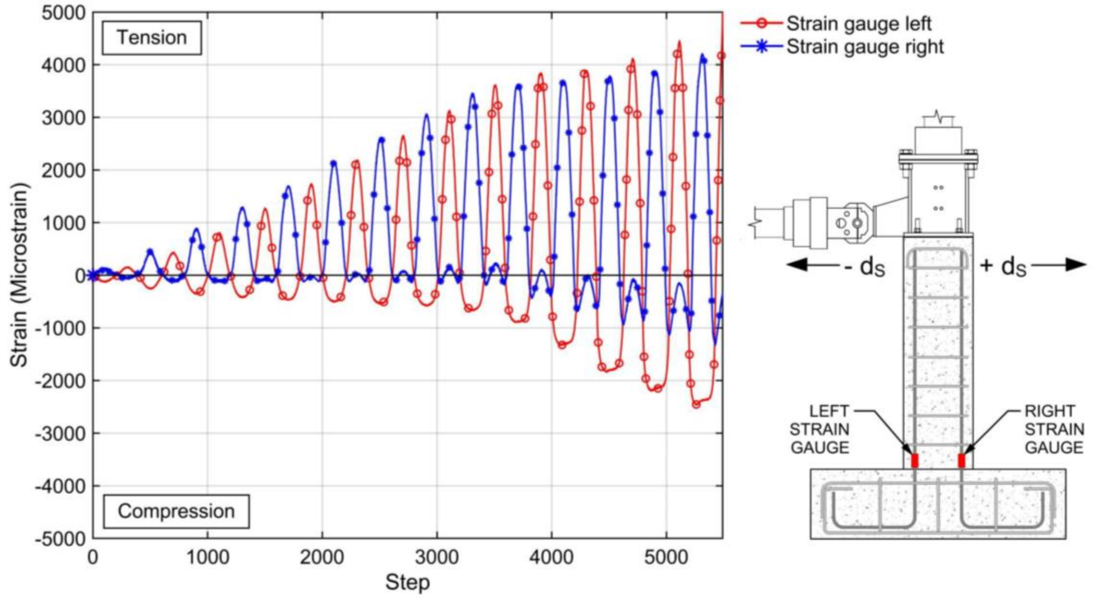

Figure 4-7 Cyclic test 2 strain gauge readings

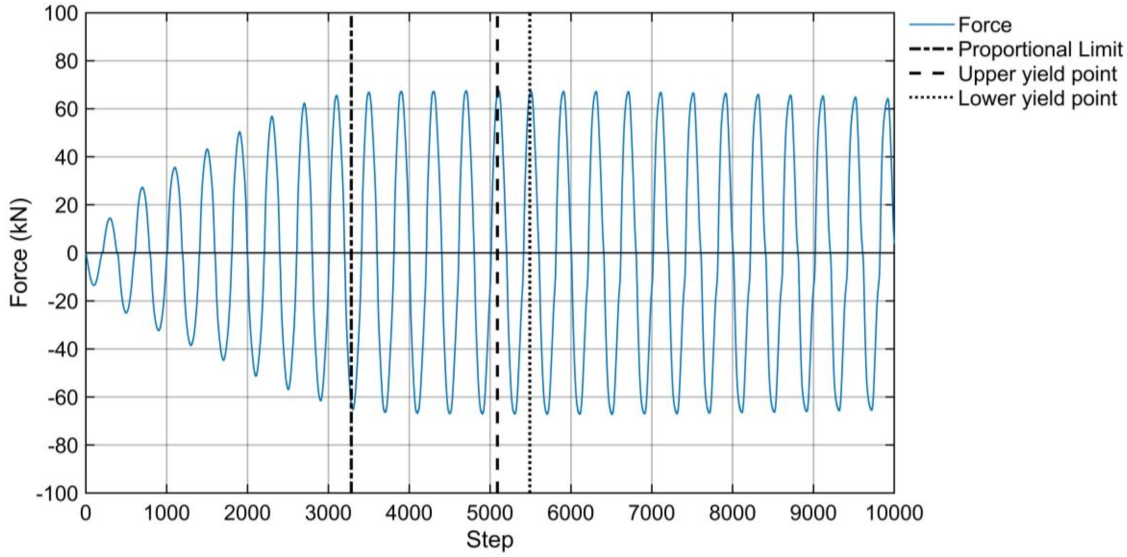

Figure 4-8 Lateral shear force capacity of the reinforced concrete footing

4.2 NATURAL FREQUENCY AND DAMPING PROPERTIES

Rayleigh damping was used to account for energy loss within the overall frame structure that remained linear elastic for the duration of the applied earthquake excitation. Ignoring damping in the frame structure would overpredict the amount of damage incurred by the reinforced concrete footing as the footing would provide the only mechanism of energy loss in the analysis. A damping ratio of 5% was used from SANS 10160-4:2017 for each of the pseudo-dynamic experiments. Figure 4-9 shows the variation of the damping ratio with increasing modal frequencies for the frame structure used during the pseudo-dynamic experiments. As can be seen from Figure 4-9, the damping ratio of 5% is only true at the first two modes and produces higher damping ratios at frequencies less than ω_1 and greater than ω_2. However, at intermittent frequencies between ω_1 and ω_2, the damping ratio is less than the specified 5%.

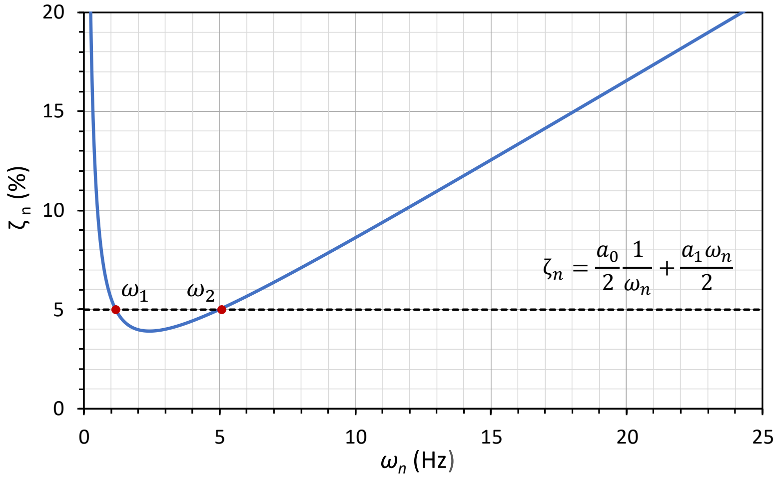

Figure 4-9 Effect of frequency on the damping ratio

Because of the change in the lateral stiffness of the reinforced concrete footing during the pseudo-dynamic experiments, a sensitivity analysis was undertaken to determine the impact that the lateral stiffness of the footing would have on the Rayleigh damping coefficients. The aim was to determine whether the Rayleigh damping coefficients would have to be updated at each time increment within the analysis or whether just calculating the Rayleigh damping coefficients at the start of the analysis would be enough. Having to calculate the damping coefficients at each time increment would result in a significant increase in the computational time that results from the time it takes solve numerically for the eigenvalues in the pseudo-dynamic algorithm as shown in Appendix A.

Assuming an initial lateral stiffness of the footing that is less than the actual elastic stiffness of the footing would result in premature damage being incurred to the reinforced concrete footing as the analysis progresses and would thus produce an unrealistic response. To ensure that the correct response was obtained during the pseudo-dynamic tests, it was considered conservative to select an initial lateral stiffness value greater than that calculated from the cyclic load tests to account for potential variability between the test samples. Thus, the sensitivity analysis would also provide insight into the impact of selecting a larger lateral stiffness value would have on the Rayleigh damping coefficients.

Figure 4-10 shows the results of varying the initial elastic stiffness of the footing on the damping coefficients a_0 and a_1 using 2%, 5% and 10% damping. The Rayleigh damping coefficients are used to calculate the damping matrix $[C]$ from the mass $[M]$ and the stiffness matrices $[K]$. Selecting a larger initial stiffness of the footing to perform the pseudo-dynamic analysis has no significant influence on the damping within the structure. However, the selection of the damping ratio has a significant influence on the overall energy lost, which is expected. Reducing the damping ratio will result in more damage to the footing because more energy needs to be absorbed by the footing with a concomitant reduction in energy loss due to damping.

Figure 4-10 shows that as the lateral stiffness of the footing approaches zero, the Rayleigh damping coefficient a_0 reduces and the coefficient a_1 increases. There is a reduction in the influence of the mass component on the Rayleigh damping matrix $[C]$ as the stiffness of the footing reduces with a subsequent increase in the influence in the stiffness component on the Rayleigh damping matrix $[C]$.

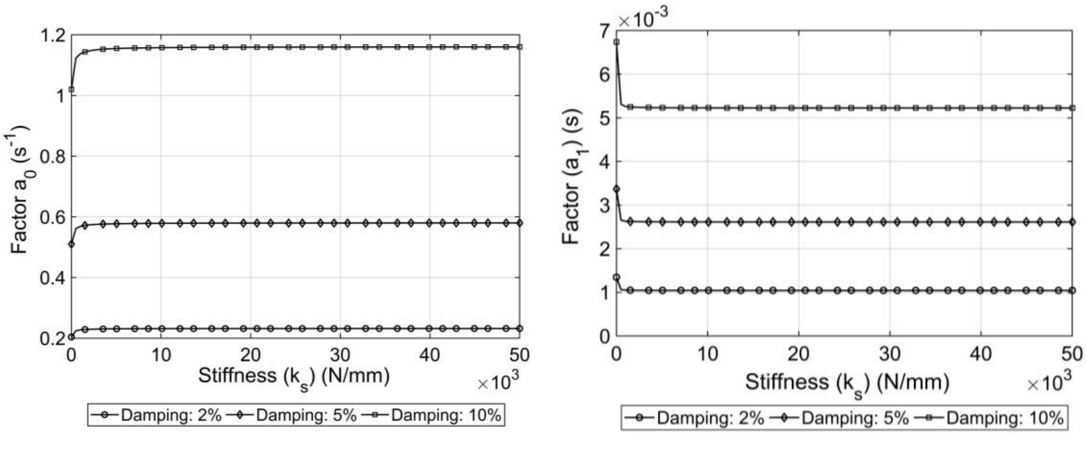

(a) **(b)**

Figure 4-10 Variation of Rayleigh damping coefficients versus the initial elastic horizontal stiffness of the reinforced concrete footing

The selection of the initial stiffness of the footing that was used for the pseudo-dynamic experiments was not critical, particularly when selecting an initial stiffness that is greater than the predicted stiffness of the reinforced concrete footing. However, the selection of damping ration has a significant influence on the amount of energy absorbed by the frame structure and the subsequent damage suffered by the reinforced concrete footing. Using this information and the initial stiffness obtained from the cyclic load tests, the Rayleigh damping coefficients with 5% damping was calculated as follows:

$$a_0 = 0.59\ s^{-1} \ \text{ and } \ a_1 = 0.0256\ s$$

4.3 PSEUDO-DYNAMIC ANALYSIS HYSTERETIC TEST RESULTS

The hysteretic curves for each of the pseudo-dynamic experiments are discussed in this section. Figure 4-11 shows the five linear elastic response spectra for each of the scaled El Centro ground motion records that were used to perform the pseudo-dynamic experiments. The fundamental period of vibration of the structure used during the pseudo-dynamic tests was equal to 0.86 s and calculated using the initial elastic stiffness of the footing. However, the building period formula given by Equation 2.15 produces an approximate fundamental period of vibration equal to 0.40 s for a two-storey steel structure, which is lower than the calculated value determined in Chapter 3. The disparity is likely due to the simple configuration of the frame structure as well as ignoring the stiffness contribution of the concrete slabs in the frame structure and the stiffness of the masonry infill panels when calculating the structural stiffness matrix. However, similar pseudo-accelerations (PSa) are produced by using either fundamental period of vibration from the response spectrum determined using the El Centro ground motion record.

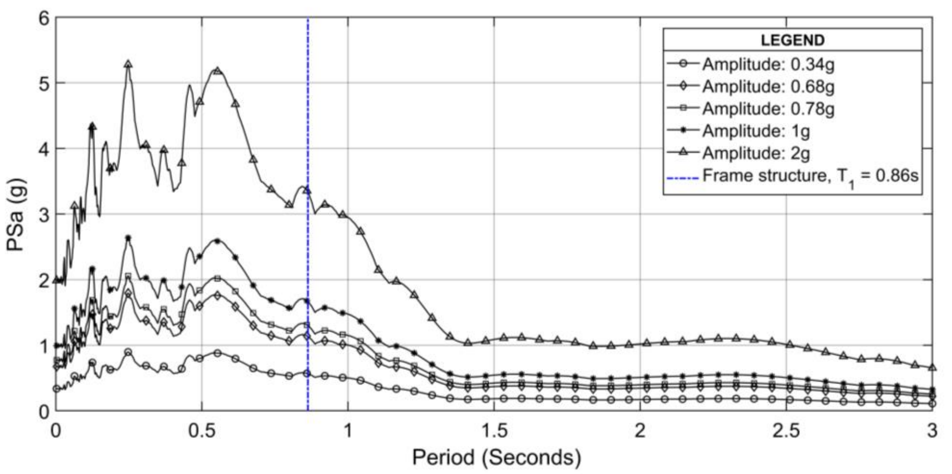

Figure 4-11 Elastic response spectra for each of the scaled El Centro earthquake records

Figure 4-11 also indicates that the fundamental period of vibration of the structure has a considerable influence on the overall response of the structure. A larger fundamental period of vibration of the structure will result in a lower shear force being applied to the top of the footing with a concomitant increase in the lateral deflection of the structure. Reducing the fundamental period of vibration indicates a stiffer structure that generally results in larger shear forces being placed on the footing and a subsequent increase in damage suffered by the footings.

4.3.1 SPECIMEN 1 – 0.34 G PEAK GROUND ACCELERATION

The first pseudo-dynamic test was undertaken at a maximum peak ground acceleration of 0.34 g and continued for the full duration of the El Centro earthquake record. The experiment took 5 hours and 8 minutes to run the full 53.76 s of the amplified earthquake record. Figure 4-12 shows the hysteretic response of the reinforced concrete column that was produced from the pseudo-dynamic experiment and shows that slippage occurred between the base plate and the top of the footing at the start of the applied load. The hysteretic curve of the footing showed a decrease in stiffness at a displacement of 2 mm, which indicates the onset of concrete cracking. Figure 4-13 shows the displacement versus time graph and Figure 4-14 shows the force versus time graph for the duration of the earthquake record. The profiles that are produced by both the displacement versus time graph and the force versus time graph each follow a similar profile of the El Centro ground motion record.

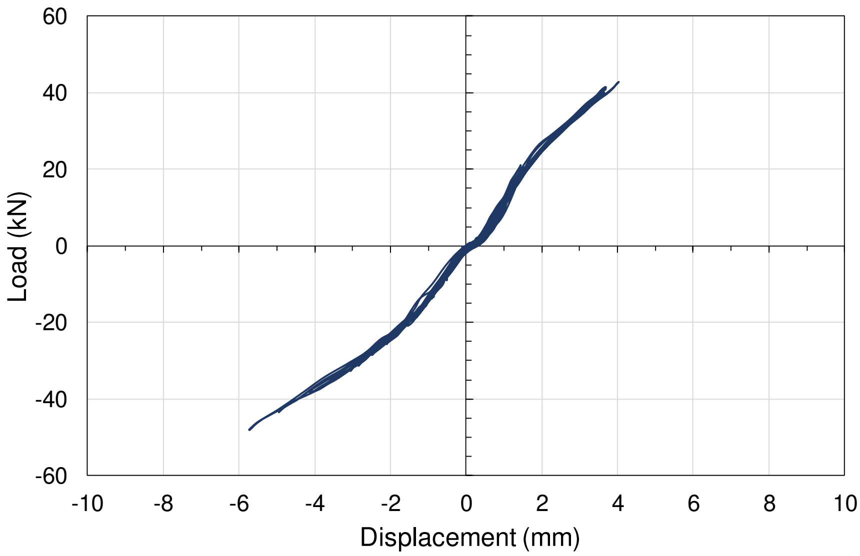

Figure 4-12 Hysteretic response under the El Centro Earthquake scaled to 0.34 g

Figure 4-15 shows a 1 mm horizontal crack opened at the maximum applied lateral displacement on either face of the column in the direction of the applied shear load. Upon load reversal, the cracks closed with some spalling of concrete occurring at the corners of the columns. The response of the footing remains predominantly elastic-perfectly plastic as there was no significant permanent deformation upon unloading. Yielding of the reinforcement did not occur, and none of the reinforcement become exposed by the end of the experiment.

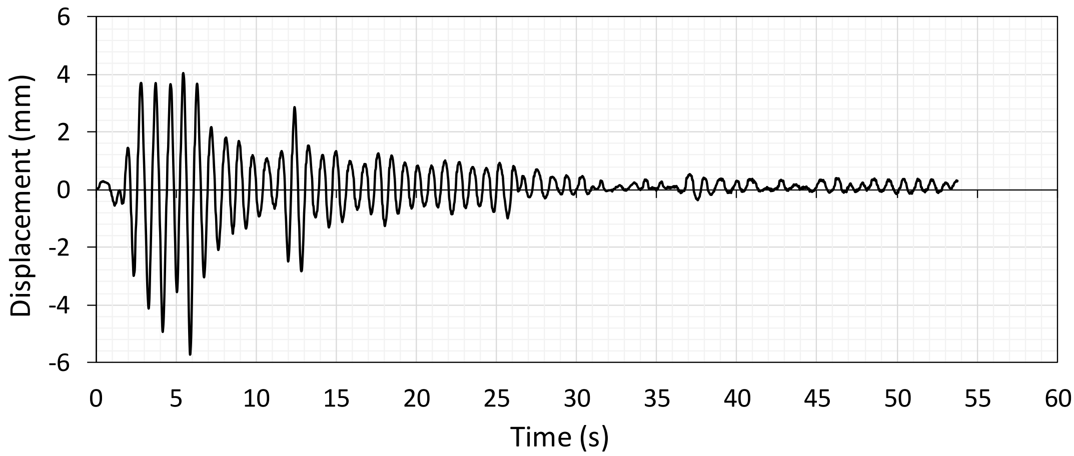

Figure 4-13 Displacement vs time for the 0.34 g experiment

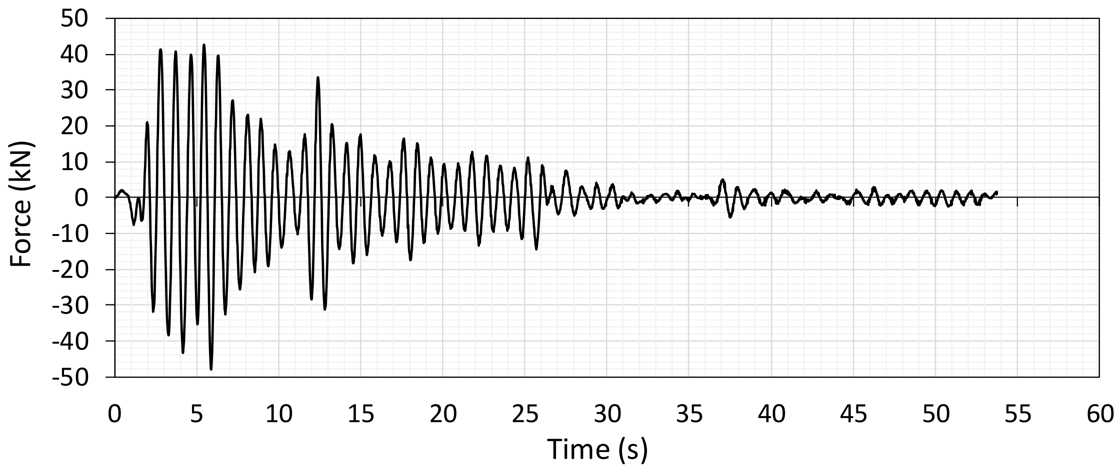

Figure 4-14 Force vs time graph for the 0.34 g experiment

(a) **(b)**

Figure 4-15 Crack patterns at the base of the column at the end of the experiment with (a) the left face of the column and (b) the right face of the column

4.3.2 SPECIMEN 2 – 0.68 G PEAK GROUND ACCELERATION

The second pseudo-dynamic experiment was conducted by amplifying the El Centro earthquake to produce a maximum peak ground acceleration of 0.68 g, with the hysteretic response shown in Figure 4-16. The experiment took 6 hours and 52 minutes to run the full 53.76 s of the amplified earthquake record. Figure 4-17 shows the displacement versus time graph and Figure 4-18 shows the force versus time graph and both follow the profile of the El Centro earthquake ground motion record. The footing did not collapse during the earthquake record, and therefore the full duration of the earthquake record was applied to the structure.

From the hysteretic response, the footing underwent significant deformation resulting in the formation of large cracks on either face of the column in the direction of loading. The reinforcement yielded on either face of the footing, and therefore the maximum shear capacity of the footing was reached. Figure 4-19 shows a crack of 5 mm opening on the left face (the face to which the actuator was connected) of the column at a time of 3.8 s. Figure 4-20 shows visible crushing of the concrete that occurred after 4.8 s on the right face of the column. Although the concrete showed visible crushing and spalling, the footing was still able to maintain the applied axial load of 300 kN by the end of the earthquake record.

The hysteretic response shows that a permanent degradation of lateral stiffness of the footing occurs with an increase in concrete cracking and yielding of the reinforcement. The pinching effect of reinforced concrete was observed. The load path followed upon unloading from the backbone curve shows an initial increase in stiffness at the unloading point from the backbone curve, which approximates to the initial elastic stiffness of the footing. With further reduction in the lateral load, there is an associated reduction in the lateral stiffness of the footing. Upon unloading, the displacement at which the shear force is equal to zero occurs at approximately the same displacement at which the reinforcement first started yielding. Therefore, the displacement at which yielding first occurred can provide an indication of the maximum displacement the structure will suffer by the end of the earthquake provided the structure does not collapse.

It appears that the maximum deformation encountered in either direction of the applied load dictates the extent of stiffness degradation upon unloading and reloading in the same direction. The reloading of the footing in either direction tends to form a parabolic curve with the stiffness decreasing with increasing displacement and the reloading branch tends to the maximum displacement and force that had occurred previously in the direction of loading.

Figure 4-16 shows the cyclic loading that occurred within the bounds of the maximum displacement that had previously being reached and indicates that the same reloading path is followed up until the maximum displacement in the reloading direction is exceeded. Therefore, indicating that the reloading path is governed by the maximum displacement reached in the reloading direction.

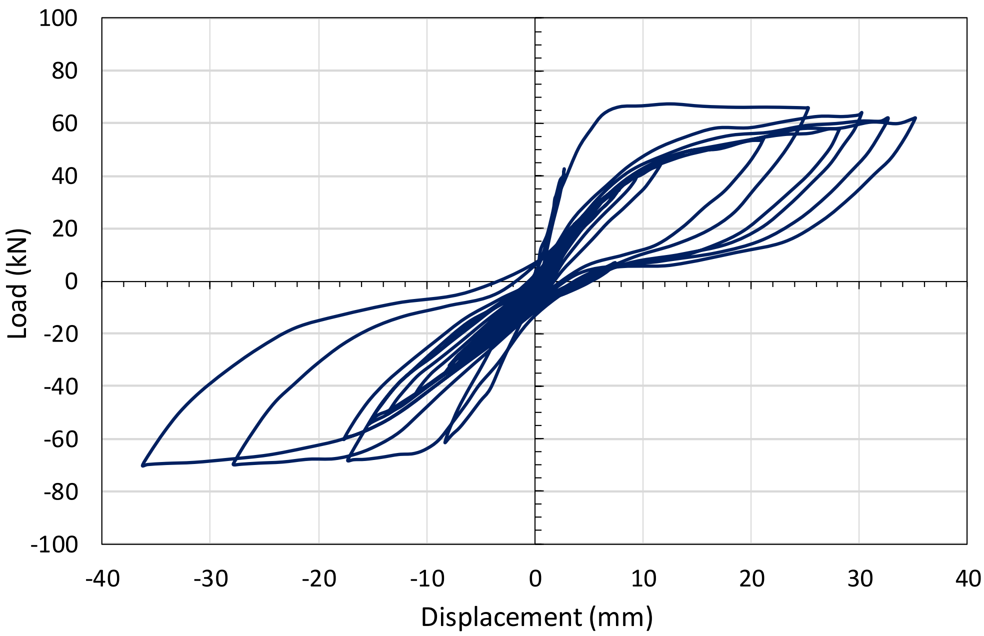

Figure 4-16 Hysteretic response under the El Centro Earthquake scaled to 0.68 g

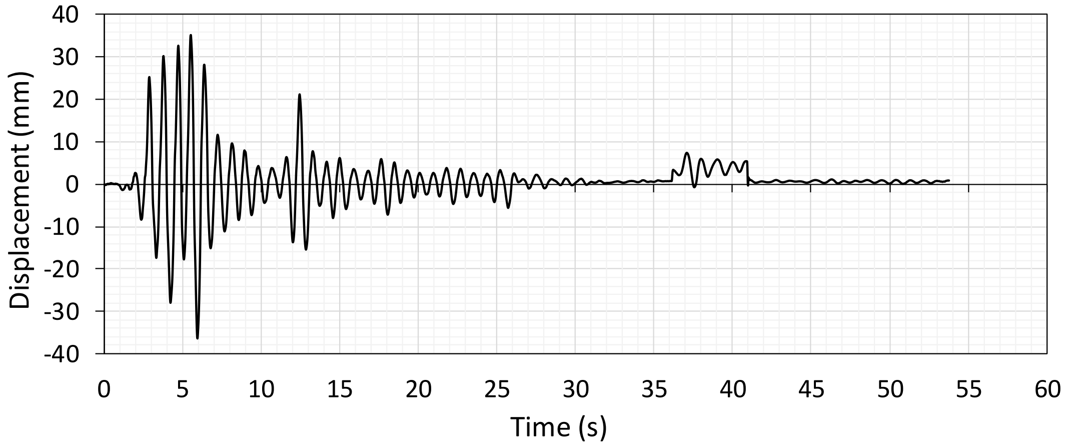

Figure 4-17 Displacement vs time for the 0.68 g experiment

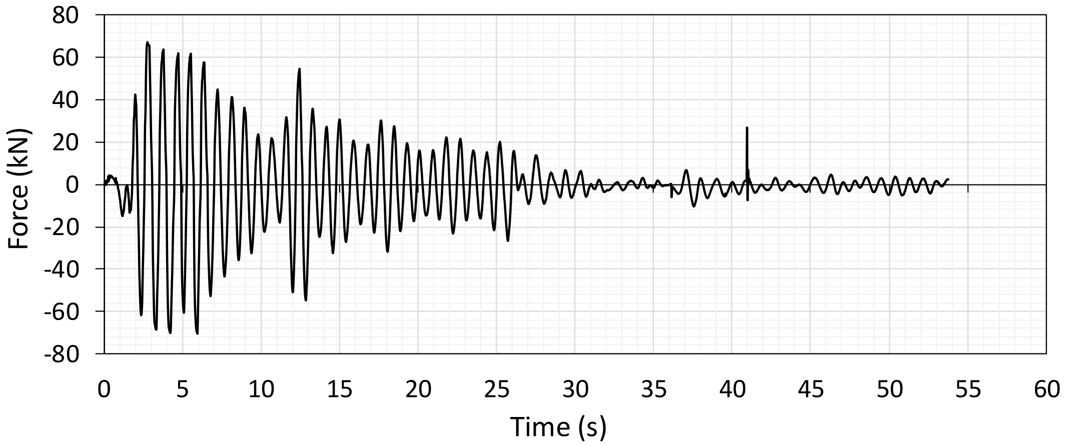

Figure 4-18 Force vs time graph for the 0.68 g experiment

Figure 4-19 Cracking of concrete after the maximum acceleration had been applied to the footing during the El Centro earthquake at 0.68 g

Figure 4-20 Crushing of the concrete after the maximum acceleration had been applied to the footing during the El Centro earthquake at 0.68 g

4.3.3 SPECIMEN 3 – 0.78 G PEAK GROUND ACCELERATION

The El Centro ground motion record was scaled to produce a maximum peak ground acceleration of 0.78 g. The experiment took 45 minutes to run the 5.88 s of the amplified earthquake record. Figure 4-21 shows the resultant hysteretic response of the footing obtained from the pseudo-dynamic experiment. Figure 4-22 shows the displacement versus time graph and Figure 4-23 shows the force versus time graph, which both show that the displacement and force follow a similar profile to the El Centro earthquake ground motion record. Upon reaching the maximum earthquake intensity, large deformations of the column had occurred resulting in the reinforcement yielding and the maximum shear capacity of the footing having been reached.

Figure 4-24(a) shows the initial crack patterns on the left face (the side of the actuator) and Figure 4-24(b) shows the initial crack patterns and spalling of the concrete on the right face of the columns (opposite face to the actuator) before exceeding a lateral deflection of $\pm$30 mm. A reduction in the shear capacity occurred primarily at a lateral displacement exceeding approximately 30 mm. Significant concrete spalling occurred on each face of the column due to the buckling of the tensile reinforcement during load reversal from tension to compression, which had previously undergone significant permanent plastic elongation. The pronounced pinching effect is likely due to the buckling of the reinforcement, which becomes more pronounced as the horizontal load is reduced and the axial load is distributed to the reinforcement prior to closing the crack in the concrete. The loss of compatibility between the permanent elongation of the ductile reinforcement and the cracking of the brittle concrete resulted in the plastically elongated reinforcement carrying all the compression force upon load reversal. For the concrete to become mobilised in compression, the reinforcement would need to buckle, which results in significant spalling of the concrete and the reinforcement becoming exposed. Thus, producing significant observed damage. Most of the concrete spalling occurred on either face of the column due to the buckling of the reinforcement due to the cyclic behaviour and not at the maximum lateral deformation of the column. The points at which significant concrete spalling occurred are shown in the unloading branch in Figure 4-21 where the lateral force approximates -10 kN and shows a substantial reduction in lateral displacement with a relatively small reduction in lateral load. This indicates that the vertical axial load governs the reduction in displacement as the horizontal load is removed, contributing to the pinching effect.

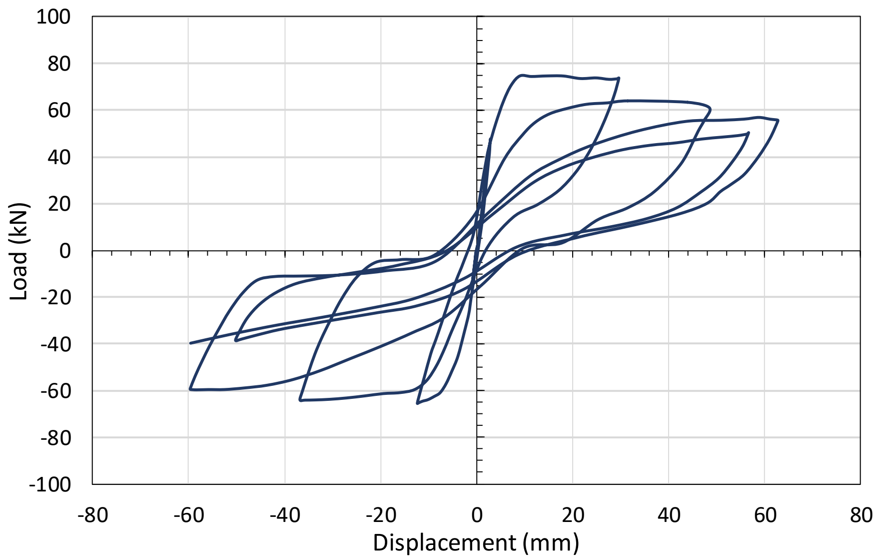

Figure 4-21 Hysteretic response under the El Centro Earthquake scaled to 0.78 g

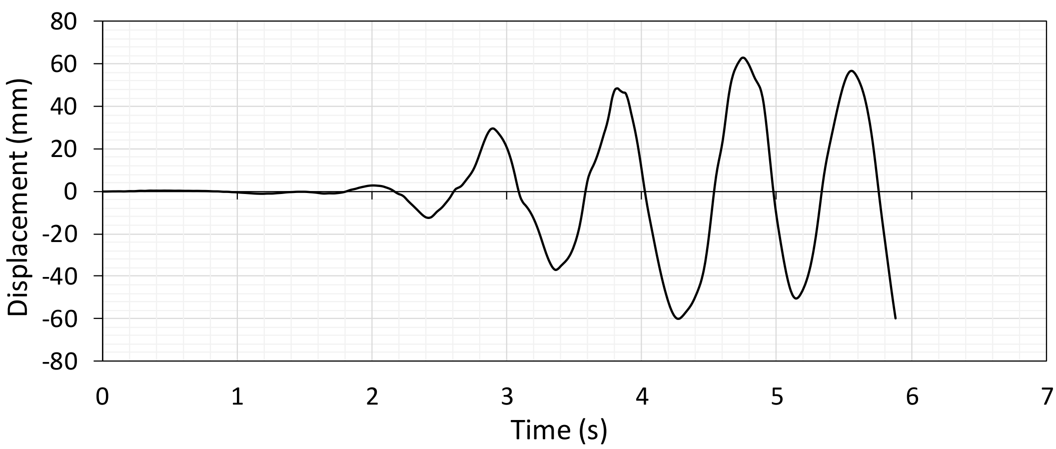

Figure 4-22 Displacement vs time for the 0.78 g experiment

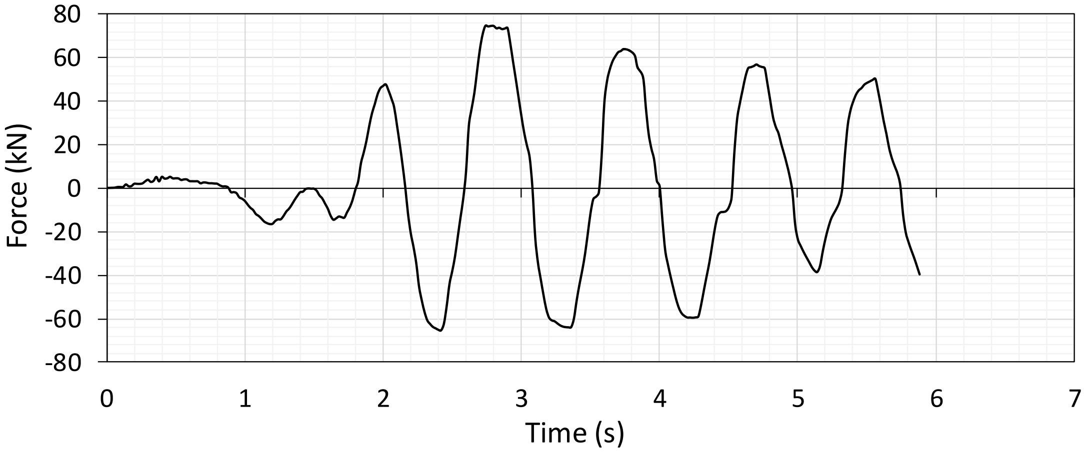

Figure 4-23 Force vs time graph for the 0.78 g experiment

The spalling of the concrete resulted in a reduction in the gross cross-sectional area of the column and the concomitant reduction in the shear capacity of the footing. The lateral resistance of the footing degraded due to the footing being subjected to repeated cyclic loading at large deformations until collapse occurred due to the fracturing of the tensile reinforcement. The column continued to carry the axial load until the cross-sectional area had reduced substantially, resulting in the axial capacity of the footing being exceeded and the subsequent collapse of the structure. Figure 4-25 shows the buckled and fractured reinforcement and Figure 4-26 shows the formation of the plastic hinge at the point of collapse.

(a) Left face **(b) Right face**

Figure 4-24 Initial crack patterns and concrete spalling on (a) left face and (b) right face of the column during the 0.78 g test

(a) (b)

Figure 4-25 Resultant damage to the reinforced concrete footing with (a) outward buckling of the reinforcement and (b) reinforcement fracturing during the 0.78 g test

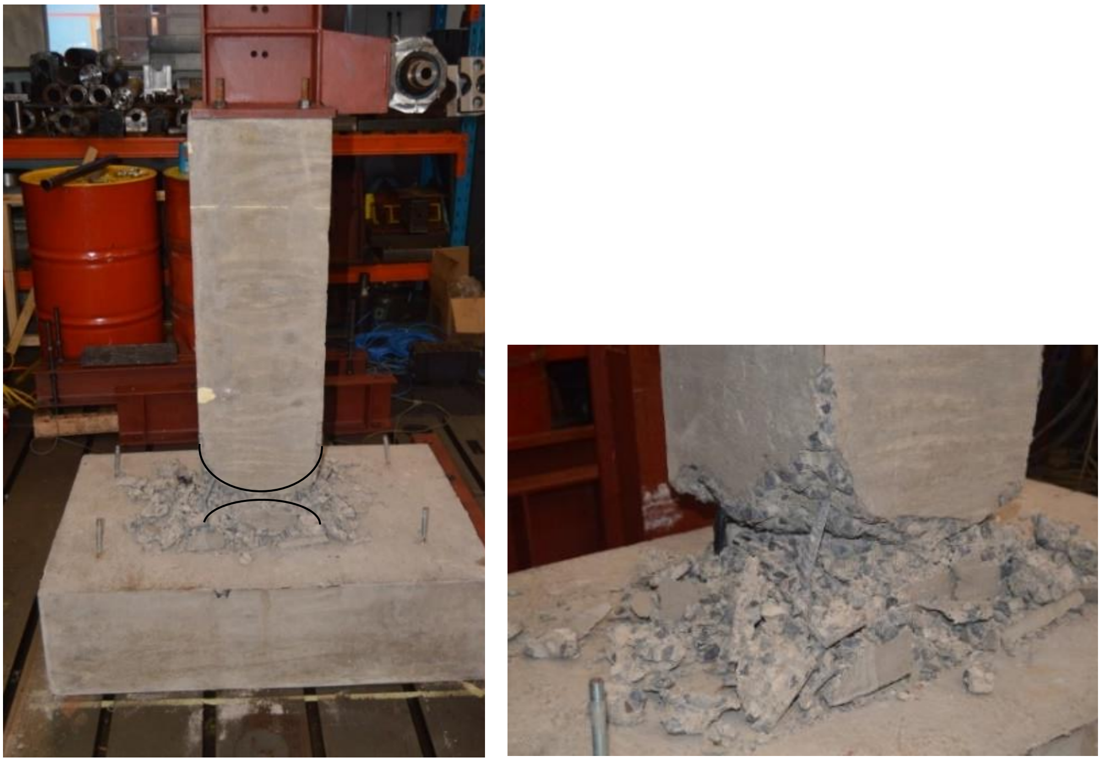

(a) (b)

Figure 4-26 Plastic hinge formation at the base of the column at collapse during the 0.78 g test

4.3.4 SPECIMEN 4 – 1 G PEAK GROUND ACCELERATION

The El Centro ground motion record was scaled to produce a maximum peak ground acceleration of 1 g, and Figure 4-27 shows the hysteretic response produced from the pseudo-dynamic experiment. Figure 4-28 shows the displacement versus time graph and Figure 4-29 shows the force versus time graph and both follow a similar profile to that produced by the El Centro ground motion record. The structure could only sustain a maximum of 2.8 s of the applied earthquake load before failure occurred, which took 37 minutes to run the pseudo-dynamic experiment. However, the maximum peak ground acceleration of 1 g was reached before failure.

The structural failure occurred due to the fracturing of the tensile reinforcement and crushing of the concrete at a horizontal displacement of 62 mm. Figure 4-30(a) shows the horizontal cracking that occurred on the left face at the base of the column and Figure 4-30(b) shows the horizontal cracking that occurred on the right face at the base of the column without any significant spalling of the concrete occurring at the failure displacement. There was no loss in shear capacity before the structure failed, which indicates that the degradation of shear capacity of the footing was dominated by the repeated cyclic loading that is placed on the footing, which results in an increase in concrete spalling. Figure 4-31 shows the crushing of the concrete at the end of the 1 g experiment.

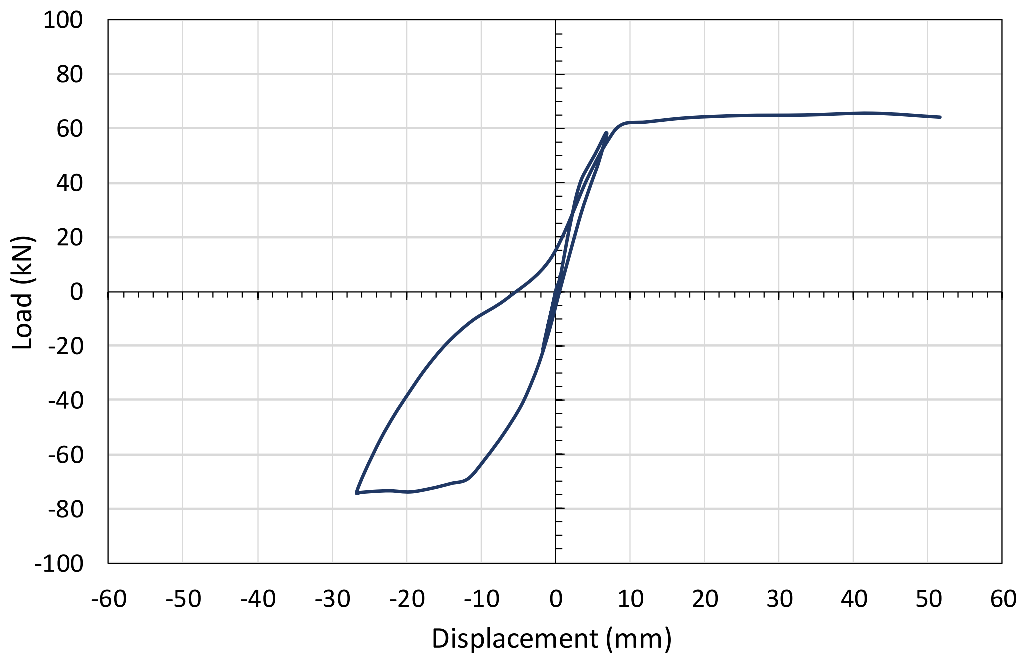

Figure 4-27 Hysteretic response under the El Centro Earthquake scaled to 1 g

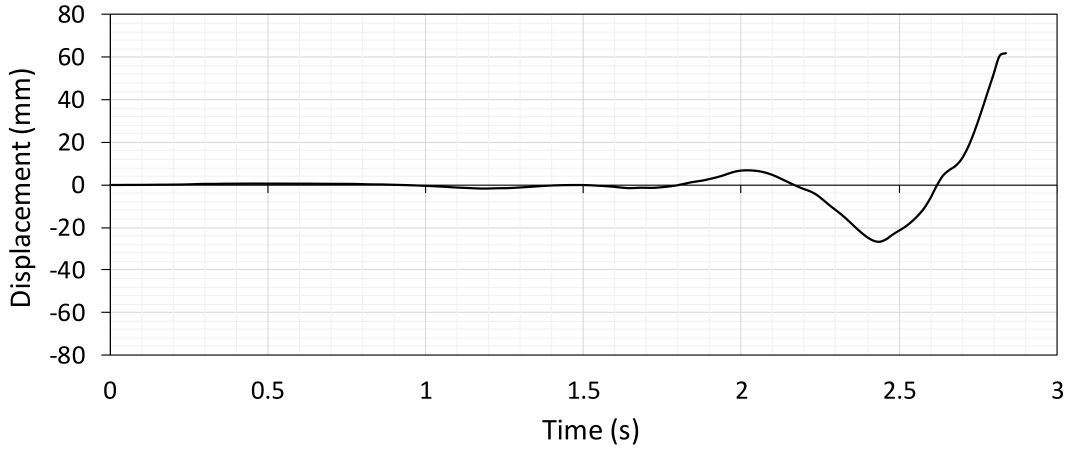

Figure 4-28 Displacement vs time graph for the 1 g experiment

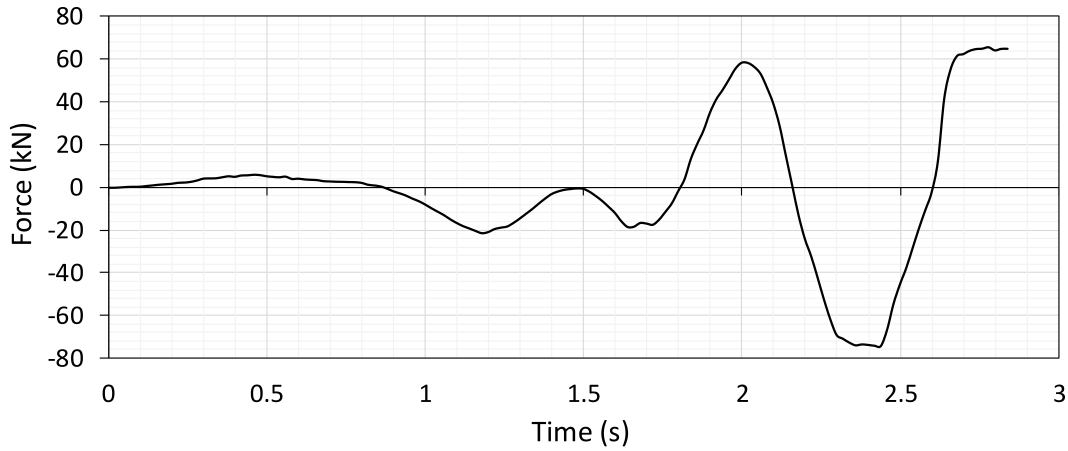

Figure 4-29 Force vs time graph for the 1 g experiment

(a) (b)

Figure 4-30 Damage and cracking to the footing during the 1 g experiment

Figure 4-31 Crushing of the concrete during the 1 g experiment

4.3.5 SPECIMEN 5 – 2 G PEAK GROUND ACCELERATION

The final test was undertaken by scaling the El Centro earthquake record to produce a maximum peak ground acceleration of 2 g, and Figure 4-32 shows the hysteretic response produced during the pseudo-dynamic experiment. The experiment took 33 minutes to run the 2.06 s of the amplified earthquake record. Figure 4-33 shows the displacement versus time graph and Figure 4-34 shows the force versus time graph and both produce a similar profile to the El Centro ground motion record. The footing could only sustain the applied earthquake record for 2.02 s and a maximum peak ground acceleration of 1.21 g before the reinforcement fractured and the footing failed. Therefore, the structure did not achieve a peak ground acceleration of 2 g. The footing remained in the linear region before drifting to the right and achieving a maximum displacement of 62 mm before the reinforcement fractured.

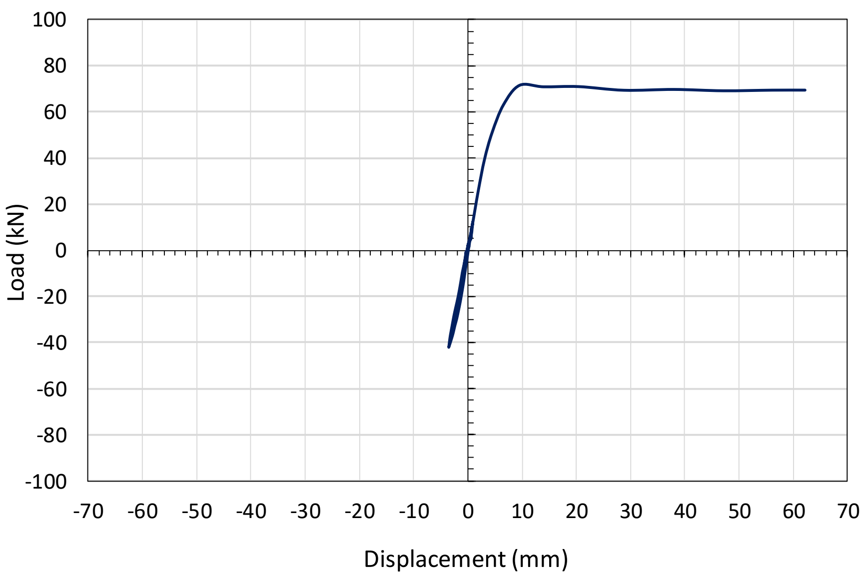

Figure 4-32 Hysteretic response under the El Centro Earthquake scaled to 2 g

Figure 4-35 shows the cracking that occurred on the left face of the reinforced concrete column, and unlike the previous tests, the cracks occurred at approximately 110 mm from the base of the concrete column. Figure 4-36 shows the crushing of the concrete at structural failure and similar to the test carried out at a PGA of 1 g, no significant degradation in shear capacity was observed at the failure displacement.

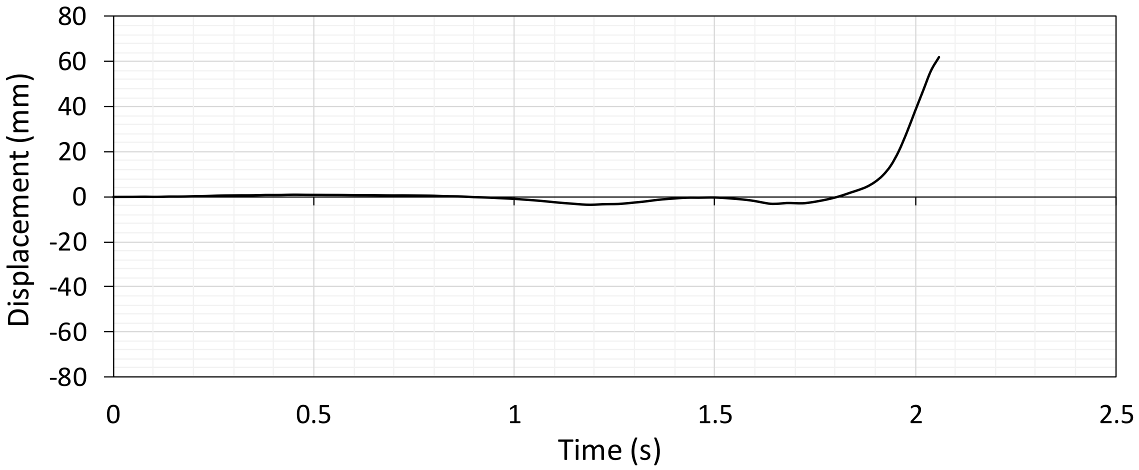

Figure 4-33 Displacement vs time graph for the 2 g experiment

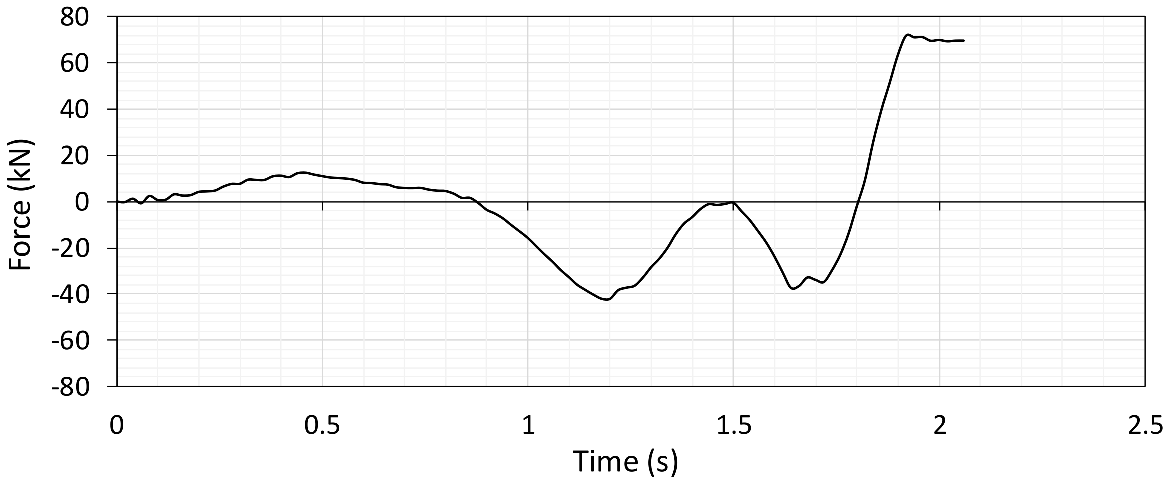

Figure 4-34 Force vs time graph for the 2 g experiment

(a) (b)

Figure 4-35 Cracking of the concrete during the 2 g experiment

Figure 4-36 Concrete crushing during the 2 g experiment

4.3.6 PSEUDO-DYNAMIC ANALYSIS REINFORCEMENT STRAIN RESULTS

The aim of using the strain gauges in the research was to determine the points at which the concrete cracks and the reinforcement yields, and to relate the data obtained from the strain gauges with the hysteretic curves produced during the pseudo-dynamic tests. The strain gauges performed well at the low peak ground accelerations (PGA) as the strain in the reinforcement remained in the elastic region. At high PGAs, the strain gauges failed soon after the strain exceeded the yield strength of the reinforcement, despite having used high post yield strain gauges with a maximum strain of 10 % to 15 %. Because the strain gauges failed soon after the yield capacity of the reinforcement was reached, the results produced by the strain gauges were not meaningful for the tests at a PGA of 0.68 g and greater. The failure of the strain gauges can be presumed to be caused by the failure of the connecting wires to the strain gauges.

Figure 4-37 shows the strain gauge results for the El Centro earthquake scaled to a peak ground acceleration of 0.34 g. The recorded strain at the base of the column indicates that the yield strain was not reached and that the strain results followed a similar profile to the applied ground motion record. The maximum strain occurred in the right strain gauge, with the maximum strain point lagging the maximum PGA that occurs at 2.14 s during the El Centro ground motion record.

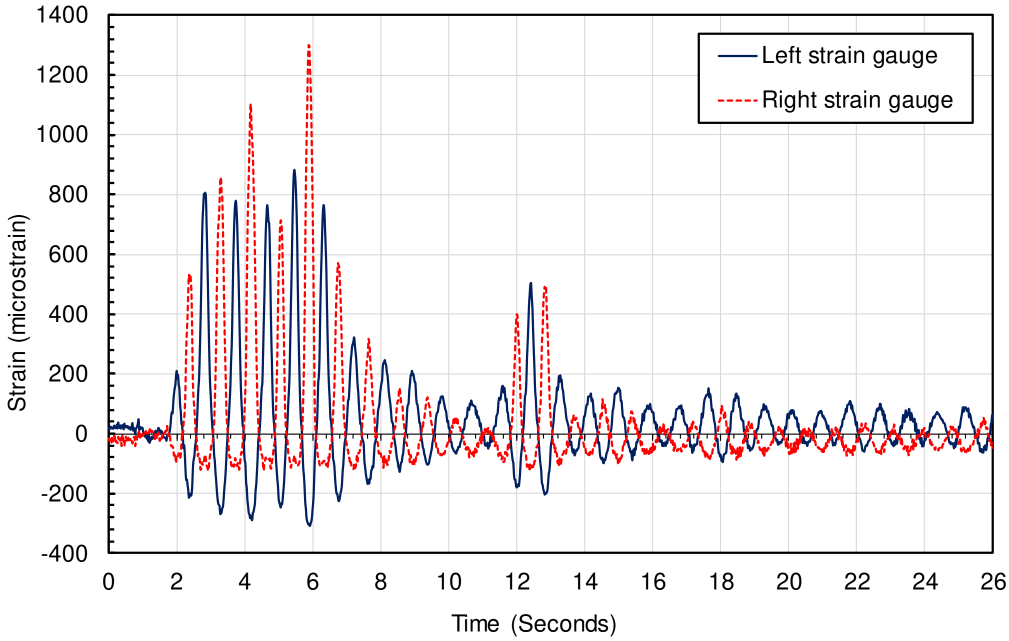

Figure 4-37 Reinforcement strain measurement under the El Centro Earthquake record scaled to 0.34 g

4.3.7 ENERGY-RELATED RESULTS

The amount of energy imparted to the structure due to the earthquake is distributed between the kinetic energy (E_M), damping energy (E_C), strain energy (E_K) and hysteretic energy (E_H). This section shows the distribution of energy within the structure for each of the pseudo-dynamic experiments. Figure 4-38 shows the time history of the total energy imparted to the structure for the duration of each of the scaled earthquake ground motion records during the pseudo-dynamic experiments and is either shown for the entire duration of the earthquake record or until structural failure of the footing. The experiments conducted at 0.34 g and 0.68 g ran for the full duration of the earthquake, whereas the 0.78 g, 1 g and 2 g experiments all failed before completion of the earthquake record. The maximum energy imparted to the structure occurred during the experiment with a maximum peak ground acceleration of 0.68 g and the tests conducted at higher peak ground accelerations showed a reduction in the total energy imparted to the structure before failure of the reinforced concrete footing occurred.

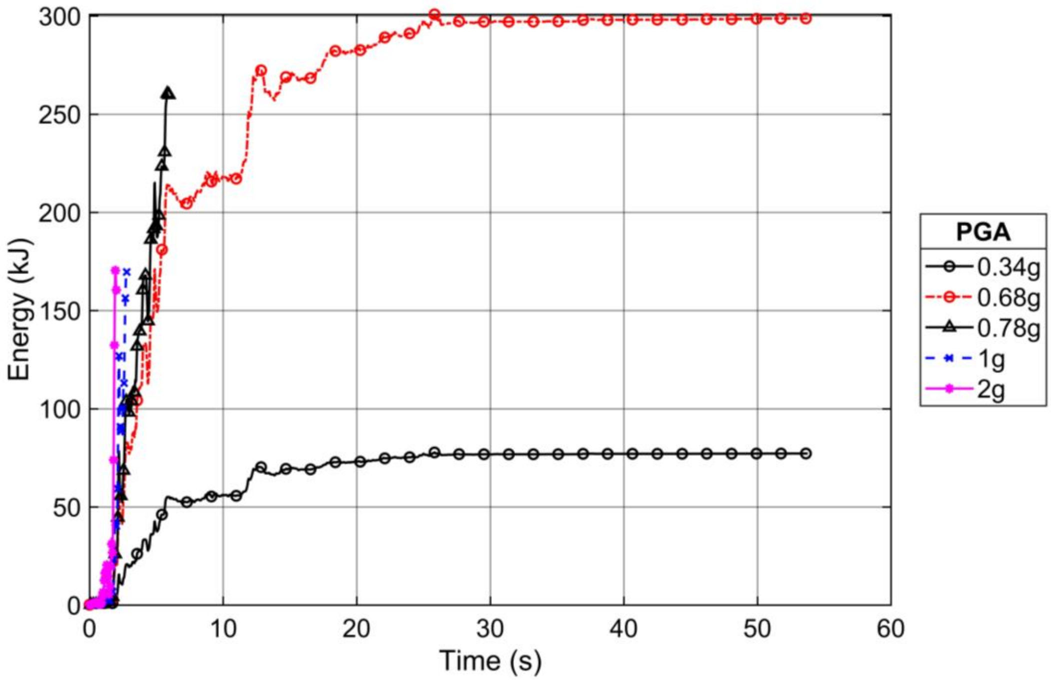

Figure 4-38 Total energy imparted to the structure at the scaled peak ground accelerations (PGAs)

Figure 4-39 shows the total hysteretic energy absorbed as time progressed with the application of the scaled El Centro ground motion record for each of the pseudo-dynamic experiments. The footings that showed more substantial observed damage during the experiments absorbed the largest quantity of energy. The 0.78 g ground motion record resulted in the most observed damage and absorbed the greatest quantity of energy, which can be seen in Figure 4-39. Even though the 1 g and 2 g ground motion records resulted in the failing of the structure, the amount of energy absorbed by the footing is lower than that absorbed by the 0.68 g and 0.78 g PGA earthquake tests.

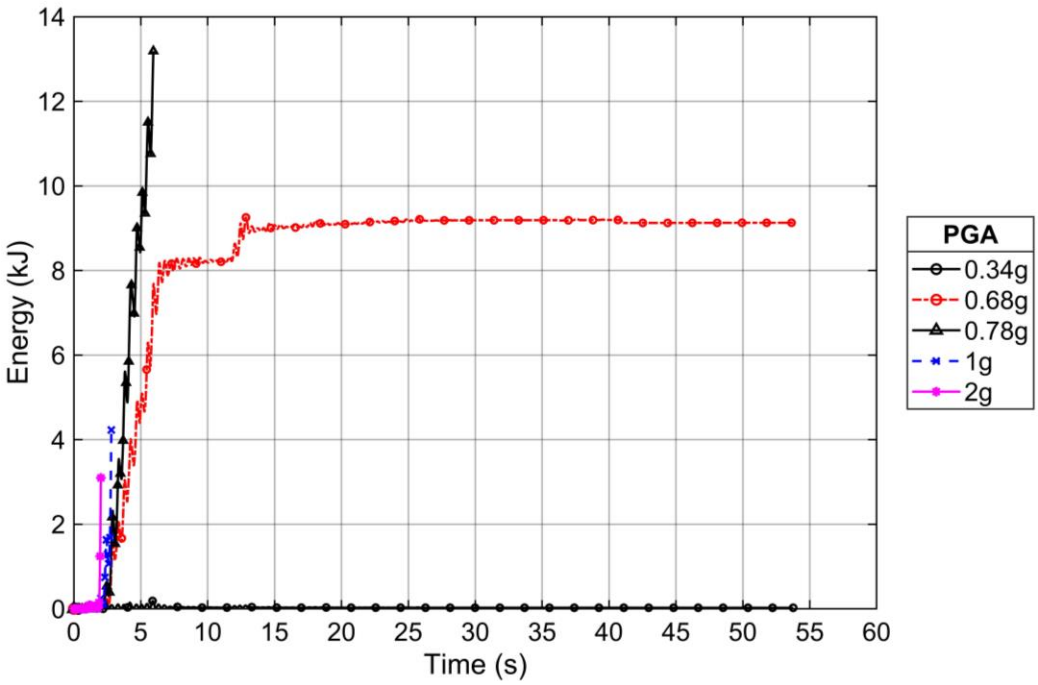

Figure 4-39 Hysteretic energy of the reinforced concrete footings during the pseudo-dynamic tests

Table 4-1 shows the distribution of energy within the structure for each of the scaled amplitudes of the ground motion records, which is either recorded at the end of the earthquake motion record or at the point of failure of the footing during the applied earthquake. For each of the pseudo-dynamic experiments, the hysteretic energy absorbed by the footing was determined as a percentage of the total energy imparted to the structure. The 0.78 g earthquake absorbed the largest percentage of the total energy imparted to the structure by the earthquake during the pseudo-dynamic experiment, which correlates with the observed damage regarding cracking and spalling of the concrete. Although the observed damage to the footing subjected to a PGA of 0.68 g was greater when considering cracking and spalling of concrete than that observed by the 1 g and 2 g experiments, the 1 g and 2 g reinforced concrete footings still failed due to the fracturing of the reinforcement and crushing of the concrete. The hysteretic energy absorbed by the footing during the induced ground motion record is a good indicator of the damage incurred by the reinforced concrete member; however, it does not necessarily indicate whether the structure has failed.

Table 4-1 Distribution of energy at the end of the ground motion record or at failure

PGA (g)	Total energy imparted (kJ)	Hysteretic (E_H) (kJ)	Inertia (E_M) (kJ)	Damping (E_C) (kJ)	Strain (E_K) (kJ)	Percentage energy absorbed (%)
0.34	77.3	0.02	0.0	77.0	0.3	0.03
0.68	298.8	9.1	0.0	289.4	0.3	3.1
0.78	259.9	13.2	5.3	182.4	59.0	5.1
1	169.6	4.2	1.1	56.3	108.0	2.5
2 (1.21*)	158.6	3.1	0.2	33.0	122.3	2.0

* The maximum acceleration achieved by the structure before failure

Figure 4-40 and Figure 4-41 show the energy components for the frame structure for the entire duration of the ground motion record scaled to 0.34 g and 0.68 g peak ground acceleration. The structure subjected to the 0.34 g peak ground acceleration resulted in damping absorbing all the energy imparted to the structure. The 0.68 g peak ground acceleration resulted in the footing absorbing hysteretic energy and therefore indicates a correlation between the number of cycles of vibration and the resultant damage in terms of observed concrete spalling, yielding of the reinforcement and buckling of the reinforcement. The ductility provided by the reinforcement has a significant influence on the amount of energy that can be absorbed by the footing before the failure displacement is exceeded. The energy-time histories show that with an increase in the number of cycles of vibration the amount of energy absorbed by the footing is increased as expected. The test at 0.34 g did not absorb a large amount of energy as the footing did not undergo significant lateral deformation and the reinforcement did not yield.

Figure 4-42 to Figure 4-44 show the energy components of the 0.78 g, 1 g and 2 g pseudo-dynamic tests that all failed before the full duration of the amplified El Centro record could be applied to the structure. For the tests at peak ground accelerations of 0.68 g and 0.78 g, the footing underwent a larger number of cycles of vibration in the plastic region of the reinforcement, which consequently resulted in more damage to the footing due to the spalling of the concrete cover. The spalling of the concrete cover occurred predominately due to the buckling of the permanently elongated reinforcement upon load reversal from tension to compression and to a lesser extent due to compression capacity of the concrete being exceeded. The test carried out a 1 g and 2 g had fewer or no cycles of vibration, as shown in Figure 4-43 and Figure 4-44 respectively, before the reinforcement fractured and visually did not experience the same amount of damage in terms of concrete crushing and spalling than that observed from the tests conducted at the lower peak ground accelerations.

It is evident that most of the energy absorbed in the structure is due to Rayleigh damping, with only a small percentage of the overall energy being absorbed by the reinforced concrete footing. The hysteretic energy correlates well with the cumulative damage to the reinforced concrete footing and the observed damage experienced by the specimens during the pseudo-dynamic experiments.

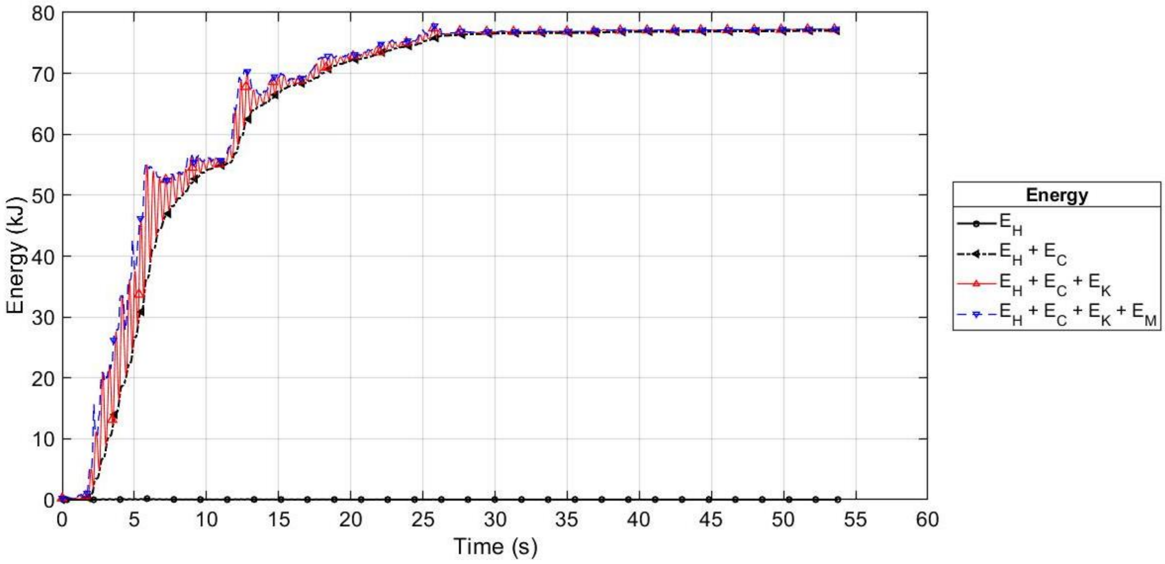

Figure 4-40 Time histories for energy terms during the El Centro earthquake scaled to a PGA of 0.34 g

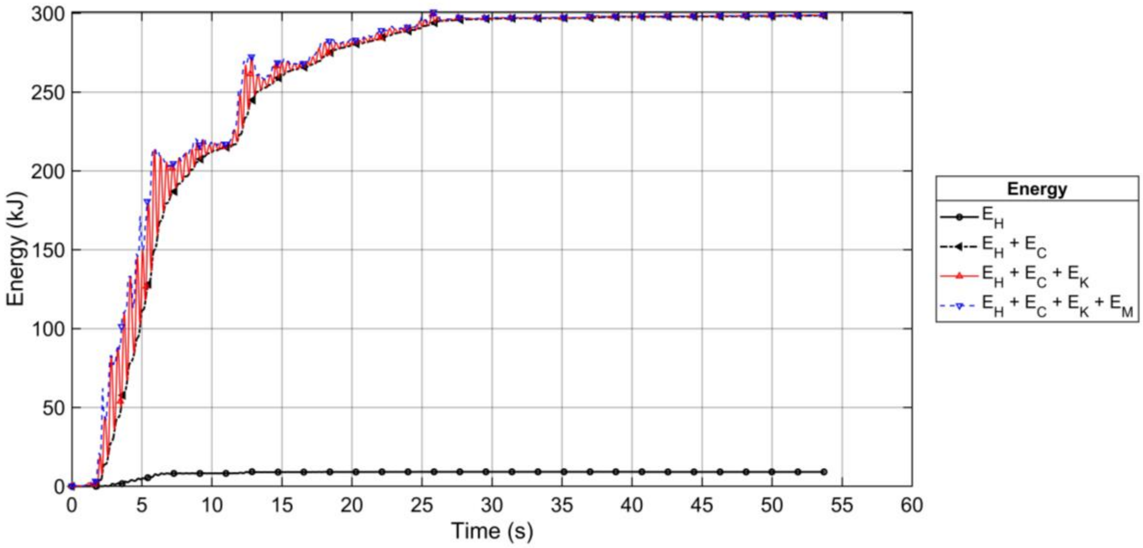

Figure 4-41 Time histories for energy terms during the El Centro earthquake scaled to a PGA of 0.68 g

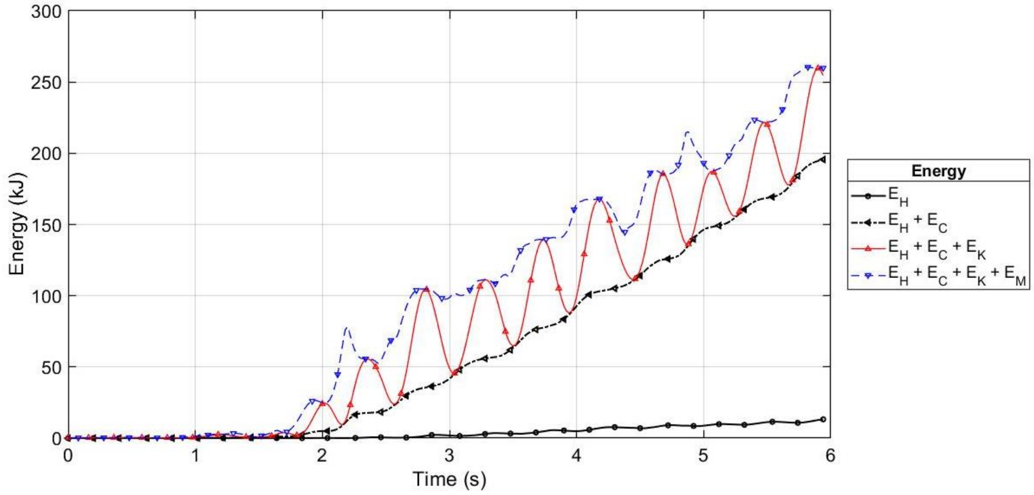

Figure 4-42 Time histories for energy terms during the El Centro earthquake scaled to a PGA of 0.78 g

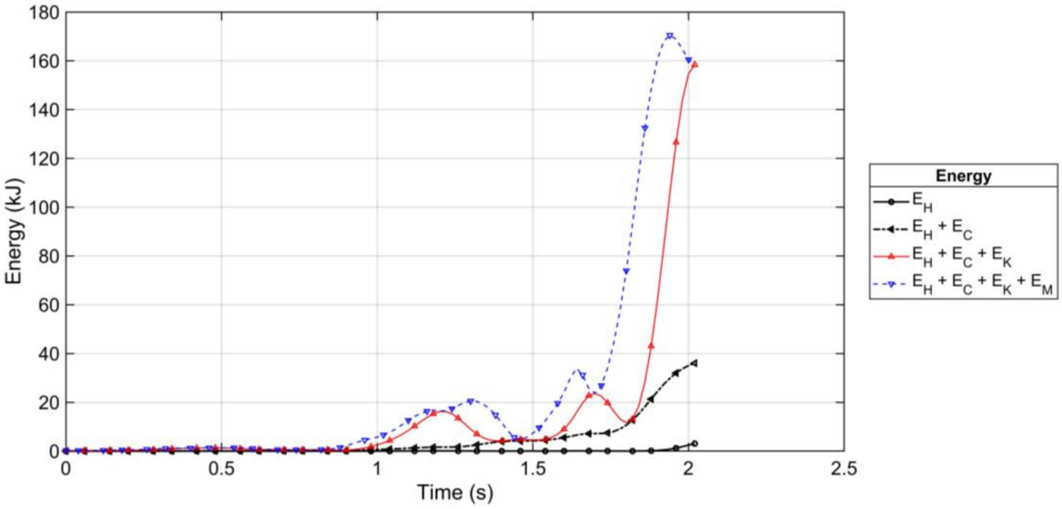

Figure 4-43 Time histories for energy terms during the El Centro earthquake scaled to a PGA of 1 g

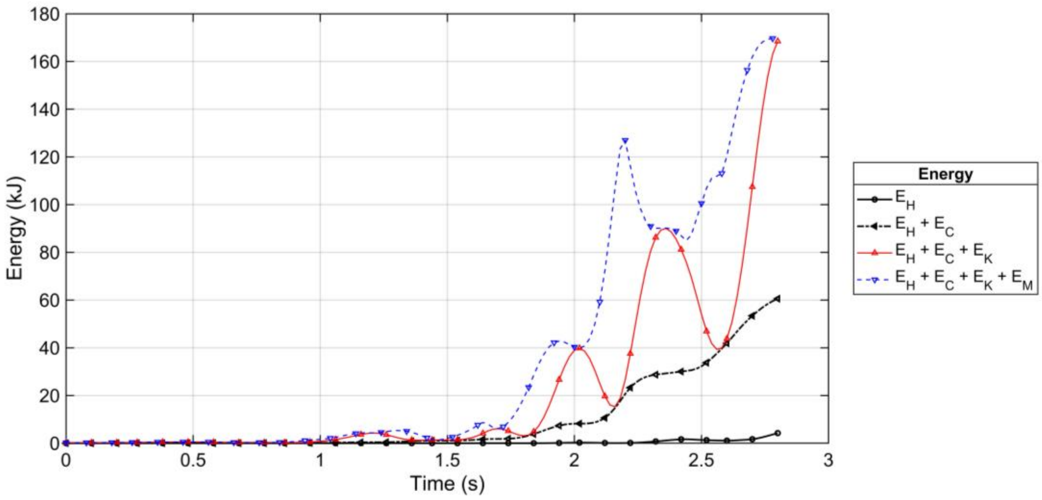

Figure 4-44 Time histories for energy terms during the El Centro earthquake scaled to a PGA of 2 g

4.4 PSEUDO-DYNAMIC ANALYSIS OVERALL STRUCTURE RESPONSE

The response of the overall frame structure is discussed in this section with the results presented for the maximum structural deflections with its corresponding bending moment and shear force diagrams. The resultant axial loads applied to each of the supports are also presented. Table 4-2 shows the moment capacities for the overall frame structure used during the pseudo-dynamic experiments and the strong axis moment of inertia for each of the members.

Table 4-2 Members moment capacities for the steel frame moment resisting structure

Member	Moment capacity M_r (kN.m)	Moment of inertia I_{xx} (mm^4)
305 x 305 118 H-Section (External columns)	586	276 x 10^6
203 x 203 x 52 H-Section (Internal columns)	185	52.5 x 10^6
533 x 210 x 101 I-Section (Beams)	476	616 x 10^6

Figure 4-45 shows the initial deflection of the structure under static loads for all the pseudo-dynamic tests. Under the initial conditions, the horizontal deflection at node 2 was equal to zero due to the symmetry of the loading. Figure 4-46 shows the initial shear force diagram and bending moment diagram of the structure before the earthquake load was applied. The bending moments in each of the members are less than the capacities of the members.

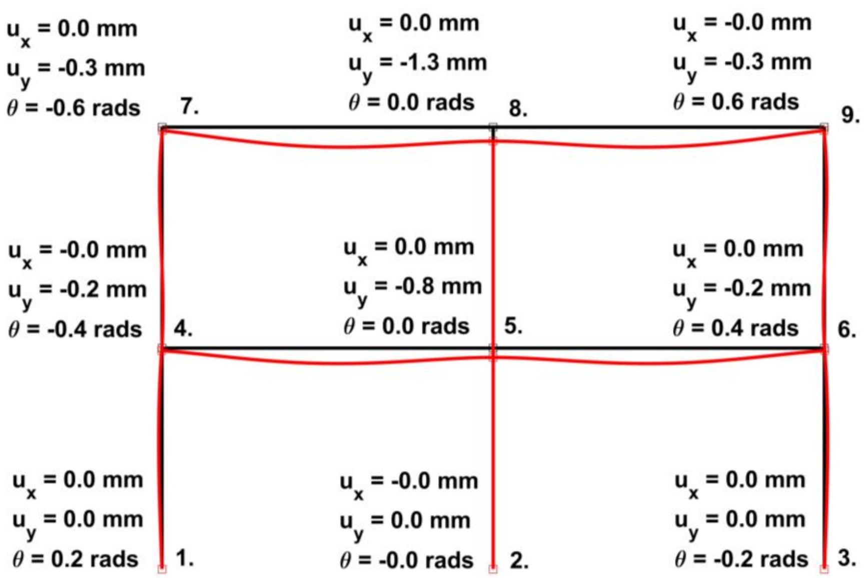

Figure 4-45 Initial deflection of the structure under static loads

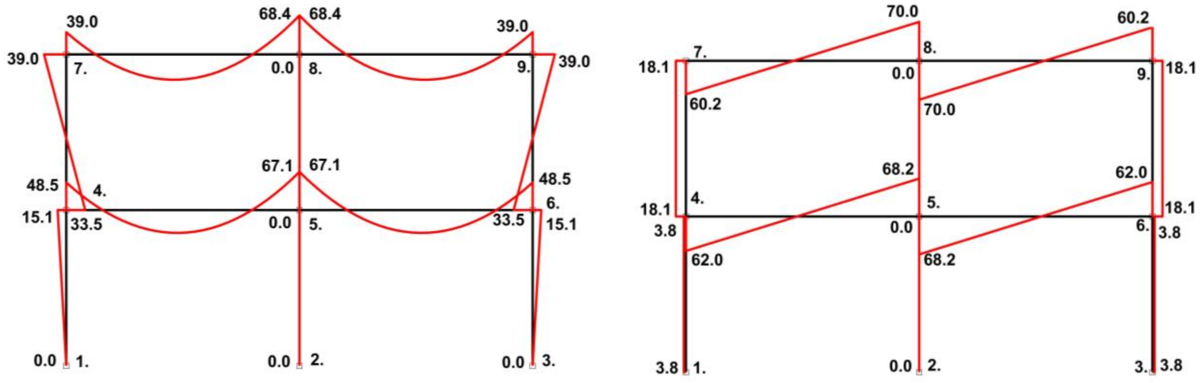

(a) Bending moment diagram

(b) Shear force diagram

Figure 4-46 The initial state of the structure before earthquake loading

Figure 4-48 to Figure 4-56 shows the response of the structure at the maximum displacement reached during the 0.34 g to 2 g peak ground acceleration pseudo-dynamic experiments. As can be seen from Figure 4-48(b), the maximum bending moment reached in the external column and beam exceeds the capacity of the members, and therefore the beam would have failed before the external column due to the beam having a lower moment capacity than the external columns. The maximum bending moment that was reached by the internal column only marginally exceeded the steel member's capacity, and therefore a plastic hinge would have formed resulting in the loss of structural stability with the combination of steel members used to perform the pseudo-dynamic tests.

At a peak ground acceleration of 0.68 g and greater, the maximum bending moment reached in all the steel members exceeded the capacity of the steel members, and therefore the structure would have failed before the footing failed. However, a variation in the design of the frame and the selection of the structural members and connections all influence the behaviour of the overall structure.

Figure 4-57 to Figure 4-61 shows the axial load in each of the supports for the duration of the applied earthquake record. The axial load is shown either for the entire duration of the earthquake loading or until failure of the reinforced concrete footing during the applied earthquake loading. For each of the experiments, the axial load in the centre support (Node 2) is constant, whereas the external footings are subjected to varying axial load for the duration of the earthquake record. The pseudo-dynamic experiment undertaken at a maximum peak ground acceleration of 0.34 g resulted in zero tensile forces in the external columns for the duration of the applied earthquake record. However, the footings subjected to a PGA of 0.68 g and greater all resulted in tensile forces and uplift being experienced by the external footings. The variation in axial load for the duration of the earthquake in combination with the lateral load will result in the performance of the reinforced concrete footing varying substantially. Therefore, it is recommended that future studies focus on the response of the footing that is subjected to both a varying axial and shear load and to investigate the effect this would have on the performance of the foundation. Future studies can also focus on the influence that progressive failure within the superstructure would have on the fragility of the footing as this study only assumed a linear elastic frame structure with 5 % damping.

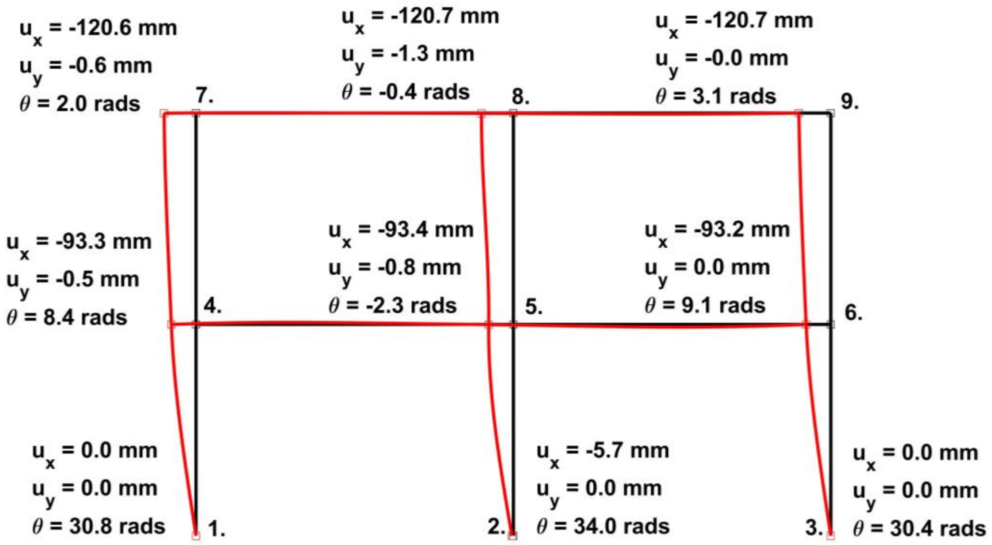

Figure 4-47 Maximum deflection of the overall frame structure at the maximum lateral displacement of the footing at a PGA of 0.34 g

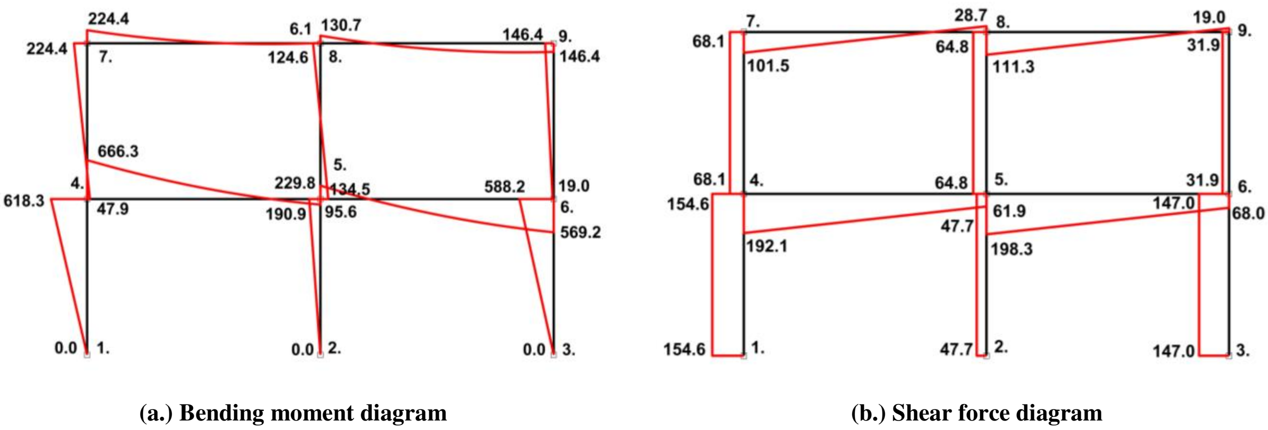

Figure 4-48 Bending moment diagram and shear force diagram at the maximum displacement during the 0.34 g PGA experiment

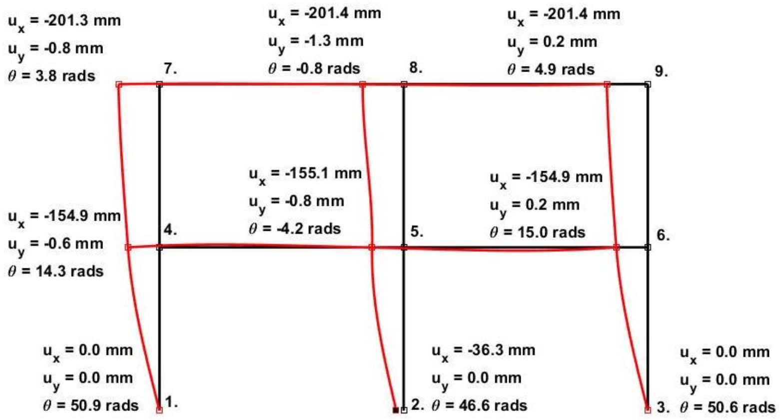

Figure 4-49 Maximum deflection of the overall frame structure at the maximum lateral displacement of the footing at a PGA of 0.68 g

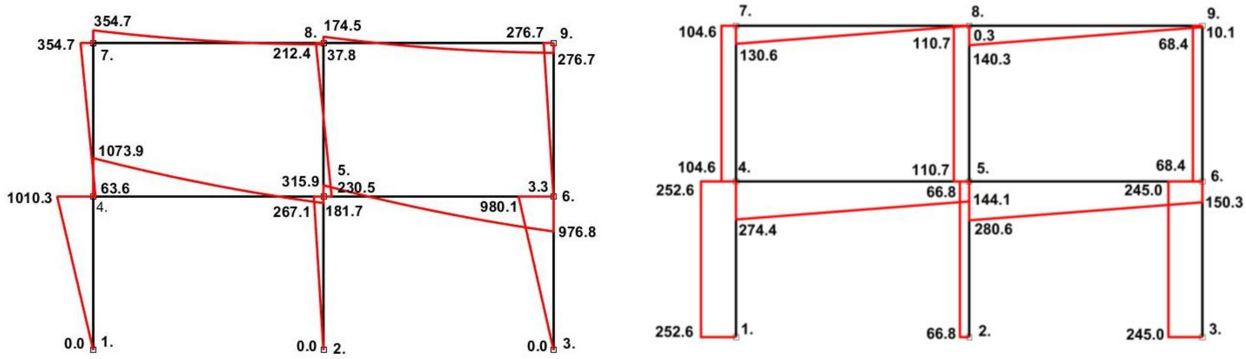

(a.) Bending moment diagram **(b.) Shear force diagram**

Figure 4-50 Bending moment diagram and shear force diagram at the maximum displacement during the 0.68 g PGA experiment

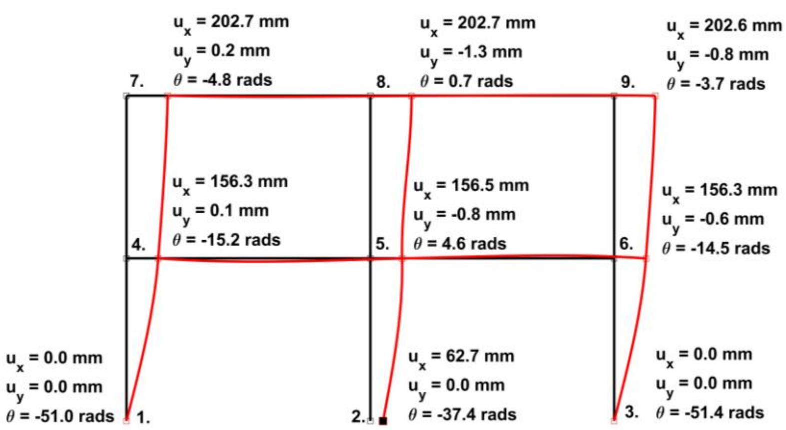

Figure 4-51 Maximum deflection of the overall frame structure at the maximum lateral displacement of the footing at a PGA of 0.78 g

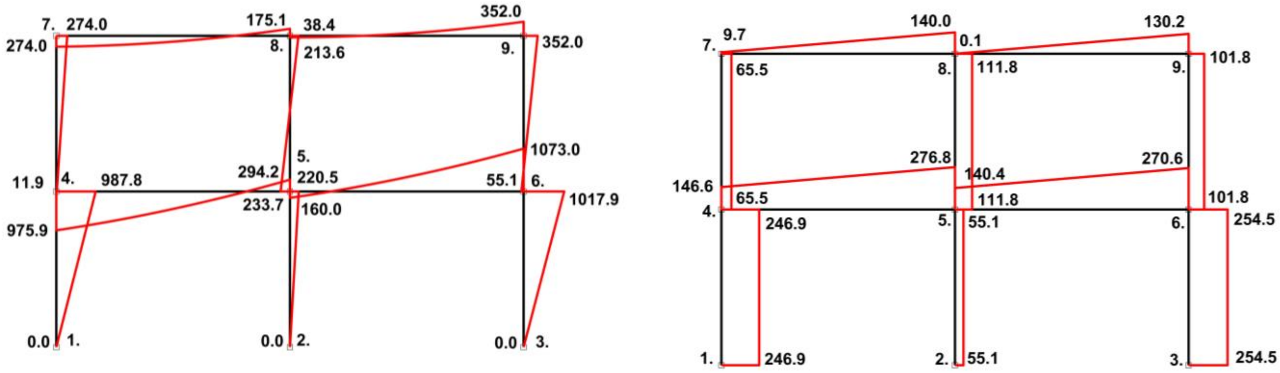

(b.) Bending moment diagram **(c.) Shear force diagram**

Figure 4-52 Bending moment diagram and shear force diagram at the maximum displacement during the 0.78 g PGA experiment

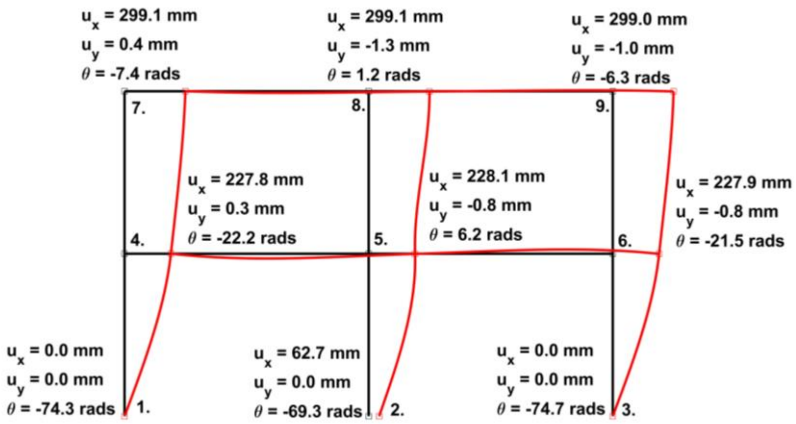

Figure 4-53 Maximum deflection of the overall frame structure at the maximum lateral displacement of the footing at a PGA of 1 g

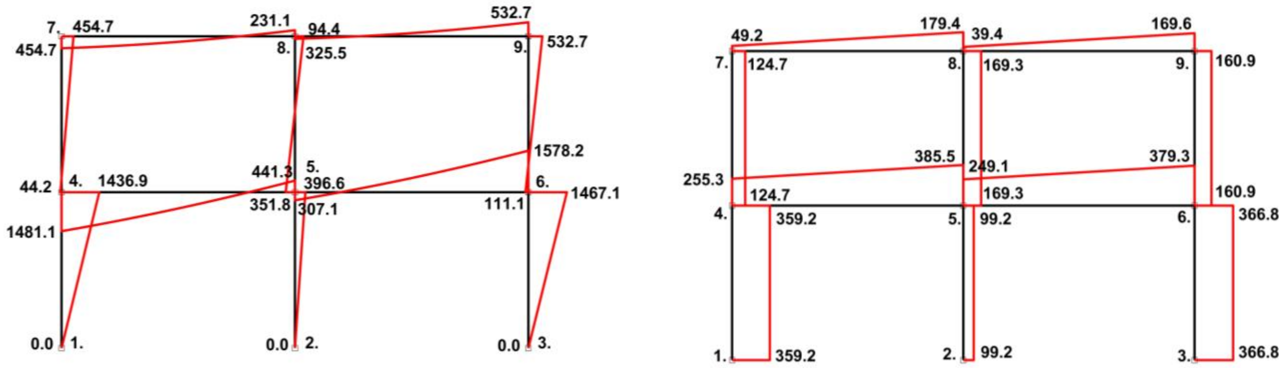

(b.) Bending moment diagram **(c.) Shear force diagram**

Figure 4-54 Bending moment diagram and shear force diagram at the maximum displacement during the 1 g PGA experiment

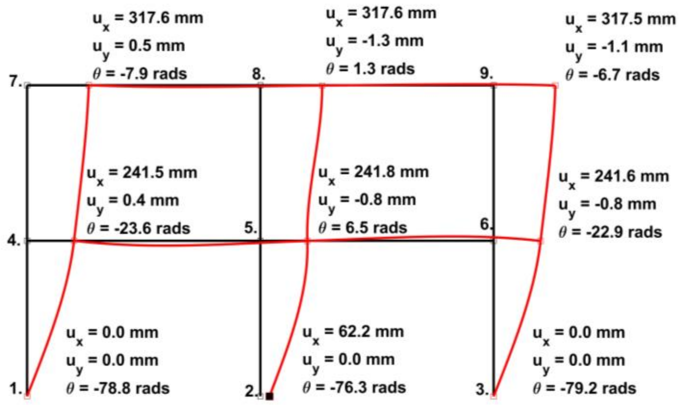

Figure 4-55 Maximum deflection of the overall frame structure at the maximum lateral displacement of the footing at a PGA of 2 g

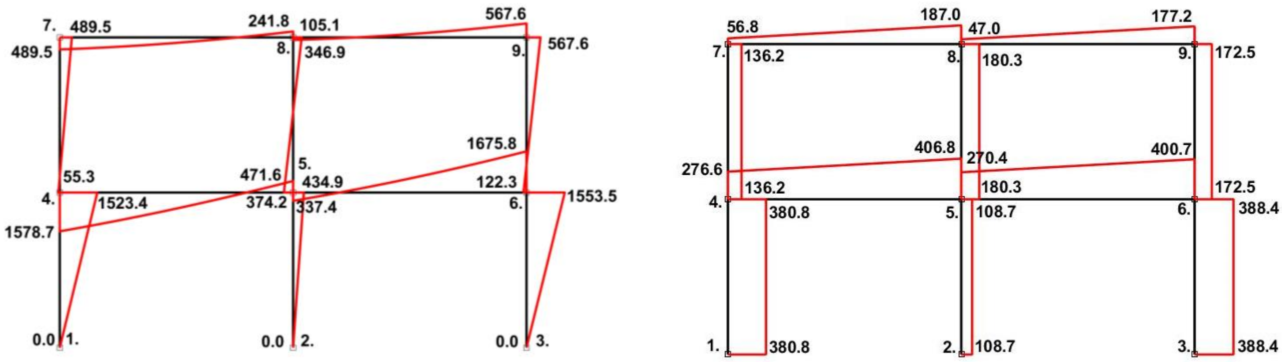

(b.) Bending moment diagram

(c.) Shear force diagram

Figure 4-56 Bending moment diagram and shear force diagram at the maximum displacement during the 2 g PGA experiment

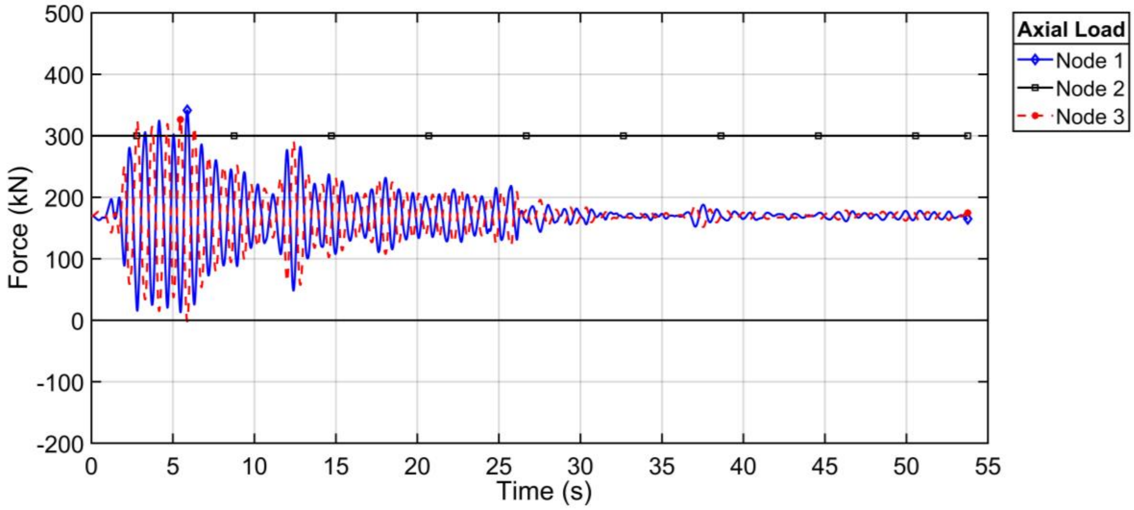

Figure 4-57 Axial force reactions in each of the columns for the duration of the 0.34 g experiment

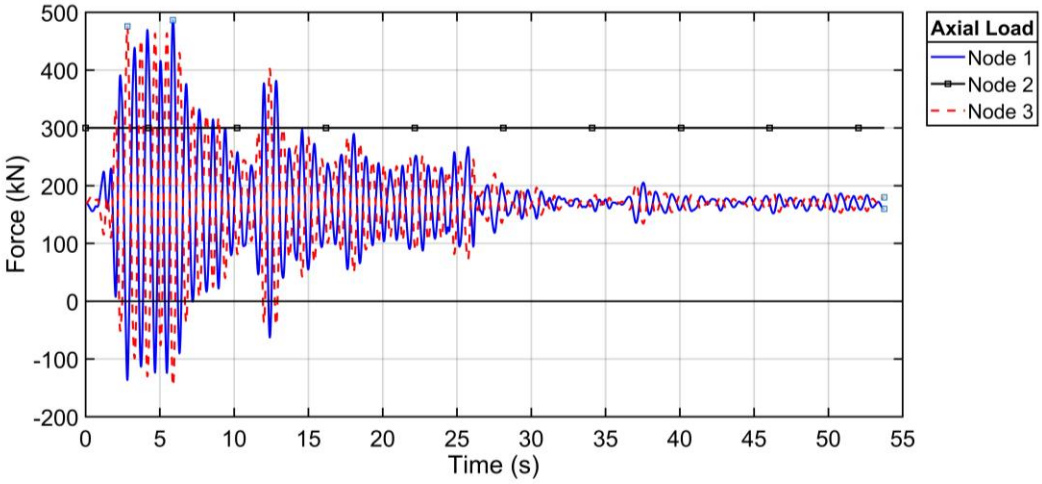

Figure 4-58 Axial force reactions in each of the columns for the duration of the 0.68 g experiment

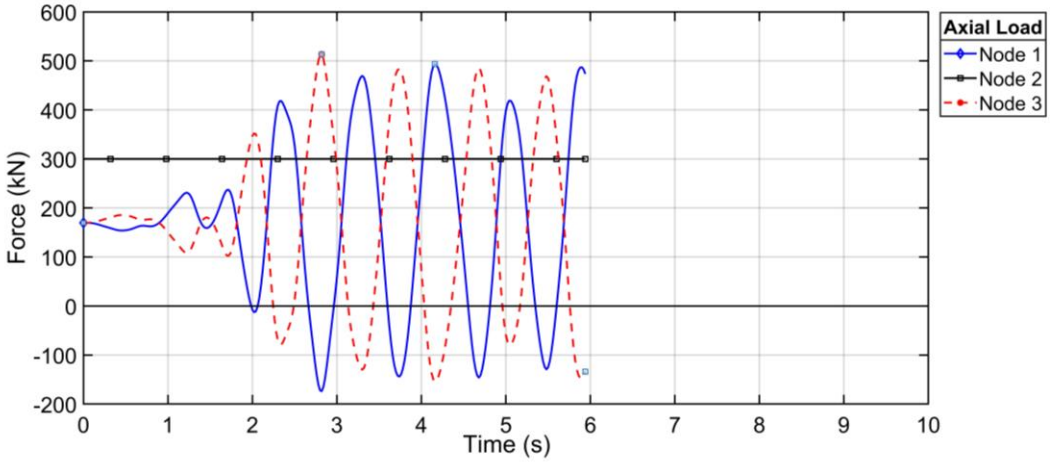

Figure 4-59 Axial force reactions in each of the columns for the duration of the 0.78 g experiment

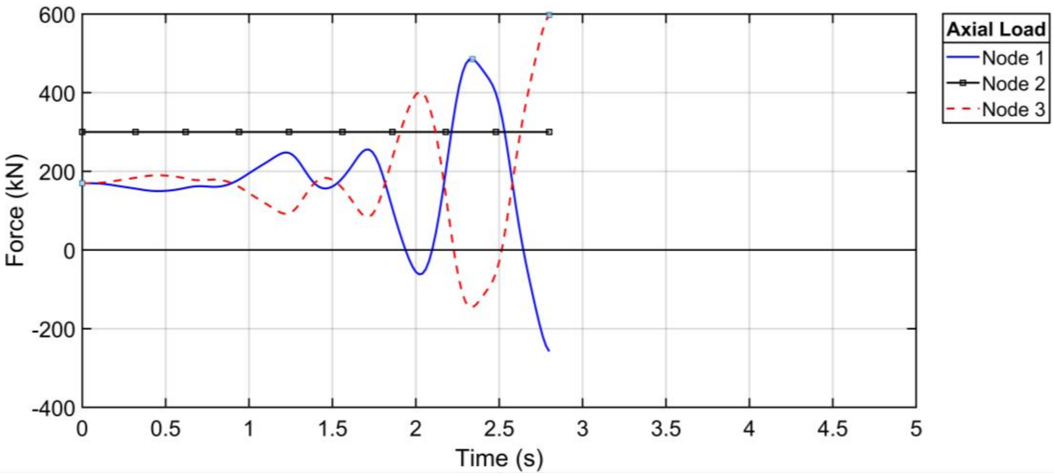

Figure 4-60 Axial force reactions in each of the columns for the duration of the 1 g experiment

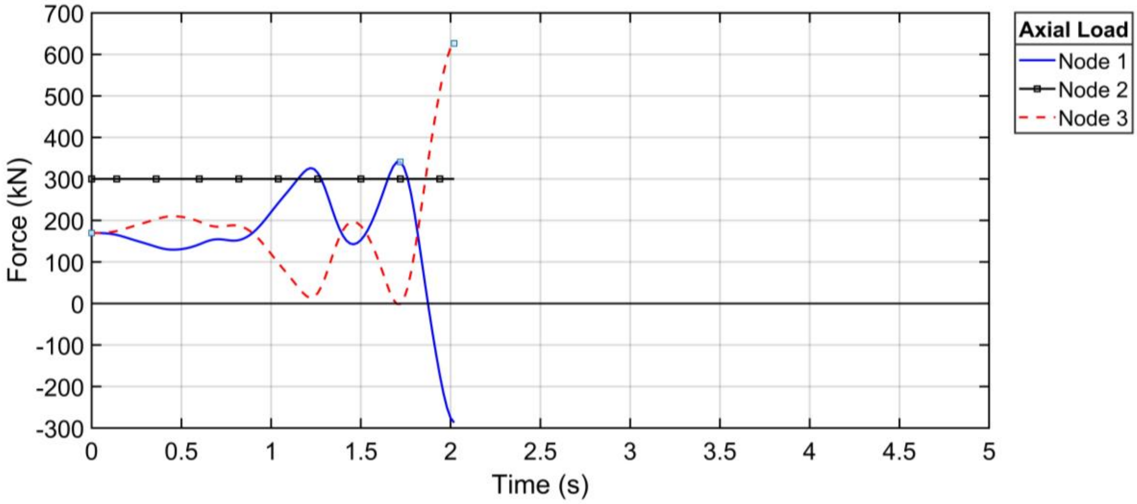

Figure 4-61 Axial force reactions in each of the columns for the duration of the 2 g experiment

4.5 CONCLUSION AND SUMMARY

Pseudo-dynamic experiments were undertaken on five reinforced concrete footing at different peak ground accelerations, which were obtained by amplifying the El Centro earthquake ground motion record. The peak ground accelerations (PGA) ranged from 0.34 g to 2 g. Only minimal cracking resulted at a PGA of 0.34 g, with complete failure having occurred at a PGA of 2 g. Table 4-3 summarises the results obtained during the pseudo-dynamic experiments for the following critical points: the minimum cracking force (F_c) and cracking deformation (u_c), the minimum reinforcement yielding force (F_y) and deformation (u_y), and the maximum achieved force (F_m) and deformation (u_m). The following observations were made during the pseudo-dynamic experiments:

- Increasing the amplitude of the El Centro ground motion record showed that there is a maximum PGA that can be sustained by the footing before failure occurs. For example, the pseudo-dynamic test that was undertaken by amplifying the El Centro ground motion record to produce a PGA of 2 g, only managed to achieve a maximum PGA of 1.21 g before failure occurred;
- An increase in the applied lateral deformation to the reinforced concrete footing results in cracking and yielding of the reinforcement, which in turn results in a reduction in the lateral stiffness of the footing;
- The lateral capacity of the reinforced concrete footing and subsequent damage is predominately controlled by the yield strength and ductility of the reinforcement;

- The ductility of the reinforced concrete footing is controlled by the tensile reinforcement and the shear reinforcement;
- Cracks occurred near the base of the column where the maximum moment was expected, however, the cracks do not always open at the interface between the base of the column and the top of the footing;
- The number of cycles of vibration increases the damage to the reinforced concrete footing, particularly when the load reverses after the reinforcement has yielded in tension;
- Spalling of concrete occurs due to the buckling of reinforcement during load reversal from tensile loading to compression loading on either face of the concrete column in the direction of loading. This occurs due to the incompatibility between the brittle concrete material and the ductile reinforcement. Upon load reversal, the permanently elongated reinforcement is first mobilised in compression before the crack that has formed in the concrete can close and mobilise in compression. To overcome this incompatibility, the reinforcement buckles, resulting in the spalling of the concrete. The spalling of the concrete subsequently results in a reduction in the gross cross-sectional area of the column, which in turn results in a decrease in the axial and shear capacity of the footing;
- The axial load applied to the footing contributes to pinching effect, which was observed in the pseudo-dynamic hysteretic curves. As the horizontal load is reduced the axial load stabilises the column by causing the column to pivot back to its original vertical position and closing the cracks in the concrete;
- The unloading stiffness from the backbone curve of the footing is greater than the reloading stiffness into the backbone curve, which indicates that the structure is absorbing energy and incurring damage;
- Before the reinforcement yields, the response under cyclic loading remains predominantly perfectly plastic without any significant permanent deformation;
- The hysteretic energy absorbed by the footing gives a good indication of damage incurred by the footing under repeated cyclic loading but does not indicate structural failure at large deformations with few or no loading cycles. Therefore, the results correlate with the Park and Ang damage index, as discussed in Chapter 2, that incorporates both damage due to excessive deformation and repeated cyclic loading; and

- The loss of moment capacity due to the formation of a plastic hinge is governed by the repeated cycling of the footing at a displacement less than the failure displacement of the footing and greater than the yielding displacement of the reinforcement.
- Plastic hinges and progressive failure within the frame structure were not considered in the numerical model. However, depending on the capacity of the members used within the frame structure, plastic hinges would have formed, which could have resulted in the frame structure failing before the reinforced concrete footing. The progressive failure of the structure could have altered the response of the footing with increasing earthquake intensity.

Table 4-3 Results from pseudo-dynamic analysis at 5% damping and a natural period of vibration of 0.86 s

Intensity (MMI)	PGA (g)	Cracking (1)		Yielding (1)		Maximum		Damage state
		F_c (kN)	u_c (mm)	F_y (kN)	u_y (mm)	F_m (kN)	u_m (mm)	
7.45	0.34	22.1	1.68	-	-	48	5.72	Onset of cracking, still serviceable
8.29	0.68	40.5	2.48	67.4	6.85	70.3	36.3	Large cracks, extensive damage
8.45	0.78	45.8	2.75	74.6	7.21	74.6	62.7	Collapse
8.75	1	40.84	3.37	62.0	7.41	74	62.7	Collapse
9.59	2 (1.21(2))	35.8	2.47	71.5	7.81	71.6	62.2	Collapse

(1) Minimum lateral force and displacement that results in cracking of the concrete and yielding of the reinforcement

(2) The maximum acceleration achieved by the structure before failure

5 DAMAGE FORMULATION WITH EARTHQUAKE INTENSITY

The aim of this chapter is to show the procedure that was followed to formulate the damage and fragility curves for the analysed reinforced concrete footing, which forms part of an overall linear elastic moment resisting frame structure, by utilising the results obtained from the laboratory experiments in the previous chapter. The results obtained from the cyclic load tests and pseudo-dynamic tests were used to formulate an analytical hysteretic model for the reinforced concrete footing under the constant axial load of 300 kN, which was then used to replace the laboratory test setup. The results produced during the cyclic load tests and pseudo-dynamic experiments were utilised to formulate the hysteretic model to enable the requisite degradation of stiffness and pinching effect of reinforced concrete to be incorporated into the damage formulation at peak ground accelerations and fundamental period of vibration that were not undertaken during the pseudo-dynamic laboratory experiments.

The force value produced from the analytical hysteretic model is used to circumvent the force reading from the load cell in the pseudo-dynamic experiment. The damage to the reinforced concrete footing could be interpolated at amplified peak ground accelerations and overall structural fundamental periods of vibration that were not undertaken during the laboratory experiments by using the pseudo-dynamic testing algorithm in combination with the developed analytical hysteretic model described in this chapter.

5.1 ANALYTICAL HYSTERETIC MODEL

Figure 5-1 shows the numerical hysteretic shear model that was formulated using the limited results produced during the cyclic load tests and the pseudo-dynamic tests to determine the damage states of the footing over a range of earthquake intensities, structural stiffnesses and damping ratios that were not undertaken during the laboratory work. The numerical model was predominately formulated from the results from the second cyclic load test and the trilinear model that is typically used to model reinforced concrete.

The same numerical analysis model that was used to perform the pseudo-dynamic experiments, as previously shown in Figure 3-27, was used to perform the analysis using the formulated hysteretic model. The displacement calculated using pseudo-dynamic computational algorithm was input into the hysteretic model, instead of being applied directly to the test specimen, which then calculates the resultant force that is based on the historical response of the footing at previous time increments.

The hysteretic model for cyclic loading was purely based on the observed results from the experimental analysis that only considered an axial load of 300 kN and the minimally reinforced concrete footing. The accuracy of the model under different axial loads and different structural configurations has not been verified. Three curves can be deduced from the observations made during the cyclic load tests and are shown in Figure 5-1 and described below:

- Primary Curves (PC): Is the backbone curve of the analytical model and produces the same response under monotonic loading. The backbone curve provides the envelope to which the unloading and reloading curves are confined. Two points are defined on the primary curve and represent the maximum displacement points reached in either direction of loading from the initial vertical position of the footing. The maximum deformation in either direction governs the shape of the unloading and reloading curves. The value $\mathrm{u}_{\mathrm{max\_neg}}$ is the maximum negative lateral deformation achieved by the footing from the start of ground motion load application, and $\mathrm{u}_{\mathrm{max\_pos}}$ is the maximum positive deformation achieved by the footing since the start of the earthquake.
- Secondary Curves (SC): Is the response of the footing due to a change in direction from the initial direction of loading along the backbone curve and accounts for the softening of the reinforced concrete due to concrete cracking, yielding of the reinforcement and the pinching effect. The hysteretic analytical model is driven by the maximum positive and negative deformation points ($\mathrm{u}_{\mathrm{max\_neg}}$ and $\mathrm{u}_{\mathrm{max\_pos}}$) along the backbone curve for each time increment as defined in Figure 5-1. The point u_{UL} indicates a point where the path changes from the primary curve to the secondary curve and the point u_{RL} indicates the point where there is a transition from the secondary curve into the primary curve. If the footing is unloading from the positive direction along the backbone curve, then the unloading point $u_{UL} = \mathrm{u}_{\mathrm{max\_pos}}$ and the reloading point is $u_{RL} = \mathrm{u}_{\mathrm{max\_neg}}$, otherwise, if the footing is unloading from the backbone curve in the negative direction, then the unloading point $u_{UL} = \mathrm{u}_{\mathrm{max\_neg}}$ and the reloading point is $u_{RL} = \mathrm{u}_{\mathrm{max\_pos}}$. The response of the footing travels down the path of unloading until it reaches the origin and starts reloading in the opposite direction.
- Tertiary curves (TC): When reloading and unloading occur in the same quadrant without a load direction reversal. The tertiary curve is driven by the point where there is a change in direction from the secondary curve and the initial unloading point from the primary curve.

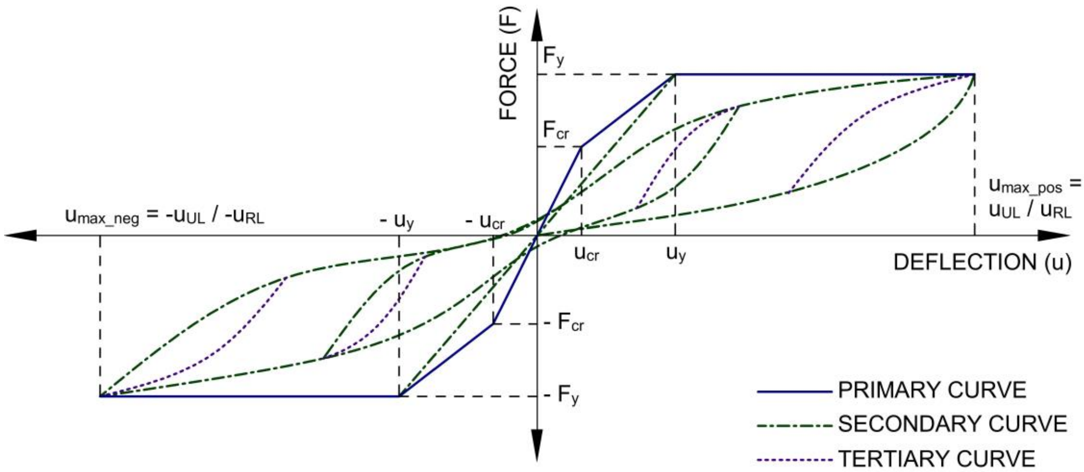

Figure 5-1 Numerical hysteretic shear model showing the primary, secondary, and tertiary curves

Figure 5-2 shows the calculation model used to drive the hysteretic model, which depends on the change in sign of displacement from the final displacement from the previous time increment and the calculated displacement at the current time increment. Using Figure 5-2, a positive change in displacement will result in the path remaining in the same direction as the previous time increment. However, if the change in displacement is negative, it indicates a load reversal whereby the path changes from Path 1 to Path 2. Only the force (F_s) produced from the calculated displacement u_i in the current iteration and time step is used further in the analysis. However, the model also outputs the maximum positive and negative displacement of the footing and the current load path, which is then used in the next iteration or time increment.

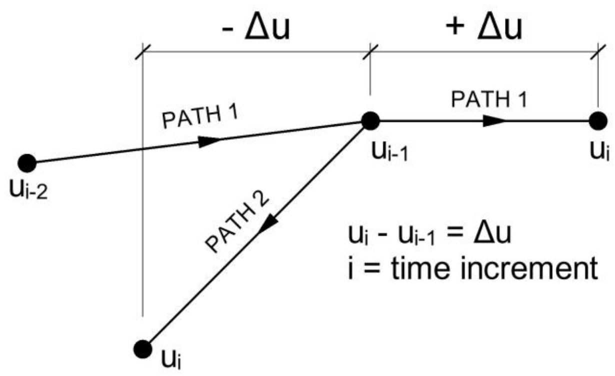

Figure 5-2 Basis of the analytical numerical analytical hysteretic model formulation

5.1.1 PRIMARY BRANCHES

Figure 5-3 shows the primary curve of the hysteretic model, which is the same as the backbone curve produced during monotonic load testing. The primary curve is initialised at the start of the analysis and consists of three regions using a trilinear model:

1. Before cracking, $|u_i| \leq |\pm u_{cr}|$, Region O – A or O – D: the model follows a linear elastic response model.
2. Concrete cracking, $|\pm u_{cr}| \leq |u_i| \leq |\pm u_y|$, Region A – B or Region D – E: after cracking of the concrete in either direction there is a reduction in the stiffness of the cross section. With a continued increase in the load applied to the footing, the loading path follows Path A – B or D – E. However, upon unloading, the path follows region O - A' or O – D' and therefore there is a permanent reduction in the stiffness of the footing due to the cracking of the concrete. Point A' and Point D' then becomes the new reloading point into the backbone curve. If the displacement exceeds the new u_{cr} point, the path will continue along the backbone curve (Path 1). From the cyclic load tests and pseudo-dynamic tests, it was observed that upon unloading, and before the reinforcement yields, the displacement returns to the original position without any permanent deformation. Further experimentation will be needed to verify this, however, for this model the unloading curve follows a linear line from the unloading point on the backbone curve to the origin before the reinforcement yields.
3. Yielding of the reinforcement, $|u_i| \geq |\pm u_y|$, Region B – C or Region E – G: once the displacement of the footing exceeds the yield strength of the reinforcement, the stiffness of the backbone curve becomes equal to zero with a further increase in the displacement. The secondary path is calculated using the maximum displacement achieved on the primary curve and used to interpolate the unloading and reloading curves obtained from the second cyclic load test. If the change in displacement from the current time step and the previous time step is positive $\left(|u_{i,j}| - |u_{i-1}| \geq 0\right)$, where i indicates the time increment and j the iteration step, then the path continues along the backbone curve. However, if the change in displacement is negative $\left(|u_{i,j}| - |u_{i-1}| < 0\right)$, then the unloading displacement follows the secondary curve. The point of unloading along the backbone curve then governs the point of reloading upon load reversal.

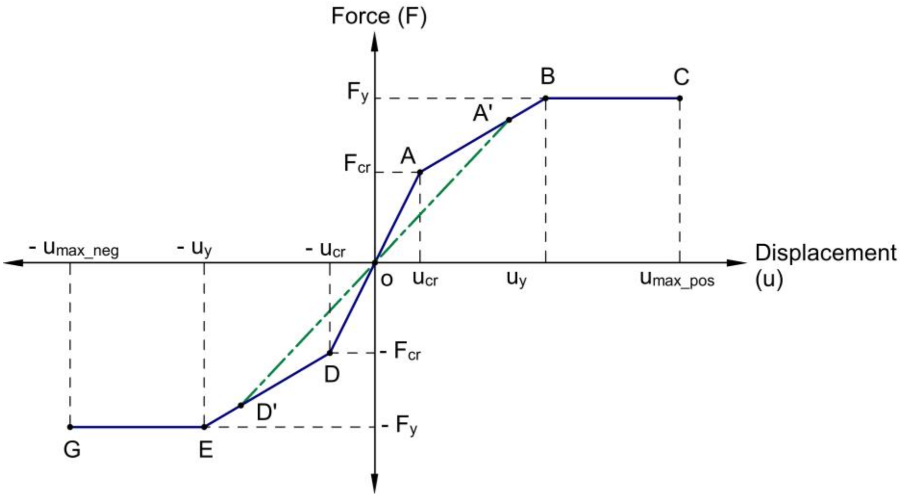

Figure 5-3 Primary curve

5.1.2 SECONDARY BRANCHES: UNLOADING AND RELOADING CURVES

Figure 5-4 shows the unloading and reloading branches of the secondary curves for the analytical hysteretic material, which are driven by the maximum deformations ($u_{\max\_pos}$ and $u_{\max\_neg}$) that have been reached in both directions along the primary curve. The secondary curves account for the degradation in stiffness with each cycle of loading due to the cracking and yielding of the reinforcement.

The unloading branch is defined as a path that is formed upon load reversal whereby the path changes from the primary curve to the secondary curve and tends to have a concave up shape. The maximum slope along the unloading curve occurs at the unloading point along the primary curve and decreases to the minimum slope at the point of zero shear force. The reloading branch is defined as the path that transitions from the secondary curve into the primary curve and tends to have a concave down shape with the maximum slope occurring at the point of zero shear force and the minimum slope occurring at the transition point (u_{RL}) back into the primary curve.

The unloading curves are shown in Figure 5-6 and are tabulated in Table 5-1 and the reloading curves are shown in Figure 5-7 and tabulated in Table 5-2. The unloading and reloading curves were interpolated from the second cyclic load test, as previously shown in Figure 4-5, and compared to the results produced during the pseudo-dynamic experiments. The unloading point along the backbone curve, which occurs due to load reversal, is used to calculate the unloading curve by interpolating the values given in Table 5-1. The reloading point along the primary curve is used to calculate the reloading curve by interpolating the values in Table 5-2.

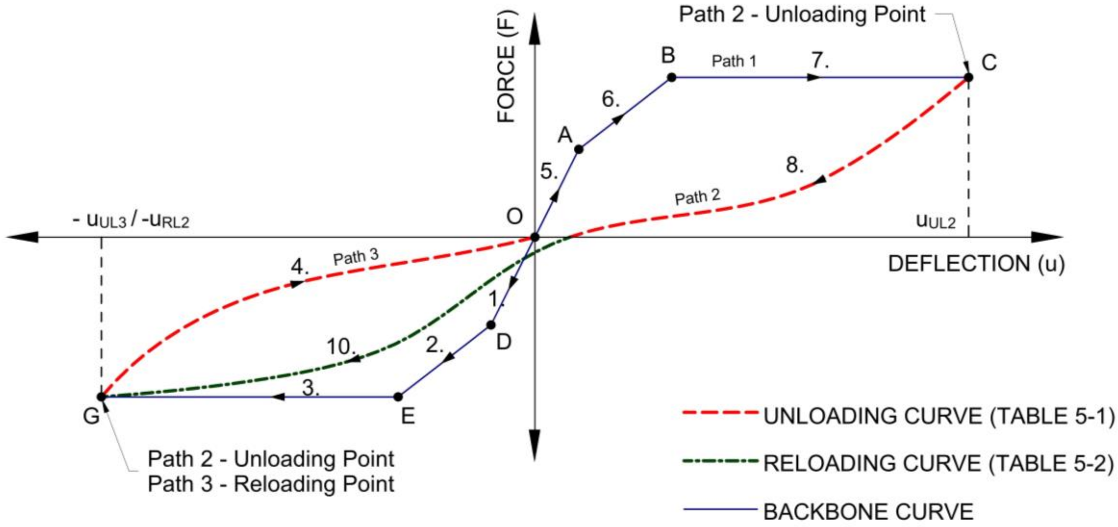

Figure 5-4 Unloading and reloading curves

The problem that arises when separately interpolating the unloading and reloading curves is that the points of intersection produced by the unloading and reloading curves at the x-axis typically does not intercept the axis at the same point. To overcome the incompatibility at the x-axis intercept, the average between the two x-axis points is determined between the unloading curve and the reloading curve. The two curves are then scaled equally until the points of intersection along the x-axis occurs at the same point. Figure 5-5 shows the method followed to produce the final secondary curve that is used upon unloading from the primary curve and reloading back into the primary curve in the opposite direction from the unloading point. Further experimentation will be needed to verify this.

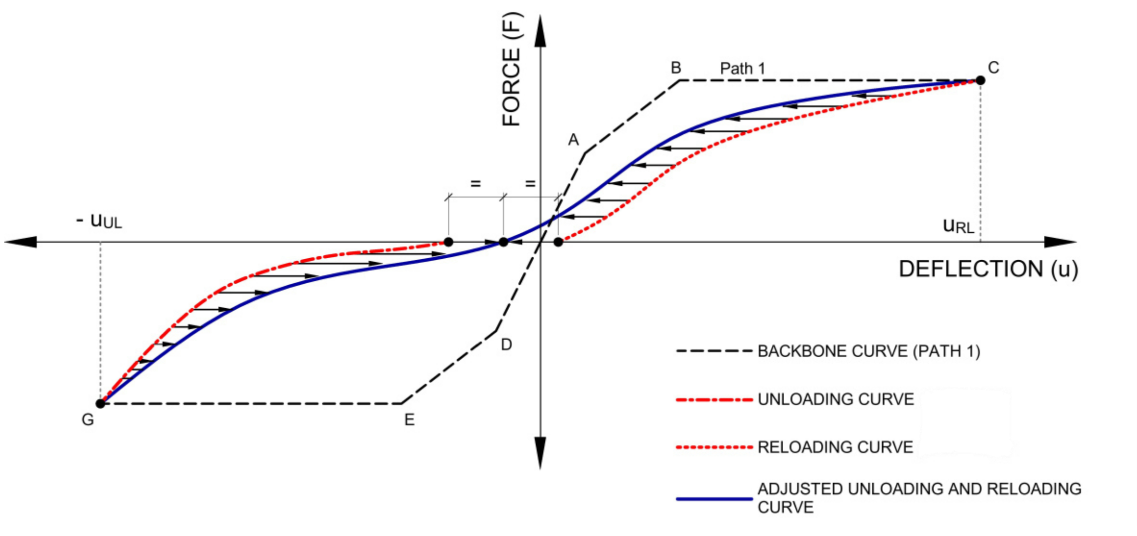

Figure 5-5 Adjusted unloading and reloading curves from the interpolated data

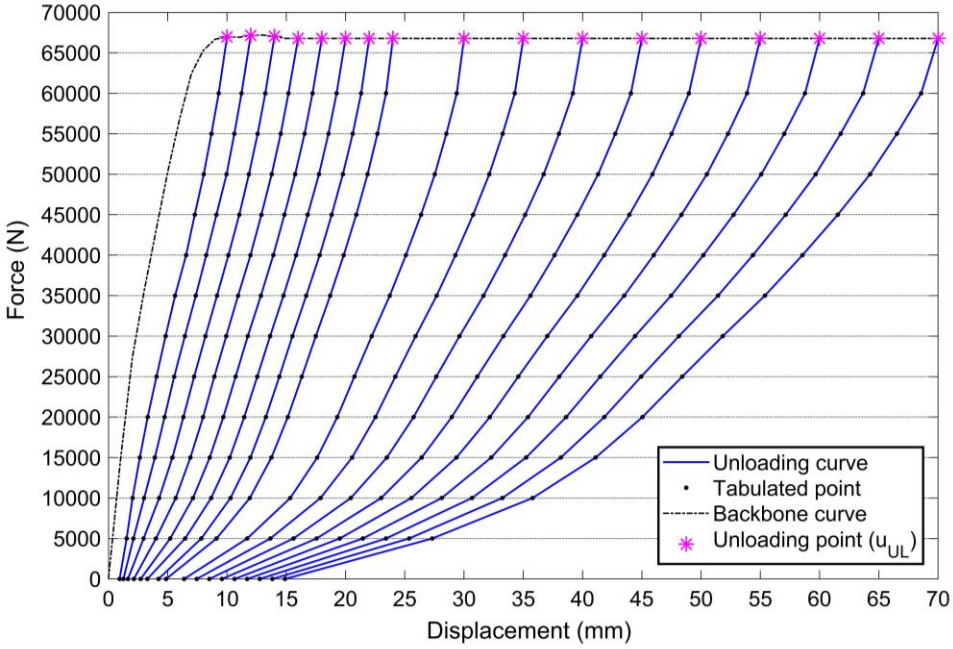

Figure 5-6 Unloading curves as a function of the point of unload along the primary curve

Table 5-1 Tabulated displacement points along the unloading curve as a function of the point of unloading along the primary curve

Backbone curve unloading displacement (u_{UL}) (mm)	Backbone curve force (N)	Force (N): 0	5000	10000	15000	20000	25000	30000	35000	40000	45000	50000	55000	60000
0	0	0.00	0.00	0.00	-	-	-	-	-	-	-	-	-	-
1	14523	0.11	0.53	0.78	1.09	1.38	1.68	-	-	-	-	-	-	-
2	27215	0.16	0.61	0.88	1.16	1.48	1.83	2.28	2.70	-	-	-	-	-
3	35497	0.21	0.67	0.95	1.24	1.58	1.98	2.45	2.95	3.41	-	-	-	-
4	42976	0.30	0.73	1.02	1.34	1.67	2.09	2.63	3.20	3.71	4.13	4.61	-	-
5	50278	0.37	0.81	1.09	1.40	1.76	2.20	2.76	3.38	4.01	4.49	4.99	5.41	-
6	56819	0.45	0.90	1.20	1.51	1.92	2.35	2.92	3.60	4.25	4.85	5.37	5.87	6.12
7	62439	0.57	1.01	1.32	1.64	2.05	2.52	3.16	3.82	4.53	5.16	5.77	6.32	6.82
8	65307	0.68	1.13	1.47	1.87	2.30	2.86	3.51	4.25	4.99	5.67	6.39	6.96	7.52
9	66677	0.81	1.31	1.70	2.18	2.73	3.38	4.10	4.86	5.66	6.40	7.11	7.78	8.34
10	66960	0.94	1.53	2.03	2.65	3.31	4.05	4.82	5.62	6.55	7.28	8.04	8.69	9.30
11	66921	1.12	1.79	2.51	3.28	4.02	4.79	5.61	6.49	7.38	8.21	8.98	9.66	10.30
12	67146	1.26	2.11	3.01	3.91	4.74	5.55	6.45	7.37	8.25	9.11	9.96	10.62	11.23
13	67199	1.40	2.45	3.60	4.60	5.49	6.34	7.27	8.21	9.13	10.00	10.86	11.58	12.19
14	67026	1.64	2.97	4.28	5.40	6.32	7.23	8.18	9.16	10.12	11.04	11.85	12.59	13.24
15	66774	1.92	3.50	4.97	6.17	7.14	8.08	9.06	10.07	11.04	11.96	12.81	13.57	14.21
16	66774	2.14	4.01	5.67	6.91	7.99	8.94	9.93	10.94	11.98	12.90	13.77	14.53	15.19
17	66774	2.42	4.60	6.37	7.74	8.81	9.82	10.86	11.89	12.91	13.89	14.78	15.53	16.20
18	66774	2.71	5.21	7.13	8.54	9.69	10.73	11.76	12.86	13.91	14.85	15.75	16.55	17.22
19	66774	2.96	5.84	8.14	9.37	10.57	11.62	12.68	13.80	14.86	15.84	16.74	17.53	18.22
20	66774	3.28	6.47	8.66	10.24	11.46	12.56	13.64	14.76	15.84	16.81	17.76	18.56	19.25
21	66774	3.78	7.12	9.47	11.11	12.36	13.49	14.60	15.72	16.83	17.84	18.79	19.57	20.28
22	66774	4.22	7.83	10.30	11.97	13.28	14.42	15.53	16.69	17.82	18.84	19.78	20.61	21.32
23	66774	4.61	8.50	11.09	12.88	14.20	15.35	16.52	17.69	18.81	19.86	20.79	21.65	22.33
24	66774	4.86	9.12	11.93	13.75	15.13	16.32	17.50	18.71	19.85	20.91	21.86	22.69	23.42
25	66774	5.32	9.76	12.78	14.68	16.09	17.29	18.51	19.78	20.91	21.98	22.95	23.76	24.49
30	66774	6.38	11.71	15.34	17.62	19.31	20.75	22.21	23.73	25.09	26.37	27.54	28.51	29.39
35	66774	7.45	13.66	17.89	20.55	22.53	24.20	25.92	27.69	29.28	30.77	32.13	33.26	34.28
40	66774	8.51	15.61	20.45	23.49	25.74	27.66	29.62	31.65	33.46	35.16	36.72	38.01	39.18
45	66774	9.57	17.56	23.00	26.42	28.96	31.12	33.32	35.60	37.64	39.56	41.31	42.76	44.08
50	66774	10.64	19.51	25.56	29.36	32.18	34.58	37.02	39.56	41.82	43.95	45.90	47.51	48.98
55	66774	11.70	21.46	28.12	32.30	35.40	38.04	40.73	43.51	46.01	48.35	50.49	52.27	53.87
60	66774	12.77	23.41	30.67	35.23	38.62	41.49	44.43	47.47	50.19	52.74	55.08	57.02	58.77
65	66774	13.83	25.37	33.23	38.17	41.83	44.95	48.13	51.43	54.37	57.14	59.67	61.77	63.67
70	66774	14.89	27.32	35.78	41.10	45.05	48.41	51.83	55.38	58.55	61.53	64.26	66.52	68.57

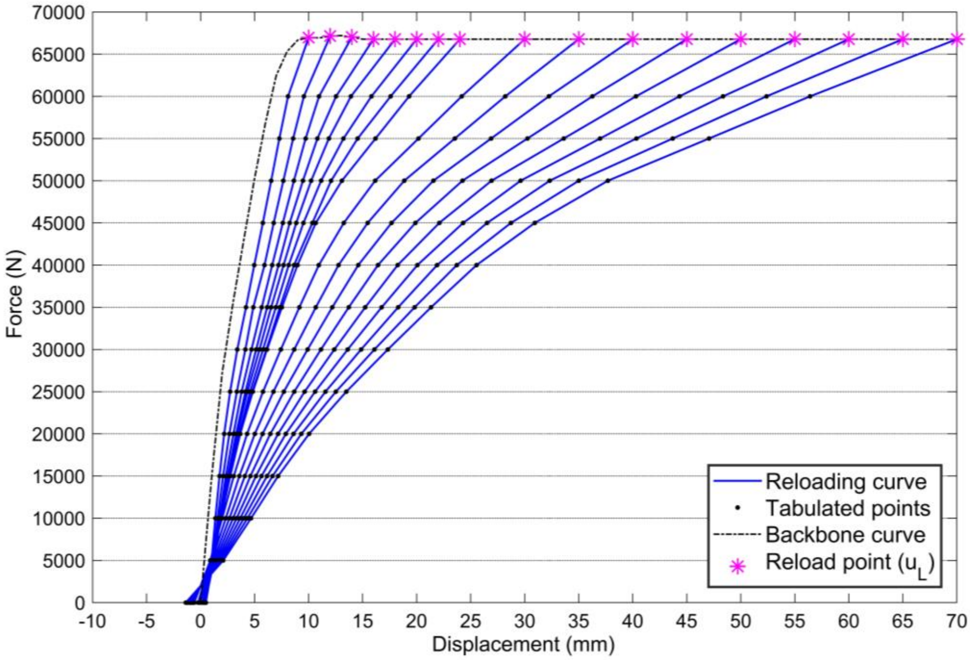

Figure 5-7 Reloading curves as a function of the point of reload along the primary curve

Table 5-2 Tabulated displacement points along the reloading curve as a function of the point of reloading along the primary curve

Backbone curve reloading displacement (u_L) (mm)	Backbone curve force (N)	Force (N) 0	5000	10000	15000	20000	25000	30000	35000	40000	45000	50000	55000	60000
0	0	0.00	0.00	0.00	-	-	-	-	-	-	-	-	-	-
1	14523	0.02	0.45	0.73	1.02	1.35	1.73	-	-	-	-	-	-	-
2	27215	0.12	0.54	0.81	1.10	1.43	1.80	2.27	2.83	-	-	-	-	-
3	35497	0.14	0.60	0.88	1.17	1.50	1.87	2.37	2.94	3.47	-	-	-	-
4	42976	0.20	0.68	0.96	1.25	1.57	1.97	2.47	3.04	3.62	4.14	4.80	-	-
5	50278	0.26	0.75	1.03	1.33	1.66	2.05	2.57	3.15	3.77	4.33	4.95	5.57	-
6	56819	0.38	0.82	1.09	1.42	1.76	2.17	2.69	3.30	3.92	4.52	5.11	5.77	6.33
7	62439	0.38	0.86	1.18	1.49	1.83	2.26	2.78	3.43	4.06	4.66	5.32	5.97	6.62
8	65307	0.41	0.92	1.23	1.55	1.90	2.35	2.90	3.55	4.23	4.92	5.58	6.25	6.91
9	66677	0.42	0.96	1.28	1.64	2.01	2.50	3.10	3.79	4.52	5.24	6.01	6.70	7.42
10	66960	0.42	1.01	1.37	1.75	2.19	2.73	3.40	4.21	4.97	5.77	6.54	7.29	8.10
11	66921	0.45	1.07	1.47	1.91	2.41	3.05	3.79	4.65	5.46	6.27	7.13	7.96	8.84
12	67146	0.49	1.14	1.58	2.08	2.67	3.36	4.15	4.88	5.92	6.77	7.66	8.57	9.56
13	67199	0.49	1.19	1.66	2.22	2.86	3.59	4.42	5.36	6.29	7.18	8.14	9.17	10.27
14	67026	0.44	1.21	1.74	2.34	3.04	3.80	4.71	5.66	6.63	7.61	8.64	9.72	10.97
15	66774	0.42	1.23	1.78	2.42	3.15	3.99	4.93	5.95	6.91	7.97	9.07	10.26	11.71
16	66774	0.43	1.25	1.85	2.52	3.29	4.15	5.14	6.16	7.22	8.25	9.47	10.82	12.54
17	66774	0.39	1.25	1.88	2.58	3.38	4.26	5.31	6.38	7.41	8.62	9.84	11.31	13.22
18	66774	0.30	1.21	1.86	2.58	3.40	4.34	5.45	6.54	7.68	8.85	10.24	11.87	13.92
19	66774	0.21	1.14	1.86	2.61	3.47	4.42	5.57	6.75	7.89	9.20	10.60	12.39	14.89
20	66774	0.17	1.16	1.89	2.69	3.58	4.58	5.78	6.97	8.15	9.52	11.16	13.23	15.82
21	66774	-0.01	1.09	1.89	2.73	3.62	4.67	5.92	7.13	8.41	9.81	11.69	13.99	16.58
22	66774	-0.03	1.06	1.89	2.75	3.68	4.79	6.09	7.34	8.66	10.35	12.08	14.54	17.59
23	66774	-0.05	1.06	1.89	2.74	3.69	4.82	6.12	7.40	8.89	10.51	12.52	15.07	18.79
24	66774	-0.23	0.93	1.79	2.66	3.66	4.84	6.15	7.53	8.97	10.67	13.08	16.19	19.30
25	66774	-0.49	0.75	1.67	2.56	3.59	4.82	6.19	7.62	9.12	11.05	13.47	16.81	20.15
30	66774	-0.59	0.90	2.00	3.08	4.30	5.78	7.43	9.14	10.95	13.26	16.16	20.17	24.18
35	66774	-0.69	1.05	2.34	3.59	5.02	6.74	8.67	10.67	12.77	15.47	18.85	23.53	28.21
40	66774	-0.78	1.20	2.67	4.10	5.74	7.71	9.90	12.19	14.59	17.68	21.54	26.89	32.24
45	66774	-0.88	1.35	3.00	4.61	6.46	8.67	11.14	13.72	16.42	19.89	24.24	30.25	36.26
50	66774	-0.98	1.50	3.34	5.13	7.17	9.63	12.38	15.24	18.24	22.10	26.93	33.61	40.29
55	66774	-1.08	1.65	3.67	5.64	7.89	10.60	13.62	16.76	20.07	24.31	29.62	36.97	44.32
60	66774	-1.17	1.80	4.00	6.15	8.61	11.56	14.86	18.29	21.89	26.52	32.32	40.33	48.35
65	66774	-1.27	1.95	4.34	6.66	9.33	12.52	16.09	19.81	23.72	28.72	35.01	43.70	52.38
70	66774	-1.37	2.10	4.67	7.18	10.04	13.49	17.33	21.33	25.54	30.93	37.70	47.06	56.41

Another path that needs to be considered during the analysis is a change in direction from a secondary path before it transitions back into the backbone curve. This typically occurs when the footing has previously been displaced to its maximum position in the direction of loading and load reversal occurs at a displacement that is less than the maximum displacement reached on the primary curve. Because of this, the cyclic behaviour of the footing and load reversals occurs within the maximum displacements achieved on the primary curve. Figure 5-8 shows a load reversal that has occurred along a secondary curve before reaching the maximum displacement u_{max_pos}. Figure 5-9 shows diagrammatically the method used to determine the unloading path that occurs from a reloading path along the secondary curve. The unloading path is determined by adjusting and scaling the unloading curve that would otherwise have been calculated from the maximum point u_{max_pos} along the primary curve.

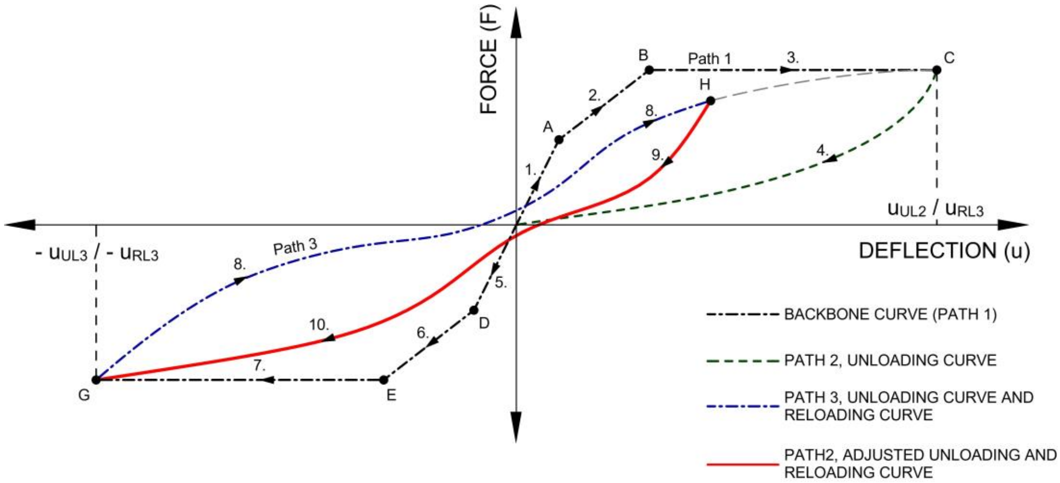

Figure 5-8 Adjusted unloading from a secondary reloading curve

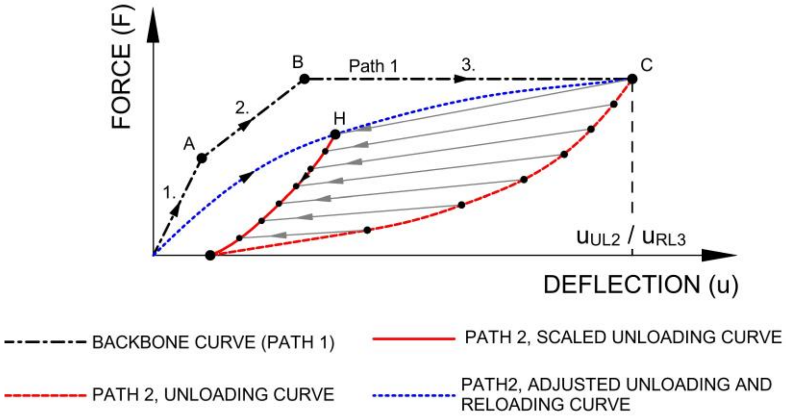

Figure 5-9 Scaling of the unloading curve to produce the adjusted unload curve

5.1.3 TERTIARY CURVES: INTERMEDIATE CURVES

Tertiary curves account for unloading and reloading behaviour that occurs within the same quadrant without crossing the origin as shown in Figure 5-10. The tertiary curves are determined by mirroring the secondary curve about a straight line drawn from the unloading point (Point C in Figure 5-10) along the backbone curve and the point of load reversal (Point D in Figure 5-10) along the secondary curve. The new curve is then mirrored about a line perpendicular and equidistant along the line drawn between Point D and Point C, which is shown by Line D'-C' in Figure 5-10, to produce the final tertiary curve. The same procedure is followed for each cycle of vibration within the quadrant. Double mirroring of the curve about two perpendicular lines ensures that the slope at point D and Point F is greater than the slope at point C and Point E as shown in Figure 5-10.

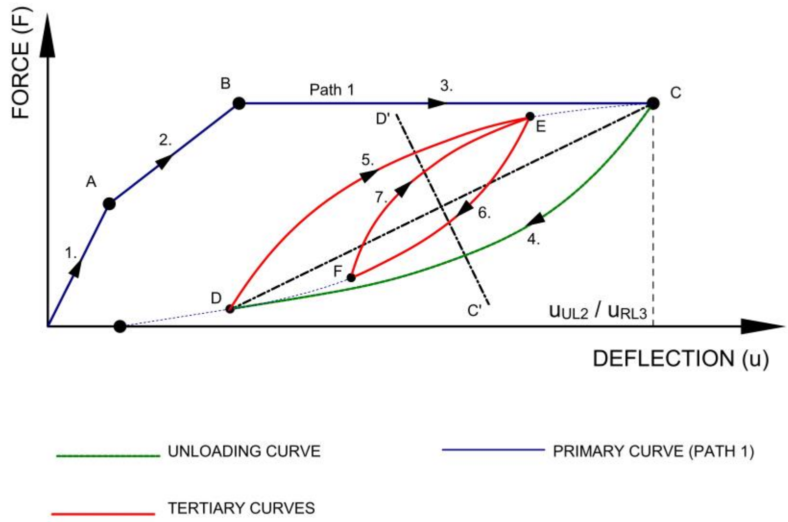

Figure 5-10 Tertiary curves

5.2 ANALYTICAL MODEL HYSTERETIC RESULTS

The hysteretic curves produced using the analytical hysteretic model for cyclic loading are compared to the hysteretic curves that were generated during the pseudo-dynamic experiments. The comparisons for the five tests are shown in Figure 5-11 to Figure 5-15. The numerical model was run using the analytical hysteretic material with the El Centro earthquake and was scaled to a peak ground acceleration of 0.34 g and Figure 5-11 shows the comparison of the two hysteretic curves. The hysteretic response produced using the analytical model resulted in more hysteresis during the unloading cycle than that observed during the pseudo-dynamic laboratory test. The slight disparity between the formulated hysteretic model analysis and the result produced during the laboratory test is due to the unloading rule specified in the hysteretic model before the reinforcement had yielded. However, the developed analytical hysteretic model provides a maximum shear force and backbone curve that is similar to the result produced during the pseudo-dynamic experiments.

Figure 5-12 shows the comparison between the result produced using the analytical hysteretic model and pseudo-dynamic experiment at a PGA of 0.68 g. The analytical hysteretic model for cyclic loading provides a similar hysteretic response to the result produced during the pseudo-dynamic experiments. The response is particularly evident by the maximum shear force and displacement being almost the same for both the hysteretic curves. Figure 5-13 shows the comparison between the analytical model and experimental tests at a PGA of 0.78 g. The hysteretic response produced from the analytical hysteretic model shows that the unloading and reloading branches differ from that generated from the experimental result. The difference in response was most likely due to the reduction in cross section due to spalling of the concrete not being incorporated into the model. The pinching effect is captured by the analytical hysteretic model as shown in Figure 5-12 and Figure 5-13.

Figure 5-14 and Figure 5-15 shows the comparison between the results generated using the analytical hysteretic model and the experimental tests at a PGA of 1 g and 2 g respectively. The analytical material model provided a similar response to the results produced during the pseudo-dynamic experiments for both the 1 g and 2 g. For the 1 g experiment, the analytical hysteretic model produces a single loop in the negative direction before drifting off in the positive direction and failing. The test that was undertaken at a PGA of 2 g resulted in a similar hysteretic curve being formed between the analytical hysteretic model and the laboratory test, with only a linear-elastic displacement of the footing in the negative direction before drifting off to the right and failing.

The comparison between the experimental test results and the results produced using the analytical hysteretic model indicate that the formulated analytical hysteretic model provides a relatively accurate means to predict damage at peak ground accelerations and structural fundamental periods of vibration that were not undertaken during the laboratory experiments. Cognisance should be taken that the analytical hysteretic model was produced using the limited set of results for the given reinforced concrete footing design. However, the model provides a better method to interpolate the damage sustained by the given reinforced concrete footing at various peak ground accelerations and overall structural fundamental periods of vibration.

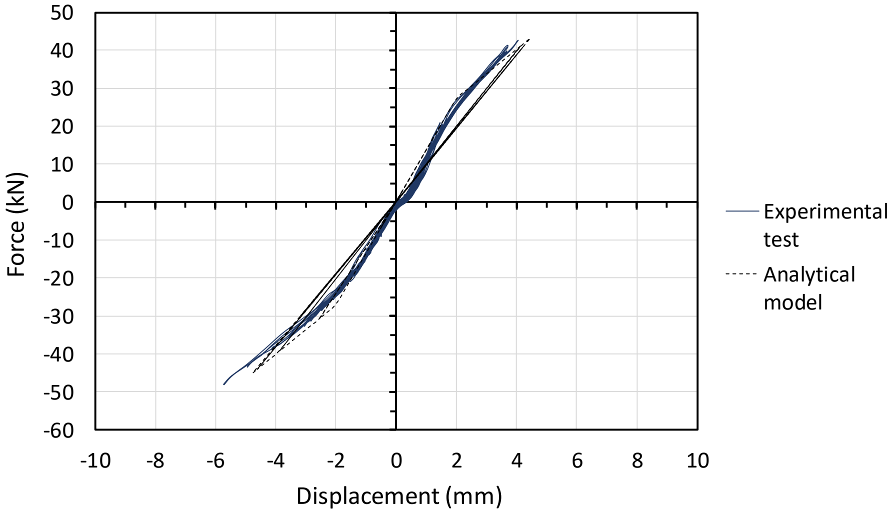

Figure 5-11 Analytical hysteretic model comparison with experimental results at a PGA of 0.34 g

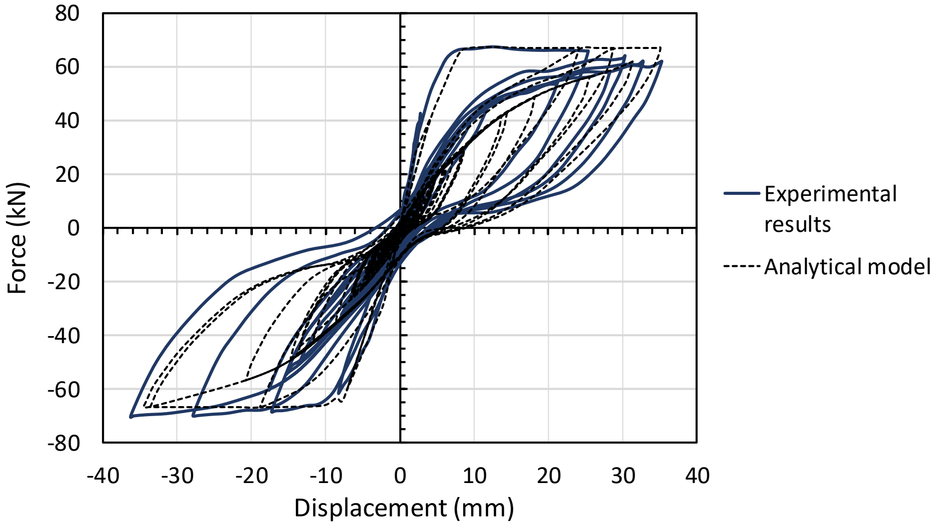

Figure 5-12 Analytical hysteretic model comparison with experimental results at a PGA of 0.68 g

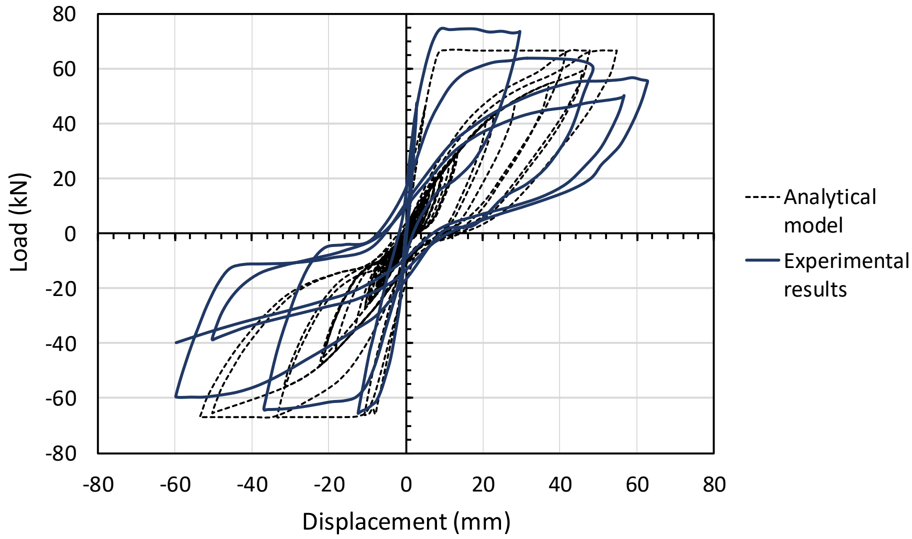

Figure 5-13 Analytical hysteretic model comparison with experimental results at a PGA of 0.78 g

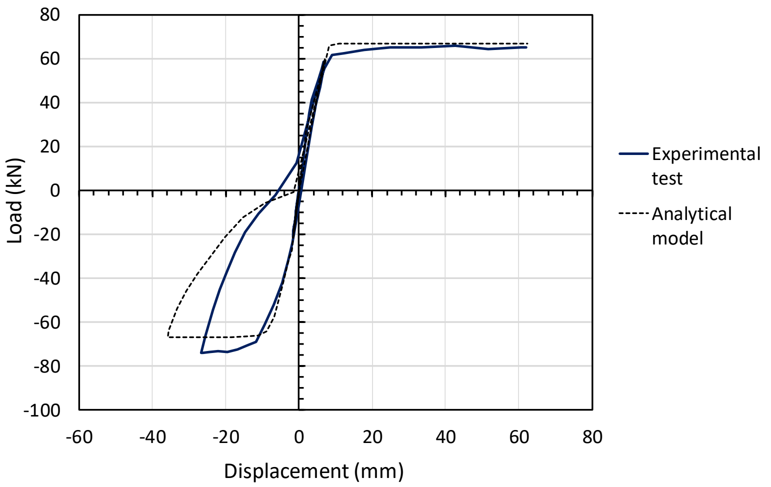

Figure 5-14 Analytical hysteretic model comparison with experimental results at a PGA of 1 g

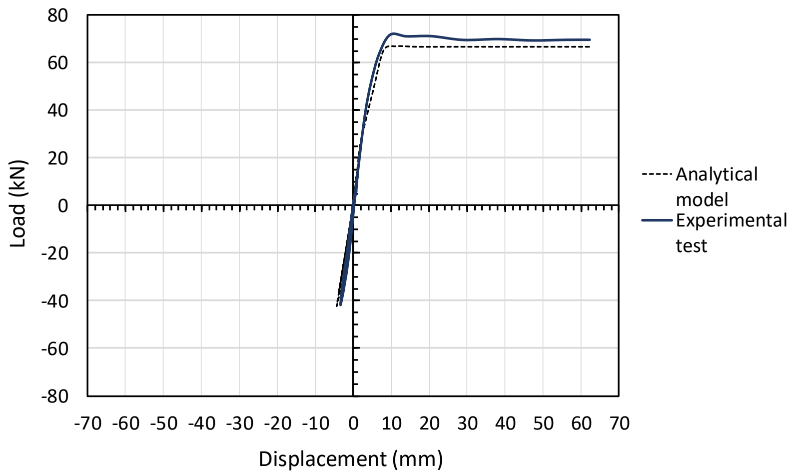

Figure 5-15 Analytical hysteretic model comparison with experimental results at a PGA of 2 g

5.3 DAMAGE AND FRAGILITY ANALYSIS

The numerical model was run using the analytical hysteretic model that was developed in the previous section over a range of scaled peak ground accelerations using the El Centro ground motion record to evaluate the extent of damage sustained by the reinforced concrete footing. The same frame structure that was used during the pseudo-dynamic experiments, with a fundamental period of vibration of 0.86 s was used to run the computational model with the developed analytical hysteretic model for the reinforced concrete footing. The conversion between PGA and intensity was done using Equation 2.1 in Section 2.1.1, which was developed by Ambraseys (1974).

A damage index was formulated using the Park and Ang (1985) damage model by utilising the results produced during the pseudo-dynamic experiments and the results produced using the analytical hysteretic model. Equation 4.1 shows the Park and Ang (1985) damage index formula for brevity and the values used within the formula for each of the analytical hysteretic model analysis. The values used within the Park and Ang damage model were obtained from the cyclic load tests and the pseudo-dynamic tests, which were summarised in Table 4-3. The maximum shear capacity of the footing was determined by averaging the absolute values of the maximum shear values obtained from both the negative and positive displacements from each of the pseudo-dynamic tests and cyclic load tests. The damage index ranges from 0 to 1, with 0 indicating an undamaged structure and 1 indicating a complete collapse of the structure.

$$DI = \frac{d_m}{d_u} + \frac{\beta}{V_y d_u} \int dE_h \leq 1 \qquad (4.1)$$

With:

$d_u =$ 0.062 m (maximum displacement before collapse, Table 4-3)

$V_y =$ 66775 N (shear capacity at yielding averaged from the experiments)

$\beta =$ 0.1 (equation 2.27 in section 2.8.1 for the analysed footing)

$E_h =$ Hysteretic energy absorbed by the reinforced concrete footing

The value of β represents the effect that cyclic loading has on the cumulative structural damage incurred by the reinforced concrete footing for the duration of the earthquake record. The value of β was calculated using the recommended formula provided by Park and Ang (1985) using the characteristics of the reinforced concrete used during the research.

Figure 5-16 and Figure 5-17 shows the five damage index values determined from the pseudo-dynamic experiments superimposed on the damage index values produced using the analytical hysteretic model that was used to run the analysis over a range of peak ground accelerations. Figure 5-16 is given in terms of PGA and Figure 5-17 is given in terms of earthquake intensity. The damage index values calculated from the numerical hysteretic model for each of the five tested specimens compares well with the calculated values determined from the pseudo-dynamic experiments. By running the analysis over a range of peak ground accelerations, two distinct points can be observed where there is a change in the rate of damage with increasing peak ground acceleration. The first point occurs at a damage index of 0.03, which indicates a point of softening of the reinforced concrete footing and relates to the onset of concrete cracking. The second point occurs at a damage index of 0.13 and corresponds to the point at which the reinforcement starts to yield. The first two points are pronounced and consistent with the cracking and the yielding of the reinforcement.

A third point can be characterised due to concrete spalling, which is directly related to the number of cycles of vibration and the resultant reduction in shear capacity. From the results and observations made during the pseudo-dynamic tests, the third point occurs at a damage index of approximately 0.4, which correlates with the value produced in literature. A loss of shear capacity with increased cycles of vibration was observed to occur at a damage index exceeding 0.4 during the pseudo-dynamic experiments undertaken at peak ground accelerations of 0.68 g and 0.78 g.

Comparing the damage index values with the Modified Mercalli intensity scale, as previously shown in Table 2-1, indicates that there is a correlation between the observed damage to the footings and the descriptions given by the Modified Mercalli Intensity scale. At an intensity of between VIII and IX, the damage to the reinforced concrete footing varies between being slightly damaged to considerably damaged in ordinary buildings. At an intensity of IX, the footings had failed, which corresponds with the description given in Table 2-1 that indicates buildings having shifted off of their foundations.

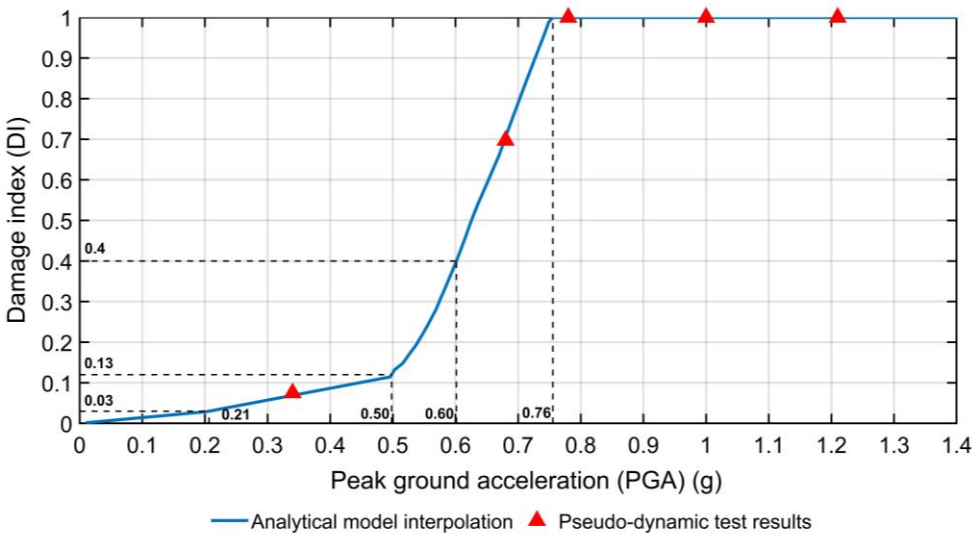

Figure 5-16 PGA vs Damage Index of a reinforced concrete footing using the derived analytical hysteretic model and the laboratory results with 5% structural damping and a linear structural natural period of vibration of 0.86 s

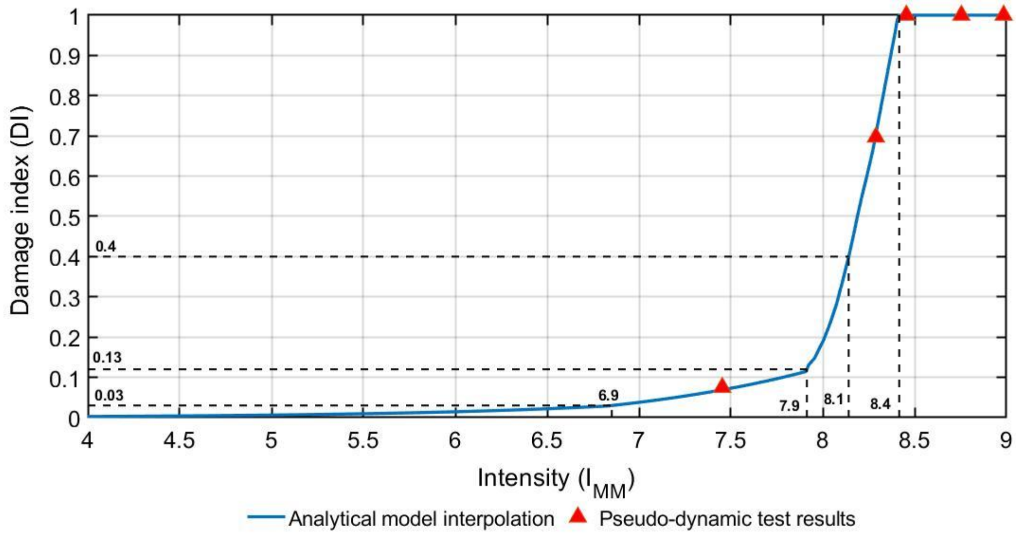

Figure 5-17 Earthquake Intensity vs Damage Index of a reinforced concrete footing using the derived analytical hysteretic model and the laboratory results with 5% structural damping and a linear structural natural period of vibration of 0.86 s

Figure 5-18 compares the influence that the structural damping ratio has on the damage incurred by the reinforced concrete footing. The same natural period of vibration of 0.86 s was used for each of the tests, and the damping ratio was varied for each of the series of tests. The series of tests comprised of analysing the structure over a range of peak ground accelerations and determining the extent of damage at each of the peak ground accelerations. Figure 5-18 shows that the damping ratio is independent of the damage index value due to concrete cracking and reinforcement yielding. However, the damping ratio has a significant influence on the amount of damage incurred by the reinforced concrete footing at any given peak ground acceleration. The damage sustained by the footing decreases with a concomitant increase in the damping ratio used in the overall frame structure. The large difference in damage incurred by the reinforced concrete footing at the different damping ratios is most likely due to the reinforced concrete footing only forming a small component within the overall frame structure and therefore does not consider the extent of damage sustained by the elements that comprise the overall superstructure. Therefore, the distribution of damage within the overall structure has a significant influence on the damage to the footing.

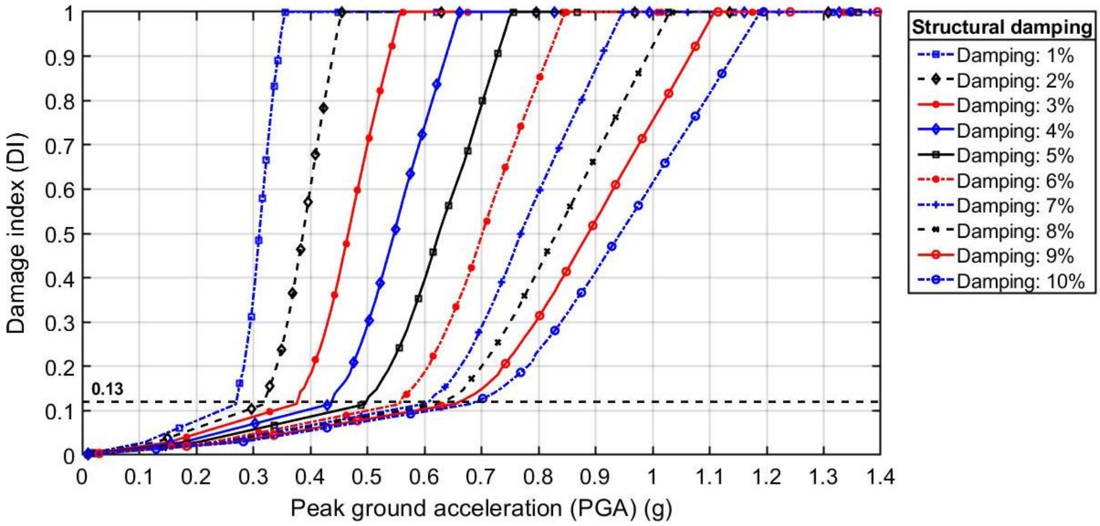

Figure 5-18 Earthquake Intensity vs Damage Index of a reinforced concrete footing at various damping ratios with linear structural natural period of vibration of 0.86 s

5.3.1 DAMAGE STATES

Five categories of damage were deduced from the results and observations made during the experimental tests and the numerical analysis run using the analytical hysteretic model. The first three damage states were obtained from plotting the damage index with increasing intensity and identifying the points at which the rate of damage increased with increasing earthquake intensity. The fourth damage state was obtained from visual observations made during the pseudo-dynamic tests and from literature. The damage states are as follows:

1) Undamaged (Damage Index < 0.03): The maximum load applied to the footing does not exceed the tensile capacity of the concrete and therefore cracking of the concrete does not occur.
2) Minor damage ($0.03 <$ Damage Index ≤ 0.13): Formation of cracks in the concrete and opening of existing cracks. Occurs when the maximum deformation does not exceed the yield displacement of the footing. The maximum shear load capacity of the footing has not been reached. Basic visual inspection advised with limited and isolated remedial work.
3) Moderate damage ($0.13 <$ Damage Index ≤ 0.4): Occurs when the reinforcement yields, which results in a significant loss of stiffness within the footing and the subsequent increase in the overall displacement of the structure. The loss of concrete cover is not observed, and the reinforcement has not become exposed. The footing can still carry the axial load from the structure above and therefore allows occupants time to evacuate. Repair and retrofitting

of the foundations will be required post-earthquake to ensure that the structure conforms to relevant design codes of practice.

4) Extensive damage ($0.40 < \text{Damage Index} < 1$): Large lateral displacement of the footing resulting in the visible crushing of the concrete and the loss of concrete cover to the reinforcement. Buckling of the exposed reinforcement and significant reduction in the load carrying capacity of the footing. The structure is still standing but is at risk of collapse and not safe for occupation. The structure is subsequently condemned, requiring demolition.
5) Collapse ($\text{Damage Index} = 1$): The capacity of the footing has been reduced significantly resulting in the applied load exceeding the carrying capacity of the footing and the subsequent collapse of the structure.

5.3.2 DAMAGE CURVES

The analytical hysteretic model was used in conjunction with the pseudo-dynamic algorithm, as shown in Figure 3-27, to determine damage curves and fragility curves for the various damage states described in Section 5.3.1 for the minimally reinforced concrete footing. The response of the footing was analysed over a range of earthquake intensities and fundamental periods of vibration using the scaled El Centro ground motion record and the formulated hysteretic model.

The majority of the building classes, specifically low to medium rise buildings, are placed on reinforced concrete footings, and one of the main structural characteristics that separate the response of different buildings is the fundamental period of vibration of the structure. Many seismic codes distinguish the extent of seismic loading on the structure by the structure's resultant fundamental period of vibration in the form of response spectra, and therefore the damage curves were produced in terms of the overall structural fundamental period of vibration.

Utilising the same frame structure that was used during the pseudo-dynamic experiments, the stiffness of the column and beam elements were increased by changing the moment inertia of each of the members by a constant value to ensure a similar stiffness distribution within the frame. Figure 5-19 shows the damage contour plot in terms of peak ground acceleration (PGA) and the fundamental period of vibration of the structure and shows that the fundamental period of vibration of the overall structure has a significant influence on the damage incurred by the reinforced concrete footing. The reinforced concrete footing that will incure the most damage at lower earthquake intensities are those that have an overall structural fundamental period of vibration in the order of 0.53 s.

Figure 5-20 shows the damage contour plot between earthquake intensity and overall structural fundamental period of vibration. The variation in damage defined at each of the Modified Mercalli intensity values is most likely due to structures with different fundamental periods of vibration experiencing different levels of damage for a given peak ground acceleration. At a Modified Mercalli intensity of VIII, the extent of damage to the structure varies between being slight to considerable. Structures with very low and very high fundamental periods of vibration will incur slight to moderate damage at an intensity of VIII when subjected to the scaled El Centro earthquake record. However, structures with a fundamental period in the order of 0.53 s will suffer considerable damage and even collapse, which indicates that the Modified Mercalli intensity scale can be subjective and dependent on the type of structure, and the mass and stiffness distribution within the structure.

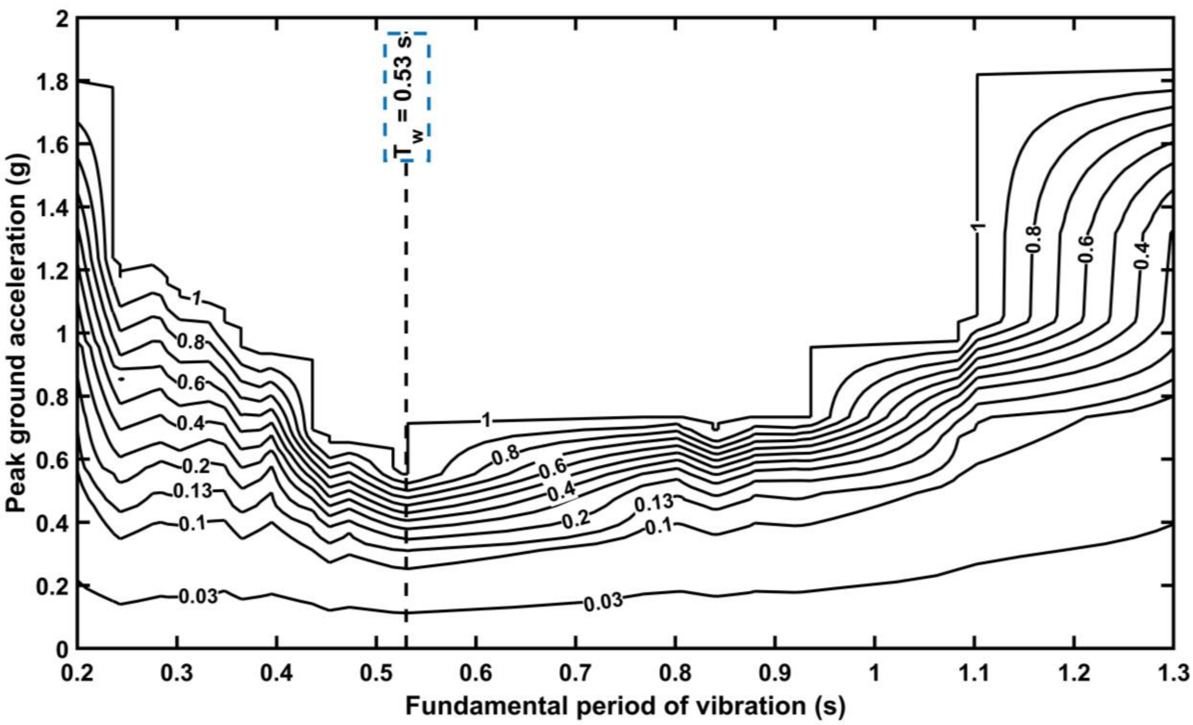

Figure 5-19 Damage contour plot in terms of peak ground acceleration at 5% damping

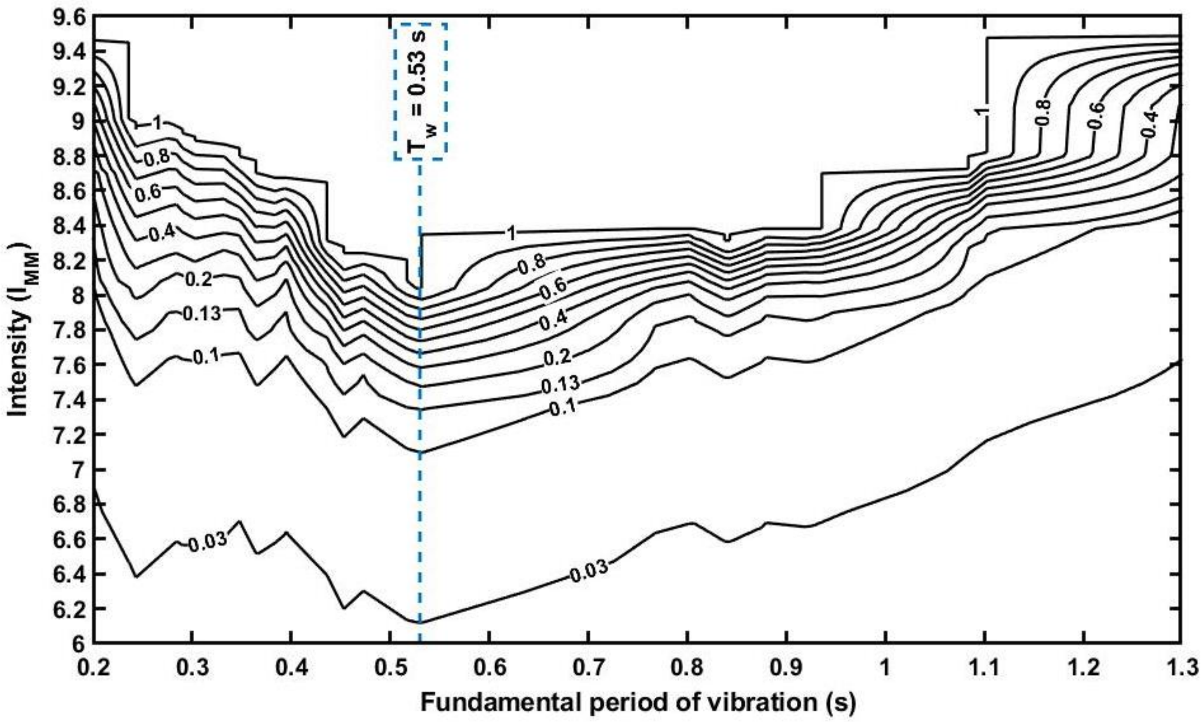

Figure 5-20 Damage contour plot in terms of intensity at 5% damping

Cognisance should be given to the fact that the analysis that was undertaken during this research only considered a single reinforced concrete foundation design and a single design for the moment resisting frame structure that was analysed using a single earthquake ground motion record. Therefore, the contour plot of damage could substantially differ in Figure 5-19 and Figure 5-20 if a different earthquake ground motion record was used or a different combination of structural steel members was used. Therefore, when predicting the extent of damage at different earthquake intensities, it would be conservative to assume a damage curve plotted for the worst-case fundamental period of vibration. In this case, under the analysed conditions, the fundamental period of vibration of 0.53 s produced the worst-case damage curve and is shown in Figure 5-21 in terms of PGA and Figure 5-22 in terms of intensity. Under the worse-case fundamental period of vibration for the reinforced concrete footing analysed using the El Centro ground motion record, moderate damage can be expected in reinforced concrete structures that are subjected to earthquake intensities greater than 0.31 g. Extensive damage can be expected in reinforced concrete structures subjected to earthquake intensities exceeding 0.41 g, thus indicating that some footings will require demolition and therefore a total loss of the asset. Earthquakes producing intensities exceeding 0.55 g will result in the total collapse of footings and therefore collapse of the overall structure.

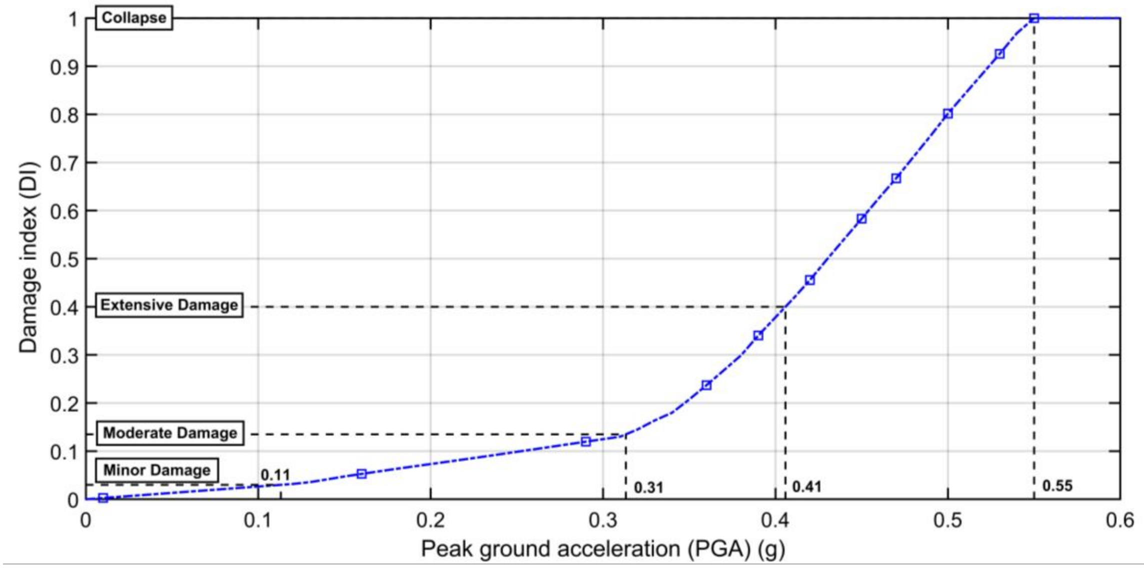

Figure 5-21 Worst case damage curve for the analysed nominally reinforced concrete footing in terms of PGA

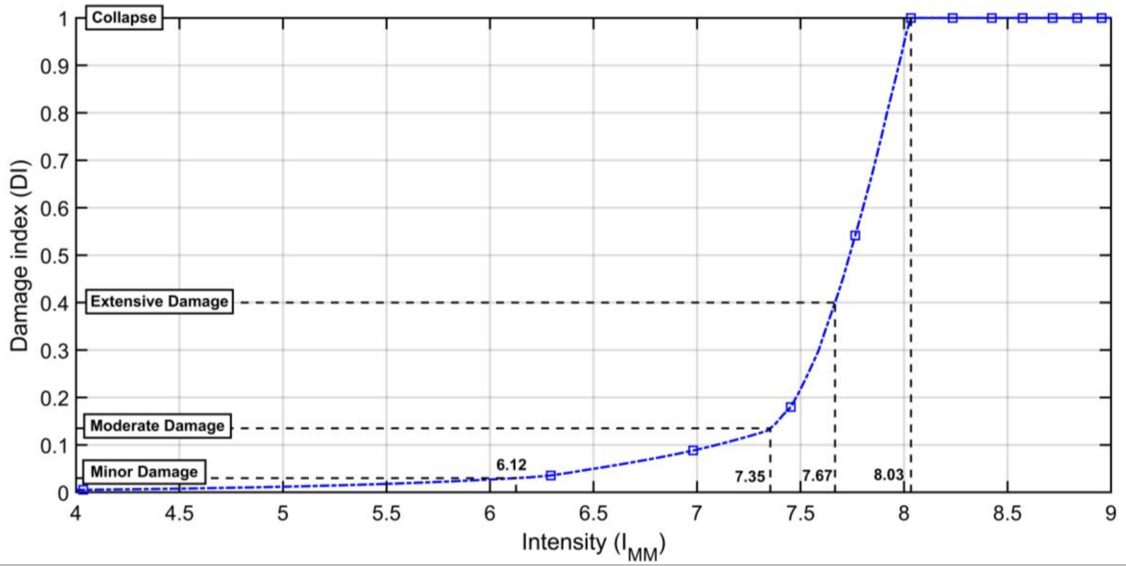

Figure 5-22 Worst case damage curve for the analysed nominally reinforced concrete footing in terms of intensity

5.3.3 FRAGILITY CURVES

A method of producing fragility curves is proposed using the formulated damage contour plots produced in the previous section. The fragility curves are calculated for each damage state over a range of fundamental periods of vibration that are deemed to be representative of low-rise structures from the building period formulas specified in SANS 10160-4:2017. The fragility curves were developed by considering the following assumptions and limitations:

- The fragility curves were determined using the procedure given in FEMA P-58-1 (2012) that results in a lognormal distribution from the demand data obtained from results produced by running the pseudo-dynamic algorithm using the formulated analytical hysteretic model;
- The range of fundamental periods of vibration used to develop the fragility curves were determined by using the building period formulas given by Equations 2.15 and Equation 2.16 for steel and reinforced concrete moment resisting frame structures. The lowest fundamental period of vibration and the maximum period of vibration for one storey to three storey high structures, which range between 4 m to 12 m in height, was used to develop the fragility curves;
- A continuous uniform distribution of fundamental periods of vibration was determined as shown in Figure 5-23. Therefore. the probability of each period occurring with the range of fundamental period of vibrations is equal. The exact distribution of structures that could reasonably be placed on the footing is unknown, and therefore a uniform distribution is assumed when calculating the median value, θ, and logarithmic standard deviation, β.

Table 5-3 shows the fundamental period of vibration of low-rise structures between one-storey and three stories and produces a minimum fundamental period of vibration of 0.21 s for a one-storey reinforced concrete moment resisting frame structure with a 4 m height, and a maximum fundamental period of vibration of 0.55 s for a three-storey steel frame moment resisting structure. Selecting structures between one storey and three stories account for the variability in fundamental periods of vibrations and compare with the distribution of fundamental periods of vibration as previously shown in Figure 2-17, which shows the fundamental period of vibration for a range of 2622 Chilean buildings. The range of fundamental periods of vibration is deemed to satisfy all strength and deformation requirements as specified in the South African structural design codes of practice.

Table 5-3 Fundamental period of vibration for 1 storey to 3 storey structures calculated using the building period formulas in SANS 10160:4-2017

	C_T (1)	Fundamental period of vibration (1) (s)		
		1 storey(2) $h_t = 4m$	2 storey(2) $h_t = 8m$	3 storey(2) $h_t = 12m$
Steel frame structures (Equation 2.15)	0.085	0.24	0.40	**0.55**
Reinforced concrete moment resisting frame structures (Equation 2.16)	0.075	**0.21**	0.36	0.48

(1) Building period formula $T = C_T \times h_t^{3/4}$ from SANS 10160-4:2017

(2) A storey is taken as 4 m

Figure 5-23 shows the contour lines representing each of the damage states that are extracted from Figure 5-19 with the continuous uniform distribution used to determine the median value, θ, and logarithmic standard deviation, β. Using the equations given in Section 2.8.2 and the produced median value, θ, and standard deviation, β, for each damage state, the fragility curves were determined. Figure 5-24 shows the fragility curves for the minimally reinforced concrete footing subjected to the El Centro ground motion record for structures with periods that range between 0.21 s and 0.55 s. At a peak ground acceleration of 0.128 g or earthquake intensity of 6.3, only minor damage is expected in approximately 30% of low-rise structure's reinforced concrete footings with a period in the range of 0.21 s to 0.55 s when subjected to the El Centro ground motion record.

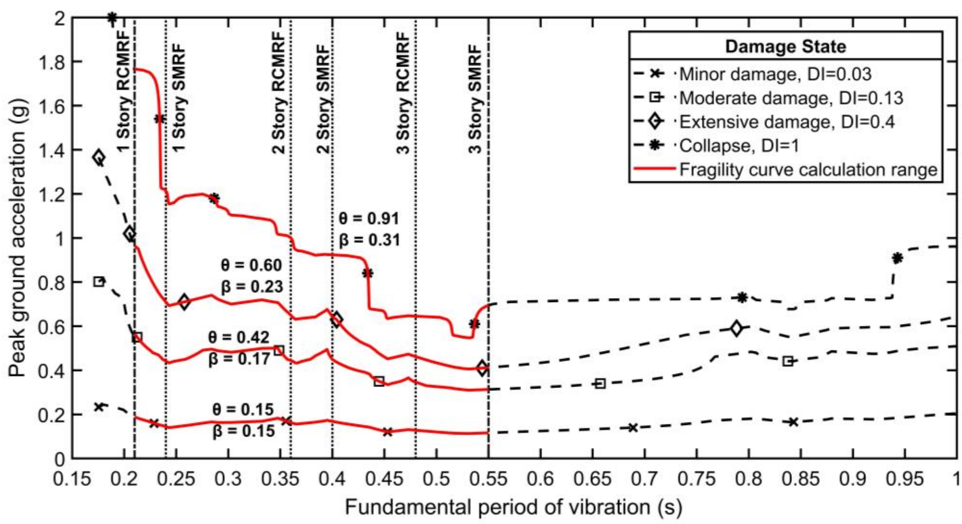

Figure 5-23 Continuous range for each of the damage states to formulate the fragility curves

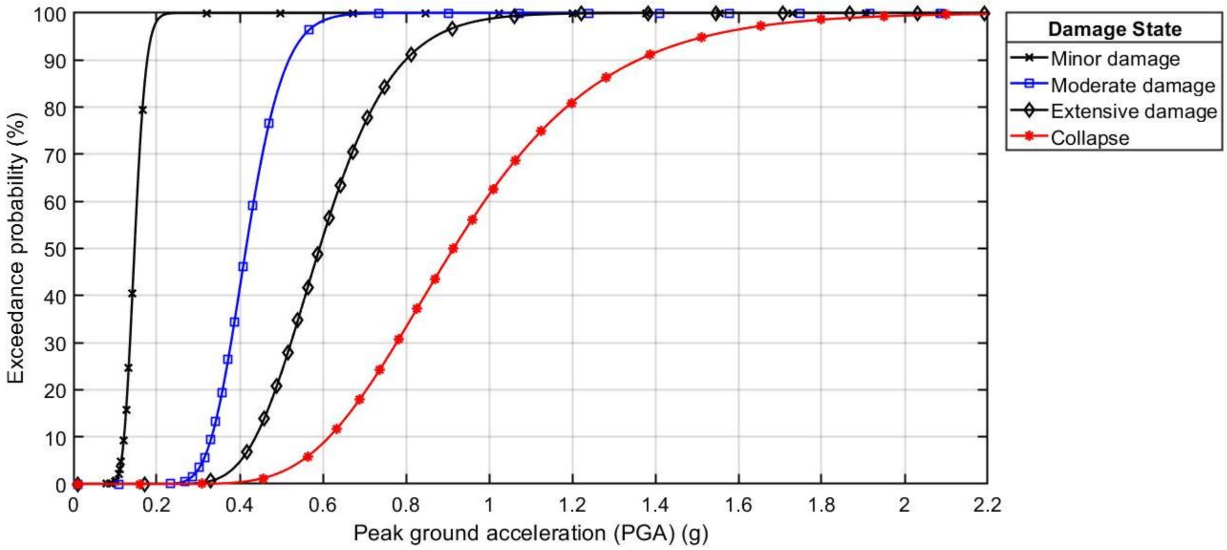

(a)

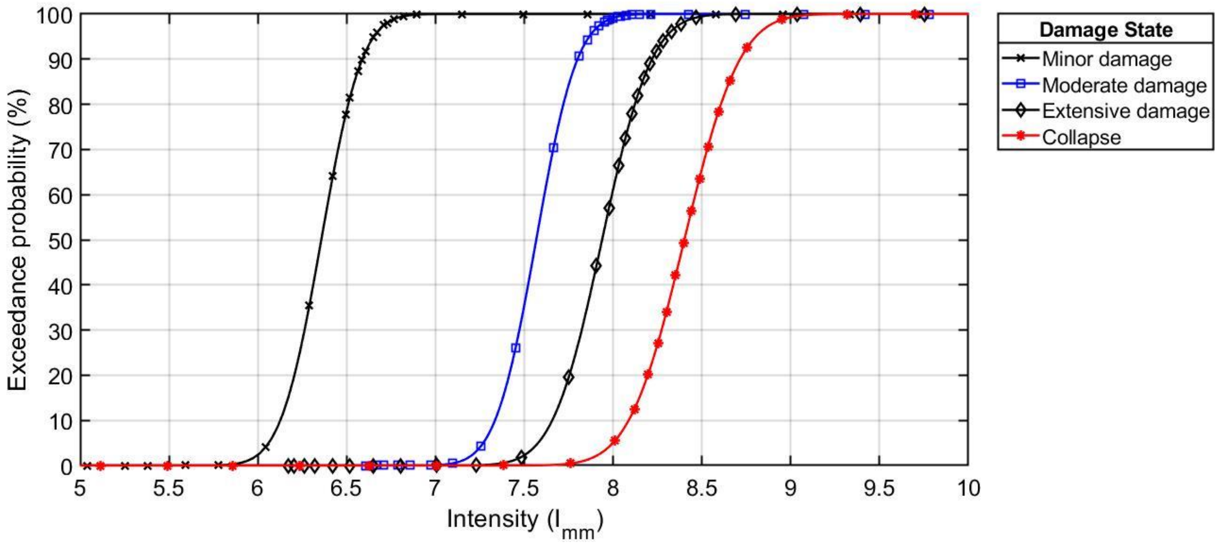

(b)

Figure 5-24 Fragility curves for minimally reinforced concrete footing of fundamental period range of 0.21 s to 0.55 s

5.4 CONCLUSION

This chapter described a method to approximate the damage curves and fragility curves for a structural component by utilising the results produced during the pseudo-dynamic tests and cyclic load tests. To interpolate damage at PGAs that were not undertaken during the laboratory tests, an analytical hysteretic model was developed to replace the physical test setup in the laboratory that was used to perform the pseudo-dynamic tests. Running the analysis over a range of peak ground accelerations and overall structural fundamental periods of vibration showed that the rate of damage increased at distinct points, which were independent of the damping ratio used for the frame structure. Damage states were formulated using the results produced during the analysis using the analytical hysteretic model and the results and observations made during the laboratory tests.

The produced damage contour plots, which show the amount of damage as a function of the overall fundamental period of vibration and the PGA, indicated the extent of damage sustained by the reinforced concrete footing correlates with the descriptions given by the Modified Mercalli intensity scale. However, the variation in damage expected at any given intensity within the Modified Mercalli intensity scale is likely due to the influence that the fundamental period of vibration has on the extent of damage sustained by the reinforced concrete footing. The fundamental period of vibration is a characteristic that relies on the mass and stiffness distribution of the structure, the type of structure, and the composition of the structure that is placed on the footing. Therefore, knowing the fundamental period of vibration of the structure will better enable the risk of damage at various earthquake intensities to be quantified. This chapter shows that quantifying the expected damage to a structure and individual structural components is complex and dependant on several variables that define the structure.

6 CONCLUSIONS AND RECOMMENDATIONS

In the following section conclusions are made regarding the viability of using the pseudo-dynamic experimental method to relate structural damage with increasing earthquake intensity for an axially loaded reinforced concrete footing, which forms part of a two-bay, two-storey moment resisting frame structure. A total of five reinforced concrete footings were tested using the pseudo-dynamic experimentation method and two reinforced concrete footings were cyclic load tested. The results produced during the experiments were used to formulate an analytical hysteretic model to interpolate damage at peak ground accelerations and overall structural fundamental periods of vibration that were not undertaken during the pseudo-dynamic experiments. The results produced during the pseudo-dynamic tests and those produced using the analytical hysteretic model aided in the development of a damage index and the formulation of damage curves and fragility curves for the analysed reinforced concrete footing. Furthermore, this section provides recommendations for further work.

6.1 CONCLUSIONS FROM THE STUDY

The pseudo-dynamic experimentation method provides a viable approach to correlate the damage that has occurred to a physical model of a reinforced concrete footing, which forms part of an overall linear elastic structure, with increasing earthquake intensity. The use of the implicit Newmark's method provides a stable and accurate algorithm to quantify the damaged incurred to the reinforced concrete footing due to the overall response of the structure that has been subjected to an applied seismic excitation. The initial stiffness that is used within in the implicit Newmark's algorithm must be greater than the maximum achievable stiffness of the specimen being tested to ensure the stability of the analysis and to prevent premature damage.

By using the pseudo-dynamic method, the hysteretic response of the footings could be related to earthquake intensity and observations could be made on the extent of damage incurred by the footing due to the applied earthquake loading. The time history of energy terms and hysteretic energy dissipation characteristics could be determined for each time increment during the application of the scaled El Centro earthquake record, which enabled the amount of energy dissipated by the footing to be calculated as a percentage of the total energy imparted to the structure. The reinforced concrete footing only dissipates a small percentage of the overall energy imparted to the structure in the form of hysteretic energy, with the remainder of the energy being dissipated due to damping within the frame structure. The pseudo-dynamic method enables the determination of the energy dissipation potential for individual structural components during an applied earthquake record to the overall structure, which is comprised of many structural elements.

With an increase in the hysteretic energy dissipated by the reinforced concrete footing there is an associated increase in the observed damage to the footing in the form of concrete cracking, reinforcement yielding and spalling of the concrete. The repeated cyclic loading at deformations exceeding the yield strength of the reinforcement but not exceeding the failure deformation results in the largest quantity of hysteretic energy being absorbed. At large PGAs, the hysteretic energy does not give an indication of whether the footing has failed, therefore demonstrating the applicability of the Park and Ang damage index that consists of two terms that depends on the maximum deformation of the structure and the cumulative hysteretic energy. At large PGAs the structure tends to fail due to excessive deformation before undergoing cyclic loading and at lower PGAs the absorbed hysteretic energy tends to govern the damage and failure of the footing due to the larger number of cycles of vibration.

The research showed that by using the pseudo-dynamic method to analyse a single component of a much larger structure, which is assumed to be linear elastic for the duration of the analysis, does have its limitations. The capacity of structural members and connections within the overall frame structure is not accounted for during the analysis due to the linear elastic assumption, and therefore, the formation of plastic hinges and the resulted loss of stiffness within the overall structure is not considered in the response of the reinforced concrete footing.

Five damage states can be deduced for the analysed reinforced concrete footing, with the damaged states being linked to the material characteristics of the concrete and reinforcement. The extent of damage to the reinforced concrete footing is governed predominately by the yield strength of the reinforcement, which results in the rate of damage increasing substantially once the reinforcement had yielded. The mechanisms that resulted in the failure of the reinforced concrete footing due to increasing earthquake intensity are as follows:

- The shear capacity of the reinforced concrete footing was reached soon after the reinforcement yielded, and large cracks had formed at the interface between the base of the column and the top of the concrete base slab. Upon reaching the maximum shear strength, the stiffness of the footing approached zero with a subsequent increase in the horizontal displacement at the top of the reinforced concrete footing;
- Spalling of the concrete is predominately governed due to the buckling of the yielded and elongated reinforcement upon load reversal from tension to compression;

- The pinching effect was observed in the pseudo-dynamic and cyclic load tests and is due to the presence of the axial load. With a reduction in the horizontal load, the vertical load overcomes the overturning moment produced by the horizontal shear force and attempts to stabilise the member by returning the footing back to its original vertical position. Upon load reversal the plastically elongated reinforcing steel is first mobilised in compression by the axial load prior to the closure of the crack resulting in a reduction in the lateral displacement that is independent of the applied horizontal load;
- An increase in the number of cycles of vibration results in an increase in the degree of concrete spalling, which governs the failure of the footing at lower earthquake intensities;
- Significant spalling of the concrete resulted in the reduction and loss of axial capacity and shear capacity of the footing, which ultimately resulted in the failure of the reinforced concrete footing's column; and
- A reduction in shear capacity was not observed at tests conducted at large earthquake intensities and at large deformations. The fracturing of the reinforcement and loss of stability of the structure governed the failure of the test specimen at large PGAs.

Although pseudo-dynamic testing between computer modelling and laboratory testing provides an alternative and more cost-effective solution to full scale testing, the cost and time required to produce a single result under a single set of structural conditions limits the amount of data that can be produced to formulate complete set of damage curves and fragility curves. Therefore, to develop damage curves and fragility curves, an analytical hysteretic plastic hinge model had to be formulated for the analysed footing from the results produced during the pseudo-dynamic tests and cyclic load tests to interpolate damage at PGAs and overall structural fundamental periods of vibration that were not undertaken during the laboratory tests.

By performing the pseudo-dynamic tests by scaling the El Centro ground motion record showed that the footing could only sustain a maximum PGA with further increase in the amplitude of the ground motion record. The pseudo-dynamic test that was undertaken by amplifying the El Centro ground motion record to a PGA of 2 g, only managed to achieve a maximum PGA of 1.21 g before failure. This observation was further clarified by the damage contour plots and curves that were produced during the computational analysis using the analytical hysteretic model derived from the cyclic load tests and pseudo-dynamic tests. The analysis shows that with increasing amplitude of the ground motion record, the reinforced concrete footing is only able to endure a maximum peak ground acceleration before failure. The level of damage incurred by the reinforced concrete footing at a given earthquake intensity is dependent on the fundamental period of vibration of the structure and the frequency characteristics of the earthquake record to which the structure is subjected. The damage contour plot, in terms of earthquake intensity and fundamental period of vibration tends to follow the profile of the linear response spectrum that is produced using the same earthquake record.

The investigation shows that the resultant damage to the reinforced concrete footing is complex and it depends on several characteristics that relates to the overall super structure. The structural configuration, the distributed loading within the structure and the initial stress state of the structural component all plays a critical role in the resultant damage to the reinforced concrete footing. The results obtained from this research enabled a better understanding of the performance of a reinforced concrete footing that accounts for the overall response of a moment resisting frame structure subjected to an earthquake excitation. The research shows how the damage to the reinforced concrete footing manifests at different peak ground accelerations when subjected to the El Centro earthquake excitations and can be used to better understand the material response of reinforced concrete and improve the selection of PGAs for future pseudo-dynamic tests.

6.2 RECOMMENDATIONS FOR FURTHER WORK

Cognisance should be given to the fact that the analysis undertaken during this research only considered a single reinforced concrete foundation design that was analysed using a single earthquake ground motion record and the overall superstructure remained linear elastic for the duration of the earthquake record. Therefore, recommendation for future work would include the following:

- Analysing the structure by varying the longitudinal and shear reinforcement to determine the influence it has on the damage to the footing;
- Perform pseudo-dynamic tests on reinforced concrete footings by incorporating non-linear behaviour within the overall structure and determining the influence that the reduction in stiffness within the overall frame structure has on the performance of the footing;
- Investigating reinforced concrete footings that are designed to the seismic structural design code of practice (SANS 10160-4:2017) and comparing their capacity with results produced in this research. Testing reinforced concrete footings with closed seismic stirrups and comparing the capacity with the results produced using traditional stirrups;

- Performing pseudo-dynamic experiments that account for both a varying shear and axial loading as could be experienced by foundations placed on the exterior of a building;
- Soil structure interaction is one of the most important factors that influences the overall response of the foundation system. Pseudo-dynamic experiments can be performed by embedding footings within soil to determine the response and resultant damage to the reinforced concrete footing at various earthquake intensities;
- Developing a hysteretic model from a series of cyclic load tests that can account for a variation in both horizontal and vertical load for the duration of the earthquake record for a range of reinforced concrete footing designs will be beneficial in evaluating the damage encountered to number of different structural types;
- Account for several elements within the structure during a pseudo-dynamic experiment to investigate the progressive failure of the structure and determine the contribution of each element to the overall energy dissipation and fragility of the structure;
- Investigation can be done to determine the distribution of fundamental periods of vibration of all structures that form part of the insured portfolio as this will improve the formulation of the fragility curves;
- Investigation into improving the experimental test setup to reduce external noise experienced during the pseudo-dynamic experiments. Base isolation of the experimental test setup is recommended;
- Performing pseudo-dynamic experiments that enables the analysis of the reinforced concrete footing under biaxial bending and shear; and
- Use hybrid testing methods combined with machine learning algorithms to analyse a large sample of footings or reinforced concrete members by varying all significant parameters to develop a hysteretic model that can be used during earthquake loading and cyclic loading. The model can be developed to account for cyclic behaviour, degradation in strength due to reinforcement buckling and spalling, and varying axial loads on the section. The material can be further developed to account for variability in material properties and reinforcement configuration. Such a hysteretic model can be programmed into finite element analyse software packages to evaluate the progression of damage under different earthquake loadings for different structural configurations.

7 REFERENCES

ABAQUS. 2003. ABAQUS version 6.4 documentation. ABAQUS Inc.

Ambraseys N.N. 1974. *The correlation of intensity with ground motions*. Earthquake Engineering Research Library: California

Brandt, M. 2011. *Seismic Hazard in South Africa*. Council for Geoscience Report number: 2011-0061

Bursi, O. & Shing, P.B. 1996. *Evaluation of some implicit time-stepping algorithms for pseudo dynamic tests*. Earthquake Engineering and Structural Dynamics, Vol 25, 333-355.

CatmanAP. (2016). Version V4.2.2.14. Darmstadt, Germany: Hottinger Balswin Messtechnik GmbH

Chang S. 2009. *Bidirectional Pseudodynamic Testing*. Journal of Engineering Mechanics. 135(11): 1227-1236.

Chopra, A.K. 2012. *Dynamics of structures, Theory and Applications to Earthquake Engineering*. Prentice Hall: Upper Saddle River

Cusson, D. & Paultre, P. 1994. *High-Strength Concrete Columns Confined by Rectangular Ties. Journal of Structural Engineering*. 120(3).

Elmenshawi, A. & Brown, T. 2009. *Hysteretic energy and damping capacity of flexural elements constructed with different concrete strengths*. Engineering Structures. 32:297-305.

FEMA P-58-1. 2012. *Seismic Performance Assessment of Buildings: Volume 1 – Methodology*. Federal Emergency Management Agency: Washington

Ghosh S. & Datta, D. & Katakdhoud, A. 2011. *Estimation of the Park-Ang damage index for planar multi-storey frames using equivalent single-degree systems*. Engineering Structures. 33:2509-2524.

Goel, R.K. & Chopra, A.K.1996. *Evaluation of code formulas for fundamental period of buildings.* Paper No. 1127 Eleventh World Conference on Earthquake Engineering.

Hall, J.F. 2006. *Problems encountered from the use (or misuse) of Rayleigh damping*. Earthquake Engineering and Structural Dynamics. 35:525-545.

Ibarra, L.F., Medina, R.A. and Krawinkler, H., 2005. *Hysteretic models that incorporate strength and stiffness deterioration*. Earthquake engineering & structural dynamics, 34(12), pp.1489-1511.

Jeon, J.J. & Lowes, L.N & DesRoches, R. & Brilakis, I. 2014. *Fragility curves for non-ductile reinforced concrete frames that exhibit different component response mechanisms*. Engineering Structures 85:127-143.

Kent, D.C. and Park, R. 1971. *Flexural members with confined concrete*. Journal of the Structural Division, 97(7).

Kijko, A & Kahle, B & Smit, A & Esterhuyse, S. 2015. *Hydraulic Fracturing, Waste-Water Pumping and Seismicity*.

Kijko, A. & Davies, N. 2003. *Seismic Risk Assessment: With an application to the South African Insurance Industry*. South African Actuarial Journal, 3.

Kijko, A. & Smit, A. & Van De Coolwijk, N. 2015. *A scenario approach to estimate the maximum foreseeable loss for buildings due to an earthquake in Cape Town*. South African Actuarial Journal, 15.

Kijko, A. 2008. *Strong ground motion and earthquake hazard*. Presentation at the 2nd Seismology Workshop 2008 Characterisation of Strong Motion for Damage Potential CGS, 11 November 2008

Kurt, E.G. 2010. *Investigation of strengthening techniques using pseudo-dynamic testing*. Middle East Technical University: Ankara

Lagos, R. & Kupfer, M., 2012. *Performance of high-rise buildings under the February 27th 2010 Chilean earthquake*. In Proceedings of the 4th Structural Engineering World Congress, Structural Engineering World Congress (SEWC).

Li, Y.W., Li, G.Q., Jiang, J. and Wang, Y.B., 2019. *Experimental study on seismic performance of RC frames with Energy-Dissipative Rocking Column system*. Engineering Structures, 194, pp.406-419.

Linzer, L.M. & Bejaichund, M. & Cichowicz, A. & Durrheim, R, J. & Goldbach, O.D. & Kataka, M.O. & Kijko, A. & Milev, A.M. & Saunders, I. Spottiswoode, S.M. & Webb, S.J. 2007. *Recent research in seismology in South Africa*. South African Journal of Science 103.

Logan, D.L. 2012. *A first course in the finite element method*. 5th Ed. Cengage Learning: Stamford

Low, S.S & Moehle, J.P. 1987. *Experimental Study of Reinforced Concrete Columns Subjected to Multi-Axial Cyclic Loading*. Earthquake Engineering Research centre. Report No. UCB/EERC-87/14.

Mahin, S.A & Shing, P.B & Thewalt, C.R & Hanson R.D. 1989. *Pseudodynamic Test Method – Current Status and Future Directions*. Journal of Structural Engineering. 115(8), 2113-2128.

Manzunzu, B. & Midzi, V. & Mangongolo, A. & Essrich, F. 2017. *The aftershock sequence of the 5 August 2014 Orkney earthquake (ML 5.5), South Africa*. Journal of Seismology.

Matlab. (2017). Version R2017b (9.3.0.713579) 64-bit (win64). Natick, Massachusetts, United States: The MathWorks, Inc.

Mosalam, K.M & White, R.N & Ayala, G.1998. *Response of infilled frames using pseudo-dynamic experimentation*. Earthquake Engineering and Structural Dynamics. 27, 589-608.

Mosalam, K.M. & White R.N. & Gergely, P. 1997. *Seismic Evaluation of Frames with Infill Walls Using pseudo-dynamic Experiments*. Technical Report NCEER-97-0020. Cornell University: Ithaca

Nielson, B.G. 2005. *Analytical Fragility Curves for Highway Bridges in Moderate Seismic Zones. Doctoral Thesis*. Georgia Institute of Technology: Atlanta.

Ozcebe, G, & Saaioglu, M. 1989. *Hysteretic shear model for reinforced concrete members*. Journal of Structural Engineering, 115(1):132-148.

Park, D & Hashash, Y, M, A. 2004. *Soil damping formulation in nonlinear time domain site response analysis*. Journal of Earthquake Engineering, 8(2):249-274.

Park, R., Priestley, M.J. and Gill, W.D. 1982. *Ductility of square-confined concrete columns*. Journal of the structural division, 108(4).

Park, Y.J. & Ang, A.H. & Wen, Y.K. 1984. *Seismic Damage Analysis and Damage-Limiting Design of R.C. Buildings*. Report no. UILU-ENG-84-2007. Department of Civil Engineering, University of Illinois at Urbana-Champaign.

Park, Y.J. & Ang, A.S. 1985. *Mechanistic Seismic Damage Model for Reinforced Concrete*. Journal of Structural Engineering. 111(4).

Pegan, P. & Pinto, A.V. 2000. *Pseudo-dynamic testing with substructuring at the ELSA Laboratory*. Earthquake Engineering and Structural Dynamics. 29:905-925.

Penelis, G.G. & Kappos, A.J. 2010. *Earthquake-Resistant Concrete Structures*. Taylor & Francis: Oxon

Pinto A.V. & Pegan, P. & Magonette, G. & Tsionis, G. 2004. *Pseudo-dynamic testing of bridges using non-linear substructuring*. Earthquake Engineering and Structural Dynamics. 33:1125-1146.

Rabbat, B.G. & Russell, H.G. 1985. *Friction Coefficient of Steel on Concrete or Grout*. Journal of Structural Engineering. 111(3).

Rajabi, Ro. Barghi, M. & Rajabi, Re. 2012. *Investigation of Park-Ang damage index model for flexural behaviour of reinforced concrete columns*. The Structural design of tall and special buildings. 22:1350-1358.

Razvi, S.R. & Saatcioglu, M. 1989. *Confinement of reinforced concrete columns with welded wire fabric*. Structural Journal. 86(5).

Robberts, J.M. & Marshall, V. 2010. *Analysis and Design of Concrete Structure*. Nuclear Structural Engineering: Cape Town

Saatcioglu, M. & Razvi, S. 1992. *Strength and Ductility of Confined Concrete*. Journal of Structural Engineering. 118(6).

SAISC. 2010. Southern African Steel Construction Handbook. Southern African Institute of steel construction. CTP Printers: Cape Town

SANS 10100-1. 2000. *The structural use of concrete Part 1: Design*. Standards South Africa. SANS 10100-1: 2000. Pretoria

SANS 10160-1. 2011. *Basis of structural design and actions for buildings and industrial structures – Part 1: Basis of Structural Design*. Standards South Africa. SANS 10160-1: 2011. Pretoria

SANS 10160-2. 2011. *Basis of structural design and actions for buildings and industrial structures – Part 2: Self weight and imposed loads*. Standards South Africa. SANS 10160-2: 2011. Pretoria

SANS 10160-3. 2011. *Basis of structural design and actions for buildings and industrial structures – Part 3: Wind actions*. Standards South Africa. SANS 10160-3: 2011. Pretoria

SANS 10160-4. 2017. *Basis of structural design and actions for buildings and industrial structures – Part 4: Seismic actions and general requirements for buildings*. Standards South Africa. SANS 10160-4: 2011. Pretoria

SANS 10162-1. 2011. *The structural use of steel Part 1: Limits-states design of hot-rolled steelwork. Standards South Africa*. SANS 10100-1: 2011. Pretoria

Scott, B.D., Park, R, and Priestley, M.J.N. 1982. *Stress-strain behaviour of concrete confined by overlapping hoops at low and high strain rates*. Journal Proceedings, 79(1).

Sengupta, P. and Li, B. 2017. *Hysteresis modelling of reinforced concrete structures: state of the art*. ACI Structural Journal, 114(1), 25-38.

Sezen H. 2000. *Evaluation and testing of existing reinforced concrete building columns*. CE299 Report. University of California, Berkeley

Shing P.B & Mahin S.A. 1988. *Rate-of-Loading Effects on pseudo dynamic tests.* Journal of Structural Engineering. 114(11).

Shing P.B & Mahin S.A. 1990. *Experimental Error Effects in pseudo dynamic testing*. Journal of Engineering Mechanics. 116(14).

Shing, P.B. & Mahin S.A. 1984. *Pseudodynamic test method for seismic performance evaluation: Theory and Implementation*. Report No. UCB/EERC-84/01. Earthquake Engineering Research centre, University of California Berkeley: California

Spencer, B.F., Elnashai, A.S., Kwon, O., Park, K., Nakata, N., B. 2007. *The UI-SimCor Hybrid Simulation Framework*. Conference Paper

Takanashi K. & Udagawa K. 1989. *Behaviour of Steel and Composite Beams at Various Displacement Rates*. Journal of Structural Engineering. 115(8).

Takanashi, K & Udagawa, K. & Seki, M. & Okada, T. & Tanaka, H. 1975. *Non-linear earthquake response analysis of structures by a computer-actuator on-line system*. Earthquake Engineering Research centre: University of California.

Takanashi, K. & Nakashima, M. 1987. *Japanese Activities on On-Line Testing*. J. Eng. Mech 113(7): 1014-1032.

Thewalt, C.R & Mahin, S.A. 1987. *Hybrid solution techniques for generalised pseudo dynamic testing*. Report No. UCB/EERC-87/09. Earthquake Engineering Research Centre, University of California Berkeley: California

Udagawa K. & Mimura H. 1988. *Equivalent stiffness of composite beams in frames during earthquake*. Proceedings of the Ninth World Conference on Earthquake Engineering. Tokyo-Kyoto, Japan Vol 6, 59-64

Udagawa K. & Mimura H. 1991. *Behaviour of Composite Beam Frame by pseudo dynamic Testing*. Journal of Structural Engineering. 117(5).

Udagawa, K., Takanashi, K., and Kato, B. 1984. *Effects of displacement rates on the behaviour of steel beams and composite beams*. Proc. 8th World Conf. on Earthquake Engrg., San Francisco, Calif., 6, 177-184.

Wang, T. & Nakashima, M. & Pan, P. 2006. *On-line hybrid test combining with general-purpose finite element software*. Earthquake Engineering and Structural Dynamics. 35:1471-1488.

Xing, G., Ozbulut, O.E., Lei, T. and Liu, B., 2017. *Cumulative seismic damage assessment of reinforced concrete columns through cyclic and pseudo‐dynamic tests*. The Structural Design of Tall and Special Buildings, 26(2).

Yu, J., Yu, K., Shang, X. and Lu, Z. 2016. *New Extended Finite Element Method for Pinching Effect in Reinforced Concrete Columns*. ACI Structural Journal, 113(4).

Zahrah, T.F. & Hall, W.J. 1984. *Earthquake Energy Absorption in SDOF Structures*. Journal of Structural Engineering. 110(8).

APPENDIX A

PSEUDO-DYNAMIC EXPERIMENTATION SCRIPT

```
Sub Main
'EA_Job.Start(Job1)

'Activating plots in the panel and setting them to zero
EA_Graph.RemovePlot(Panel1,"Graph1",1)
EA_Graph.Refresh(Panel1,"Graph1")
EA_Graph.RemovePlot(Panel1,"Graph2",1)
EA_Graph.Refresh(Panel1,"Graph2")
EA_Graph.RemovePlot(Panel1,"Energy_plot",1)
EA_Graph.Refresh(Panel1,"Energy_plot")

EA_Graph.RemovePlot(Panel2,"Strain_out_disp",1)
EA_Graph.Refresh(Panel2,"Strain_out_disp")
EA_Graph.RemovePlot(Panel2,"Disp_read_LVDT",1)
EA_Graph.Refresh(Panel2,"Disp_read_LVDT")

EA_Panel.SetValue(Panel1,"Increment_out",0)
EA_Panel.SetValue(Panel1,"Time_out",0)
EA_Panel.SetValue(Panel1,"PGA",0)
EA_Panel.SetValue(Panel1,"Iteration_out",0)
EA_Panel.SetValue(Panel1,"Convergence_out",0)
EA_Panel.SetValue(Panel,"Damage_out",0)
EA_Panel.SetValue(Panel1,"DispRead_out",0)
EA_Panel.SetValue(Panel1,"DispRead_in",0)
EA_Panel.SetValue(Panel1,"Interal_counter",0)

'Sets analog output to zero volts
EA_IO.SetAnalogOut("PMX_1 CH 9",1,0,OperMode)

'Zeros input data

EA_IO.ZeroBalanceControl("MX840_SR",1)          'Zeros right strain gauge
EA_IO.ZeroBalanceControl("MX840_SL",1)          'Zeros left strain gauge

EA_IO.ZeroBalanceControl("PMX_LVDT1",1)         'Zeros LVDT1
EA_IO.ZeroBalanceControl("PMX_LVDT2",1)         'Zeros LVDT2
EA_IO.ZeroBalanceControl("PMX_LVDT3",1)         'Zeros LVDT3
EA_IO.ZeroBalanceControl("PMX_LVDT4",1)         'Zeros LVDT4

EA_IO.ZeroBalanceControl("Displacement_Hor",1)  'Zeros Horizontal displacement
EA_IO.ZeroBalanceControl("Force_Hor",1)         'Zeros Horizontal force

End Sub
Sub Axial_load
'Runs data logging during axial load application
Dim Analysis As Variant 'Input to change for the number of analysis being performed
Analysis=1

Dim objXls_a As Object
Set objXls_a = CreateObject("Excel.Application")
objXls_a.Workbooks.Add
objXls_a.Worksheets(1).Name = "Linear results"
objXls_a.Workbooks(1).SaveAs
"C:\Octave\Dynamics\Pseudo\Pseudo_test_"+CStr(Analysis)+".xlsx"  '
"C:\Octave\Dynamics\Pseudo\OutputDispOutput4.xls"

objXls_a.Worksheets(1).Cells(1,1).Value ="Counter"
objXls_a.Worksheets(1).Cells(1,2).Value ="Axial load (kN)"
objXls_a.Worksheets(1).Cells(1,3).Value ="Strain gauge left (micro)"
objXls_a.Worksheets(1).Cells(1,4).Value ="Strain gauge right (micro)"

Dim Force_axial As Double
Dim Strain_Left As Double
Dim Strain_right As Double

Dim Axial_load_applied() As Double
Dim Strain_Left_disp() As Double
Dim Strain_right_disp() As Double
Dim StepInc() As Double

Dim Button2 As Variant
Button2=0
Dim counter As Variant
```

```
counter=0

EA_Panel.SetCell(Panel2,"Axial_stop_table",1,1,0)

        Do While Button2=0 'Convergence at each time step

        EA_Panel.GetCell(Panel2,"Axial_stop_table",1,1,Button2)

        ReDim Preserve StepInc(counter+1)
        ReDim Preserve Axial_load_applied(counter+1)
        ReDim Preserve Strain_Left_disp(counter+1)
        ReDim Preserve Strain_right_disp(counter+1)

        StepInc(counter)=CDbl(counter) 'Counter to array
        objXls_a.Worksheets(1).Cells(counter+2,1).Value =counter

        'Read out axial force from servo controller
        EA_IO.Measure("Load cell",Force_axial,1) 'Axial force read out
        objXls_a.Worksheets(1).Cells(counter+2,2).Value =Force_axial 'Saves axial force to excel spreadsheet
        Axial_load_applied(counter)=CDbl(Force_axial) 'Saves axial force to a array

        'Read out Strain gauge Left from servo controller
        EA_IO.Measure("MX840_SL",Strain_Left,1) 'Strain gauge left read out
        objXls_a.Worksheets(1).Cells(counter+2,3).Value =Strain_Left 'Saves strain gauge left to excel spreadsheet
        Strain_Left_disp(counter)=CDbl(Strain_Left) 'Saves Strain gauge left to array

        'Read out Strain gauge Right from servo controller
        EA_IO.Measure("MX840_SR",Strain_right,1) 'Strain gauge right to read out
        objXls_a.Worksheets(1).Cells(counter+2,4).Value =Strain_right 'Saves strain gauge right to excel spreadsheet
        Strain_right_disp(counter)=CDbl(Strain_right) 'Strain gauge right to array

        'Axial load out (Plotting)
        EA_Graph.PlotArrayXY(Panel3,"Axial_load_initial",1,counter+1, StepInc(), Axial_load_applied())
        EA_Graph.SetPlotProperty(Panel3,"Axial_load_initial",1,2,vbRed)
        EA_Graph.Refresh(Panel3,"Axial_load_initial")

        'Plots Strain values (Plotting)
        EA_Graph.PlotArrayXY(Panel3,"Strain_gauge_axial",1,counter+1, StepInc(), Strain_right_disp())
        EA_Graph.SetPlotProperty(Panel3,"SStrain_gauge_axial",1,2,vbBlue)
        EA_Graph.SetPlotProperty(Panel3,"Strain_gauge_axial",1,5,0)

        counter=counter+1 'Step counter
        objXls_a.Workbooks(1).Save
        Loop
        objXls_a.Workbooks(1).Save
        objXls_a.Quit

End Sub

Sub Pseudo_analysis 'Pseudo analysis algorithm
'Performs a single degree of freedom pseudo dynamic analysis on multi degree of freedom system

Dim Analysis As Variant 'Input to change for the number of analysis being performed
Analysis=1

'In SI Units kg, N , m, otherwise indicated

'Earthquake record time step
Dim dt As Variant
dt=0.02 'Seconds

'Analog output
Dim analog_out As Variant
analog_out=0
EA_IO.SetAnalogOut("PMX_1 CH 9",1,analog_out,OperMode)

'Convergence criteria
```

```
Dim ConvergC As Variant
ConvergC=0.0005

'If the analysis has to be restarted during the test
Dim Restart As Variant
Restart=0 'Restart = 0 (Start new analysis) 'Restart=1 (Continue existing analysis)
Dim time_restart As Variant
time_restart=0 'Last time recorded
Dim i_Lres As Variant
i_Lres=time_restart/dt
'Amplify record
Dim AeR As Variant
AeR=1 'Amplify the import earthqauke record

Dim Load_axial As Variant

Dim objXls_u As Object
Set objXls_u = CreateObject("Excel.Application")

If Restart=0 Then
'Data files - Excel output of the data
objXls_u.Workbooks.Add
objXls_u.Worksheets.Add
objXls_u.Worksheets.Add
objXls_u.Worksheets.Add
objXls_u.Worksheets.Add
objXls_u.Worksheets.Add
objXls_u.Worksheets.Add
objXls_u.Worksheets.Add
objXls_u.Worksheets.Add
objXls_u.Worksheets.Add
objXls_u.Worksheets.Add
objXls_u.Worksheets.Add
objXls_u.Worksheets.Add
objXls_u.Worksheets.Add
objXls_u.Worksheets.Add

objXls_u.Worksheets(1).Name = "Input_and_loading"
objXls_u.Worksheets(2).Name = "Earthquake"
objXls_u.Worksheets(3).Name = "Displacement"
objXls_u.Worksheets(4).Name = "Velocity"
objXls_u.Worksheets(5).Name = "Acceleration"
objXls_u.Worksheets(6).Name = "Energy"
objXls_u.Worksheets(7).Name = "Stiffness"
objXls_u.Worksheets(8).Name = "Mass"
objXls_u.Worksheets(9).Name = "Local_matrices"
objXls_u.Worksheets(10).Name = "Spring_DF"
objXls_u.Worksheets(11).Name = "Force_FDOF"
objXls_u.Worksheets(12).Name = "Force_M"
objXls_u.Worksheets(13).Name = "Force_C"
objXls_u.Worksheets(14).Name = "It_disp"
objXls_u.Worksheets(15).Name = "It_force"

objXls_u.Workbooks(1).SaveAs "C:\Octave\Dynamics\Pseudo\Pseudo_Test_analysis1112_"+CStr(Analysis)+".xlsx"  ' "C:\Octave\Dynamics\Pseudo\OutputDispOutput4.xls"

ElseIf Restart=1 Then

objXls_u.Workbooks.Open "C:\Octave\Dynamics\Pseudo\Pseudo_Test_analysis1112_"+CStr(Analysis)+".xlsx"  ' "C:\Octave\Dynamics\Pseudo\OutputDispOutput4.xls"

End If

'Structural frame input
Dim Bays As Variant
Bays=2  'Number of bays
objXls_u.Worksheets(1).Cells(2,1).Value ="Number of bays ="
objXls_u.Worksheets(1).Cells(2,2).Value =Bays
Dim Stories As Variant
Stories = 2 'Number of stories
objXls_u.Worksheets(1).Cells(3,1).Value ="Number of stories ="
```

```
objXls_u.Worksheets(1).Cells(3,2).Value =Stories
Dim h As Variant
h=4 'm (Height of the story)
objXls_u.Worksheets(1).Cells(4,1).Value ="Story height (h) ="
objXls_u.Worksheets(1).Cells(4,2).Value =h
objXls_u.Worksheets(1).Cells(4,3).Value ="m"
Dim b As Variant
b=6 'm (Width of a bay)
objXls_u.Worksheets(1).Cells(5,1).Value ="Bay width (b) ="
objXls_u.Worksheets(1).Cells(5,2).Value =b
objXls_u.Worksheets(1).Cells(5,3).Value ="m"

'Steel sections
Dim nmat As Variant 'Number of material properties
nmat= 3 'Number
Dim fy As Variant 'Structural steel strength
fy=350 'MPa

'Material 1 (Internal Columns)
objXls_u.Worksheets(1).Cells(7,1).Value ="Material properties"
objXls_u.Worksheets(1).Cells(8,1).Value ="Material 1 (Internal columns)"

objXls_u.Worksheets(1).Cells(8,2).Value ="203.00 x 203.00 x 52.00"
Dim E1 As Variant 'E1 of material type 1
E1=200*10^9             'Pa
objXls_u.Worksheets(1).Cells(9,1).Value ="E1 ="
objXls_u.Worksheets(1).Cells(9,2).Value =E1
objXls_u.Worksheets(1).Cells(9,3).Value ="Pa"

Dim I1 As Variant 'I1 of material type 1
I1=52500000/1000^4  'm^4
objXls_u.Worksheets(1).Cells(10,1).Value ="I1 ="
objXls_u.Worksheets(1).Cells(10,2).Value =I1
objXls_u.Worksheets(1).Cells(10,3).Value ="m^4"

Dim A1 As Variant 'A1 of material type 1
A1=6640/1000^2          'm^2
objXls_u.Worksheets(1).Cells(11,1).Value ="A1 ="
objXls_u.Worksheets(1).Cells(11,2).Value =A1
objXls_u.Worksheets(1).Cells(11,3).Value ="m^2"

Dim Den1 As Variant 'Den1 of material type 1
Den1=7850               'kg/m^3
objXls_u.Worksheets(1).Cells(12,1).Value ="Material density ="
objXls_u.Worksheets(1).Cells(12,2).Value =Den1
objXls_u.Worksheets(1).Cells(12,3).Value ="kg/m^3"

'Material 2 (Beams)
objXls_u.Worksheets(1).Cells(8,5).Value ="Material 2 (Beams)"
objXls_u.Worksheets(1).Cells(8,6).Value ="533.00 x 210.00 x 101.00"
Dim E2 As Variant 'E2 of material type 2
E2=200*10^9             'Pa
objXls_u.Worksheets(1).Cells(9,5).Value ="E2 ="
objXls_u.Worksheets(1).Cells(9,6).Value =E2
objXls_u.Worksheets(1).Cells(9,7).Value ="Pa"

Dim I2 As Variant 'I2 of material type 2
I2=616000000/1000^4     'm^4
objXls_u.Worksheets(1).Cells(10,5).Value ="I2 ="
objXls_u.Worksheets(1).Cells(10,6).Value =I2
objXls_u.Worksheets(1).Cells(10,7).Value ="m^4"

Dim A2 As Variant 'A2 of material type 2
A2=12900/1000^2         'm^2
objXls_u.Worksheets(1).Cells(11,5).Value ="A2 ="
objXls_u.Worksheets(1).Cells(11,6).Value =A2
objXls_u.Worksheets(1).Cells(11,7).Value ="m^2"

Dim Den2 As Variant 'Den2 of material type 2
Den2=7850                   'kg/m^3
objXls_u.Worksheets(1).Cells(12,5).Value ="Material density ="
objXls_u.Worksheets(1).Cells(12,6).Value =Den2
objXls_u.Worksheets(1).Cells(12,7).Value ="kg/m^3"
```

```
'Material 3 (External Columns)
objXls_u.Worksheets(1).Cells(8,9).Value ="Material 3 (External columns)"
objXls_u.Worksheets(1).Cells(8,10).Value ="305.00 x 305.00 x 118.00"
Dim E3 As Variant
E3=200*10^9                  'Pa
objXls_u.Worksheets(1).Cells(9,9).Value ="E3 ="
objXls_u.Worksheets(1).Cells(9,10).Value =E3
objXls_u.Worksheets(1).Cells(9,11).Value ="Pa"

Dim I3 As Variant
I3=276000000/1000^4      'm^4
objXls_u.Worksheets(1).Cells(10,9).Value ="I3 ="
objXls_u.Worksheets(1).Cells(10,10).Value =I3
objXls_u.Worksheets(1).Cells(10,11).Value ="m^4"

Dim a3 As Variant
a3=15000/1000^2          'm^2
objXls_u.Worksheets(1).Cells(11,9).Value ="A3 ="
objXls_u.Worksheets(1).Cells(11,10).Value =a3
objXls_u.Worksheets(1).Cells(11,11).Value ="m^2"

Dim Den3 As Variant
Den3=7850                'kg/m^3
objXls_u.Worksheets(1).Cells(12,9).Value ="Material density ="
objXls_u.Worksheets(1).Cells(12,10).Value =Den3
objXls_u.Worksheets(1).Cells(12,11).Value ="kg/m^3"

'Get earthquake record
Dim nt As Variant
nt=2689 'Number of rows (Data points) of earthquake record
Dim uppe() As Variant
ReDim Preserve uppe(nt-1,1)
uppe=Import_data(nt)

objXls_u.Worksheets(2).Cells(1,1).Value ="Time (s)"
objXls_u.Worksheets(2).Cells(1,2).Value ="Accleration (m/s^2)"
For i=0 To nt-1
    objXls_u.Worksheets(2).Cells(i+2,1).Value =uppe(i,0)
    objXls_u.Worksheets(2).Cells(i+2,2).Value =uppe(i,1)
Next

'Dead load Is imposed On the model by a concrete slab that Is one way
'spaning between the frames
objXls_u.Worksheets(1).Cells(13,1).Value ="Loading on structure"
objXls_u.Worksheets(1).Cells(14,1).Value ="Dead loading"
Dim Span As Variant
Span=2.5                     'm (Transverse span distance between the frames
objXls_u.Worksheets(1).Cells(15,1).Value ="Transverse span ="
objXls_u.Worksheets(1).Cells(15,2).Value =Span
objXls_u.Worksheets(1).Cells(15,3).Value ="m"

'Concrete slab
Dim tc As Variant
tc=0.25                      'm (Thickness of the slab
objXls_u.Worksheets(1).Cells(16,1).Value ="Slab thickness ="
objXls_u.Worksheets(1).Cells(16,2).Value =tc
objXls_u.Worksheets(1).Cells(16,3).Value ="m"

Dim Den_conc As Variant
Den_conc=2400                'kg/m^3 (Density of the concrete)
objXls_u.Worksheets(1).Cells(17,1).Value ="Concrete density ="
objXls_u.Worksheets(1).Cells(17,2).Value =Den_conc
objXls_u.Worksheets(1).Cells(17,3).Value ="kg/m^3"

'Live load
objXls_u.Worksheets(1).Cells(19,1).Value ="Live loading"
Dim LL As Variant
LL=2400                      'N/m^2 (Live load imposed On the frame structure)
objXls_u.Worksheets(1).Cells(19,1).Value ="Live load ="
objXls_u.Worksheets(1).Cells(19,2).Value =LL
objXls_u.Worksheets(1).Cells(19,3).Value ="N/m^2"
```

```
'Masonary walls
Dim Den_mas As Variant
Den_mas=1800    'kg/m3
Dim t_wall As Variant
t_wall=0.23     'm
Dim M_mas As Variant
M_mas=Den_mas*t_wall*h*Span 'kg
Dim W_mas As Variant
W_mas=M_mas*9.81 'N

'Dynamic properties
objXls_u.Worksheets(1).Cells(21,1).Value ="Dynamic properties"
Dim Dp As Variant
Dp=0.05                       '(Damping ratio)
objXls_u.Worksheets(1).Cells(22,1).Value ="Damping ratio ="
objXls_u.Worksheets(1).Cells(22,2).Value =Dp

'Footing placement And initial stiffness
objXls_u.Worksheets(1).Cells(23,1).Value ="Footing initial stiffness"
Dim Column_hinge As Variant
Column_hinge=2
'%%%%%%%%%%%%%%%%%%%%%%%%%%%%%%%%%%%%%%%%%%%%%%%%%%%%%%%%%%%%%%%%%%%%%
Dim kinitial As Variant
kinitial=30000000 'N/m

objXls_u.Worksheets(1).Cells(24,1).Value ="ki ="
objXls_u.Worksheets(1).Cells(24,2).Value =kinitial
objXls_u.Worksheets(1).Cells(24,3).Value ="N/m"

'%%%%%%%%%%%%%%%%%%%%%%%%%%%%%%%%%%%%%%%%%%%%%%%%%%%%%%%%%%%%%%%%%%%%%%

Dim Prop(3,2) As Variant 'Table of material properties

Prop(0,0)=E1
Prop(2,0)=I1
Prop(1,0)=A1
Prop(3,0)=Den1

Prop(0,1)=E2
Prop(2,1)=I2
Prop(1,1)=A2
Prop(3,1)=Den2

Prop(0,2)=E3
Prop(2,2)=I3
Prop(1,2)=a3
Prop(3,2)=Den3

'Preprocessor
Dim nnode As Variant
nnode=(Bays+1)*(Stories+1)

'Coordinates of the nodes
Dim NodeNumber() As Variant
ReDim Preserve NodeNumber(Stories,Bays)
Dim Node_x() As Variant
ReDim Preserve Node_x(Stories,Bays)
Dim Node_y() As Variant
ReDim Preserve Node_y(Stories,Bays)
Dim coord() As Variant 'Dim coord(nnode,2)
ReDim Preserve coord(1,nnode-1)
Dim N_mas As Variant
N_mas=(Stories-1)*2
Dim Nodes_mas() As Variant
ReDim Preserve Nodes_mas(N_mas-1,0)

'Node Numbers
Dim counter As Variant
counter=0
Dim count_mas As Variant
count_mas=-1

For i=0 To Stories
```

```
Dim width As Variant
width = 0
    For j=0 To Bays
    counter=counter+1
    NodeNumber(-i+2,j)=counter
    If j=0 Then
    width =0
    Node_x(i,j)=width
    Else
    width=width+b
    Node_x(i,j)=width
    End If
    Node_y(i,j)=(-i+2)*h
        If j=0 Or j=Bays Then
            If i>0 And i<Stories Then
            count_mas=count_mas+1
            Nodes_mas(count_mas,0)=counter
            End If
        End If
    Next
Next

For i=0 To Stories
    For j=0 To Bays
    coord(0,NodeNumber(i,j)-1)=Node_x(i,j)
    coord(1,NodeNumber(i,j)-1)=Node_y(i,j)
    Next
Next

Dim N_columns As Variant
N_columns=Stories*(Bays+1)
Dim N_beams As Variant
N_beams=Stories*Bays
Dim nbc As Variant
nbc=N_columns+N_beams 'Number of beam elements

'Assign the columns first To the idbc matrix
Dim idbc() As Variant 'Dim idbc(nbc-1,2)
ReDim Preserve idbc(nbc-1,2)

counter=-1
For i=0 To Bays
    If i=0 Or i=Bays Then
        For j=0 To Stories-1
        counter=counter+1
        idbc(counter,0)=NodeNumber(-j+2,i)
        idbc(counter,1)=NodeNumber(-j+1,i)
        idbc(counter,2)=3
        Next
    Else
        For j=0 To Stories-1
        counter=counter+1
        idbc(counter,0)=NodeNumber(-j+2,i)
        idbc(counter,1)=NodeNumber(-j+1,i)
        idbc(counter,2)=1
        Next
    End If
Next

'Assign the beams Second To the idbc matrix
For i=1 To 2
    For j=0 To 1
        counter=counter+1
        idbc(counter,0)=NodeNumber(-i+2,j)
        idbc(counter,1)=NodeNumber(-i+2,j+1)
        idbc(counter,2)=2
    Next
Next

'Supports of the frame structure
Dim support() As Variant
ReDim Preserve support(3,Bays)
```

```
For i=0 To Bays
    If i=Column_hinge-1 Then    'Nonlinear support
    support(0,i)=NodeNumber(Stories,i)
    support(1,i)=0
    support(2,i)=1
    support(3,i)=0
    Else                        'Rest of the supports In the model
    support(0,i)=NodeNumber(Stories,i)
    support(1,i)=1
    support(2,i)=1
    support(3,i)=0
    End If

Next

'Loading On the structure that includes
'Point loads And beam distributed loads On the structure
'Wind loading Not included

Dim loading() As Variant 'loading=zeros(4,nnode);
ReDim Preserve loading(3,nnode-1)

For i=0 To nnode-1
    loading(0,i)=i+1
Next

For i=0 To nbc-1
    If idbc(i,2)=1 Then
    loading(2,idbc(i,0)-1)=loading(2,idbc(i,0)-1)-Prop(3,0)*Prop(1,0)*9.81*h/2
    loading(2,idbc(i,1)-1)=loading(2,idbc(i,1)-1)-Prop(3,0)*Prop(1,0)*9.81*h/2
    ElseIf idbc(i,2)=3 Then
    loading(2,idbc(i,0)-1)=loading(2,idbc(i,0)-1)-Prop(3,2)*Prop(1,2)*9.81*h/2
    loading(2,idbc(i,1)-1)=loading(2,idbc(i,1)-1)-Prop(3,2)*Prop(1,2)*9.81*h/2
    End If
Next

'Add masonary loading
For i=0 To N_mas-1
loading(2,Nodes_mas(i,0)-1)=loading(2,Nodes_mas(i,0)-1)-W_mas
Next

'Distributed loading columns And beams
Dim Distributed_loads(2,1) As Variant               'Distributed_loads=zeros(3,2);

Distributed_loads(0,0)=LL*Span                      'Beams live loads
Distributed_loads(0,1)=0                            'Columns live loads
Distributed_loads(1,0)=Den_conc*Span*tc*9.81        'Beams dead load
Distributed_loads(1,1)=0                            'Columns dead load
Distributed_loads(2,0)=Prop(3,1)* Prop(1,1)*9.81    'Beams dead load
Distributed_loads(2,1)=0                            'Columns dead load

Dim loading_beam() 'loading_beam=zeros(nbc,2);
ReDim Preserve loading_beam(nbc-1,1)

For i=0 To nbc-1
    If idbc(i,2)=2 Then

    loading_beam(i,1)=Distributed_loads(0,0)+Distributed_loads(1,0)+Distributed_loads(2,0)
    loading_beam(i,0)=i+1
    Else

    loading_beam(i,1)=Distributed_loads(0,1)+Distributed_loads(1,1)+Distributed_loads(2,1)
    loading_beam(i,0)=i+1
    End If
Next

'Static calculations
'___________________________________________________________________________________________

Dim supp() As Variant
```

```
ReDim Preserve supp(2,nnode-1)

For i=0 To 2
    For j=0 To 8
    supp(i,j)=0
    Next
Next

For i=1 To 3 'Dim support(3,2) As Double
    For j=0 To 2
    supp(i-1,support(0,j)-1)=support(i,j)
    Next
Next

'Determines the dof of freedom
Dim dof() As Variant
ReDim Preserve dof(2,nnode-1)
counter=0

'First assigns the free dof numbers

For i=0 To 8 'Number of nodes-1
    For j=0 To 2
        If supp(j,i)=0 Then
        counter=counter+1
        dof(j,i)=counter
        End If
    Next
Next
Dim nfdof As Variant
nfdof=counter

'Assigns the fixed dof numbers

For i=0 To 8 'Number of nodes-1
    For j=0 To 2
        If supp(j,i)=1 Then
        counter=counter+1
        dof(j,i)=counter
        End If
    Next
Next
Dim tdof As Double
tdof=counter+1 'Total degrees of freedom + DOF of the footing hinge

'Calculates the point loads on the nodes
Dim ptfof() As Variant
ReDim Preserve ptfof(tdof-1,0)  'ptfof=zeros(tdof,1);
Dim aL As Variant

For i=0 To nnode-1
    For j=0 To 2
        If dof(j,loading(0,i)-1)<=tdof Then
        ptfof(dof(j,loading(0,i)-1)-1,0)=loading(j+1,i)
        End If
    Next
Next

Dim P() As Variant
ReDim Preserve P(nfdof-1,0)

For i=0 To nfdof-1
P(i,0)=ptfof(i,0)
Next

'Calculates the member information
Dim mem_info() As Variant
ReDim Preserve mem_info(1,nbc-1) 'mem_info=zeros(2,nbc);

'Calculates the length of Each of the members And places it In mem_info(1,i)
For i=0 To nbc-1
mem_info(0,i)=((coord(0,idbc(i,1)-1)-coord(0,idbc(i,0)-1))^2+(coord(1,idbc(i,1)-1)-coo
rd(1,idbc(i,0)-1))^2)^(1/2)
```

```
Next

'Calculates the rotation of the member where anticlockwise Is positive
Dim x1 As Variant
Dim y1 As Variant
Dim x2 As Variant
Dim y2 As Variant
Dim pi As Variant
pi=4*Atn(1)

For i=0 To nbc-1
'Obtain the nodal coordinates from the coord Array
x1 = coord (0,idbc(i,0)-1)
y1 = coord (1,idbc(i,0)-1)
x2 = coord (0,idbc(i,1)-1)
y2 = coord (1,idbc(i,1)-1)
'Calculate the rotation angle
    If (x2-x1)=0 Then
    mem_info(1,i)=pi/2
    Else
    mem_info(1,i)=Atn((y2-y1)/(x2-x1))
    End If
Next

'Calculates the member degrees of freedom
Dim mdof() As Variant
ReDim Preserve mdof(5,nbc-1) 'mdof=zeros(6,nbc)

For i=0 To nbc-1
counter=-1
    For K=0 To 1
        For j=0 To 2
        counter=counter+1
        mdof(counter,i)=dof(j,idbc(i,K)-1)
        Next
    Next
Next

Dim estiff_local() As Variant
ReDim Preserve estiff_local(5,5,nbc-1) 'estiff_local{1,nbc}=[]
Dim etran_local() As Variant
ReDim Preserve etran_local(5,5,nbc-1) 'estiff_local{1,nbc}=[]
Dim etranT_local() As Variant
ReDim Preserve etranT_local(5,5,nbc-1) 'estiff_local{1,nbc}=[]
Dim K_beam_local() As Variant
ReDim Preserve K_beam_local(5,5,nbc-1) 'estiff_local{1,nbc}=[]

Dim global_stiffness() As Variant
ReDim Preserve global_stiffness(tdof-1,tdof-1)
Dim KSpring() As Variant
ReDim Preserve KSpring(1,1)
Dim Smdof() As Variant
ReDim Preserve Smdof(1,0)

'Zeros the global stiffness matrix
For i=0 To tdof-1
    For j=0 To tdof-1
    global_stiffness(i,j)=0
    Next
Next

assemble_local_stiffness_beam(estiff_local,etran_local,K_beam_local,etranT_local,nbc,Prop,idbc,mem_info)
assemble_beam_stiffness(global_stiffness,tdof,K_beam_local,nbc,mdof)
KSpring=Spring_stiff(global_stiffness,Column_hinge,dof,tdof,kinitial,Smdof)

Dim Pw_local() As Variant
ReDim Preserve Pw_local(5,nbc-1)
Dim DOF_c() As Variant
ReDim Preserve DOF_c(5,nbc-1)
Dim Pwout() As Variant
ReDim Preserve Pw(nfdof-1,0)
Dim Pwtdof() As Variant
```

```
ReDim Preserve Pwtdof(tdof-1,0)

For i=0 To tdof-1
    Pwtdof(i,0)=0
Next

Pw=beam_loads(loading_beam,nbc,etranT_local,dof,mem_info,idbc,tdof,nfdof,Pw_local,DOF_c,Pwtdof)

R=Matrix_addition(P,Pw,nfdof,1)

Disp=solve(global_stiffness,R,nfdof)

Dim Rs() As Variant
Rs=reactions(global_stiffness,Disp,nfdof,tdof)

If Restart=0 Then
objXls_u.Worksheets(3).Cells(1,1).Value =0
objXls_u.Worksheets(11).Cells(1,1).Value =0
For i = 0 To nfdof-1
    objXls_u.Worksheets(3).Cells(i+2,1).Value =Disp(i,0)
    objXls_u.Worksheets(11).Cells(i+2,1).Value =R(i,0)
Next
objXls_u.Workbooks(1).Save
End If

Dim IMF_L() As Variant
ReDim Preserve IMF_L(5,nbc-1)
Dim IMD_L() As Variant
ReDim Preserve IMD_L(5,nbc-1)
Dim IMD_G() As Variant
ReDim Preserve IMD_G(5,nbc-1)
Dim IMF_G() As Variant
ReDim Preserve IMF_G(5,nbc-1)
Dim fso() As Variant
ReDim Preserve fso(5,nbc-1)

memf(IMF_L,IMD_L,IMD_G,IMF_G,fso,supp,nnode,Disp,nbc,idbc,etran_local,etranT_local,estiff_local,Pw_local)

Dim ds() As Variant
ReDim Preserve ds(1,0)
Dim IMFs() As Variant
ReDim Preserve IMFs(1,0)
memf_spring(KSpring,Disp,Smdof,ds,IMFs)

'Dynamic calculations
'_____________________________________________________________________________________

Dim fyspring As Variant
Dim k2 As Variant
Dim Mf As Variant

fyspring=37830.3235480421       'N
k2=0.146706193729911*kinitial   'N/m
Mf=770.3                        'kg

'Damage index
Dim Dpa As Variant
Dpa=0
Dim di As Variant
di=0
Dim dumax As Variant
dumax=0.00504481947024698
Dim bPa As Variant
bPa=0.05

'Initial calculations
Dim Fsi1 As Variant
ReDim Preserve Fsi1(tdof-1,0)

Dim Ui1 As Variant
```

```
ReDim Preserve Uil(tdof-1,0)
For i=0 To tdof-1
Uil(i,0)=0
Next

If Restart=1 Then
    For i=0 To 5
        For j=0 To nbc-1
        IMD_G(i,j)=objXls_u.Worksheets(9).Cells(6*i_Lres+2+i,j+2).Value
        fso(i,j)=objXls_u.Worksheets(9).Cells(6*i_Lres+2+i,j+nbc+4).Value
        Next
    Next

    For i=0 To 1
        IMFs(i,0)=objXls_u.Worksheets(10).Cells(i+2,i_Lres+1).Value
        ds(i,0)=objXls_u.Worksheets(10).Cells(i+4,i_Lres+1).Value
    Next
    Dpa=objXls_u.Worksheets(2).Cells(i_Lres+2,5).Value

End If

initial_conditions_static(Fsi1,Uil,fso,IMD_G,mdof,tdof,IMFs,Smdof,nbc)

Dim global_mass() As Variant
ReDim global_mass(tdof-1,tdof-1)

'Zeros the global mass matrix
For i=0 To tdof-1
    For j=0 To tdof-1
    global_mass(i,j)=0
    Next
Next

global_mass_self=assemble_mass_self(global_mass,nbc,Prop,idbc,mem_info,mdof,tdof) 'Self weight
global_mass_DL=assemble_mass_DL(global_mass,nbc,idbc,mem_info,mdof,tdof,tc,Span,Den_conc) 'Dead load (Concrete slab)
global_mass_LL=assemble_mass_LL(global_mass,nbc,idbc,mem_info,mdof,tdof,Span,LL) 'Live load
global_mass_Point=assemble_mass_Point(global_mass,dof,tdof,N_mas,Nodes_mas,M_mas,mdof)  'Mass due to masonary walls load

'Foundation mass
global_mass(Smdof(1,0)-1,Smdof(1,0)-1)=global_mass(Smdof(1,0)-1,Smdof(1,0)-1)+Mf

Dim tmdof As Variant
Dim kttv() As Variant
Dim Mttf() As Variant
Dim Uto() As Variant
ReDim Preserve Uto(nfdof-1,0)
Dim eig() As Variant
ReDim Preserve eig(1,0)
Dim Lm() As Variant
ReDim Preserve Lm(nfdof-1,0)

static_condensation_initial(Lm,kttv,Uto,tmdof,Mttf,global_stiffness,global_mass,mdof,nfdof,Fsi1,Uil,nbc)
eig=eigenvalues(Mttf,kttv,tmdof)

For i=0 To tmdof-1
    For j=0 To tmdof-1
    objXls_u.Worksheets(7).Cells(i+1,j+1).Value =kttv(i,j)
    objXls_u.Worksheets(8).Cells(i+1,j+1).Value =Mttf(i,j)
    Next
Next

If Restart=0 Then
objXls_u.Worksheets(1).Cells(26,1).Value ="Eigenvalues"
objXls_u.Worksheets(1).Cells(27,1).Value ="Eig1 = "
objXls_u.Worksheets(1).Cells(28,1).Value ="Eig2 = "
objXls_u.Worksheets(1).Cells(27,2).Value =eig(0,0)
objXls_u.Worksheets(1).Cells(28,2).Value =eig(1,0)
End If
```

```
Dim Cff() As Variant
'ReDim Preserve Damp(1,0)

Cff=Rayleigh_damping_nonlinear(eig,Mttf,kttv,Dp,tmdof)

Dim ui() As Variant
ReDim Preserve ui(tmdof-1,1)
Dim upi() As Variant
ReDim Preserve upi(tmdof-1,1)
Dim uppi() As Variant
ReDim Preserve uppi(tmdof-1,1)
Dim fsi() As Variant
ReDim Preserve fsi(tmdof-1,0)

If Restart=0 Then
    For I=0 To tmdof-1
    ui(i,1)=Uto(i,0)
    upi(i,1)=0
    uppi(i,1)=0
    Next

ElseIf Restart=1 Then

    For I=0 To tmdof-1
    ui(i,1)=Uto(i,0)
    upi(i,1)=objXls_u.Worksheets(4).Cells(i+2,i_Lres+2).Value
    uppi(i,1)=objXls_u.Worksheets(5).Cells(i+2,i_Lres+2).Value
    Next
End If

fsi=Matrix_multiplication(kttv,ui,tmdof,tmdof,tmdof,1)

Dim IMF_Li() As Variant
ReDim Preserve IMF_Li(5,nbc-1,1)
Dim IMD_Li() As Variant
ReDim Preserve IMD_Li(5,nbc-1,1)
Dim IMD_Gi() As Variant
ReDim Preserve IMD_Gi(5,nbc-1,1)
Dim IMF_Gi() As Variant
ReDim Preserve IMF_Gi(5,nbc-1,1)
Dim fsiE() As Variant
ReDim Preserve fsiE(5,nbc-1,1)

For i=0 To 5
    For j=0 To nbc-1
    IMD_Gi(i,j,0)=0
    IMD_Gi(i,j,1)=1
    fsiE(i,j,0)=0
    fsiE(i,j,1)=1
    Next
Next

Sort_matrix(IMF_Li,IMF_L,6,nbc)
Sort_matrix(IMD_Li,IMD_L,6,nbc)
Sort_matrix(IMD_Gi,IMD_G,6,nbc)
Sort_matrix(IMF_Gi,IMF_G,6,nbc)
Sort_matrix(fsiE,fso,6,nbc)

If Retart=0 Then
'Saves local matrices to output file
objXls_u.Worksheets(9).Cells(1,2).Value ="IMD_Gi"
objXls_u.Worksheets(9).Cells(1,nbc+4).Value ="fsiE"
objXls_u.Worksheets(9).Cells(1,1).Value ="Time (s)"
objXls_u.Worksheets(9).Cells(1,nbc+3).Value ="Time (s)"
objXls_u.Worksheets(9).Cells(2,1).Value =0
objXls_u.Worksheets(9).Cells(2,nbc+3).Value =0

    For i=0 To 5
        For j=0 To nbc-1
        objXls_u.Worksheets(9).Cells(i+2,j+2).Value =IMD_G(i,j)
        objXls_u.Worksheets(9).Cells(i+2,j+nbc+4).Value =fso(i,j)
        Next
```

```
        Next
    End If

    Dim IMDsi() As Variant
    ReDim Preserve IMDsi(1,nt-1)
    Dim IMFsi() As Variant
    ReDim Preserve IMFsi(1,nt-1)

    If Restart=0 Then
    vector_sort(IMFsi,IMFs,2,0)
    vector_sort(IMDsi,ds,2,0)
    'Saves force matrix
    objXls_u.Worksheets(10).Cells(1,1).Value =0
        For i=0 To 1
            objXls_u.Worksheets(10).Cells(i+2,1).Value =IMFs(i,0)
            objXls_u.Worksheets(10).Cells(i+4,1).Value =ds(i,0)
        Next
    ElseIf Restart=1 Then
        For i=0 To i_Lres
            For j=0 To 1
            IMFsi(j,i)=objXls_u.Worksheets(10).Cells(j+2,i+1).Value
            IMDsi(j,i)=objXls_u.Worksheets(10).Cells(j+4,i+1).Value
            Next
        Next
    End If

    'Energy calculations
    Dim Energy_Ps As Variant
    Dim Energy_Ms() As Variant
    ReDim Preserve Energy_Ms(nt-1,0)
    Dim Energy_Cs() As Variant
    ReDim Preserve Energy_Cs(nt-1,0)
    Dim Energy_Ks() As Variant
    ReDim Preserve Energy_Ks(nt-1,0)
    Dim Energy_Hs() As Variant
    ReDim Preserve Energy_Hs(nt-1,0)

    Dim Energy_K As Variant
    Dim Energy_H As Variant
    Dim Energy_M As Variant
    Dim Energy_C As Variant

    'Internal energy
    Dim Energy_Total() As Double
    ReDim Preserve Energy_Total(nt-1)
    Dim Energy_Stiffness() As Double
    ReDim Preserve Energy_Stiffness(nt-1)
    Dim Energy_Damping() As Double
    ReDim Preserve Energy_Damping(nt-1)
    Dim Energy_Hys() As Double
    ReDim Preserve Energy_Hys(nt-1)

    'Load cell, strain gauges and LVDT readings

    Dim Strain_Left As Double
    Dim Strain_right As Double

    Dim Strain_Left_disp() As Double
    ReDim Preserve Strain_Left_disp(nt-1)
    Dim Strain_right_disp() As Double
    ReDim Preserve Strain_right_disp(nt-1)

    Dim LVDT1 As Double
    Dim LVDT2 As Double
    Dim LVDT3 As Double
    Dim LVDT4 As Double

    Dim LVDT1_disp() As Double
    ReDim Preserve LVDT1_disp(nt-1)
    Dim LVDT2_disp() As Double
    ReDim Preserve LVDT2_disp(nt-1)
    Dim LVDT3_disp() As Double
    ReDim Preserve LVDT3_disp(nt-1)
```

```
Dim LVDT4_disp() As Double
ReDim Preserve LVDT4_disp(nt-1)

'External energy
Dim Disp_P() As Variant
ReDim Preserve Disp_P(nfdof-1,1)
Dim Force_P() As Variant
ReDim Preserve Force_P(nfdof-1,1)

If Restart= 0 Then
    Energy_K=0
    Energy_H=0
    Energy_M=0
    Energy_C=0

    For i=0 To 5
        For j=0 To nbc-1
        Energy_K=Energy_K+0.5*IMD_G(i,j)*fso(i,j)
        Next
    Next
    Energy_H=0.5*IMDsi(1,0)*IMFsi(1,0)

    Energy_Ms(0,0)=0
    Energy_Cs(0,0)=0
    Energy_Ks(0,0)=Energy_K
    Energy_Hs(0,0)=Energy_H

    Energy_Ps=0
    For i=0 To nfdof-1
    Energy_Ps=Energy_Ps+0.5*R(i,0)*Disp(i,0)
    Next

    'External energy

    For i=0 To nfdof-1
    Disp_P(i,1)=Disp(i,0)
    Force_P(i,1)=R(i,0)
    Next

    Energy_Total(0)=Energy_Ms(0,0)+Energy_Cs(0,0)+Energy_Ks(0,0)+Energy_Hs(0,0)
    Energy_Stiffness(0)=Energy_Ks(0,0)+Energy_Hs(0,0)+Energy_Cs(0,0)
    Energy_Damping(0)=Energy_Hs(0,0)+Energy_Cs(0,0)
    Energy_Hys(0)=Energy_Hs(0,0)

    'Readings from LVDTS, load cells and strain gauges
    EA_IO.Measure("MX840_SL",Strain_Left,1)
    EA_IO.Measure("MX840_SR",Strain_right,1)
    EA_IO.Measure("Load cell",Load_axial,1)

    objXls_u.Worksheets(2).Cells(2,8).Value =Load_axial

    objXls_u.Worksheets(2).Cells(2,10).Value =Strain_Left
    objXls_u.Worksheets(2).Cells(2,11).Value =Strain_right

    Strain_Left_disp(0)=Strain_Left
    Strain_right_disp(0)=Strain_right

    EA_IO.Measure("PMX_LVDT1",LVDT1,1)
    EA_IO.Measure("PMX_LVDT2",LVDT2,1)
    EA_IO.Measure("PMX_LVDT3",LVDT3,1)
    EA_IO.Measure("PMX_LVDT4",LVDT4,1)

    objXls_u.Worksheets(2).Cells(2,13).Value =LVDT1
    objXls_u.Worksheets(2).Cells(2,14).Value =LVDT2
    objXls_u.Worksheets(2).Cells(2,15).Value =LVDT3
    objXls_u.Worksheets(2).Cells(2,16).Value =LVDT4

    LVDT1_disp(0)=LVDT1
    LVDT2_disp(0)=LVDT2
    LVDT3_disp(0)=LVDT3
    LVDT4_disp(0)=LVDT4

ElseIf Restart=1 Then
```

```
    Energy_K=objXls_u.Worksheets(6).Cells(i_Lres+2,4).Value
    Energy_H=objXls_u.Worksheets(6).Cells(i_Lres+2,5).Value
    Energy_M=objXls_u.Worksheets(6).Cells(i_Lres+2,2).Value
    Energy_C=objXls_u.Worksheets(6).Cells(i_Lres+2,3).Value
    Energy_Ps=objXls_u.Worksheets(6).Cells(i_Lres+2,6).Value

    For i=0 To i_Lres
        Energy_Ms(i,0)=objXls_u.Worksheets(6).Cells(i+2,2).Value
        Energy_Cs(i,0)=objXls_u.Worksheets(6).Cells(i+2,3).Value
        Energy_Ks(i,0)=objXls_u.Worksheets(6).Cells(i+2,4).Value
        Energy_Hs(i,0)=objXls_u.Worksheets(6).Cells(i+2,5).Value

        Energy_Total(i)=CDbl(Energy_Ms(i,0)+Energy_Cs(i,0)+Energy_Ks(i,0)+Energy_Hs(i,
        0))
        Energy_Stiffness(i)=CDbl(Energy_Ks(i,0)+Energy_Hs(i,0)+Energy_Cs(i,0))
        Energy_Damping(i)=CDbl(Energy_Hs(i,0)+Energy_Cs(i,0))
        Energy_Hys(i)=CDbl(Energy_Hs(i,0))
        Strain_Left_disp(i)=objXls_u.Worksheets(2).Cells(i+2,10).Value
        Strain_right_disp(i)=objXls_u.Worksheets(2).Cells(i+2,11).Value
        LVDT1_disp(i)=objXls_u.Worksheets(2).Cells(i+2,13).Value
        LVDT2_disp(i)=objXls_u.Worksheets(2).Cells(i+2,14).Value
        LVDT3_disp(i)=objXls_u.Worksheets(2).Cells(i+2,15).Value
        LVDT4_disp(i)=objXls_u.Worksheets(2).Cells(i+2,16).Value

    Next

    For i=0 To nfdof-1
    Disp_P(i,1)=objXls_u.Worksheets(3).Cells(i+2,i_Lres+1).Value
    Force_P(i,1)=objXls_u.Worksheets(11).Cells(i+2,i_Lres+1).Value
    Next

End If


Dim Force_M() As Variant
ReDim Preserve Force_M(tmdof-1,1)
Dim Force_C() As Variant
ReDim Preserve Force_C(tmdof-1,1)

If Restart=0 Then
For i=0 To tmdof-1
    For j=0 To 1
    Force_M(i,j)=0
    Force_C(i,j)=0
    Next
    objXls_u.Worksheets(12).Cells(i+2,1).Value =0
    objXls_u.Worksheets(13).Cells(i+2,1).Value =0
Next

ElseIf Restart=1 Then
    For i=0 To tmdof-1
        Force_M(i,0)=objXls_u.Worksheets(12).Cells(i+2,i_Lres+1).Value
        Force_C(i,0)=objXls_u.Worksheets(13).Cells(i+2,i_Lres+1).Value
    Next
End If

'----------------------------------------------------------
'Output data initial
If Restart=0 Then
objXls_u.Worksheets(4).Cells(1,1).Value ="DOF \ t(s)"
objXls_u.Worksheets(5).Cells(1,1).Value ="DOF \ t(s)"
For i = 0 To tmdof-1
    objXls_u.Worksheets(4).Cells(i+2,1).Value =Lm(i,0)+1
    objXls_u.Worksheets(5).Cells(i+2,1).Value =Lm(i,0)+1
Next

objXls_u.Worksheets(4).Cells(1,2).Value =0
objXls_u.Worksheets(5).Cells(1,2).Value =0
For i = 0 To tmdof-1
    objXls_u.Worksheets(4).Cells(i+2,2).Value =0
    objXls_u.Worksheets(5).Cells(i+2,2).Value =0
Next
```

```
'Energy data
objXls_u.Worksheets(6).Cells(1,1).Value ="Time (s)"
objXls_u.Worksheets(6).Cells(1,2).Value ="Mass energy (J)"
objXls_u.Worksheets(6).Cells(1,3).Value ="Damping (J)"
objXls_u.Worksheets(6).Cells(1,4).Value ="Stiffness (J)"
objXls_u.Worksheets(6).Cells(1,5).Value ="Hysteretic (J)"
objXls_u.Worksheets(6).Cells(1,6).Value ="Input Energy (J)"

objXls_u.Worksheets(6).Cells(1,8).Value ="H"
objXls_u.Worksheets(6).Cells(1,9).Value ="H+D"
objXls_u.Worksheets(6).Cells(1,10).Value ="H+D+S"
objXls_u.Worksheets(6).Cells(1,11).Value ="H+D+S+M"

objXls_u.Worksheets(6).Cells(2,1).Value =0
objXls_u.Worksheets(6).Cells(2,2).Value =0          'Mass or inertia energy / kinetic energy
objXls_u.Worksheets(6).Cells(2,3).Value =0          'Damping energy
objXls_u.Worksheets(6).Cells(2,4).Value =Energy_K   'Stiffness energy/potential energy
objXls_u.Worksheets(6).Cells(2,5).Value =Energy_H   'Hysteretic energy of the footing
objXls_u.Worksheets(6).Cells(2,6).Value =Energy_Ps  'Input energy
objXls_u.Worksheets(6).Cells(2,8).Value =Energy_H
objXls_u.Worksheets(6).Cells(2,9).Value =Energy_H+0
objXls_u.Worksheets(6).Cells(2,10).Value =Energy_H+0+Energy_K
objXls_u.Worksheets(6).Cells(2,11).Value =Energy_H+0+Energy_K+0

'Earthquake and numerical results output
objXls_u.Worksheets(2).Cells(1,3).Value ="Displacement (mm)"
objXls_u.Worksheets(2).Cells(1,4).Value ="Force (kN)"
objXls_u.Worksheets(2).Cells(1,5).Value ="Damage Index"
objXls_u.Worksheets(2).Cells(1,6).Value ="Convergence"
objXls_u.Worksheets(2).Cells(1,7).Value ="Iterations"
objXls_u.Worksheets(2).Cells(1,8).Value ="Axial Load (kN)"
objXls_u.Worksheets(2).Cells(2,3).Value =ds(1,0)
objXls_u.Worksheets(2).Cells(2,4).Value =IMFs(1,0)
objXls_u.Worksheets(2).Cells(2,5).Value =0

'Strain gauges output data
objXls_u.Worksheets(2).Cells(1,10).Value ="Strain gauge left (micro)"
objXls_u.Worksheets(2).Cells(1,11).Value ="Strain gauge right (micro)"

'LVDTs output data
objXls_u.Worksheets(2).Cells(1,13).Value ="LVDT1 (mm)"
objXls_u.Worksheets(2).Cells(1,14).Value ="LVDT2 (mm)"
objXls_u.Worksheets(2).Cells(1,15).Value ="LVDT3 (mm)"
objXls_u.Worksheets(2).Cells(1,16).Value ="LVDT4 (mm)"

End If

Dim count As Variant
Dim num As Variant
Dim ks As Variant

EA_Graph.ClearPlots(Panel1,"Graph1")
EA_Graph.Refresh(Panel1,"Graph1")
Dim xSpring() As Double
ReDim Preserve xSpring(nt)
Dim ySpring() As Double
ReDim Preserve ySpring(nt)
xSpring(0)=0
ySpring(0)=0

EA_Graph.PlotArrayXY(Panel1,"Graph1",1,nt+1, xSpring(), ySpring())
EA_Graph.SetPlotProperty(Panel1,"Graph1",1,2,vbRed)
EA_Graph.Refresh(Panel1,"Graph1")

EA_Graph.ClearPlots(Panel1,"Graph2")
EA_Graph.Refresh(Panel1,"Graph2")
Dim xEarth() As Double
ReDim Preserve xEarth(nt)
Dim yEarth() As Double
ReDim Preserve yEarth(nt)
xEarth(0)=0
yEarth(0)=0
```

```
EA_Graph.PlotArrayXY(Panel1,"Graph2",1,nt+1, xEarth(), yEarth())
EA_Graph.SetPlotProperty(Panel1,"Graph2",1,2,vbBlue)
EA_Graph.Refresh(Panel1,"Graph2")
Dim LVDT_counter As Variant
LVDT_counter=0
Dim PGAmax As Variant
PGAmax=0
Dim Disp_read_servo As Double
Dim Force_read_servo As Double

EA_IO.ZeroBalanceControl("Displacement_Hor",1)  'Zeros Horizontal displacement
EA_IO.ZeroBalanceControl("Force_Hor",1)         'Zeros Horizontal force

Dim ncpts As Variant
ncpts=50
Dim Fsavg As Variant
Dim Disp_i_1 As Variant
Disp_i_1=0
Dim axial_read As Double
'Start of time stepping
'--------------------------------------------------------
For i_Load=i_Lres+1 To nt-1 'Starts the earthquake record
EA_Panel.SetValue(Panel1,"Increment_out",i_Load)
EA_Panel.SetValue(Panel1,"Time_out",uppe(i_Load,0))
objXls_u.Worksheets(14).Cells(1,i_Load).Value =uppe(i_Load,0)
objXls_u.Worksheets(15).Cells(1,i_Load).Value =uppe(i_Load,0)

EA_IO.Measure("Load cell",axial_read,1)
EA_Panel.SetValue(Panel1,"Axial_load",CVar(axial_read))
objXls_u.Worksheets(2).Cells(i_Load+2,8).Value =CVar(axial_read)

If Abs(uppe(i_Load,1))>PGAmax Then
PGAmax=Abs(uppe(i_Load,1))
End If
EA_Panel.SetValue(Panel1,"PGA",PGAmax)

Initial_sort_vec(ui,tmdof,1,0)
Initial_sort_vec(upi,tmdof,1,0)
Initial_sort_vec(uppi,tmdof,1,0)

Initial_sort_vec(Disp_P,nfdof,1,0)
Initial_sort_vec(Force_P,nfdof,1,0)

'Initial_sort_mat(IMF_Li,6,nbc,1,0)
'Initial_sort_mat(IMD_Li,6,nbc,1,0)
Initial_sort_mat(IMD_Gi,6,nbc,1,0)
'Initial_sort_mat(IMF_Gi,6,nbc,1,0)
Initial_sort_mat(fsiE,6,nbc,1,0)

For i=0 To tdof-1
    For j=0 To 0
    EA_Panel.SetCell(Panel2,"PropTable",j+1,i+1,Fsi1(i,j))
    Next
Next

Initial_sort_vec(IMFsi,2,i_Load-1,i_Load)
Initial_sort_vec(IMDsi,2,i_Load-1,i_Load)
count=count+1
num=0
Fsavg=0
EA_Panel.SetCell(Panel1,"Converge_table",2,1,0)

ks=kinitial

xEarth(i_Load)=CDbl(uppe(i_Load,0))
yEarth(i_Load)=CDbl(AeR*uppe(i_Load,1))
EA_Graph.PlotArrayXY(Panel1,"Graph2",1,nt+1, xEarth(), yEarth())
EA_Graph.SetPlotProperty(Panel1,"Graph2",1,2,vbBlue)
EA_Graph.Refresh(Panel1,"Graph2")

Dim converge_time_step As Variant
converge_time_step=0
```

```
EA_Panel.SetCell(Panel1,"Converge_time_table",1,1,0)

    Do While num<5000 'Convergence at each time step
    EA_Panel.GetCell(Panel1,"Converge_time_table",1,1,converge_time_step)

        'Zeros the global stiffness matrix
        For i=0 To tdof-1
            For j=0 To tdof-1
            global_stiffness(i,j)=0
            Next
        Next
        assemble_beam_stiffness(global_stiffness,tdof,K_beam_local,nbc,mdof)
        KSpring=Spring_stiff(global_stiffness,Column_hinge,dof,tdof,ks,Smdof)

        Dim Mfft() As Variant
        Dim lh() As Variant
        Dim Ps() As Variant
        Dim koof() As Variant
        Dim ktof() As Variant
        Dim kotf() As Variant


        static_condensation(Lm,kotf,kttv,fsi,ktof,koof,Ps,lh,Mttf,global_stiffness,mdof,nfdof,Fsi1,Ui1,global_mass,Pwtdof,ptfof,i_Load,nbc,tdof)

        Dim a_1() As Variant
        Dim a_2() As Variant
        Dim a_3() As Variant

        Dynamic_analysis_coefficients(a_1,a_2,a_3,dt,Mttf,Cff,tmdof)
        'P=-Mttf*lh*uppe(i_Load,2);
        Dim PEarth() As Variant
        ReDim Preserve PEarth(tmdof-1,0)

        PEarth=Matrix_multiplcation_constant(-AeR*uppe(i_Load,1),Matrix_multiplication(Mttf,lh,tmdof,tmdof,tmdof,1),tmdof,1)
        'Pa=P+Ps(1:tmdof,1)-ktof*(koof\Ps(tmdof+1:nfdof,1))
        Pa_calc(tmdof,nfdof,Ps,PEarth,ktof,koof)
        Dim Pa() As Variant
        ReDim Preserve Pa(tmdof-1,0)
        Pa=Pa_calc(tmdof,nfdof,Ps,PEarth,ktof,koof)
        'Pp=Pa+a1*ui(:,i_Load-1)+a2*upi(:,i_Load-1)+a3*uppi(:,i_Load-1)
        Dim Pp() As Variant
        ReDim Preserve Pp(tmdof-1,0)
        Pp=Pp_calcs(Pa,tmdof,ui,upi,uppi,a_1,a_2,a_3)
        'R=Pp-fsi(:,i_Load)-a1*ui(:,i_Load)
        Dim Residual() As Variant
        ReDim Preserve Residual(tmdof-1,0)
        Residual=R_calc(Pp,fsi,a_1,ui,tmdof)
        'Norm_max=max(abs(R))
        Dim Norm_max As Variant
        Norm_max=Norm_Residual(Residual,tmdof)
        num=num+1

    EA_Panel.SetValue(Panel1,"Iteration_out",num)
    EA_Panel.SetValue(Panel1,"Convergence_out",Norm_max)

    If Norm_max<ConvergC Then Exit Do

    If converge_time_step=1 Then Exit Do

    'Calculates the Newmarks pseudo stiffness
    'ktp=kttv+A1
    Dim ktp() As Variant
    ReDim Preserve ktp(tmdof-1,tmdof-1)
    ktp=Matrix_addition(kttv,a_1,tmdof,tmdof)
    Dim du() As Variant
    ReDim Preserve du(tmdof-1,0)
    du=Matrix_solver(ktp,Residual,tmdof)
    'ui(:,i_Load)=ui(:,i_Load)+du
    For i= 0 To tmdof-1
        ui(i,1)=ui(i,1)+du(i,0)
    Next
```

```
    Dim uig() As Variant
    Dim uigdu() As Variant
    Dim Puig() As Variant

    static_condensation_out(uig(),uigdu(),Puig(),ui,kotf,koof,Ps,Lm,i_Load,tmdof,nfdof
    ,tdof,du,PEarth)
    Dim Fsi2() As Variant

    internal_dynamic_loads(IMD_G,IMD_L,IMF_L,IMF_G,Fsi2,nbc,uig,mdof,etran_local,etran
    T_local,estiff_local,Pw_local)
    Dim Fs As Variant
    memf_spring_dynamic(Fs,IMFsi,IMDsi,KSpring,uig,Smdof,uigdu,i_Load)

'%%%%%%%%%%%%%%%%%%%%%%%%%%%%%%%%%%%%%%%%%%%%%%%%%
'Sends displacement reading to actuator
'Reads from load cell and LVDTS

'EA_IO.SetAnalogOut(ByVal Channel As Variant, ByVal Connector As Integer, ByVal
Voltage As Double, ByVal OperMode As Long, Optional ByVal OutputNumber As Integer)
As Long
'Dim LVDT_read As Double
'EA_IO.Measure("MX410_1_CH 1",LVDT_read,1)

    If num<=ncpts  Then

    'Analog output
    Dim anolog_step As Variant
    Dim time_step_analog As Variant
    Dim change_disp As Variant

    change_disp=Abs(uig(Smdof(1,0)-1,0)*1000-Disp_i_1)
    anolog_step=Int(2*change_disp)+1
    time_step_analog=(uig(Smdof(1,0)-1,0)*1000-Disp_i_1)/anolog_step

    For i_as=1 To anolog_step
    analog_out=(1/-6.5025)*(Disp_i_1+i_as*time_step_analog) 'volts from mm
    EA_Panel.SetValue(Panel1,"DispRead_out",(Disp_i_1+i_as*time_step_analog)) 'mm
    EA_IO.SetAnalogOut("PMX_1 CH 9",1,analog_out,1)
    Wait 0.05
    Next

    End If
Disp_i_1=uig(Smdof(1,0)-1,0)*1000

analog_out=(1/-6.5025)*uig(Smdof(1,0)-1,0)*1000 'volts from mm
EA_IO.SetAnalogOut("PMX_1 CH 9",1,analog_out,1)
EA_Panel.SetValue(Panel1,"DispRead_out",uig(Smdof(1,0)-1,0)*1000) 'mm

objXls_u.Worksheets(2).Cells(i_Load+2,18).Value =analog_out 'Volts
objXls_u.Worksheets(14).Cells(num+1,i_Load).Value =uig(Smdof(1,0)-1,0) 'm

Dim diff_servo As Variant
Dim Disp_check_in As Variant

        EA_IO.Measure("Displacement_Hor",Disp_read_servo,1) 'mm from servo controller
        Disp_check_in=CVar(Disp_read_servo)
        EA_Panel.SetValue(Panel1,"DispRead_in",Disp_check_in)

        diff_servo=Abs(Disp_check_in-uig(Smdof(1,0)-1,0)*1000)
        EA_Panel.SetValue(Panel1,"Analog_diff",diff_servo)

        Dim Internal_loop As Variant
        Internal_loop=0
        EA_Panel.SetValue(Panel1,"Interal_counter",0)
        EA_Panel.SetCell(Panel1,"Converge_table",1,1,0)
        Dim Internal_count1 As Variant
        Internal_count1=0

        Do While diff_servo>20 'Determines the difference between output and input
        voltage
        Internal_count1=Internal_count1+1
```

```
        EA_Panel.SetValue(Panel1,"Interal_counter",Internal_count1)

        EA_Panel.GetCell(Panel1,"Converge_table",1,1,Internal_loop)
            If Internal_loop=1 Then Exit Do
        EA_IO.Measure("Displacement_Hor",Disp_read_servo,1)
        EA_Panel.SetValue(Panel1,"DispRead_in",Disp_read_servo)
        Disp_check_in=CVar(Disp_read_servo)
        diff_servo=Abs(Disp_check_in-uig(Smdof(1,0)-1,0)*1000)
        EA_Panel.SetValue(Panel1,"Analog_diff",diff_servo)
            If diff_servo<20 Then Exit Do
        Loop

        EA_IO.Measure("Force_Hor",Force_read_servo,1)

        If num<=ncpts  Then
        Wait 0.1 'Waits for displacement to be applied and to settle
        Fs=CVar(Force_read_servo) 'N
        Fsavg=Fs
        ElseIf num>ncpts Then
        Fs=Fsavg
        EA_Panel.SetCell(Panel1,"Converge_table",2,1,1)
        EA_Panel.SetCell(Panel1,"Converge_table",2,2,Fs)
        End If

        EA_Panel.SetValue(Panel1,"Force_servo_in",Fs)



objXls_u.Worksheets(2).Cells(i_Load+2,19).Value =Fs
objXls_u.Worksheets(15).Cells(num+1,i_Load).Value =Fs


'%%%%%%%%%%%%%%%%%%%%%%%%%%%%%%%%%%%%%%%%%%%%%%%%%

'[Fsi1,ks,IMFsi]=Post_calcs_nonlinear_dynamic(Fsi2,Fs,mdof,Smdof,tdof,IMFsi,IMDsi,i_Load);

    Post_calcs_nonlinear_dynamic(Fsi1,ks,IMFsi,Fsi2,Fs,mdof,Smdof,tdof,IMDsi,i_Load,nbc)
    'objXls_u.Workbooks(1).Save
    Loop

'[upi,uppi]=velocity_acceleration(ui,upi,uppi,i_Load,dt);
velocity_acceleration(ui,upi,uppi,dt,tmdof)
'Calculates the reactions
Rs=reactions(global_stiffness,Disp,nfdof,tdof)

'Reads strain gauge data
EA_IO.Measure("MX840_SL",Strain_Left,1)
EA_IO.Measure("MX840_SR",Strain_right,1)

objXls_u.Worksheets(2).Cells(i_Load+2,10).Value =Strain_Left
objXls_u.Worksheets(2).Cells(i_Load+2,11).Value =Strain_right

Strain_Left_disp(i_Load)=Strain_Left
Strain_right_disp(i_Load)=Strain_right

EA_IO.Measure("PMX_LVDT1",LVDT1,1)
EA_IO.Measure("PMX_LVDT2",LVDT2,1)
EA_IO.Measure("PMX_LVDT3",LVDT3,1)
EA_IO.Measure("PMX_LVDT4",LVDT4,1)

objXls_u.Worksheets(2).Cells(i_Load+2,13).Value =LVDT1
objXls_u.Worksheets(2).Cells(i_Load+2,14).Value =LVDT2
objXls_u.Worksheets(2).Cells(i_Load+2,15).Value =LVDT3
objXls_u.Worksheets(2).Cells(i_Load+2,16).Value =LVDT4

LVDT1_disp(i_Load)=LVDT1
LVDT2_disp(i_Load)=LVDT2
LVDT3_disp(i_Load)=LVDT3
LVDT4_disp(i_Load)=LVDT4

'Saves local stiffness matrices
```

```
objXls_u.Worksheets(9).Cells(6*i_Load+2,1).Value =uppe(i_Load,0)
objXls_u.Worksheets(9).Cells(6*i_Load+2,nbc+3).Value =uppe(i_Load,0)
For i=0 To 5
    For j=0 To nbc-1
    objXls_u.Worksheets(9).Cells(6*i_Load+2+i,j+2).Value =IMD_G(i,j)
    objXls_u.Worksheets(9).Cells(6*i_Load+2+i,j+nbc+4).Value =Fsi2(i,j)
    Next
Next

'Saves force matrix
objXls_u.Worksheets(10).Cells(1,i_Load+1).Value =uppe(i_Load,0)
For i=0 To 1
    objXls_u.Worksheets(10).Cells(i+2,i_Load+1).Value =IMFsi(i,i_Load)
    objXls_u.Worksheets(10).Cells(i+4,i_Load+1).Value =IMDsi(i,i_Load)
Next

'LVDT_counter=LVDT_counter+1
'EA_Panel.SetValue(Panel2,"DIGIT_1",LVDT_read)

'Energy calculations
'Force_M(:,2)=Mttf*uppi(:,i_Load);

Dim upiE() As Variant
ReDim Preserve upiE(tmdof-1,0)

Dim uppiE() As Variant
ReDim Preserve uppiE(tmdof-1,0)

For i=0 To 5
    For j=0 To nbc-1
    fsiE(i,j,1)=Fsi2(i,j)
    IMD_Gi(i,j,1)=IMD_G(i,j)
    Next
Next

For i=0 To tmdof-1
upiE(i,0)=upi(i,1)
uppiE(i,0)=uppi(i,1)
Next

Dim FeM() As Variant
ReDim Preserve FeM(tmdof-1,0)
FeM=Matrix_multiplication(Mttf,uppiE,tmdof,tmdof,tmdof,1)

Dim FeC() As Variant
ReDim Preserve FeC(tmdof-1,0)
FeC=Matrix_multiplication(Cff,upiE,tmdof,tmdof,tmdof,1)

For i=0 To tmdof-1
Force_M(i,1)=FeM(i,0)
Force_C(i,1)=FeC(i,0)
objXls_u.Worksheets(12).Cells(i+2,i_Load+1).Value =FeM(i,0)
objXls_u.Worksheets(13).Cells(i+2,i_Load+1).Value =FeC(i,0)
Next

For i=0 To nfdof-1
Disp_P(i,1)=uig(i,0)
Force_P(i,1)=Puig(i,0)
Next

For i=0 To nfdof-1
    Energy_Ps=Energy_Ps+0.5*(Disp_P(i,1)-Disp_P(i,0))*(Force_P(i,1)+Force_P(i,0))
Next

For i=0 To tmdof-1
    Energy_M=Energy_M+0.5*(ui(i,1)-ui(i,0))*(Force_M(i,1)+Force_M(i,0))
    Energy_C=Energy_C+0.5*(ui(i,1)-ui(i,0))*(Force_C(i,1)+Force_C(i,0))
Next

For i=0 To 5
    For j=0 To nbc-1
    Energy_K=Energy_K+0.5*(IMD_Gi(i,j,1)-IMD_Gi(i,j,0))*(fsiE(i,j,1)+fsiE(i,j,0))
```

```
        Next
    Next

    Energy_H=Energy_H+0.5*(IMDsi(1,i_Load)-IMDsi(1,i_Load-1))*(IMFsi(1,i_Load)+IMFsi(1,i_Load-1))

    Energy_Ms(i_Load,0)=Energy_M
    Energy_Cs(i_Load,0)=Energy_C
    Energy_Ks(i_Load,0)=Energy_K
    Energy_Hs(i_Load,0)=Energy_H

    For i=0 To tmdof-1
    Force_M(i,0)=Force_M(i,1)
    Force_C(i,0)=Force_C(i,1)
    Next

    Energy_Total(i_Load)=CDbl(Energy_Ms(i_Load,0)+Energy_Cs(i_Load,0)+Energy_Ks(i_Load,0)+Energy_Hs(i_Load,0))
    Energy_Stiffness(i_Load)=CDbl(Energy_Ks(i_Load,0)+Energy_Hs(i_Load,0)+Energy_Cs(i_Load,0))
    Energy_Damping(i_Load)=CDbl(Energy_Hs(i_Load,0)+Energy_Cs(i_Load,0))
    Energy_Hys(i_Load)=CDbl(Energy_Hs(i_Load,0))

    'Plots Total Energy
    EA_Graph.PlotArrayXY(Panel1,"Energy_plot",1,nt+1, xEarth(), Energy_Total())
    EA_Graph.SetPlotProperty(Panel1,"Energy_plot",1,2,vbBlack)
    EA_Graph.SetPlotProperty(Panel1,"Energy_plot",1,5,0)

    EA_Graph.PlotArrayXY(Panel1,"Energy_plot",2,nt+1, xEarth(), Energy_Stiffness())
    EA_Graph.SetPlotProperty(Panel1,"Energy_plot",2,2,vbMagenta)
    EA_Graph.SetPlotProperty(Panel1,"Energy_plot",2,5,0)

    EA_Graph.PlotArrayXY(Panel1,"Energy_plot",3,nt+1, xEarth(), Energy_Damping())
    EA_Graph.SetPlotProperty(Panel1,"Energy_plot",3,2,vbBlue)
    EA_Graph.SetPlotProperty(Panel1,"Energy_plot",3,5,0)

    EA_Graph.PlotArrayXY(Panel1,"Energy_plot",4,nt+1, xEarth(), Energy_Hys())
    EA_Graph.SetPlotProperty(Panel1,"Energy_plot",4,2,vbRed)
    EA_Graph.SetPlotProperty(Panel1,"Energy_plot",4,5,0)

    EA_Graph.Refresh(Panel1,"Energy_plot")

    'Plots Strain values
    EA_Graph.PlotArrayXY(Panel2,"Strain_out_disp",1,nt+1, xEarth(), Strain_Left_disp())
    EA_Graph.SetPlotProperty(Panel2,"Strain_out_disp",1,2,vbBlue)
    EA_Graph.SetPlotProperty(Panel2,"Strain_out_disp",1,5,0)

    EA_Graph.PlotArrayXY(Panel2,"Strain_out_disp",2,nt+1, xEarth(), Strain_right_disp())
    EA_Graph.SetPlotProperty(Panel2,"Strain_out_disp",2,2,vbRed)
    EA_Graph.SetPlotProperty(Panel2,"Strain_out_disp",2,5,0)

    EA_Graph.Refresh(Panel2,"Strain_out_disp")

    'Plots LVDT values out
    EA_Graph.PlotArrayXY(Panel2,"Disp_read_LVDT",1,nt+1, xEarth(), LVDT1_disp())
    EA_Graph.SetPlotProperty(Panel2,"Disp_read_LVDT",1,2,vbBlack)
    EA_Graph.SetPlotProperty(Panel2,"Disp_read_LVDT",1,5,0)

    EA_Graph.PlotArrayXY(Panel2,"Disp_read_LVDT",2,nt+1, xEarth(), LVDT2_disp())
    EA_Graph.SetPlotProperty(Panel2,"Disp_read_LVDT",2,2,vbRed)
    EA_Graph.SetPlotProperty(Panel2,"Disp_read_LVDT",2,5,0)

    EA_Graph.PlotArrayXY(Panel2,"Disp_read_LVDT",3,nt+1, xEarth(), LVDT3_disp())
    EA_Graph.SetPlotProperty(Panel2,"Disp_read_LVDT",3,2,vbBlue)
    EA_Graph.SetPlotProperty(Panel2,"Disp_read_LVDT",3,5,0)

    EA_Graph.PlotArrayXY(Panel2,"Disp_read_LVDT",4,nt+1, xEarth(), LVDT4_disp())
    EA_Graph.SetPlotProperty(Panel2,"Disp_read_LVDT",4,2,vbMagenta)
    EA_Graph.SetPlotProperty(Panel2,"Disp_read_LVDT",4,5,0)

    EA_Graph.Refresh(Panel2,"Disp_read_LVDT")

    'Calculates the Park and Ang damage intensity
```

```
If Abs(IMDsi(1,i_Load))>di Then
    di=Abs(IMDsi(1,i_Load))
End If

If (di/dumax)+(bPa/(fyspring*dumax))*Energy_H>Dpa Then
Dpa=(di/dumax)+(bPa/(fyspring*dumax))*Energy_H
End If
EA_Panel.SetValue(Panel,"Damage_out",Dpa)

'Saves data to output file
objXls_u.Worksheets(3).Cells(1,i_Load+1).Value =uppe(i_Load,0)
objXls_u.Worksheets(11).Cells(1,i_Load+1).Value =uppe(i_Load,0)
For i = 0 To nfdof-1
    objXls_u.Worksheets(3).Cells(i+2,i_Load+1).Value =uig(i,0)
    objXls_u.Worksheets(11).Cells(i+2,i_Load+1).Value =Puig(i,0)
Next

'Saves the velocity and acceleration data
objXls_u.Worksheets(4).Cells(1,i_Load+2).Value =uppe(i_Load,0)
objXls_u.Worksheets(5).Cells(1,i_Load+2).Value =uppe(i_Load,0)
For i = 0 To tmdof-1
    objXls_u.Worksheets(4).Cells(i+2,i_Load+2).Value =upi(i,1)
    objXls_u.Worksheets(5).Cells(i+2,i_Load+2).Value =uppi(i,1)
Next

'Saves the energy data
objXls_u.Worksheets(6).Cells(i_Load+2,1).Value =uppe(i_Load,0)
objXls_u.Worksheets(6).Cells(i_Load+2,2).Value =Energy_M  'Mass or inertia energy / kinetic energy
objXls_u.Worksheets(6).Cells(i_Load+2,3).Value =Energy_C  'Damping energy
objXls_u.Worksheets(6).Cells(i_Load+2,4).Value =Energy_K  'Stiffness energy/potential energy
objXls_u.Worksheets(6).Cells(i_Load+2,5).Value =Energy_H  'Hysteretic energy of the footing
objXls_u.Worksheets(6).Cells(i_Load+2,6).Value =Energy_Ps  'External energy input

objXls_u.Worksheets(6).Cells(i_Load+2,8).Value =Energy_H
objXls_u.Worksheets(6).Cells(i_Load+2,9).Value =Energy_H+Energy_C
objXls_u.Worksheets(6).Cells(i_Load+2,10).Value =Energy_H+Energy_C+Energy_K
objXls_u.Worksheets(6).Cells(i_Load+2,11).Value =Energy_H+Energy_C+Energy_K+Energy_M

xSpring(i_Load)=CDbl(IMDsi(1,i_Load)*1000)
ySpring(i_Load)=CDbl(IMFsi(1,i_Load)/1000)
EA_Graph.PlotArrayXY(Panel1,"Graph1",1,nt+1, xSpring(), ySpring())
EA_Graph.SetPlotProperty(Panel1,"Graph1",1,2,vbRed)
EA_Graph.Refresh(Panel1,"Graph1")

'Output for foundation and numerical procedure

objXls_u.Worksheets(2).Cells(i_Load+2,3).Value =IMDsi(1,i_Load)*1000
objXls_u.Worksheets(2).Cells(i_Load+2,4).Value =IMFsi(1,i_Load)/1000

objXls_u.Worksheets(2).Cells(i_Load+2,5).Value =Dpa
objXls_u.Worksheets(2).Cells(i_Load+2,6).Value =Norm_max
objXls_u.Worksheets(2).Cells(i_Load+2,7).Value =num
'objXls_u.Worksheets(2).Cells(i_Load+2,8).Value =Load_axial


objXls_u.Workbooks(1).Save
Next

objXls_u.Quit

End Sub

Sub static_condensation(ByRef Lm() As Variant,ByRef kotf() As Variant,ByRef kttv() As Variant,ByRef fsi() As Variant,ByRef ktof() As Variant,ByRef koof() As Variant,ByRef Ps() As Variant,ByRef lh() As Variant,ByRef Mttf() As Variant,ByVal K As Variant,ByVal mdof As Variant,ByVal nfdof As Variant,ByVal fso As Variant,ByVal Uio As Variant,ByVal global_mass As Variant,ByVal Pwtdof As Variant,ByVal ptfof As Variant,ByVal i_Load As Variant,ByVal nbc As Variant,ByVal tdof As Variant)

Dim Lmi() As Variant
```

```
ReDim Preserve Lmi(nfdof-1,0)
Dim Lhi() As Variant
ReDim Preserve Lhi(nfdof-1,0)
Dim Lvi() As Variant
ReDim Preserve Lvi(nfdof-1,0)

For i=0 To nfdof-1
Lmi(i,0)=0
Lhi(i,0)=0
Lvi(i,0)=0
Next

For i=0 To 5
    For j=0 To nbc-1
        If i<>2 And i<>5 Then
            If mdof(i,j)<=nfdof Then
                Lmi(mdof(i,j)-1,0)=1
            End If
        End If
        If i=0 Or i=3 Then
            If mdof(i,j)<=nfdof Then
            Lhi(mdof(i,j)-1,0)=1
            End If
        End If
        If i=1 Or i=4 Then
            If mdof(i,j)<=nfdof Then
            Lvi(mdof(i,j)-1,0)=1
            End If
        End If
    Next
Next

Dim Lms As Variant
Lms=Matrix_sum(Lmi,nfdof,1)

ReDim Preserve Lm(nfdof-1,0)

Dim counter As Variant
counter=-1
For i=0 To nfdof-1
    If Lmi(i,0)<>0 Then
        counter=counter+1
        Lm(counter,0)=i
    End If
Next
tmdof=counter+1

For i=0 To nfdof-1
    If Lmi(i,0)=0 Then
        counter=counter+1
        Lm(counter,0)=i
    End If
Next

Dim psi() As Variant
ReDim Preserve psi(tdof-1,0)
psi=Matrix_addition(Pwtdof,ptfof,tdof,1)

Dim Kff() As Variant
ReDim Preserve Kff(nfdof-1,nfdof-1)

Dim Mff() As Variant
ReDim Preserve Mff(nfdof-1,nfdof-1)

For i=0 To nfdof-1
    For j=0 To nfdof-1
    Kff(i,j)=K(i,j)
    Mff(i,j)=global_mass(i,j)
    Next
Next

Dim Kfft() As Variant
ReDim Preserve Kfft(nfdof-1,nfdof-1)
```

```
ReDim Preserve Mfft(nfdof-1,nfdof-1)

For i=0 To nfdof-1
    For j=0 To nfdof-1
        Kfft(i,j)=0
        Mfft(i,j)=0
    Next
Next

Dim Fsto() As Variant
ReDim Preserve Fsto(nfdof-1,0)

ReDim Preserve Ps(nfdof-1,0)

For i=0 To nfdof-1
    Fsto(i,0)=0
    Ps(i,0)=0
Next

Dim lv() As Variant
ReDim Preserve lv(tmdof-1,0)

ReDim Preserve lh(tmdof-1,0)

For i=0 To tmdof-1
lv(i,0)=0
lh(i,0)=0
Next

For i=0 To nfdof-1
    Fsto(i,0)=fso(Lm(i,0),0)
    Ps(i,0)=psi(Lm(i,0),0)
    For j=0 To nfdof-1
        Kfft(i,j)=Kff(Lm(i,0),Lm(j,0))
        Mfft(i,j)=Mff(Lm(i,0),Lm(j,0))
    Next
Next

Dim kttf() As Variant
ReDim Preserve kttf(tmdof-1,tmdof-1)

For i=0 To tmdof-1
    For j=0 To tmdof-1
    kttf(i,j)=Kfft(i,j)
    Next
Next

ReDim Preserve ktof(tmdof-1,nfdof-tmdof-1)

For i=0 To tmdof-1
    For j=0 To nfdof-tmdof-1
    ktof(i,j)=Kfft(i,j+tmdof)
    Next
Next

ReDim Preserve kotf(nfdof-tmdof-1,tmdof-1)

For i=0 To nfdof-tmdof-1
    For j=0 To tmdof-1
    kotf(i,j)=Kfft(i+tmdof,j)
    Next
Next

ReDim Preserve koof(nfdof-tmdof-1,nfdof-tmdof-1)

For i=0 To nfdof-tmdof-1
    For j=0 To nfdof-tmdof-1
    koof(i,j)=Kfft(i+tmdof,j+tmdof)
    Next
Next

Dim koofinv() As Variant
ReDim Preserve koofinv(nfdof-tmdof-1,nfdof-tmdof-1)
```

```
koofinv=Matrix_inverse(koof,nfdof-tmdof,nfdof-tmdof)

Dim kttvi() As Variant

'kttv=kttf-ktof*inv(koof)*kotf;
kttvi=Matrix_multiplication(ktof,koofinv,tmdof,nfdof-tmdof,nfdof-tmdof,nfdof-tmdof)
kttvi=Matrix_multiplication(kttvi,kotf,tmdof,nfdof-tmdof,nfdof-tmdof,tmdof)
ReDim kttv(tmdof,tmdof)
kttv=Matrix_subtraction(kttf,kttvi,tmdof,tmdof)

'Mttf=Mfft(1:tmdof,1:tmdof)
ReDim Mttf(tmdof-1,tmdof-1)
For i=0 To tmdof-1
    For j=0 To tmdof-1
    Mttf(i,j)=Mfft(i,j)
    Next
Next

'fsi(:,i_Load)=Fsto(1:tmdof,1)-ktof*inv(koof)*Fsto(tmdof+1:nfdof,1);
ReDim Preserve fsi(tmdof-1,0)

Dim fsiinv() As Variant

Dim Fsto1() As Variant
ReDim Preserve Fsto1(tmdof-1,0)
For i=0 To tmdof-1
    Fsto1(i,0)=Fsto(i,0)
Next

Dim Fsto2() As Variant
ReDim Preserve Fsto2(nfdof-tmdof-1,0)

For i=0 To nfdof-tmdof-1
    Fsto2(i,0)=Fsto(i+tmdof,0)
Next

fsiinv=Matrix_multiplication(ktof,koofinv,tmdof,nfdof-tmdof,nfdof-tmdof,nfdof-tmdof)
fsiinv=Matrix_multiplication(fsiinv,Fsto2,tmdof,nfdof-tmdof,nfdof-tmdof,1)
fsi=Matrix_subtraction(Fsto1,fsiinv,tmdof,1)

For i=0 To tmdof-1
    lv(i,0)=Lvi(Lm(i,0),0)
    lh(i,0)=Lhi(Lm(i,0),0)
Next

End Sub

Private Sub PrintMatrix(ByRef Prop As Variant) ' Keeps giving a ) error, I need to pass a multidimensional array into a sub
'The code works when I run it In visual studio
    For i = 0 To 3
        For j = 0 To 2
         EA_Panel.SetCell(Panel1,"PropTable",i+1,j+1,Prop(i,j))
       Next
    Next
End Sub

Function assemble_beam_stiffness(ByRef global_stiffness As Variant,ByVal tdof As Variant,ByVal K_beam_local As Variant,ByVal nbc As Variant,ByVal mdof As Variant) As Variant
    For i = 0 To tdof-1
        For j = 0 To tdof-1
        global_stiffness(i,j)=0
        Next
    Next

'Assembles the Global stiffness matrix

For i=0 To nbc-1
    For j=0 To 5
        For K=0 To 5

        global_stiffness(mdof(j,i)-1,mdof(K,i)-1)=global_stiffness(mdof(j,i)-1,mdof(K,
```

```
        i)-1)+K_beam_local(j,K,i)
        Next
    Next
Next

End Function

Sub assemble_local_stiffness_beam(ByRef estiff_local As Variant,ByRef etran_local As Variant,ByRef K_beam_local As Variant,ByRef etranT_local As Variant,ByVal nbc As Variant,ByVal Prop As Variant,ByVal idbc As Variant,ByVal mem_info As Variant)

For j=0 To nbc-1

Dim local_stiff() As Variant
Dim local_etran() As Variant
Dim local_etranTrans() As Variant
Dim local_Kbeam() As Variant

phi=mem_info(1,j)
local_stiff=estiff_BEAM(Prop(1,idbc(j,2)-1),Prop(0,idbc(j,2)-1),Prop(2,idbc(j,2)-1),mem_info(0,j))
local_etran=etrans(phi)
local_etranTrans=eTransT(phi)

'M_beam_local{1,j}=transpose(gamma)*mass*gamma
local_Kbeam=Matrix_multiplication(local_etranTrans,local_stiff,6,6,6,6)
local_Kbeam=Matrix_multiplication(local_Kbeam,local_etran,6,6,6,6)

    For i=0 To 5
        For K= 0 To 5
        estiff_local(i,K,j)=local_stiff(i,K)
        etran_local(i,K,j)=local_etran(i,K)
        etranT_local(i,K,j)=local_etranTrans(i,K)
        K_beam_local(i,K,j)=local_Kbeam(i,K)
        Next
    Next
Next

End Sub

Function estiff_BEAM(ByVal a As Variant,ByVal e As Variant,ByVal i As Variant,ByVal l As Variant ) As Variant

Dim elk() As Variant
ReDim Preserve elk(5,5)

elk(0,0)=(a*e)/l
elk(0,1)=0
elk(0,2)=0
elk(0,3)=(-a*e)/l
elk(0,4)=0
elk(0,5)=0

elk(1,0)=0
elk(1,1)=(12*e*i)/l^3
elk(1,2)=(6*e*i)/l^2
elk(1,3)=0
elk(1,4)=(-12*e*i)/l^3
elk(1,5)=(6*e*i)/l^2

elk(2,0)=0
elk(2,1)=(6*e*i)/l^2
elk(2,2)=(4*e*i)/l
elk(2,3)=0
elk(2,4)=(-6*e*i)/l^2
elk(2,5)=(2*e*i)/l


elk(3,0)=(-a*e)/l
elk(3,1)=0
elk(3,2)=0
elk(3,3)=(a*e)/l
elk(3,4)=0
```

```
elk(3,5)=0

elk(4,0)=0
elk(4,1)=(-12*e*i)/l^3
elk(4,2)=(-6*e*i)/l^2
elk(4,3)=0
elk(4,4)=(12*e*i)/l^3
elk(4,5)=(-6*e*i)/l^2

elk(5,0)=0
elk(5,1)=(6*e*i)/l^2
elk(5,2)=(2*e*i)/l
elk(5,3)=0
elk(5,4)=(-6*e*i)/l^2
elk(5,5)=(4*e*i)/l

estiff_BEAM=elk

End Function

Function etrans(ByVal phi As Variant) As Variant

Dim Gamma() As Variant
ReDim Preserve Gamma(5,5)

For i=0 To 5
    For j=0 To 5
    Gamma(i,j)=0
    Next
Next

Gamma(0,0)=Cos(phi)
Gamma(0,1)=Sin(phi)
Gamma(1,0)=-Sin(phi)
Gamma(1,1)=Cos(phi)
Gamma(2,2)=1
Gamma(3,3)=Cos(phi)
Gamma(3,4)=Sin(phi)
Gamma(4,3)=-Sin(phi)
Gamma(4,4)=Cos(phi)
Gamma(5,5)=1

etrans=Gamma

End Function

Function eTransT(ByVal phi As Variant) As Variant
Dim Gamma() As Variant
ReDim Preserve Gamma(5,5)

For i=0 To 5
    For j=0 To 5
    Gamma(i,j)=0
    Next
Next

Gamma(0,0)=Cos(phi)
Gamma(0,1)=-Sin(phi)
Gamma(1,0)=Sin(phi)
Gamma(1,1)=Cos(phi)
Gamma(2,2)=1
Gamma(3,3)=Cos(phi)
Gamma(3,4)=-Sin(phi)
Gamma(4,3)=Sin(phi)
Gamma(4,4)=Cos(phi)
Gamma(5,5)=1

eTransT=Gamma

End Function

Function Matrix_multiplication(ByVal matrix1 As Variant, ByVal Matrix2 As
Variant,ByVal m1 As Variant,ByVal n1 As Variant, ByVal m2 As Variant, ByVal n2 As
```

```
Variant) As Variant

Dim result() As Variant
ReDim Preserve result(m1-1,n2-1)
'EA_Panel.SetCell(Panel1,"PropTable",1,1,m1)
'EA_Panel.SetCell(Panel1,"PropTable",1,2,n2)

For i =0 To m1-1
    For j = 0 To n2-1
        For K=0 To n1-1
        result(i,j)=result(i,j)+matrix1(i,K)*Matrix2(K,j)
        Next
    Next
Next
Matrix_multiplication=result

End Function

Function Matrix_solver(ByVal a As Variant,ByVal b As Variant,ByVal n As Variant) As Variant

'To reduce the coefficient matrix To the upper triangular form And Then solve With backward substitution
'Reduce the coefficient matrix To upper triangular form
Dim m As Variant
Dim pt() As Variant
Dim pivot As Variant
Dim counter As Variant

For K=0 To n-2
    For i=K+1 To n-1
        If a(K,K)<>0 Then
        m=a(i,K)/a(K,K)
        ElseIf a(K,K)=0 Then
        pt=eye(n)
        pivot=a(K,K)
        counter=K
            While pivot =0 And counter<n-1
            counter=counter+1
            pivot=a(counter,K)
            Wend
        pt(K,K)=0
        pt(K,counter)=1
        pt(counter,K)=1
        pt(counter,counter)=0
        a=Matrix_multiplication(pt,a,n,n,n,n)
        b=Matrix_multiplication(pt,b,n,n,n,1)
        m=a(i,K)/a(K,K)
        End If
            For j=K+1 To n-1
            a(i,K)=0
            a(i,j)=a(i,j)-m*a(K,j)
            Next
        b(i,0)=b(i,0)-m*b(K,0)
    Next
Next

'Solve With backward substitution
Dim x() As Variant 'x=zeros(n,1);
ReDim Preserve x(n-1,0)
    For i=0 To n-1
    x(i,0)=0
    Next
Dim s As Variant

For K=n-1 To 0 Step -1
s=0
    For j=K To n-1
        If K<>j Then
        s=s+a(K,j)*x(j,0)
        End If
    Next
    x(K,0)=(b(K,0)-s)/a(K,K)
```

```
Next
Matrix_solver=x


End Function

Function eye(ByVal n As Variant) As Variant

Dim a() As Variant
ReDim Preserve a(n-1,n-1)

For i=0 To n-1
    For j=0 To n-1
        If i=j Then
        a(i,j)=1
        Else
        a(i,j)=0
        End If
    Next
Next
eye=a

End Function


Function Spring_stiff(ByRef global_stiffness As Variant ,ByVal Column_hinge As Variant,ByVal dof As Variant,ByVal tdof As Variant,ByVal ks As Variant,ByRef Smdof As Variant)

'Adds the spring stiffness In the Global matrix

Smdof(0,0)= tdof
Smdof(1,0)= dof(0,Column_hinge-1)

Dim KSpring() As Variant
ReDim Preserve KSpring(1,1)

KSpring(0,0)=ks
KSpring(0,1)=-ks
KSpring(1,0)=-ks
KSpring(1,1)=ks

'Assembles the Global stiffness matrix
For j=0 To 1
    For K=0 To 1

    global_stiffness(Smdof(j,0)-1,Smdof(K,0)-1)=global_stiffness(Smdof(j,0)-1,Smdof(K,0)-1)+KSpring(j,K)
    Next
Next

Spring_stiff=KSpring

End Function

Function beam_loads(ByVal loading_beam As Variant,ByVal nbc As Variant,ByVal etranT_local As Variant,ByVal dof As Variant,ByVal mem_info As Variant,ByVal idbc As Variant,ByVal tdof As Variant,ByVal nfdof As Variant,ByRef Pw_local As Variant,ByRef DOF_c As Variant,ByRef Pwtdof() As Variant) As Variant

For i=0 To nbc-1
    For j=0 To 5
    Pw_local(j,i)=0
    DOF_c(j,i)=0
    Next
Next

Dim Wbeam() As Variant
ReDim Preserve Wbeam(nbc-1,0)

For i=0 To nbc-1
    Pw_local(0,loading_beam(i,0)-1)=0

```

```
        Pw_local(1,loading_beam(i,0)-1)=-(loading_beam(i,1)*mem_info(0,loading_beam(i,0)-1))/2
        Pw_local(2,loading_beam(i,0)-1)=-(loading_beam(i,1)*mem_info(0,loading_beam(i,0)-1)^2)/12
        Pw_local(3,loading_beam(i,0)-1)=0
        Pw_local(4,loading_beam(i,0)-1)=-(loading_beam(i,1)*mem_info(0,loading_beam(i,0)-1))/2
        Pw_local(5,loading_beam(i,0)-1)=(loading_beam(i,1)*mem_info(0,loading_beam(i,0)-1)^2)/12
        Wbeam(loading_beam(i,0)-1,0)=loading_beam(i,1)
    Next

    Dim Pw_global() As Variant
    ReDim Preserve Pw_global(5,nbc-1)

    For i=0 To nbc-1
        Dim trans() As Variant
        ReDim Preserve trans(5,5) As Variant
        Dim LocalPW() As Variant
        ReDim Preserve LocalPW(5,5) As Variant

        For j=0 To 5
            For K=0 To 5
            trans(j,K)=etranT_local(j,K,i)
            Next
        LocalPW(j,0)=Pw_local(j,i)
        Next

        local_Kbeam=Matrix_multiplication(trans,LocalPW,6,6,6,1)

        For K=0 To 5
        Pw_global(K,i)=local_Kbeam(K,0)
        Next

        For K=0 To 2
            DOF_c(K,i)=dof(K,idbc(i,0)-1)
            DOF_c(K+3,i)=dof(K,idbc(i,1)-1)
        Next
    Next

    Dim Pw() As Variant
    ReDim Preserve Pw(nfdof-1,0)

    For i=0 To nfdof-1
        Pw(i,0)=0
    Next

    For i=0 To nbc-1
        For j=0 To 5
        Pwtdof(DOF_c(j,i)-1,0)=Pwtdof(DOF_c(j,i)-1,0)+Pw_global(j,i)
        Next
    Next

    For i=0 To nfdof-1
    Pw(i,0)=Pwtdof(i,0)
    Next

    beam_loads=Pw

    End Function

    Function solve(ByVal global_stiffness As Variant,ByVal R As Variant,ByVal nfdof As Variant) As Variant

    Dim Kff() As Variant
    ReDim Preserve Kff(nfdof-1,nfdof-1)

    For i=0 To nfdof-1
        For j=0 To nfdof-1
        Kff(i,j)=global_stiffness(i,j)
```

```
        Next
    Next

    solve=Matrix_solver(Kff,R,nfdof)

    End Function

    Function Matrix_addition(ByVal a As Variant,ByVal b As Variant,ByVal m1 As
    Variant,ByVal n1 As Variant) As Variant

    Dim Out() As Variant
    ReDim Preserve Out(m1-1,n1-1)

    For i=0 To m1-1
        For j=0 To n1-1
        Out(i,j)=a(i,j)+b(i,j)
        Next
    Next
    Matrix_addition=Out

    End Function

    Function Matrix_subtraction(ByVal a As Variant,ByVal b As Variant,ByVal m1 As
    Variant,ByVal n1 As Variant) As Variant

    Dim Out() As Variant
    ReDim Preserve Out(m1-1,n1-1)

    For i=0 To m1-1
        For j=0 To n1-1
        Out(i,j)=a(i,j)-b(i,j)
        Next
    Next
    Matrix_subtraction=Out

    End Function

    Sub memf(ByRef IMF_L As Variant,ByRef IMD_L As Variant,ByRef IMD_G As Variant,ByRef
    IMF_G As Variant,ByRef fso As Variant,ByVal supp As Variant,ByVal nnode As
    Variant,ByVal Disp As Variant,ByVal nbc As Variant,ByVal idbc As Variant,ByVal
    etran_local As Variant,ByVal etranT_local As Variant,ByVal estiff_local As
    Variant,ByVal Pw_local As Variant)
    '[IMF_L,IMD_L,IMD_G,IMF_G,fso,coord_out]=memf(supp,Disp,estiff_local,etran_local,idbc,
    nbc,coord,nnode,Pw_local)

    Dim displacement_out() As Variant
    ReDim Preserve displacement_out(2,nnode-1)
    'displacement_out=zeros(m,n)
    Dim count As Variant
    count=-1

    For j=0 To nnode-1
        For i=0 To 2
            If supp(i,j)=1 Then
            displacement_out(i,j)=0
            ElseIf supp(i,j)=0 Then
            count=count+1
            displacement_out(i,j)=Disp(count,0)
            End If
        Next
    Next

    'Transform {displacement_out} from Global To local coordinates by multiplying With
    member local stiffness matrix
    'And transformation matrix

    For i=0 To nbc-1

            For K=0 To 2
            IMD_G(K,i)=displacement_out(K,idbc(i,0)-1)
            IMD_G(K+3,i)=displacement_out(K,idbc(i,1)-1)
            Next
```

```
            Dim IMDLi() As Variant
            ReDim Preserve IMDLi(5,0)
            Dim IMFLi() As Variant
            ReDim Preserve IMFLi(5,0)
            Dim IMFGi() As Variant
            ReDim Preserve IMFGi(5,0)
            Dim fsoi() As Variant
            ReDim Preserve fsoi(5,0)
            Dim PwL() As Variant
            ReDim Preserve PwL(5,0)

            Dim trans As Variant
            ReDim Preserve trans(5,5)
            Dim transT As Variant
            ReDim Preserve transT(5,5)
            Dim estiff As Variant
            ReDim Preserve estiff(5,5)

            For j=0 To 5
                For K=0 To 5
                trans(j,K)=etran_local(j,K,i)
                transT(j,K)=etranT_local(j,K,i)
                estiff(j,K)=estiff_local(j,K,i)
                Next
            IMDLi(j,0)=IMD_G(j,i)
            PwL(j,0)=Pw_local(j,i)
            Next

        IMDLi=Matrix_multiplication(trans,IMDLi,6,6,6,1)
        IMFLi=Matrix_multiplication(estiff,IMDLi,6,6,6,1)
        fsoi=Matrix_multiplication(transT,IMFLi,6,6,6,1)
        IMFLi=Matrix_subtraction(IMFLi,PwL,6,1)
        IMFGi=Matrix_multiplication(transT,IMFLi,6,6,6,1)

        For j=0 To 5
        IMD_L(j,i)=IMDLi(j,0)
        IMF_L(j,i)=IMFLi(j,0)
        IMF_G(j,i)=IMFGi(j,0)
        fso(j,i)=fsoi(j,0)
        Next

    Next

    End Sub

    Sub memf_spring(ByVal KSpring As Variant,ByVal Disp As Variant,ByVal Smdof As
    Variant,ByRef ds As Variant,ByRef IMFs As Variant)
    'Calculates the New spring stiffness

    ds(0,0)=0
    ds(1,0)=Disp(Smdof(1,0)-1,0)
    Dim IMFsi() As Variant
    IMFsi=Matrix_multiplication(KSpring,ds,2,2,2,1)

    For i=0 To 1
    IMFs(i,0)=IMFsi(i,0)
    Next

    End Sub

    Sub initial_conditions_static(ByRef Fsi1 As Variant,ByRef Ui1 As Variant,ByVal fso
    As Variant,ByVal IMD_G As Variant,ByVal mdof As Variant,ByVal tdof As Variant,ByVal
    IMFs As Variant,ByVal Smdof As Variant,ByVal nbc As Variant)

    For i=0 To nbc-1
        For j=0 To 5
        Fsi1(mdof(j,i)-1,0)=Fsi1(mdof(j,i)-1,0)+fso(j,i)
        Ui1(mdof(j,i)-1,0)=IMD_G(j,i)
        Next
    Next

    Fsi1(Smdof(0,0)-1,0)=Fsi1(Smdof(0,0)-1,0)+IMFs(0,0)
    Fsi1(Smdof(1,0)-1,0)=Fsi1(Smdof(1,0)-1,0)+IMFs(1,0)
```

```
End Sub

Function assemble_mass_self(ByRef global_mass As Variant,ByVal nbc As Variant,ByVal
Prop As Variant,ByVal idbc As Variant,ByVal mem_info As Variant,ByVal mdof As
Variant,ByVal tdof As Variant)

Dim M_beam_local As Variant
ReDim Preserve M_beam_local(5,5,nbc-1)

For j=0 To nbc-1

Dim local_mass() As Variant
Dim local_etran() As Variant
Dim local_etranTrans() As Variant
Dim local_Mself() As Variant

'e=Prop(0,idbc(j,2)-1)
'a=Prop(1,idbc(j,2)-1)
'i=Prop(2,idbc(j,2)-1)
'l=mem_info(0,j)
'den=Prop(3,idbc(j,2)-1)

phi=mem_info(1,j)

local_mass=mass_local(Prop(1,idbc(j,2)-1),mem_info(0,j),Prop(3,idbc(j,2)-1))
local_etran=etrans(phi)
local_etranTrans=eTransT(phi)

'M_beam_local{1,j}=transpose(gamma)*mass*gamma
local_Mself=Matrix_multiplication(local_etranTrans,local_mass,6,6,6,6)
local_Mself=Matrix_multiplication(local_Mself,local_etran,6,6,6,6)

    For i=0 To 5
        For K= 0 To 5
        M_beam_local(i,K,j)=local_Mself(i,K)
        Next
    Next
Next

assemble_mass_self=M_beam_local

For i=0 To nbc-1
    For j=0 To 5
        For K=0 To 5

        global_mass(mdof(j,i)-1,mdof(K,i)-1)=global_mass(mdof(j,i)-1,mdof(K,i)-1)+M_be
        am_local(j,K,i)
        Next
    Next
Next

End Function

Function mass_local(ByVal a As Variant,ByVal l As Variant,ByVal den As Variant) As
Variant

Dim Mass As Variant
ReDim Preserve Mass(5,5)

For i=0 To 5
    For j= 0 To 5
    Mass(i,j)=0
    Next
Next

Mass(0,0)=(a*l*den)/2
Mass(1,1)=(a*l*den)/2
Mass(3,3)=(a*l*den)/2
Mass(4,4)=(a*l*den)/2

mass_local=Mass
```

```
End Function

Function assemble_mass_DL(ByRef global_mass As Variant,ByVal nbc As Variant,ByVal idbc As Variant,ByVal mem_info As Variant,ByVal mdof As Variant,ByVal tdof As Variant,ByVal tc As Variant,ByVal Span As Variant,ByVal Den_conc As Variant)

Dim a As Variant
a=tc*Span

Dim M_beam_local As Variant
ReDim Preserve M_beam_local(5,5,nbc-1)

For j=0 To nbc-1

    If idbc(j,2)=2 Then
    Dim local_mass() As Variant
    Dim local_etran() As Variant
    Dim local_etranTrans() As Variant
    Dim local_MDL() As Variant

    phi=mem_info(1,j)

    local_mass=mass_local(a,mem_info(0,j),Den_conc)
    local_etran=etrans(phi)
    local_etranTrans=eTransT(phi)

    'M_beam_local{1,j}=transpose(gamma)*mass*gamma
    local_MDL=Matrix_multiplication(local_etranTrans,local_mass,6,6,6,6)
    local_MDL=Matrix_multiplication(local_MDL,local_etran,6,6,6,6)

        For i=0 To 5
            For K= 0 To 5
            M_beam_local(i,K,j)=local_MDL(i,K)
            Next
        Next

    Else
        For i=0 To 5
            For K= 0 To 5
            M_beam_local(i,K,j)=0
            Next
        Next
    End If

Next

assemble_mass_DL=M_beam_local

For i=0 To nbc-1
    For j=0 To 5
        For K=0 To 5

        global_mass(mdof(j,i)-1,mdof(K,i)-1)=global_mass(mdof(j,i)-1,mdof(K,i)-1)+M_beam_local(j,K,i)
        Next
    Next
Next


End Function

Function assemble_mass_LL(ByRef global_mass As Variant,ByVal nbc As Variant,ByVal idbc As Variant,ByVal mem_info As Variant,ByVal mdof As Variant,ByVal tdof As Variant,ByVal Span As Variant,ByVal LL As Variant)

Dim a As Variant
a=Span
Dim den As Variant
den=LL/9.81

Dim M_beam_local As Variant
ReDim Preserve M_beam_local(5,5,nbc-1)

```

```
For j=0 To nbc-1

    If idbc(j,2)=2 Then
        Dim local_mass() As Variant
        Dim local_etran() As Variant
        Dim local_etranTrans() As Variant
        Dim local_MLL() As Variant

        'e=Prop(0,idbc(j,2)-1)
        'a=Prop(1,idbc(j,2)-1)
        'i=Prop(2,idbc(j,2)-1)
        'l=mem_info(0,j)
        'den=Prop(3,idbc(j,2)-1)

        phi=mem_info(1,j)

        local_mass=mass_local(a,mem_info(0,j),den)
        local_etran=etrans(phi)
        local_etranTrans=eTransT(phi)

        'M_beam_local{1,j}=transpose(gamma)*mass*gamma
        local_MLL=Matrix_multiplication(local_etranTrans,local_mass,6,6,6,6)
        local_MLL=Matrix_multiplication(local_MLL,local_etran,6,6,6,6)

            For i=0 To 5
                For K= 0 To 5
                M_beam_local(i,K,j)=local_MLL(i,K)
                Next
            Next
    Else

        For i=0 To 5
            For K= 0 To 5
            M_beam_local(i,K,j)=0
            Next
        Next

    End If
Next

assemble_mass_LL=M_beam_local

For i=0 To nbc-1
    For j=0 To 5
        For K=0 To 5

        global_mass(mdof(j,i)-1,mdof(K,i)-1)=global_mass(mdof(j,i)-1,mdof(K,i)-1)+M_beam_local(j,K,i)
        Next
    Next
Next




End Function

Function Matrix_inverse(ByVal a As Variant,ByVal m1 As Variant,ByVal n1 As Variant)

Dim m As Variant
Dim pt() As Variant
Dim pivot As Variant
Dim counter As Variant
Dim b() As Variant
b=eye(n1)

For K=0 To n1-2
    For i=K+1 To n1-1
        If a(K,K)<>0 Then
        m=a(i,K)/a(K,K)

        ElseIf a(K,K)=0 Then
        pt=eye(n1)
```

```
            pivot=a(K,K)
            counter=K
                While pivot =0 And counter<n1-1
                counter=counter+1
                pivot=a(counter,K)
                Wend
            pt(K,K)=0
            pt(K,counter)=1
            pt(counter,K)=1
            pt(counter,counter)=0
            a=Matrix_multiplication(pt,a,n1,n1,n1,n1)
            b=Matrix_multiplication(pt,b,n1,n1,n1,n1)
            m=a(i,K)/a(K,K)
            End If
                For j=K+1 To n1-1
                a(i,K)=0
                a(i,j)=a(i,j)-m*a(K,j)
                Next
                For j=0 To n1-1
                b(i,j)=b(i,j)-m*b(K,j)
                Next
        Next
    Next

    For K=n1-1 To 1 Step -1
        For i=K-1 To 0 Step -1

            m=a(i,K)/a(K,K)

            For j=K-1 To 0 Step -1
            a(i,K)=0
            a(i,j)=a(i,j)-m*a(K,j)
            Next

            For j=0 To n1-1
            b(i,j)=b(i,j)-m*b(K,j)
            Next
        Next
    Next

    For i=0 To n1-1
        For j=0 To n1-1
        b(i,j)=b(i,j)/a(i,i)
        Next
    Next

    Matrix_inverse=b

    End Function

    Sub static_condensation_initial(ByRef Lm As Variant,ByRef kttv() As Variant,ByRef
    Uto As Variant,ByRef tmdof As Variant,ByRef Mttf() As Variant,ByVal K As
    Variant,ByVal global_mass As Variant,ByVal mdof As Variant,ByVal nfdof As
    Variant,ByVal fso As Variant,ByVal Uio As Variant,ByVal nbc As Variant)
    'The model incorporates Static condensation of the frame structure To only
    'include certain degrees of freedom where the mass will act
    'THe model accounts For only horizontal mass And vertical mass response And
    'ignores the rotational mass moment of inertia
    'The Function reorders the matrixes And solves For the equivalent
    'statically condensed stiffnes matix
    '%%%%%%%%%%%%%%%%%%%%%%%%%%%%%%%%%%%%%%%%%%%%%%%%%%%%%%%%%%%%%%%%%%%%%%%%%%%%

    Dim Lmi() As Variant
    ReDim Preserve Lmi(nfdof-1,0)
        For i=0 To nfdof-1
            Lmi(i,0)=0
        Next

    For i=0 To 5
        For j=0 To nbc-1
            If i<>2 And i<>5 Then
                If mdof(i,j)<=nfdof Then
                    Lmi(mdof(i,j)-1,0)=1
```

```
            End If
        End If
    Next
Next

Dim Lms As Variant
Lms=Matrix_sum(Lmi,nfdof,1)

Dim counter As Variant
counter=-1
For i=0 To nfdof-1
    If Lmi(i,0)<>0 Then
        counter=counter+1
        Lm(counter,0)=i
    End If
Next
tmdof=counter+1

For i=0 To nfdof-1
    If Lmi(i,0)=0 Then
        counter=counter+1
        Lm(counter,0)=i
    End If
Next

Dim Kff() As Variant
ReDim Preserve Kff(nfdof-1,nfdof-1)

Dim Mff() As Variant
ReDim Preserve Mff(nfdof-1,nfdof-1)

For i=0 To nfdof-1
    For j=0 To nfdof-1
    Kff(i,j)=K(i,j)
    Mff(i,j)=global_mass(i,j)
    Next
Next

Dim Kfft() As Variant
ReDim Preserve Kfft(nfdof-1,nfdof-1)

Dim Mfft() As Variant
ReDim Preserve Mfft(nfdof-1,nfdof-1)

For i=0 To nfdof-1
    For j=0 To nfdof-1
        Kfft(i,j)=0
        Mfft(i,j)=0
    Next
Next

Dim Fsto() As Variant
ReDim Preserve Fsto(nfdof-1,0)

For i=0 To nfdof-1
    Uto(i,0)=0
    Fsto(i,0)=0
Next

For i=0 To nfdof-1
    Fsto(i,0)=fso(Lm(i,0),0)
    Uto(i,0)=Uio(Lm(i,0),0)
    For j=0 To nfdof-1
        Kfft(i,j)=Kff(Lm(i,0),Lm(j,0))
        Mfft(i,j)=Mff(Lm(i,0),Lm(j,0))
    Next
Next

Dim kttf() As Variant
ReDim Preserve kttf(tmdof-1,tmdof-1)

For i=0 To tmdof-1
    For j=0 To tmdof-1
```

```
        kttf(i,j)=Kfft(i,j)
        Next
    Next

    Dim ktof() As Variant
    ReDim Preserve ktof(tmdof-1,nfdof-tmdof-1)

    For i=0 To tmdof-1
        For j=0 To nfdof-tmdof-1
        ktof(i,j)=Kfft(i,j+tmdof)
        Next
    Next

    Dim kotf() As Variant
    ReDim Preserve kotf(nfdof-tmdof-1,tmdof-1)

    For i=0 To nfdof-tmdof-1
        For j=0 To tmdof-1
        kotf(i,j)=Kfft(i+tmdof,j)
        Next
    Next

    Dim koof() As Variant
    ReDim Preserve koof(nfdof-tmdof-1,nfdof-tmdof-1)

    For i=0 To nfdof-tmdof-1
        For j=0 To nfdof-tmdof-1
        koof(i,j)=Kfft(i+tmdof,j+tmdof)
        Next
    Next

    Dim koofinv() As Variant
    ReDim Preserve koofinv(nfdof-tmdof-1,nfdof-tmdof-1)
    koofinv=Matrix_inverse(koof,nfdof-tmdof,nfdof-tmdof)

    Dim kttvi() As Variant

    'kttv=kttf-ktof*inv(koof)*kotf;
    kttvi=Matrix_multiplication(ktof,koofinv,tmdof,nfdof-tmdof,nfdof-tmdof,nfdof-tmdof)
    kttvi=Matrix_multiplication(kttvi,kotf,tmdof,nfdof-tmdof,nfdof-tmdof,tmdof)
    ReDim kttv(tmdof,tmdof)
    kttv=Matrix_subtraction(kttf,kttvi,tmdof,tmdof)

    'Mttf=Mfft(1:tmdof,1:tmdof)
    ReDim Mttf(tmdof-1,tmdof-1)
    For i=0 To tmdof-1
        For j=0 To tmdof-1
        Mttf(i,j)=Mfft(i,j)
        Next
    Next

    End Sub

    Function Matrix_sum(ByVal a As Variant,ByVal m As Variant,ByVal n As Variant) As
    Variant

    Dim Sumi As Variant
    Sumi=0

    For i=0 To m-1
        For j=0 To n-1
        Sumi=Sumi+a(i,j)
        Next
    Next

    Matrix_sum=Sumi

    End Function

    Function Rayleigh_damping_nonlinear(ByVal eig As Variant,ByVal m As Variant,ByVal K
    As Variant,ByVal Dp As Variant,ByVal tmdof As Variant)
    'Determine the Constants ao And a1
    'Rayleigh damping (2 modes)
```

```
'[A]{a}=2[D]
'Construction of the [A]

Dim a() As Variant
ReDim Preserve a(1,1)
Dim D() As Variant
ReDim Preserve D(1,0)
Dim R() As Variant
ReDim Preserve R(1,0)
Dim Damp() As Variant
ReDim Preserve Damp(1,0)

a(0,0)=1/eig(0,0)
a(0,1)=eig(0,0)
a(1,0)=1/eig(1,0)
a(1,1)=eig(1,0)

D(0,0)=2*Dp
D(1,0)=2*Dp

R=Matrix_solver(a,D,2)

Dim mi() As Variant
ReDim Preserve mi(tmdof-1,tmdof-1)
Dim ki() As Variant
ReDim Preserve ki(tmdof-1,tmdof-1)

mi=Matrix_multiplcation_constant(R(0,0),m,tmdof,tmdof)
ki=Matrix_multiplcation_constant(R(1,0),K,tmdof,tmdof)

Rayleigh_damping_nonlinear=Matrix_addition(mi,ki,tmdof,tmdof)

End Function


Function Matrix_multiplcation_constant(ByVal c As Variant,ByVal matrixi As
Variant,ByVal m As Variant,ByVal n As Variant) As Variant

Dim mati() As Variant
ReDim Preserve mati(m-1,n-1)

For i=0 To m-1
    For j=0 To n-1
    mati(i,j)=c*matrixi(i,j)
    Next
Next

Matrix_multiplcation_constant=mati


End Function

Function eigenvalues(ByVal Mass As Variant,ByVal Kstiff As Variant,ByVal n As Variant)

'Finds the first two eigenvalues det(K-wn^2*M)=0

Dim rangew As Variant
rangew=6000
Dim y() As Variant
ReDim Preserve y(rangew-1,0)
Dim x() As Variant
ReDim Preserve x(rangew-1,0)

x=linspace(0,200000,rangew)

For ii=0 To rangew-1
wi=x(ii,0)

Dim mi() As Variant
ReDim Preserve mi(n-1,n-1)
Dim a() As Variant
ReDim Preserve a(n-1,n-1)

```

```
mi=Matrix_multiplcation_constant(wi,Mass,n,n)
a=Matrix_subtraction(Kstiff,mi,n,n)

    Dim m As Variant
    Dim pt() As Variant
    Dim pivot As Variant
    Dim counter As Variant

    For K=0 To n-2
        For i=K+1 To n-1
            If a(K,K)<>0 Then
            m=a(i,K)/a(K,K)
            ElseIf a(K,K)=0 Then
            pt=eye(n)
            pivot=a(K,K)
            counter=K
                While pivot =0 And counter<n-1
                counter=counter+1
                pivot=a(counter,K)
                Wend
            pt(K,K)=0
            pt(K,counter)=1
            pt(counter,K)=1
            pt(counter,counter)=0
            a=Matrix_multiplication(pt,a,n,n,n,n)
            m=a(i,K)/a(K,K)
            End If
                For j=K+1 To n-1
                a(i,K)=0
                a(i,j)=a(i,j)-m*a(K,j)
                Next
        Next
    Next

    Dim deti As Variant
    deti=1
    For i=0  To n-1
        deti=deti*a(i,i)
    Next
    y(ii,0)=deti
Next

Dim counter2 As Variant
counter2=0
    Dim A1 As Variant
    Dim B1 As Variant
    Dim c1 As Variant
    Dim D1 As Variant
    Dim det As Variant
    Dim Eig_values() As Variant
    ReDim Preserve Eig_values(1,0)
    i=0
    Do Until counter2=2
    i=i+1
        If y(i,0)=0 Then
            counter2=counter2+1
            A1=y(i-1,0)
            B1=y(i,0)
            c1=x(i-1,0)
            D1=x(i,0)
            det=((-A1)*(D1-c1)/(B1-A1))+c1
            Eig_values(counter2-1,0)=Sqr(det)
        ElseIf (y(i-1,0)/y(i,0))<0 Then
            counter2=counter2+1
            A1=y(i-1,0)
            B1=y(i,0)
            c1=x(i-1,0)
            D1=x(i,0)
            det=((-A1)*(D1-c1)/(B1-A1))+c1
            Eig_values(counter2-1,0)=Sqr(det)
        End If
    Loop
```

```
eigenvalues=Eig_values

End Function

Function linspace(ByVal min As Variant,ByVal max As Variant,ByVal n As Variant) As
Variant

Dim part() As Variant
ReDim Preserve part(n-1,0)

For I=0 To n-1
part(I,0)=((max-min)/(n-1))*I+min
Next

linspace=part

End Function

Function Import_data(ByVal nt As Variant ) As Variant

Dim Earthquake() As Variant
ReDim Preserve Data(nt-1,1)
Dim objXls As Object
Set objXls = CreateObject("Excel.Application")
objXls.Workbooks.Open "C:\Octave\Dynamics\Pseudo\ElCentro0.87g.xlsx"
For i=0 To nt-1
Data(i,0)=objXls.Worksheets(1).Cells(i+1,1).Value
Data(i,1)=objXls.Worksheets(1).Cells(i+1,2).Value
Next
objXls.Quit

Import_data=Data

End Function

Sub Sort_matrix(ByRef mati As Variant,ByRef mat As Variant,ByVal m As Variant,ByVal
n As Variant)

For i=0 To m-1
    For j=0 To n-1
    mati(i,j,1)=mat(i,j)
    Next
Next

End Sub

Function vector_sort(ByRef veci As Variant,ByRef vec As Variant,ByVal m As
Variant,ByVal col As Variant)

For i=0 To m-1
    veci(i,col)=vec(i,0)
Next

End Function

Sub Initial_sort_mat(ByRef mati As Variant,ByVal m As Variant,ByVal n As
Variant,ByVal matfrom As Variant,ByVal matto As Variant)

For i=0 To m-1
    For j=0 To n-1
    mati(i,j,matto)=mati(i,j,matfrom)
    Next
Next

End Sub

Sub Initial_sort_vec(ByRef veci As Variant,ByVal m As Variant,ByVal vecfrom As
Variant,ByVal vecto As Variant)

For i=0 To m-1
    veci(i,vecto)=veci(i,vecfrom)
Next
```

```
End Sub

Sub Dynamic_analysis_coefficients(ByRef a_1() As Variant,ByRef a_2() As Variant,ByRef a_3() As Variant,ByVal dt As Variant,ByVal Mttf As Variant,ByVal Cff As Variant,ByVal tmdof As Variant )
'a_1=(1/(Beta*dt^2))*Mttf+(Gamma/(Beta*dt))*Cff
'a_2=(1/(Beta*dt))*Mttf+((Gamma/Beta)-1)*Cff
'a_3=((1/(2*Beta))-1)*Mttf+dt*((Gamma/(2*Beta))-1)*Cff

Dim Beta As Variant
Beta=0.25
Dim Gamma As Variant
Gamma=0.5

ReDim Preserve a_1(tmdof-1,tmdof-1)
ReDim Preserve a_2(tmdof-1,tmdof-1)
ReDim Preserve a_3(tmdof-1,tmdof-1)

a_1=Matrix_addition(Matrix_multiplcation_constant(1/(Beta*dt^2),Mttf,tmdof,tmdof),Matrix_multiplcation_constant(Gamma/(Beta*dt),Cff,tmdof,tmdof),tmdof,tmdof)
a_2=Matrix_addition(Matrix_multiplcation_constant(1/(Beta*dt),Mttf,tmdof,tmdof),Matrix_multiplcation_constant((Gamma/Beta)-1,Cff,tmdof,tmdof),tmdof,tmdof)
a_3=Matrix_addition(Matrix_multiplcation_constant((1/(2*Beta))-1,Mttf,tmdof,tmdof),Matrix_multiplcation_constant(dt*((Gamma/(2*Beta))-1),Cff,tmdof,tmdof),tmdof,tmdof)

End Sub

Function Pa_calc(ByVal tmdof As Variant,ByVal nfdof As Variant,ByVal Ps As Variant,ByVal PEarth As Variant,ByVal ktof As Variant,ByVal koof As Variant) As Variant
'Pa=P+Ps(1:tmdof,1)-ktof*(koof\Ps(tmdof+1:nfdof,1))
Dim Pa() As Variant
ReDim Preserve Pa(tmdof-1,0)

Dim ps1() As Variant
ReDim Preserve ps1(tmdof-1,0)
Dim ps2() As Variant
ReDim Preserve ps2(nfdof-tmdof-1,0)

For i=0 To tmdof-1
ps1(i,0)=Ps(i,0)
Next

For i=0 To nfdof-tmdof-1
ps2(i,0)=Ps(i+tmdof,0)
Next

Dim koofs() As Variant
ReDim Preserve koofs(nfdof-tmdof-1,0)
Pa=Matrix_subtraction(Matrix_addition(PEarth,ps1,tmdof,1),Matrix_multiplication(ktof,Matrix_solver(koof,ps2,nfdof-tmdof),tmdof,nfdof-tmdof,nfdof-tmdof,1),tmdof,1)
Pa_calc=Pa

End Function

Function Pp_calcs(ByVal Pa As Variant,ByVal tmdof As Variant,ByVal ui As Variant,ByVal upi As Variant,ByVal uppi As Variant,ByVal a_1 As Variant,ByVal a_2 As Variant,ByVal a_3 As Variant) As Variant

Dim Pp As Variant
ReDim Preserve Pp(tmdof-1,0)

Dim Ppdis As Variant
ReDim Preserve Ppdis(tmdof-1,0)
Dim Ppvel As Variant
ReDim Preserve Ppvel(tmdof-1,0)
Dim Ppac As Variant
ReDim Preserve Ppac(tmdof-1,0)
Dim uipp() As Variant
ReDim Preserve uipp(tmdof-1,0)
Dim upipp() As Variant
ReDim Preserve upipp(tmdof-1,0)
Dim uppipp() As Variant
```

```
ReDim Preserve uppipp(tmdof-1,0)

For i=0 To tmdof-1
uipp(i,0)=ui(i,0)
upipp(i,0)=upi(i,0)
uppipp(i,0)=uppi(i,0)
Next

Ppdis=Matrix_multiplication(a_1,uipp,tmdof,tmdof,tmdof,1)
Ppvel=Matrix_multiplication(a_2,upipp,tmdof,tmdof,tmdof,1)
Ppac=Matrix_multiplication(a_3,uppipp,tmdof,tmdof,tmdof,1)

Pp=Matrix_addition(Pa,Ppdis,tmdof,1)
Pp=Matrix_addition(Pp,Ppvel,tmdof,1)
Pp=Matrix_addition(Pp,Ppac,tmdof,1)
Pp_calcs=Pp

End Function

Function R_calc(ByVal Pp As Variant,ByVal fsi As Variant,ByVal a_1 As Variant,ByVal
ui As Variant,ByVal tmdof As Variant)
'R=Pp-fsi(:,i_Load)-a1*ui(:,i_Load)
Dim R() As Variant
ReDim Preserve R(tmdof-1,0)

Dim uiR() As Variant
ReDim Preserve uiR(tmdof-1,0)
For i=0 To tmdof-1
uiR(i,0)=ui(i,1)
Next

Dim R2() As Variant
ReDim Preserve R2(tmdof-1,0)

R2=Matrix_multiplication(a_1,uiR,tmdof,tmdof,tmdof,1)
R=Matrix_subtraction(Pp,fsi,tmdof,1)
R=Matrix_subtraction(R,R2,tmdof,1)
R_calc=R

End Function

Function Norm_Residual(ByVal Residual As Variant, ByVal tmdof As Variant) As Variant
'Calculates the norm of the array
Dim max As Variant
max=Abs(Residual(0,0))

For i=1 To tmdof-1
    If Abs(Residual(i,0))>max Then
    max=Abs(Residual(i,0))
    End If
Next
Norm_Residual=max

End Function

Sub static_condensation_out(ByRef uig() As Variant,ByRef uigdu() As Variant,ByRef
Puig() As Variant,ByVal ui As Variant,ByVal kotf As Variant,ByVal koof As
Variant,ByVal Ps As Variant,ByVal Lm As Variant,ByVal i_Load As Variant,ByVal tmdof
As Variant,ByVal nfdof As Variant,ByVal tdof As Variant,ByVal du As Variant,ByVal
PEarth As Variant)

'Reverses the static condensation
Dim ps1() As Variant
ReDim Preserve ps1(tmdof-1,0)
Dim ps2() As Variant
ReDim Preserve ps2(nfdof-tmdof-1,0)

For i=0 To tmdof-1
ps1(i,0)=Ps(i,0)
Next

For i=0 To nfdof-tmdof-1
ps2(i,0)=Ps(i+tmdof,0)
```

```
Next

'Pload=p+Ps(1:tmdof,1);
Dim Pload() As Variant
ReDim Preserve Pload(tmdof-1,0)
Pload=Matrix_addition(PEarth,ps1,tmdof,1)
Dim uiR() As Variant
ReDim Preserve uiR(tmdof-1,0)
For i=0 To tmdof-1
uiR(i,0)=ui(i,1)
Next

'uo=koof\Ps(tmdof+1:nfdof,1)-koof\(kotf*ui(:,i_Load))
Dim uo1() As Variant
ReDim Preserve uo1(nfdof-tmdof-1,0)
Dim uo2() As Variant
ReDim Preserve uo2(tmdof-1,0)
Dim uo() As Variant
ReDim Preserve uo(nfdof-tmdof-1,0)

uo1=Matrix_solver(koof,ps2,nfdof-tmdof)

uo2=Matrix_solver(koof,Matrix_multiplication(kotf,uiR,nfdof-tmdof,tmdof,tmdof,1),nfdof-tmdof)
uo=Matrix_subtraction(uo1,uo2,nfdof-tmdof,1)

'uodu=-koof\(kotf*du(:,1))
Dim uodu() As Variant
ReDim Preserve uodu(nfdof-tmdof,0)
uodu=Matrix_multiplcation_constant(-1,Matrix_solver(koof,Matrix_multiplication(kotf,du,nfdof-tmdof,tmdof,tmdof,1),nfdof-tmdof),nfdof-tmdof,1)

'uoi=[ui(:,i_Load);uo]
'uoidu=[du(:,1);uodu];
Dim uoi() As Variant
ReDim Preserve uoi(nfdof-1,0)
Dim uoidu() As Variant
ReDim Preserve uoidu(nfdof-1,0)
'Pload=[Pload;Ps(tmdof+1:nfdof,1)];
Dim counter As Variant
Dim Pload1() As Variant
ReDim Preserve Pload1(nfdof-1,0)

counter=-1
For i=0 To tmdof-1
counter=counter+1
uoi(counter,0)=uiR(i,0)
uoidu(counter,0)=du(i,0)
Pload1(counter,0)=Pload(i,0)
Next
'Pload=[Pload;Ps(tmdof+1:nfdof,1)];

For i=0 To nfdof-tmdof-1
counter=counter+1
uoi(counter,0)=uo(i,0)
uoidu(counter,0)=uodu(i,0)
Pload1(counter,0)=ps2(i,0)
Next

ReDim Preserve uig(tdof-1,0)
ReDim Preserve uigdu(tdof-1,0)
ReDim Preserve Puig(tdof-1,0)

For i=0 To tdof-1
    uig(i,0)=0
    uigdu(i,0)=0
    Puig(i,0)=0
Next

For i=0 To nfdof-1
    uig(Lm(i,0),0)=uoi(i,0)
    uigdu(Lm(i,0),0)=uoidu(i,0)
    Puig(Lm(i,0),0)=Pload1(i,0)
```

```
Next
End Sub

Sub internal_dynamic_loads(ByRef IMD_G() As Variant,ByRef IMD_L() As Variant,ByRef IMF_L() As Variant,ByRef IMF_G() As Variant,ByRef Fsi2() As Variant,ByVal nbc As Variant,ByVal uig As Variant,ByVal mdof As Variant,ByVal etran_local As Variant,ByVal etranT_local As Variant,ByVal estiff_local As Variant,ByVal Pw_local As Variant)

'duv=zeros(6,nbc)
Dim duv() As Variant
ReDim Preserve duv(5,nbc-1)

For i=0 To nbc-1
    For j=0 To 5
        duv(j,i)=uig(mdof(j,i)-1,0)
    Next
Next

'Calculate the internal member force at the time

'Transform {displacement_out} from Global To local coordinates by multiplying With member local stiffness matrix
'And transformation matrix
ReDim Preserve Fsi2(5,nbc-1)
For i=0 To nbc-1
        For K=0 To 5
        IMD_G(K,i)=duv(K,i)
        Next

        Dim IMDLi() As Variant
        ReDim Preserve IMDLi(5,0)
        Dim IMFLi() As Variant
        ReDim Preserve IMFLi(5,0)
        Dim IMFGi() As Variant
        ReDim Preserve IMFGi(5,0)
        Dim fsoi() As Variant
        ReDim Preserve fsoi(5,0)
        Dim PwL() As Variant
        ReDim Preserve PwL(5,0)

        Dim trans As Variant
        ReDim Preserve trans(5,5)
        Dim transT As Variant
        ReDim Preserve transT(5,5)
        Dim estiff As Variant
        ReDim Preserve estiff(5,5)

        For j=0 To 5
            For K=0 To 5
            trans(j,K)=etran_local(j,K,i)
            transT(j,K)=etranT_local(j,K,i)
            estiff(j,K)=estiff_local(j,K,i)
            Next
        IMDLi(j,0)=IMD_G(j,i)
        PwL(j,0)=Pw_local(j,i)
        Next
    IMDLi=Matrix_multiplication(trans,IMDLi,6,6,6,1)
    IMFLi=Matrix_multiplication(estiff,IMDLi,6,6,6,1)
    fsoi=Matrix_multiplication(transT,IMFLi,6,6,6,1)
    IMFLi=Matrix_subtraction(IMFLi,PwL,6,1)
    IMFGi=Matrix_multiplication(transT,IMFLi,6,6,6,1)

    For j=0 To 5
    IMD_L(j,i)=IMDLi(j,0)
    IMF_L(j,i)=IMFLi(j,0)
    IMF_G(j,i)=IMFGi(j,0)
    Fsi2(j,i)=fsoi(j,0)
    Next

Next
End Sub
```

```
Sub memf_spring_dynamic(ByRef Fs As Variant,ByRef IMFsi As Variant,ByRef IMDsi As Variant,ByVal KSpring As Variant,ByVal uig As Variant,ByVal Smdof As Variant,ByVal uigdu As Variant,ByVal i_Load As Variant)

Dim ds() As Variant
ReDim Preserve ds(1,0)
Dim dsidu() As Variant
ReDim Preserve dsidu(1,0)

For I=0 To 1
    ds(I,0)=0
    dsidu(I,0)=0
Next

ds(1,0)=uig(Smdof(1,0)-1,0)
dsidu(1,0)=uigdu(Smdof(1,0)-1,0)

'IMFs=KSpring*dsidu
Dim IMFs() As Variant
ReDim Preserve IMFs(1,0)
IMFs=Matrix_multiplication(KSpring,dsidu,2,2,2,1)

'IMFsi{i_Load}=IMFsi{i_Load}+IMFs;
IMFsi(0,i_Load)=IMFsi(0,i_Load)+IMFs(0,0)
IMFsi(1,i_Load)=IMFsi(1,i_Load)+IMFs(1,0)

'IMDsi{i_Load}=IMDsi{i_Load}+dsidu;
IMDsi(0,i_Load)=IMDsi(0,i_Load)+dsidu(0,0)
IMDsi(1,i_Load)=IMDsi(1,i_Load)+dsidu(1,0)

'Fs=IMFsi{i_Load}(2,1)
Fs=IMFsi(1,i_Load)

End Sub

Sub Post_calcs_nonlinear_dynamic(ByRef Fsi1 As Variant,ByRef ks As Variant,ByRef IMFsi As Variant,ByVal Fsi2 As Variant,ByVal Fs As Variant,ByVal mdof As Variant,ByVal Smdof As Variant,ByVal tdof As Variant,ByVal IMDsi As Variant,ByVal i_Load As Variant,ByVal nbc As Variant)

For i=0 To tdof-1
Fsi1(i,0)=0
Next

For i=0 To nbc-1
    For j=0 To 5
    Fsi1(mdof(j,i)-1,0)=Fsi1(mdof(j,i)-1,0)+Fsi2(j,i)
    Next
Next

Fsi1(Smdof(0,0)-1,0)=Fsi1(Smdof(0,0)-1,0)-Fs
Fsi1(Smdof(1,0)-1,0)=Fsi1(Smdof(1,0)-1,0)+Fs

IMFsi(1,i_Load)=Fs
IMFsi(0,i_Load)=-Fs

If Abs((IMDsi(1,i_Load)-IMDsi(1,i_Load-1)))*1000<0.0001 Then
EA_Panel.GetCell(Panel1,"Converge_time_table",1,1,converge_time_step)
ElseIf Abs((IMDsi(1,i_Load)-IMDsi(1,i_Load-1)))*1000>=0.0001 Then
ks=Abs((IMFsi(1,i_Load)-IMFsi(1,i_Load-1))/(IMDsi(1,i_Load)-IMDsi(1,i_Load-1)))
End If
End Sub

Sub velocity_acceleration(ByVal ui As Variant,ByRef upi As Variant,ByRef uppi As Variant,ByVal dt As Variant,ByVal tmdof As Variant)

Dim Gamma As Variant
Dim Beta As Variant
Gamma=0.5
Beta=0.25

For i= 0 To tmdof-1
upi(i,1)=(Gamma/(Beta*dt))*(ui(i,1)-ui(i,0))+(1-Gamma/Beta)*upi(i,0)+dt*(1-Gamma/(2*Be
```

```
ta))*uppi(i,0)
uppi(i,1)=(1/(Beta*dt^2))*(ui(i,1)-ui(i,0))-(1/(Beta*dt))*upi(i,0)-((1/(2*Beta))-1)*uppi(i,0)
Next

End Sub

Function reactions(ByVal global_stiffness As Variant,ByVal Disp As Variant,ByVal nfdof As Variant,ByVal tdof As Variant) As Variant

Dim Rs() As Variant
Dim Ksf() As Variant
ReDim Preserve Ksf(tdof-nfdof-1,nfdof-1)
Dim fixdof As Variant
fixdof=tdof-nfdof

For i=0 To fixdof-1
    For j=0 To nfdof-1
    Ksf(i,j)=global_stiffness(i+nfdof,j)
    Next
Next

Rs=Matrix_multiplication(Ksf,Disp,tdof-nfdof,nfdof,nfdof,1)
reactions=Rs

End Function

Function assemble_mass_Point(ByRef global_mass As Variant,ByVal dof As Variant,ByVal tdof As Variant,ByVal N_mas As Variant,ByVal Nodes_mas As Variant,ByVal M_mas As Variant,ByVal mdof As Variant) As Variant
'Assembles the mass as a result of the masonary walls

Dim global_mass_Point() As Variant
ReDim Preserve global_mass_Point(tdof-1,tdof-1)
For i=0 To tdof-1
    For j=0 To tdof-1
    global_mass_Point(i,j)=0
    Next
Next

For i=0 To N_mas-1
    For j=0 To 1
    global_mass_Point(dof(j,Nodes_mas(i,0)-1)-1,dof(j,Nodes_mas(i,0)-1)-1)=global_mass_Point(dof(j,Nodes_mas(i,0)-1)-1,dof(j,Nodes_mas(i,0)-1)-1)+M_mas
    Next
Next

For i=0 To tdof-1
    For j=0 To tdof-1
    global_mass(i,j)=global_mass(i,j)+global_mass_Point(i,j)
    Next
Next
assemble_mass_Point=global_mass_Point

End Function

Sub Axial_stop_OnClick
'Automatically created procedure: Do not change or delete name or signature!
EA_Panel.SetCell(Panel3,"Axial_stop_table",1,1,1)

End Sub

Sub Converge_OnClick
'Automatically created procedure: Do not change or delete name or signature!
EA_Panel.SetCell(Panel1,"Converge_table",1,1,1)
End Sub

Sub Converge_time_OnClick
'Automatically created procedure: Do not change or delete name or signature!
EA_Panel.SetCell(Panel1,"Converge_time_table",1,1,1)
End Sub
```

APPENDIX B

CYCLIC LOAD EXPERIMENTATION SCRIPT

```
Sub Main
'Performs a cyclic load test
EA_IO.ZeroBalanceControl("Displacement_Hor",1)
EA_IO.ZeroBalanceControl("Force_Hor",1)
EA_IO.SetAnalogOut("PMX_1 CH 9",1,0,1)

'Activating plots In the panel And setting them To zero
EA_Graph.RemovePlot(Panel1,"Graph1",1)
EA_Graph.Refresh(Panel1,"Graph1")
EA_Graph.RemovePlot(Panel1,"Displacement_out",1)
EA_Graph.Refresh(Panel1,"Displacement_out")
EA_Graph.RemovePlot(Panel1,"LVDT_plot",1)
EA_Graph.Refresh(Panel1,"LVDT_plot")
EA_Graph.RemovePlot(Panel1,"Strain_out_disp",1)
EA_Graph.Refresh(Panel1,"Strain_out_disp")
'EA_IO.ZeroBalanceControl("MX840_SR",1)
'EA_IO.ZeroBalanceControl("MX840_SL",1)
EA_IO.ZeroBalanceControl("PMX_LVDT1",1)
EA_IO.ZeroBalanceControl("PMX_LVDT2",1)
EA_IO.ZeroBalanceControl("PMX_LVDT3",1)
EA_IO.ZeroBalanceControl("PMX_LVDT4",1)
EA_IO.ZeroBalanceControl("Displacement_Hor",1)
EA_IO.ZeroBalanceControl("Force_Hor",1)

End Sub

Sub Axial_load
'Runs data logging during axial load application
Dim Analysis As Variant 'Input to change for the number of analysis being performed
Analysis=2
Dim objXls_a As Object
Set objXls_a = CreateObject("Excel.Application")
objXls_a.Workbooks.Add
objXls_a.Worksheets(1).Name = "Linear results"
objXls_a.Workbooks(1).SaveAs
"C:\Octave\Dynamics\Pseudo\Axial_unload_test_pseudo1_linear"+CStr(Analysis)+".xlsx"
' "C:\Octave\Dynamics\Pseudo\OutputDispOutput4.xls"

objXls_a.Worksheets(1).Cells(1,1).Value ="Counter"
objXls_a.Worksheets(1).Cells(1,2).Value ="Axial load (kN)"
objXls_a.Worksheets(1).Cells(1,3).Value ="Strain gauge left (micro)"
objXls_a.Worksheets(1).Cells(1,4).Value ="Strain gauge right (micro)"

Dim Force_axial As Double
Dim Strain_Left As Double
Dim Strain_right As Double
Dim Axial_load_applied() As Double
Dim Strain_Left_disp() As Double
Dim Strain_right_disp() As Double
Dim StepInc() As Double

Dim Button2 As Variant
Button2=0
Dim counter As Variant
counter=0

EA_Panel.SetCell(Panel2,"Axial_stop_table",1,1,0)

        Do While Button2=0 'Convergence at each time step

        EA_Panel.GetCell(Panel2,"Axial_stop_table",1,1,Button2)

        ReDim Preserve StepInc(counter+1)
        ReDim Preserve Axial_load_applied(counter+1)
        ReDim Preserve Strain_Left_disp(counter+1)
        ReDim Preserve Strain_right_disp(counter+1)
        StepInc(counter)=CDbl(counter)
        objXls_a.Worksheets(1).Cells(counter+2,1).Value =counter

        'Read out axial force from servo controller
        EA_IO.Measure("Load cell",Force_axial,1) 'Axial force from load cell
        objXls_a.Worksheets(1).Cells(counter+2,2).Value =Force_axial 'Saves force to
        excel spreadsheet
```

```
        Axial_load_applied(counter)=CDbl(Force_axial) 'Stores force in array for plotting

        'Read out Strain gauge Left from servo controller
        EA_IO.Measure("MX840_SL",Strain_Left,1) 'Left strain gauge reading from strain gauge
        objXls_a.Worksheets(1).Cells(counter+2,3).Value =Strain_Left 'Saves left strain gauge reading to excel spreadsheet
        Strain_Left_disp(counter)=CDbl(Strain_Left) 'Stores left strain gauge reading in array for plotting

        'Read out Strain gauge Right from servo controller
        EA_IO.Measure("MX840_SR",Strain_right,1) 'Right strain gauge reading from strain gauge
        objXls_a.Worksheets(1).Cells(counter+2,4).Value =Strain_right 'Saves right strain gauge reading to excel spreadsheet
        Strain_right_disp(counter)=CDbl(Strain_right) 'Stores right strain gauge reading in array for plotting

        'Axial load out (Plotting)
        EA_Graph.PlotArrayXY(Panel2,"Axial_load_initial",1,counter+1, StepInc(), Axial_load_applied())
        EA_Graph.SetPlotProperty(Panel2,"Axial_load_initial",1,2,vbRed)
        EA_Graph.Refresh(Panel2,"Axial_load_initial")

        'Plots Strain values (Plotting)
        EA_Graph.PlotArrayXY(Panel2,"Strain_gauge_axial",1,counter+1, StepInc(), Strain_right_disp())
        EA_Graph.SetPlotProperty(Panel2,"SStrain_gauge_axial",1,2,vbBlue)
        EA_Graph.SetPlotProperty(Panel2,"Strain_gauge_axial",1,5,0)

        counter=counter+1 'Counter per loop
        objXls_a.Workbooks(1).Save 'Save excel spreadsheet
        Loop

        objXls_a.Workbooks(1).Save 'Final save of excel spreadsheet
        objXls_a.Quit 'Closes excel spreadsheet
End Sub

Sub Cyclic_test
'Runs a cyclic test on the specimum
'Pulling (Tension)      Negative
'Pushing (Compression)  Positive
EA_IO.ZeroBalanceControl("Displacement_Hor",1)
EA_IO.ZeroBalanceControl("Force_Hor",1)

'Data files - Excel output of the data
Dim Analysis As Variant 'Input to change for the number of analysis being performed
Analysis=4
Dim objXls_u As Object
Set objXls_u = CreateObject("Excel.Application")
objXls_u.Workbooks.Add
objXls_u.Worksheets(1).Name = "Linear results"
objXls_u.Workbooks(1).SaveAs "C:\Octave\Dynamics\Pseudo\Pseudo1_load_test_0512"+CStr(Analysis)+".xlsx"  ' "C:\Octave\Dynamics\Pseudo\OutputDispOutput4.xls"
Dim n As Variant
Dim pi As Variant
pi=4*Atn(1)
Dim x() As Variant
x=Sine_increment(n)
Dim analog_out As Variant

objXls_u.Worksheets(1).Cells(1,1).Value ="Displacement (mm)"
objXls_u.Worksheets(1).Cells(1,2).Value ="Analog out (V)"
objXls_u.Worksheets(1).Cells(1,3).Value ="Displacement in (mm)"
objXls_u.Worksheets(1).Cells(1,4).Value ="Horizontal force (N)"
objXls_u.Worksheets(1).Cells(1,5).Value ="Vertical force (kN)"
objXls_u.Worksheets(1).Cells(1,7).Value ="LVDT1 (mm)"
objXls_u.Worksheets(1).Cells(1,8).Value ="LVDT2 (mm)"
objXls_u.Worksheets(1).Cells(1,9).Value ="LVDT3 (mm))"
objXls_u.Worksheets(1).Cells(1,10).Value ="LVDT4 (mm)"
objXls_u.Worksheets(1).Cells(1,12).Value ="Strain gauge left (micro)"
```

```
objXls_u.Worksheets(1).Cells(1,13).Value ="Strain gauge right (micro)"

Dim Disp_read_servo As Double
Dim Force_servo_hor As Double
Dim Force_axial As Double
Dim LVDT1 As Double
Dim LVDT2 As Double
Dim LVDT3 As Double
Dim LVDT4 As Double
Dim StrainLeft As Double
Dim StrainRight As Double
objXls_u.Workbooks(1).Save

Dim Displacement_xOut() As Double
ReDim Preserve Displacement_xOut(n-1)
Dim Displacement_xIn() As Double
ReDim Preserve Displacement_xIn(n-1)
Dim Force_hor() As Double
ReDim Preserve Force_hor(n-1)
Dim Strain_Left As Double
Dim Strain_right As Double
Dim Strain_Left_disp() As Double
ReDim Preserve Strain_Left_disp(n-1)
Dim Strain_right_disp() As Double
ReDim Preserve Strain_right_disp(n-1)

Dim LVDT1_disp() As Double
ReDim Preserve LVDT1_disp(n-1)
Dim LVDT2_disp() As Double
ReDim Preserve LVDT2_disp(n-1)
Dim LVDT3_disp() As Double
ReDim Preserve LVDT3_disp(n-1)
Dim LVDT4_disp() As Double
ReDim Preserve LVDT4_disp(n-1)
Dim Axial_load() As Double
ReDim Preserve Axial_load(n-1)
Dim StepInc() As Double
ReDim Preserve StepInc(n-1)
Dim Button_stop As Variant
Button_stop=0

EA_Panel.SetCell(Panel1,"Linear_push_stop",1,1,0)

'Starts applying the horizontal load
For i_Load=0 To n-1

EA_Panel.SetValue(Panel1,"Counter1out",i_Load)

StepInc(i_Load)=CDbl(i_Load)

Dim xout As Variant
xout=x(i_Load,0)
objXls_u.Worksheets(1).Cells(i_Load+2,1).Value =xout 'Displacement

analog_out=(1/-6.6025)*xout 'volts from mm (Check to make sure of correct direction)
EA_IO.SetAnalogOut("PMX_1 CH 9",1,analog_out,1)
objXls_u.Worksheets(1).Cells(i_Load+2,2).Value =analog_out 'Analog out

'Read out disp from servo controller
EA_IO.Measure("Displacement_Hor",Disp_read_servo,1) 'Displacement from servo controller
objXls_u.Worksheets(1).Cells(i_Load+2,3).Value =Disp_read_servo 'Saves horizontal displacement to excel spreadsheet

'Read out horizontal force from servo controller
EA_IO.Measure("Force_Hor",Force_servo_hor,1) 'Horizontal force from servo controller
objXls_u.Worksheets(1).Cells(i_Load+2,4).Value =Force_servo_hor 'Saves horizontal force to excel spreadsheet

'Read out axial force from servo controller
EA_IO.Measure("Load cell",Force_axial,1) 'Axial force from servo controller
objXls_u.Worksheets(1).Cells(i_Load+2,5).Value =Force_axial 'Saves axial force to excel spreadsheet
```

```
EA_Panel.SetValue(Panel1,"DIGIT_2_axial",Force_axial)

'Read out LVDT1 from servo controller
EA_IO.Measure("PMX_LVDT1",LVDT1,1) 'LVDT1 reading
objXls_u.Worksheets(1).Cells(i_Load+2,7).Value =LVDT1 'Saves LVDT1 reading to excel spreadsheet

'Read out LVDT2 from servo controller
EA_IO.Measure("PMX_LVDT2",LVDT2,1) 'LVDT2 reading
objXls_u.Worksheets(1).Cells(i_Load+2,8).Value =LVDT2 'Saves LVDT2 reading to excel spreadsheet

'Read out LVDT3 from servo controller
EA_IO.Measure("PMX_LVDT3",LVDT3,1) 'LVDT3 reading
objXls_u.Worksheets(1).Cells(i_Load+2,9).Value =LVDT3 'Saves LVDT3 reading to excel spreadsheet

'Read out LVDT4 from servo controller
EA_IO.Measure("PMX_LVDT4",LVDT4,1) 'LVDT4 reading
objXls_u.Worksheets(1).Cells(i_Load+2,10).Value =LVDT4 'Saves LVDT4 reading to excel spreadsheet

'Read out Strain gauge Left from servo controller
EA_IO.Measure("MX840_SL",StrainLeft,1) 'Strain gauge left reading
objXls_u.Worksheets(1).Cells(i_Load+2,12).Value =StrainLeft 'Saves strain left reading to excel spreadsheet

'Read out Strain gauge Right from servo controller
EA_IO.Measure("MX840_SR",StrainRight,1) 'Strain gauge right reading
objXls_u.Worksheets(1).Cells(i_Load+2,13).Value =StrainRight 'Saves strain right reading to excel spreadsheet

objXls_u.Workbooks(1).Save 'Saves excel spreadsheet data

Displacement_xOut(i_Load)=CDbl(xout)'Output displacement array for plotting
Displacement_xIn(i_Load)=CDbl(Disp_read_servo)'Input Displacement array for plotting

Force_hor(i_Load)=CDbl(Force_servo_hor)

LVDT1_disp(i_Load)=CDbl(LVDT1) 'LVDT1 array for plotting
LVDT2_disp(i_Load)=CDbl(LVDT2) 'LVDT2 array for plotting
LVDT3_disp(i_Load)=CDbl(LVDT3) 'LVDT3 array for plotting
LVDT4_disp(i_Load)=CDbl(LVDT4) 'LVDT4 array for plotting

Strain_Left_disp(i_Load)=CDbl(StrainLeft) 'Strain gauge left array for plotting
Strain_right_disp(i_Load)=CDbl(StrainRight) 'Strain gauge right array for plotting

Axial_load(i_Load)=CDbl(Force_axial) 'Axial load array for plotting

'Force displacement out (Plotting)
EA_Graph.PlotArrayXY(Panel1,"Graph1",1,i_Load+1, Displacement_xOut(), Force_hor())
EA_Graph.SetPlotProperty(Panel1,"Graph1",1,2,vbRed)
EA_Graph.Refresh(Panel1,"Graph1")

'Displacement load out (Plotting)
EA_Graph.PlotArrayXY(Panel1,"Displacement_out",1,i_Load+1, StepInc(), Displacement_xOut())
EA_Graph.SetPlotProperty(Panel1,"Displacement_out",1,2,vbRed)
EA_Graph.Refresh(Panel1,"Displacement_out")

EA_Graph.PlotArrayXY(Panel1,"Displacement_out",2,i_Load+1, StepInc(), Displacement_xIn())
EA_Graph.SetPlotProperty(Panel1,"Displacement_out",1,2,vbBlue)
EA_Graph.Refresh(Panel1,"Displacement_out")

'Plots Strain values (Plotting)
EA_Graph.PlotArrayXY(Panel1,"Strain_out_disp",1,i_Load+1, StepInc(), Strain_right_disp())
EA_Graph.SetPlotProperty(Panel1,"Strain_out_disp",1,2,vbBlue)
EA_Graph.SetPlotProperty(Panel1,"Strain_out_disp",1,5,0)

'EA_Graph.PlotArrayXY(Panel1,"Strain_out_disp",2,i_Load+1, StepInc(), Strain_Left_disp())
```

```
'EA_Graph.SetPlotProperty(Panel1,"Strain_out_disp",2,2,vbRed)
'EA_Graph.SetPlotProperty(Panel1,"Strain_out_disp",2,5,0)
'EA_Graph.Refresh(Panel1,"Strain_out_disp")

'Plots LVDT values out (Plotting)
EA_Graph.PlotArrayXY(Panel1,"LVDT_plot",1,i_Load+1, StepInc(), LVDT1_disp())
EA_Graph.SetPlotProperty(Panel1,"LVDT_plot",1,2,vbBlack)
EA_Graph.SetPlotProperty(Panel1,"LVDT_plot",1,5,0)

EA_Graph.PlotArrayXY(Panel1,"LVDT_plot",2,i_Load+1, StepInc(), LVDT2_disp())
EA_Graph.SetPlotProperty(Panel1,"LVDT_plot",2,2,vbRed)
EA_Graph.SetPlotProperty(Panel1,"LVDT_plot",2,5,0)

EA_Graph.PlotArrayXY(Panel1,"LVDT_plot",3,i_Load+1, StepInc(), LVDT3_disp())
EA_Graph.SetPlotProperty(Panel1,"LVDT_plot",3,2,vbBlue)
EA_Graph.SetPlotProperty(Panel1,"LVDT_plot",3,5,0)

EA_Graph.PlotArrayXY(Panel1,"LVDT_plot",4,i_Load+1, StepInc(), LVDT4_disp())
EA_Graph.SetPlotProperty(Panel1,"LVDT_plot",4,2,vbMagenta)
EA_Graph.SetPlotProperty(Panel1,"LVDT_plot",4,5,0)
EA_Graph.Refresh(Panel1,"LVDT_plot")

Wait 0.1

Next
objXls_u.Workbooks(1).Save
objXls_u.Quit

End Sub

Sub BUTTON_1_OnClick
'Automatically created procedure: Do not change or delete name or signature!
Dim Button1 As Double
Button1=1
EA_Panel.SetValue(Panel1,"Button1out",Button1)
EA_Panel.SetCell(Panel1,"TABLE_1",1,1,Button1)

End Sub

Sub Axial_stop_OnClick
'Automatically created procedure: Do not change or delete name or signature!
EA_Panel.SetCell(Panel2,"Axial_stop_table",1,1,1)
End Sub

Sub Linear_push_stop_OnClick
'Automatically created procedure: Do not change or delete name or signature!
EA_Panel.SetCell(Panel2,"Linear_push_stop",1,1,1)
End Sub

Function Sine_increment(ByRef n As Variant) As Variant
Çreates an incrementally increasing cyclic load
Dim increments As Variant
n1=100
Dim nmm As Variant
nmm=25
Dim x_inc() As Variant
ReDim Preserve x_inc(4*n1*nmm+nmm,0)
Dim pi As Variant
pi=4*Atn(1)
Dim counter As Variant
counter=0

For i=0 To nmm-1
    For j=0 To 4*n1
    x_inc(counter,0)=-1*(i+1)*Sin((pi/(2*n1))*j))
    counter=counter+1
    Next
Next
n=counter
Sine_increment=x_inc

End Function
```